

SPECTROVAS: The evaluation of biospectroscopy as a potential biomarker of disease activity in pauci-immune small vessel vasculitis

A thesis submitted to the University of Central Lancashire for the degree of MD (Res) in the Faculty of the School of Medicine

2022

Dr Adam D Morris BSc, MBChB, MRCP (Neph)

RESEARCH STUDENT DECLARATION FORM

Type of Award MD (Research) Examination

School School of Medicine

*Sections marked * delete as appropriate*

1. Concurrent registration for two or more academic awards

*I declare that while registered as a candidate for the research degree, I have not been a registered candidate or enrolled student for another award of the University or other academic or professional institution

2. Material submitted for another award

*I declare that no material contained in the thesis has been used in any other submission for an academic award and is solely my own work

3. Collaboration

Where a candidate's research programme is part of a collaborative project, the thesis must indicate in addition clearly the candidate's individual contribution and the extent of the collaboration. Please state below:

Not applicable

4. Use of a Proof-reader

*No proof-reading service was used in the compilation of this thesis.

Signature of Candidate



Print name: **Dr Adam Morris**

Table of Contents

Abstract	6
List of Tables & Figures	7
List of abbreviations	10
Declaration	12
Acknowledgements	13
Dedication	14
Chapter 1: Introduction	15
1.1 Background & study objectives	15
1.2 Pathogenesis	15
1.2.1 ANCA: origins & immunopathogenesis	15
1.2.2 Disease propagation: NETS & the complement system	16
1.2.3 B-cell T-cell cross talk	17
1.2.4 ANCA negative disease	18
1.2.5 Novel autoantibodies	18
1.2.5.1 Anti-LAMP2 autoantibodies	18
1.2.5.2 Anti-plasminogen autoantibodies	19
1.2.5.3 Anti-Moesin autoantibodies	19
1.2.5.4 Anti-endothelial cell auto-antibodies	19
1.3 A predisposition to disease	20
1.3.1 “Two hit hypothesis”	20
1.3.2 Epigenetics	20
1.3.3 Environmental factors	21
1.3.4 Silica	22
1.3.5 Drug induced disease	22
1.3.6 Infection	22
1.4 Clinical manifestation of disease	23
1.5 Epidemiology	25
1.6 Treatment	26
1.6.1 Remission induction therapy	27
1.6.1.1 Glucocorticoids	27
1.6.1.2 Cyclophosphamide	29
1.6.1.3 B-cell depleting therapy	29
1.6.1.4 Combination therapy: B-cell depletion & Cyclophosphamide	30
1.6.1.5 Mycophenolic acid	32
1.6.1.6 Methotrexate	32
1.6.1.7 Complement system inhibition	32
1.6.1.8 Anti-IL5 monoclonal antibodies	34
1.6.1.9 Intravenous immunoglobulins	34
1.6.2 Remission maintenance therapy	35
1.6.2.1 Glucocorticoids	35
1.6.2.2 Antiproliferative agents	36
1.6.2.3 Anti-TNF α	37
1.6.2.4 Rituximab	37
1.6.3 Adjuvant therapy	38
1.6.3.1 Plasma exchange	38
1.6.3.2 Anti-microbials	42
1.6.3.3 Anti-fibrotic agents	42
1.6.4 Novel therapeutic targets	42

1.7 Diagnosis & Disease Activity	43
1.7.1 Histopathology	43
1.7.2 Imaging	45
1.7.3 ANCA	46
1.7.4 B-cell population & Cytokines	48
1.7.5 Complement	49
1.7.6 Inflammatory markers	50
1.7.7 Urinary proteins	51
1.7.8 mRNA	51
1.7.9 Metabolomics	52
1.7.10 Biospectroscopy	53
1.8 Hypothesis, Aims & Objectives	56
Chapter 2: Material & Methods	57
2.1 Patients & Ethics	57
2.2 Biofluid sample collection & preparation	58
2.3 Tissue sample collection & preparation	58
2.4 ATR-FTIR spectral acquisition from biofluids	58
2.5 Raman spectral acquisition from biofluid & renal tissue samples	59
2.6 Spectral pre-processing	59
2.7 Multivariate analysis	60
2.7.1 Chemometric models for analysis of biofluids	60
2.7.2 Chemometric models for comparative analysis of tissue & urine samples	60
2.8 Model validation	62
2.9 Correlation with clinical variables	63
Chapter 3: Results	64
3.1 Study population	64
3.1.1 Biofluid samples	64
3.1.2 Renal tissue & paired urine samples	65
3.2 Biofluid sample analysis by ATR-FTIR spectroscopy	67
3.2.1 Spectral data and classification models	67
3.2.2 Correlation with clinical parameters	71
3.2.3 Key spectral biomarkers	73
3.3 Biofluid sample analysis by Raman spectroscopy	74
3.3.1 Spectral data & classification models	74
3.3.2 Key discriminating spectral bands	79
3.4 Renal tissue & paired urine sample analysis by Raman spectroscopy	80
3.4.1 Spectral data & classification models: all renal tissue samples	80
3.4.2 Spectral data & classification models: comparative results for tissue & paired urine samples	83
3.4.3 Key discriminating spectral biomarkers: tissue & paired urine samples	84
Chapter 4: Discussion	86
4.1 Biofluid sample analysis by ATR-FTIR spectroscopy	88
4.2 Biofluid sample analysis by Raman spectroscopy	89
4.3 Renal tissue & paired urine sample analysis by Raman spectroscopy	89
4.4 Study limitations & future work	91
4.5 Summary	92
Chapter 5: General Discussion & Study Overview	94
References	98
Appendix 1: Supplementary information - Distinguishing active from quiescent disease in ANCA-associated vasculitis using attenuated total reflection Fourier-transform infrared spectroscopy	125
Appendix 2: Supplementary information - A comparative analysis of different biofluids using Raman spectroscopy to determine disease activity in ANCA-associated vasculitis	139
Appendix 3: HRA approval	146

Appendix 4: Sponsor approval	153
Appendix 5: Publications in relation to the presented body of work	155

Abstract

Anti-neutrophil cytoplasmic autoantibody (ANCA)-associated vasculitis (AAV) characterises an autoimmune disorder that results in inflammation and necrosis of small- and medium-sized blood vessels, causing potential multi-organ and life threatening disease. Immunosuppressive treatment strategies are effective with improved patient survival, but carry a significant risk of treatment-related toxicity and long-term patient morbidity that often results from the sequelae of relapsing disease and required re-exposure to therapy. The current lack of a reliable biomarker of disease activity in multisystem AAV poses a significant clinical unmet need when determining relapsing or persisting disease. Biospectroscopy offers a highly versatile, non-destructive and cost-effective means of analysing a given biological sample to determine its chemical composition; in effect providing a surrogate of its metabolomic profile. This thesis aimed to evaluate the role of biospectroscopy as a candidate biomarker of disease activity in AAV with application to plasma, serum, urine and renal tissue samples.

For both initial biofluid studies, paired blood and urine samples were collected within a single UK centre from patients with active disease, disease remission, disease controls and healthy controls. Three key biofluids were evaluated; plasma, serum and urine, with subsequent chemometric analysis and blind predictive model validation. Considering ATR-FTIR, plasma proved to be the most conducive biofluid, with 100% sensitivity (F-score 92.3%) for disease remission and 85.7% specificity (F-score 92.3%) for active disease. This was independent of organ system involvement and current ANCA status. Considering Raman spectroscopy, plasma and serum samples demonstrated equal ability to discriminate disease activity: F-score 80% for plasma (specificity 93.3%, sensitivity 70%, AUC 0.95) and 80% for serum (specificity 80%, sensitivity 80%, AUC 0.92). Both techniques exhibited similar findings on analysis of paired remission samples following successful remission-induction therapy.

For renal tissue samples, consecutive patients with active ANCA-associated glomerulonephritis (AAGN) and those in disease remission were recruited from a single UK centre. In those with active disease, renal tissue and a paired urine sample were collected. Amongst those in remission at the time of recruitment, archived renal tissue samples taken at the time of initial diagnosis were attained. Using histological data, spectral analysis from unstained tissue samples was able to discriminate disease activity with a high degree of accuracy according to >25% interstitial fibrosis and tubular atrophy (F-score 95%, sensitivity 100%, specificity 90%, AUC 0.98), necrotising glomerular lesions (F-score 100%, sensitivity 100%, specificity 100%, AUC 1) and interstitial infiltrate (F-score 100%, sensitivity 100%, specificity 100%, AUC 0.97). Corresponding spectrochemical changes in paired urine samples was limited.

In this body of work, we confirm for the first time that both ATR-FTIR and Raman spectroscopy offer a novel and functional candidate biomarker in AAV, distinguishing active from quiescent disease with a high degree of accuracy using plasma and serum, as well as the application of machine learning in conjunction with Raman spectroscopy as an innovative low-cost technique for the automated computational detection of disease activity in AAGN. The promising technique of biospectroscopy is clinically translatable and warrants future larger study with longitudinal data and more varied pathology, potentially aiding earlier intervention and individualisation of treatment.

List of Tables & Figures

Chapter 1

Table 1: Definitions for AAV clinical presentations adopted by the international Chapel Hill Consensus Conference 2012

Table 2: Draft Classification criteria for the ANCA-associated vasculitides

Table 3: Risk reduction for end stage renal disease (ESRD) and increased infection risk at 12 months post plasma exchange (Adapted from - Walsh M, Collister D, Zeng L, Merkel PA, Pusey CD, Guyatt G, et al. The effects of plasma exchange in patients with ANCA-associated vasculitis: an updated systematic review and meta-analysis. *Bmj*. 2022;e064604)

Table 4: Summary of current and prospective non-invasive biomarkers in ANCA-associated vasculitis

Figure 1: Pathway of complement activation (taken from Chen M, Jayne DRW, Zhao MH. Complement in ANCA-associated vasculitis: Mechanisms and implications for management. *Nat Rev Nephrol*. 2017;13(6):359–67)

Figure 2: Proposed model for the interaction of anti-neutrophil cytoplasmic antibody (ANCA), neutrophils and complement activation in the pathogenesis of ANCA-associated vasculitis (taken from Chen M, Jayne DRW, Zhao MH. Complement in ANCA-associated vasculitis: Mechanisms and implications for management. *Nat Rev Nephrol*. 2017;13(6):359–67)

Figure 3: Distribution of vessel involvement by large vessel vasculitis, medium vessel vasculitis, and small vessel vasculitis (taken from - Jennette JC, Falk RJ, Bacon PA, N. B, Cid MC, Ferrario L., et al. 2012 Revised International Chapel Hill Consensus Conference Nomenclature of Vasculitides. *Arthritis Rheum*. 2012;65(1):1–11)

Figure 4: Graphic of the study design and treatment regimens (taken from - Merkel P, Jayne D, Harigai M, Schall T, Bekker P, Potarca A, et al. 326. a Randomized Phase 3 Trial Evaluating the Safety and Efficacy of Avacopan in Patients With New or Relapsing Anca-Associated Vasculitis. *Rheumatology*. 2019;58(Supplement_2):2–4)

Figure 5: The required stages of biomarker development

Figure 6: Pathology of ANCA-associated glomerulonephritis: light microscopy (images taken from archived biopsy samples of patients consented for participation in the studies presented in this thesis)

Chapter 3

Table 5: Characteristics of study population at the time of enrolment for biofluid analysis

Table 6: Characteristics of study population at the time of enrolment for renal tissue analysis

Table 7: Classification parameters for plasma samples in active disease (AD) vs. disease remission (DR)

Table 8: Classification parameters for plasma samples in active disease (AD) vs. paired remission (PR)

Table 9: Classification parameters for plasma samples in healthy controls (HC) vs. active disease (AD) and disease remission (DR)

Table 10: Comparative analysis between clinical variables and ATR-FTIR spectral data from plasma samples

Table 11: Potential spectral biomarkers for distinguishing active disease and disease remission using plasma samples based on the PLS-DA coefficients (ν = stretching; δ = bending)

Table 12: Classification parameters for plasma samples in active disease (AD) vs. disease remission (DR)

Table 13: Classification parameters for serum samples in active disease (AD) vs. disease remission (DR)

Table 14: Classification parameters for plasma samples in active disease (AD) vs. paired remission (PR)

Table 15: Classification parameters for serum samples in active disease (AD) vs. paired remission (PR)

Table 16: Classification model performance according to histological data for renal biopsy samples (n=27)

Table 17: Classification model performance according to histological data: comparative results for paired tissue & urine samples (n=10)

Figure 7: ATR-FTIR spectral classification of active disease vs. disease remission for plasma samples - (A) Raw spectral data (B) Pre-processed spectra (C) PCA scores plot (D) PLS-DA discriminant function graph (E) ROC curve for PLS-DA (F) PLS-DA coefficients for identification of spectral biomarkers

Figure 8: ATR-FTIR spectral classification of active disease vs. paired remission for plasma samples following successful remission induction therapy - (A) Raw spectral data (B) Pre-processed spectra (C) PCA scores plot (D) PLS-DA discriminant function graph (E) ROC curve for PLS-DA (F) PLS-DA coefficients for identification of spectral biomarkers

Figure 9: ATR-FTIR spectral classification of healthy controls (HC) vs. active disease (AD) & healthy controls (HC) vs. disease remission (DR) for plasma samples – (A) Average pre-processed spectral points for HC (n=100) & patients with AD (n=250) (B) PCA scores plot for HC & AD (C) PLS-DA discriminant function graph for classification of HC & AD using cross validation (D) Average pre-processed spectral points for HC (n=100) & DR (n=380) (E) PCA scores plot for HC & DR (F) PLS-DA discriminant function graph for classification of HC & DR using cross validation

Figure 10: Main band differences for healthy controls (HC) vs. active disease (AD) using PCA loadings on PC2 from plasma samples - 1612 cm^{-1} (higher in AD, adenine vibration in DNA), 1540 cm^{-1} (higher in HC, protein Amide II β -sheet), 1040 cm^{-1} (higher in AD, symmetric PO₂- stretching in RNA/DNA)

Figure 11: Raman spectral data for classification of active disease vs. disease remission for plasma samples - (A) Raw spectral data (B) Average pre-processed spectra (C) PCA scores plot (D) PLS-DA discriminant function graph (E) ROC curve for PLS-DA (F) PLS-DA coefficients for identification of spectral biomarkers

Figure 12: Raman spectral data for classification of active disease vs. disease remission for serum samples - (A) Raw spectral data (B) Average pre-processed spectra (C) PCA scores plot (D) PLS-DA discriminant function graph (E) ROC curve for PLS-DA (F) PLS-DA coefficients for identification of spectral biomarkers

Figure 13: Raman spectral data for classification of active disease vs. paired remission for plasma samples following successful remission induction therapy - (A) Raw spectral data (B) Pre-processed spectra (C) PCA scores plot (D) PLS-DA discriminant function graph (E) ROC curve for PLS-DA (F) PLS-DA coefficients for identification of spectral biomarkers

Figure 14: Raman spectral data for classification of active disease vs. paired remission for serum samples following successful remission induction therapy - (A) Raw spectral data (B) Pre-processed spectra (C) PCA scores plot (D) PLS-DA discriminant function graph (E) ROC curve for PLS-DA (F) PLS-DA coefficients for identification of spectral biomarkers

Figure 15: Main band differences for active disease (AD) vs. disease remission (DR) using PCA loadings on PC1 from plasma samples – 1015 cm^{-1} (higher in AD, carbohydrates peak for solids), 1446 cm^{-1} (higher in DR, CH₂ bending mode for proteins and lipids, CH₂ deformation), 1678 cm^{-1} (higher in AD, bound and free NADH)

Figure 16: Main band differences for active disease (AD) vs. disease remission (DR) using PCA loadings on PC1 from serum samples – 1311 cm^{-1} (higher in DR, CH_3/CH_2 twisting or bending mode of lipid/collagen), 1441 cm^{-1} (higher in DR, CH_2 scissoring and CH_3 bending in lipids), 1524 cm^{-1} (higher in DR, carotenoid), 1659 cm^{-1} (higher in AD, amide I vibration collagen like proteins, amide C=O stretching absorption for the α -folded polypeptide films)

Figure 17: Raman spectral data - (A) Total raw spectra for all tissue samples (n=81) (B) Total pre-processed spectra for all tissue samples (n=81) (C) Average pre-processed spectra for all tissue samples (n=27) (D) Total raw spectra for paired urine samples (n=100) (E) pre-processed spectra for paired urine samples (n=100) (F) Average pre-processed spectra paired urine tissue samples (n=10)

Figure 18: PLS-DA discriminant function graphs for the classification of histological data using spectral data from all tissue samples with corresponding receiver operating characteristic curve data as follows: focal vs. mixed disease AUC 0.85, normal glomeruli AUC 0.96, interstitial fibrosis and tubular atrophy (IFTA) severity AUC 0.98, necrotising glomerular (GN) lesions AUC 1, interstitial infiltrate AUC 0.97, extraglomerular arteritis AUC 0.89 & vessel wall necrosis AUC 0.92

Figure 19: Mean Raman spectral data for each histological group – (A) focal vs. mixed disease, (B) proportional of normal glomeruli, (C) severity of interstitial fibrosis and tubular atrophy (IFTA), (D) presence of necrotising glomerular (GN) lesions, (E) presence of interstitial infiltrate, (F) presence of extra-glomerular arteritis, (G) presence of vessel wall necrosis

Figure 20: PLS-DA coefficients for identification of spectral biomarkers in tissue and corresponding paired urine samples (n=10) – (A) Wavenumber variables associated with interstitial fibrosis & tubular atrophy (IFTA) in tissue samples – 891.92 cm^{-1} (saccharide band) (B) Wavenumber variables associated with necrotising glomerular (GN) lesions in tissue samples - 1680 cm^{-1} (C=O, stretching vibrations of cortisone), 1443 cm^{-1} (CH_2 bending mode of proteins & lipids CH_2 deformation), 1539 cm^{-1} (amide carbonyl group vibrations & aromatic hydrogens) (C) Wavenumber variables associated with interstitial infiltrate in tissue samples – 1309 cm^{-1} (CH_3/CH_2 twisting or bending mode of lipid & collagen), 1631 cm^{-1} (amide I), 1692 cm^{-1} (amide) (D) Wavenumber variables associated with interstitial fibrosis & tubular atrophy (IFTA) in paired urine samples - 1247 cm^{-1} (amide III collagen assignment), 1175 cm^{-1} (cytosine, guanine), 932 cm^{-1} (proline, hydroxyproline), 1607 cm^{-1} (C=C phenylalanine, tyrosine) (E) Wavenumber variables associated with necrotising glomerular (GN) lesions in paired urine samples - 1716 cm^{-1} (C=O of cortisone), 1316 cm^{-1} (guanine), 800 cm^{-1} (phosphate ion interactions) (F) Wavenumber variables associated with interstitial infiltrate in paired urine samples – 1458 cm^{-1} (nucleic acid), 911 cm^{-1} (glucose)

Figure 21: PLS-DA coefficients for identification of spectral biomarkers from tissue samples (n=27) – (A) Wavenumber variables associated with necrotising glomerular (GN) lesions: 1726 cm^{-1} (C=O stretching vibrations of cortisone), 1031 cm^{-1} (C-H in-plane bending mode of phenylalanine), 833 cm^{-1} (asymmetric O-P-O stretching of tyrosine), 1787 cm^{-1} (C=O stretching vibrations of cortisone) (B) Wavenumber variables associated with interstitial fibrosis & tubular atrophy (IFTA): 893 cm^{-1} (phosphodiester deoxyribose) (C) Wavenumber variables associated with interstitial infiltrate: 1533 cm^{-1} (amide carbonyl group vibrations and aromatic hydrogens), 1787 cm^{-1} (C=O stretching vibrations of cortisone), 978 cm^{-1} (C-C stretching in β -sheet proteins), 1459 cm^{-1} (deoxyribose)

Chapter 4

Figure 22: Power test based on a Fisher's exact test (two-tails, error probability = 0.05) showing the power varying the total sample size of active and remission cases

Chapter 5

Figure 23: Schematic of thesis structure

List of Abbreviations

AD	Active disease
AAGN	Anti-neutrophil cytoplasmic autoantibody associated glomerulonephritis
AAV	Anti-neutrophil cytoplasmic autoantibody associated vasculitis
AECA	Anti-endothelial cell antibody
AKI	Acute kidney injury
ANCA	Anti-neutrophil cytoplasmic autoantibodies
ATR-FTIR	Attenuated total reflection Fourier-transform infrared
AUC	Area under the curve
AWLS	Automatic weighted least squares
BAFF	B-cell activating factor
BLyS	B lymphocyte stimulator
Bregs	Regulatory B-cells
BVAS	Birmingham Vasculitis Activity Score 3
C5L2	C5a-like receptor
CFH	Complement factor H
CHCC	Chapel Hill Consensus conference
cPR3	Complementary PR3
CRP	C-reactive protein
CT	Computerised tomography
CV	Cross validation
CXCL13	Chemoattractant chemokine ligand 13
DAH	Diffuse alveolar haemorrhage
DCVAS	Diagnostic and Classification Criteria in Vasculitis
DNMT-1	DNA methyltransferase 1
DR	Disease remission
EDTA	Ethylenediaminetetraacetic acid
eGFR	Estimated glomerular filtration rate
EGPA	Eosinophilic granulomatosis with polyangitis
ELISA	Enzyme linked immunosorbent assay
ESR	Erythrocyte sedimentary rate
ESRD	End stage renal disease
EUVAS	European Vasculitis Society
FDG PET CT	Fluorodeoxyglucose positron emission tomography CT (FDG PET-CT)
FoxP3	Forkhead box P3
GA-LDA	Genetic algorithm linear discriminant analysis
GPA	Granulomatosis with polyangitis
HC	Healthy control
HR	Hazard ratio
IFTA	Interstitial fibrosis and tubular atrophy
IgA	Immunoglobulin A
IgG	Immunoglobulin G
IL	Interleukin
ILD	Interstitial lung disease
IR	Infrared
IVIG	Intravenous immunoglobulin therapy
JMJD3	Jumonji C domain-containing protein 3
LAMP-2	Lysosomal membrane protein 2
LDA	Linear discriminant analysis
LV	Latent variables
MCD	Minimal change disease
MLM	Morais-Lima-Martin
MM	Membranous nephropathy
MMF	Mycophenolate mofetil

MMP-3	Matrix metalloproteinase 3
MPA	Microscopic polyangitis
MPA	Mycophenolic acid
MPO	Myeloperoxidase
mPR3	Membrane PR3
MRI	Magnetic resonance imaging
mRNA	Messenger RNA
NADH	Nicotinamide adenine dinucleotide
NAG	N-acetyl glycoprotein
NETS	Neutrophil extracellular traps
NGAL	Neutrophil gelatinase-associated lipocalin
NMR	Nuclear magnetic resonance
OR	Odds ratio
PCA	Principal component analysis
PLEX	Plasma exchange
PLS	Partial least square
PLS-DA	Partial least squares discriminant analysis
PR3	Proteinase-3
R ²	Determination coefficient
RCT	Randomised control trial
ROC	Receiver operating characteristic
RPGN	Rapidly progressive glomerulonephritis
RUNX3	Runt-related transcription factor
<i>S. aureus</i>	<i>Staphylococcus aureus</i>
sCD163	Soluble CD163
SLE	Systemic lupus erythematosus
SVM	Support vector machines
SVV	Small vessel vasculitis
RMSECV	Root mean square error of cross-validation
Timp-1	Metalloproteinase inhibitor 1
tPA	Tissue plasminogen activator
TNF α	Tumour necrosis factor alpha
Tregs	Regulatory T-cells
uMCP-1	Urinary monocyte chemoattractant protein-1
uPCR	Urine protein creatinine ratio

Declaration

I declare that while registered as a candidate for the research degree, I have not been a registered candidate or enrolled student for another award of the University or other academic or professional institution.

I declare that no material contained in the thesis has been used in any other submission for an academic award and is solely my own work.

Acknowledgements

Above all I would like to thank my supervisor Dr Dhaygude for his support, guidance, teaching and friendship. Not only during this stage of research, but throughout my training. Dr Dhaygude is an outstanding clinician and mentor. It has always been and continues to be a privilege and joy to be able to learn from him. The same is true of the wider consultant renal team at Royal Preston Hospital. Aside from a keen interest in vasculitis, the opportunity to continue working with and learning from them was a key factor when choosing to undertake this fellowship. I am incredibly grateful for their support throughout this research project and teaching over the years. I also wish to thank Professor Rowbottom who I have been fortunate enough to receive academic supervision from, who alongside Professor Martin had the foresight for the potential novel application of biospectroscopy in the field of vasculitis.

Crucial recognition must go to Professor Martin. His experience in the field of biospectroscopy and academia is second to none. I have been exceptionally fortunate to have had him as a supervisor, with his continued support and guidance following his departure from UCLan. Professor Martin is the main reason we initially chose to register at UCLan and I have no doubt that this project would not have been a success without his knowledge, ingenuity and experience.

In addition, I would like to thank the following individuals:

Dr Morais, Professor Lima and Daniel Freitas for their collaboration in Chemometric analysis, without who this project could not have been undertaken. Thank you for all of your hard work, time and patience. It has been a pleasure working with and learning from you.

Dr Katherine Asthon for your guidance in sample processing, as well as your assistance with sample storage and preparation of archived tissue samples.

Mr Panagiotis Giamougiannis - Panos and I shared the same turbulent course in completing our respective research projects. Your initial teaching in sample analysis, support and friendship throughout the process was invaluable. Thank you.

Dr Andrew Nixon – Andy was the first clinical research fellow at Preston and I have been fortunate enough to be the second. His guidance on how to effectively run a research project, example and friendship were a source of comfort through many a long day and I hope to share his company for many years to come.

Finally I would like to thank all of the patients and healthy control who participated in this study. None of this would have possible without you and I am grateful for your time and support.

Dedication

To my wonderful wife Laura – I have thought about how to write this dedication numerous times and only hope it does you justice. All too often words do not seem enough. I love you immensely and am so lucky to have you by my side. Throughout our many years together the love and support you have shown me is immeasurable and anything I have been able to achieve is testament to this. I am a better person because of you. Both you and our son Jake bring me pure joy and the smile to my face. I dedicate this thesis to you.

Chapter 1: Introduction

1.1 Background & study objectives

Pauci-immune small vessel vasculitis (SVV) characterises a necrotising group of vasculitides with potential multi-organ and life threatening disease that is typified by the scarcity of immune complex deposits in vessel walls on histology. Current established immunosuppressive therapies are effective with markedly improved patient and renal survival, but their use requires careful consideration when balanced against the potential risks of therapy, with high rates of morbidity and the majority of deaths in the first year resulting from adverse effects of treatment (1). Current markers of disease activity are imperfect, presenting a significant challenge to treating clinicians when gauging the presence of relapsing or persistent disease. This risks either under treated disease or over-exposure to therapy and patient harm. As such, there is a clinical need for the development of a functional biomarker that accurately correlates with disease activity, enabling risk stratification and individualisation of treatment. This thesis aims to review current markers of disease activity and investigate the role of biospectroscopy as one potential innovative candidate. In the introduction that follows, an overview of disease will be provided followed by the study of biospectroscopy in the clinical setting.

1.2 Pathogenesis

1.2.1 ANCA: origins & immunopathogenesis

Central to the known pathogenesis of pauci-immune small vessel vasculitis is the activation of primed neutrophils through the interaction of circulating anti-neutrophil cytoplasmic autoantibodies (ANCA) with myeloperoxidase (MPO) and proteinase-3 (PR3) target autoantigens expressed on their cell surface (2–5). As a result, the term ANCA-associated vasculitis (AAV) is commonly used to describe disease.

The association of pauci-immune small vessel vasculitis with ANCA on indirect immunofluorescence was first described and corroborated in the early 1980s, following an Australian case series of eight patients presenting with constitutional symptoms and focal segmental necrotising glomerulonephritis on renal biopsy (6,7). Even at this time, persistent ANCA positivity at follow up despite quiescent disease was noted (6). The role of ANCA in the pathogenesis of disease has since been supported by both experimental and clinical studies. In 1988 Falk *et al* identified two auto-antibodies on enzyme linked immunosorbent assay (ELISA) that were specific to two neutrophil granule proteins with a distinct staining pattern for ANCA on indirect immunofluorescence of ethanol-fixed neutrophils; MPO with a perinuclear (p-ANCA) staining pattern and a second unidentified target with cytoplasmic (c-ANCA) immunostaining (8). The latter was later confirmed as PR3 (9). MPO is an enzyme that is normally involved in neutrophil microbicidal activity and PR3 is a serine protease involved in the generation of antimicrobial peptides. Following neutrophil priming with increased cell surface expression of MPO and PR3 mediated by cytokines such as tumour necrosis factor alpha (TNF α), ANCA binds to these auto-antigens to induce an oxidative respiratory burst and neutrophil degranulation (2,3). The ensuing release of toxic free oxygen radicals and enzyme granules results in endothelial cell damage and vascular inflammation (10,11). Both the role of TNF α

in neutrophil priming and the pathogenic role of ANCA has since been confirmed in animal studies (4,5,12,13). The former was demonstrated through disease augmentation with TNF α blockade. However, despite this potential therapeutic target, it did not translate into clinical practice with efficacy from trial evidence lacking (14). Human modelling in the form of a case report of neonatal disease following transplacental passage of ANCA supports its association with disease (15).

1.2.2 Disease propagation: NETS & the complement system

Unique to neutrophil cell death is the release of chromatin and granule proteins, including MPO and PR3, that combine to form extracellular fibres in order to trap and kill bacteria (16). Recently intra-granular MPO has been shown to be crucial to this process (17,18). The formation of these neutrophil extracellular traps (NETS) are able to trigger and propagate the process of endothelial injury in AAV by providing a platform for increased autoantigen availability, as well as activation of autoreactive B-cells and the complement cascade (19,20).

Activation of the alternative complement pathway plays a key role in the propagation of disease. The complement cascade is outlined in Figure 1. The first report of complement mediated AAV came in 2007 in an animal study of C5 and factor-B deficient mice who failed to develop disease following exposure to anti-MPO immunoglobulin G (IgG) (21). This was supported by a subsequent study that effectively utilised C5-inhibition to prevent disease (22). The downstream production of C5a is fundamental to the immunopathogenesis of the complement system in AAV. NETS are able to activate the alternative complement cascade and the resulting production of C5a is a chemoattractant, recruiting neutrophils to the site of inflammation amongst other cell types via C5a receptors expressed on their cell surface (23). The binding of C5a also facilitates neutrophil priming with translocation of the MPO and PR3 from the cytoplasm to the cell membrane surface through activation of p38 mitogen-activated protein kinase, extracellular signal-regulated kinase and phosphoinositol 3-kinase (24–27). The fallout of this is an amplification loop of disease with increased autoantigen expression and binding of ANCA. This is depicted in Figure 2. Deposition and co-localisation of Bb and C3d in line with areas and the degree of crescentic glomerulonephritis further supports the role of the alternative complement pathway in disease (28–31).

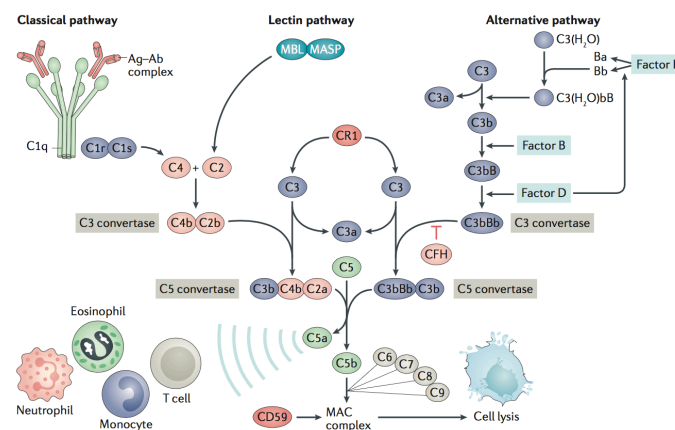


Figure 1- Pathway of complement activation (taken from Chen M, Jayne DRW, Zhao MH. Complement in ANCA-associated vasculitis: Mechanisms and implications for management. *Nat Rev Nephrol.* 2017;13(6):359–67)

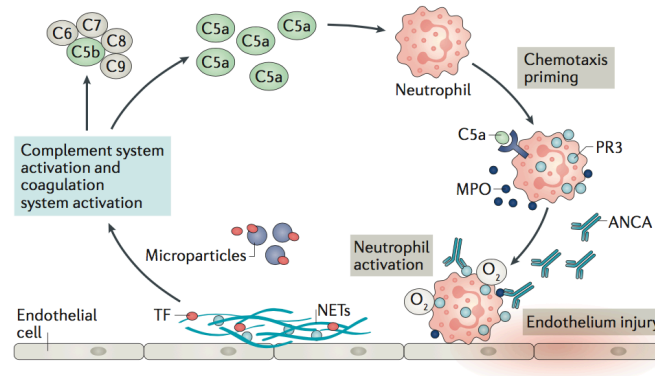


Figure 2 - Proposed model for the interaction of anti-neutrophil cytoplasmic antibody (ANCA), neutrophils and complement activation in the pathogenesis of ANCA-associated vasculitis (taken from Chen M, Jayne DRW, Zhao MH. Complement in ANCA-associated vasculitis: Mechanisms and implications for management. *Nat Rev Nephrol.* 2017;13(6):359–67)

Cross-talk also exists between the coagulation and complement systems. Neutrophil tissue factor found in NETS activate the coagulation system (32). In turn, coagulation proteases, such as plasmin, are capable of acting as C5 convertase (33). The direct cleavage of C5 and increased production of C5a that ensues further amplifies the inflammatory process with increased neutrophil recruitment, priming and tissue factor expression (33,34). A similar process of disease propagation is observed through platelet activation, with increased expression of C3a and C5a receptors in their activated state and thrombocytosis that is often seen in active disease (35–37). With these factors in mind, the hypercoagulable state and high rate of venous thromboembolism observed in patients with active disease is unsurprising (38–42).

1.2.3 B-cell T-Cell cross-talk

B-cells play a pivotal role in disease, not only through the production of resulting plasma cell derived auto-antibodies, but also through T-cell activation and downregulation of regulatory T-cells (Tregs) (43,44). This is mediated by their antigen presenting function and release of cytokines, such as interleukin (IL) 23, IL6 and TNF. The resulting B-cell T-cell cross-talk has implications for immune dysregulation in AAV, with deleterious outcomes through the loss of immune tolerance and emergence of a pathogenic ANCA response.

IL6 and TNF reduce the activity of Tregs. Tregs play a key role in downregulating the immune response to autoantigens in order to maintain self-tolerance and prevent autoimmune disease. They are characterised by the expression of CD4 T-cell co-receptors and CD25, with their development and function determined by the expression of the forkhead box P3 (FoxP3) nuclear transcription factor (45). A functional deficiency of Tregs has been identified in patients with AAV, with an associated higher rate of relapse and longer time to disease remission (45,46). Similarly, an expanded subpopulation of Tregs with reduced functional activity and a persistent increase in the number of effector memory T-cells has been demonstrated in disease remission, suggestive of a persistent immune response during quiescent disease and increased risk of relapse (47,48).

IL-23 activates Th17 cells, a CD4 T-cell subset that plays a key role in cell mediated immunity against extra-cellular pathogens through the production of IL-17. This also has implications for autoimmune disease with increased

neutrophil recruitment and upregulation other pro-inflammatory cytokines such as IL6, IL8 and TNF α (49,50). As previously outlined, upregulation of the latter has implications for increased neutrophil priming. The increased expression of IL-17 has been demonstrated in active AAV, as well as a TH17 memory cell population that persists in disease remission (51,52). The Th17 immune response is also capable of increasing the expression of the chemokine receptor CXCL5 within renal tubules, driving further neutrophil recruitment to the site of injury (53).

In parallel, CD4 cells release a range of cytokines to activate B-cells and cytotoxic CD8 cells. These CD8 cells facilitate disease through direct cell cytotoxicity and neutrophil activation through the release of interferon gamma and TNF α (54).

B-cell activating factor (BAFF), also known as B lymphocyte stimulator (BLyS), is a cytokine derived from the TNF ligand superfamily. It is important for B-cell survival and maturation through the inhibition of apoptosis and stimulation of B-cell proliferation. Significantly elevated levels are present in active AAV and the excessive expression of BAFF by activated neutrophils may facilitate autoimmune B-cell tolerance (55–58).

1.2.4 ANCA negative disease

Despite the compelling evidence base for the pathogenicity of ANCA, a subgroup of patients will develop de novo and relapsing disease in the absence of detectable circulating antibody. Indeed, the limited efficacy of plasma exchange as an adjuvant therapy for remission induction raises questions about its role in disease (59). This prompts reconsideration of the current putative pathogenesis and assays. One possibility is the presence of a novel autoantibody which is discussed in section 1.2.5. A second consideration is that anti-PR3 and anti-MPO antibodies may be present, but either remain below the detection limit of current enzyme immunoassays or that epitope masking may confound their detection (60,61). In 2013 Roth *et al* undertook a study in linear ANCA epitope mapping and disease correlation. In doing so they identified a pathogenic anti-MPO autoantibody to a new immunodominant sole linear sequence epitope in seronegative disease, the detection of which is obscured by a fragment of ceruloplasmin in serum on conventional tests (61). It is also possible that disease is mediated by immunoglobulin A (IgA) ANCA (62). Current mainstream ELISAs for ANCA detect IgG. Kelley *et al* identified the presence of IgA ANCA in a significant proportion of patients who otherwise tested negative for IgG ANCA and demonstrated the ability of IgA ANCA to mediate disease through neutrophil stimulation (62). Lastly, the pathogenic role of B-cells in ANCA negative disease may also occur independently of autoantibody production, owing to their ability to mediate Th17 cell activity and downregulate Tregs.

1.2.5 Novel autoantibodies

1.2.5.1 Anti-LAMP2 autoantibodies

Lysosomal membrane protein 2 (LAMP-2) is a heavily glycosylated membrane protein that when bound, translocates to the lysosome where it plays a key role in protein degradation and autophagy. It is co-expressed on neutrophils with PR3 and MPO, and was first identified in 1995 as a potential target antigen for ANCA in a handful of patients with pauci-immune glomerulonephritis (63). The role of anti-LAMP2 antibodies as a subtype

of ANCA and their ability to instigate disease was subsequently demonstrated in vitro and a rodent model of disease (64). This also identified a 100% homology and cross-reactivity of LAMP2 to FimH, an adhesin protein expressed on the surface of fimbriated gram-negative bacteria. Consequently, anti-LAMP2 auto-antibodies can arise as a result of molecular mimicry following infection with such organisms (64). Initial follow up studies suggested a high degree of correlation with disease activity and a potential pathogenic role in ANCA negative disease (65,66). However, these findings were not corroborated in a much larger study of 680 participants; 329 with ANCA-associated glomerulonephritis, 104 with ANCA-negative glomerulonephritis, 104 with an E.coli urinary tract infection (UTI), 124 healthy controls and 19 disease controls (67). In this study LAMP2 reactivity was present in 16% of the UTI cohort and only 21% of ANCA sera. The latter was present in very low titres and bore no correlation with disease activity. The same study also attempted to replicate the rodent model of disease with no evidence of ensuing glomerulonephritis. This confirmed that LAMP-2 is not prevalent in patients with AAV and does not play a role in disease pathogenesis.

1.2.5.2 Anti-plasminogen autoantibodies

A deficiency in plasminogen and tissue plasminogen activator (tPA) is associated with more severe glomerular injury and renal impairment in crescentic disease (68). Autoantibodies have been described to plasminogen and tPA in the sera of patients with anti-PR3 and anti-MPO positivity (69,70). The presence of anti-plasminogen antibodies correlated with the severity of renal vasculitis, with seropositive patients having a significantly higher percentage of glomeruli with fibrinoid necrosis, cellular crescents and more severe renal impairment than patients without these antibodies (69,70). Antibody formation is thought to arise from antigen mimicry with complementary PR3 (cPR3); a recombinant protein translated from the antisense strand of PR3 cDNA, with higher circulating levels of anti-plasminogen antibodies in patients with PR3-associated AAV (71). Its presence is associated with an increased venous thromboembolic risk and recent optimisation of the ELISA will aid future research of their relevance in AAV (72,73).

1.2.5.3 Anti-Moesin autoantibodies

Moesin is a heparin binding protein found on the surface of endothelial cells and neutrophils, which exhibits an epitope that cross reacts with anti-MPO autoantibody (74). A murine model of disease suggested its role in the development of glomerulonephritis as an alternative autoantigen target of MPO (74). Anti-moesin autoantibody has since been detected in the serum of patients with MPO-associated AAV alongside upregulation of inflammatory cytokines (75). The significance of this requires further study.

1.2.5.4 Anti-endothelial cell auto-antibodies

Anti-endothelial cell antibody (AECA) represent a diverse group of antibodies capable of binding endothelial cell antigens. Following in vitro depletion of PR3-ANCA, AECA was derived from patients with AAV, with the ability to cause disease when administered to a murine model (76). AECA was then evaluated in a small study of patients with ANCA positive and negative disease and was present in nearly all seropositive patients and a small subgroup

of the ANCA negative cohort (77). The authors postulated that this may represent a different pathogenic mechanism in ANCA negative pauci-immune glomerulonephritis, but its relevance remains unclear.

1.3 A predisposition to disease

1.3.1 “Two hit hypothesis”

The identification of antibody mediated disease has led to the “two-hit hypothesis”, whereby more than one event is required for activation of neutrophils by ANCA. If autoantibody formation is the first hit, then a second hit is required for autoantigen availability through neutrophil priming. It is hypothesised that the initial immunologic event in the induction of the ANCA is an immune response to an epitope bearing a structural similarity to the MPO or PR3 autoantigen. This immunogen could be endogenous or exogenous, with loss of self-tolerance and persistent autoantibody production through immune dysregulation. A combination of aberrant autoantigen gene expression as well as a pro-inflammatory event causing the release of cytokines, such as TNF α , provides the second hit. The resulting translocation of MPO and PR3 from the cytoplasm to the neutrophil cell surface facilitates binding of ANCA and the immunopathogenesis that follows.

1.3.2 Epigenetics

Epigenetics refers to an alteration in gene expression without any change to the underlying DNA sequence. This provides a basis for dysregulated autoantigen expression in AAV. Schreiber *et al* was the first study to identify a genetic variance in autoantigen membrane expression as a risk factor for disease (78). Increased degranulation and superoxide generation occurs amongst neutrophil subsets with high membrane PR3 (mPR3) expression (79). By separating cells into subsets of high a low mPR3 expression, they confirmed a significantly higher mPR3+ neutrophil population in patients with active AAV, as well as a strong correlation with monozygotic twins. Both were independent of the intracellular content of PR3 and the latter suggested a genetic influence on mPR3 expression (78). Verifying this, Yang *et al* confirmed upregulation of neutrophil granule gene transcription for MPO and PR3 which corresponded with increased disease activity (80). This transcriptional change was independent of autoantibody presence and serum cytokines.

Ciavatta *et al* explored the epigenetic changes that occur in AAV further (81). There are three primary mechanisms of epigenetic modification; histone modification, DNA methylation and RNA interference (82). Histones are nuclear based proteins that help condense DNA into chromatin and increased association with histones will reduce gene transcription. The process of methylation refers to the addition of a methyl-group to cytosine nucleotides within the DNA strand. The effect of this is reduced gene expression, either through the inhibition of transcriptional binding protein or by facilitating the formation of compact inactive chromatin. Ciavatta *et al* identified depleted levels of the histone H3K27me3 at the MPO and PRTN3 gene loci in AAV patients. Alongside this, demethylase jumoji C domain-containing protein 3 (JMJD3) which acts to demethylate H3K27me3 and contribute to depleted levels was preferentially expressed in AAV patients (81). They also identified reduced levels of runt-related transcription factor (RUNX3) through increased methylation, a protein which acts to suppress MPO

and PR3 expression by directly binding to the gene loci to cause transcriptional repression and through recruitment of H3K27me3 (81). These findings confirmed the epigenetic modifications associated with reduced gene silencing of PR3 and MPO, resulting in aberrant autoantigen expression with increased levels of PR3 and MPO messenger RNA (mRNA).

Jones et al corroborated these findings, showing hypomethylation of the MPO and PR3 genes with increased autoantigen expression in active disease and increased DNA methylation in remission (83). This had implications for relapse risk with increased methylation of the PR3 promoter region being associated with a significantly higher chance of a relapse free survival period. Conversely, patients exhibiting hypomethylation of PR3 had a much higher risk of relapse (hazard ratio, 4.55; 95% confidence interval, 2.09 to 9.91) (83). Despite evidence of these epigenetic factors, the reasons for why this occurs remains unclear.

A landmark study in 2012 undertaking a genome wide association study in AAV found that MPO and PR3 associated AAV were genetically distinct (84). This distinction according to ANCA specificity was more important than the clinical phenotype of disease. Anti-PR3 ANCA was associated with HLA-DP, as well as SERPINA1 which encodes α -1 antitrypsin and PRTN3 which encodes PR3. Anti-MPO ANCA was associated with HLA-DQ.

1.3.3 Environmental factors

Various environmental factors have been investigated as potential triggers for disease. Amongst them, farming has been correlated with a high degree of risk. Lane *et al* was the first study to identify this with an exposure to farming within 12 months prior to symptom onset or at any time during working life representing an odds ratio for disease of 2.3 (95% CI 1.2-4.6) and 2.2 (95% CI 1.2-3.8) respectively (85). This was restricted to patients with granulomatosis with polyangiitis (GPA), a clinical disease phenotype that is closely associated with anti-PR3, and was stronger for those working with livestock compared to crops (85). These observations have since been supported by more recent studies (86,87). These studies also offer some potential insight into the potential reasons for this, suggesting an association with inhaled antigens such as dust grains, chemical sprays and silica grains as potential risk factors (87). Indeed, exposure to silica from specific farming tasks related to harvesting can occur and silica has been strongly established as trigger for disease (88).

Initial studies assessing the risk of cigarette smoking and AAV suggested that smoking may be protective and that upper respiratory tract disease secondary to AAV may be less common amongst smokers (89,90). However, larger studies have since identified a positive correlation with disease and a positive association with anti-MPO AAV is suggested with a dose response relationship according to pack year history (90–93).

The presence of seasonal variation in the caseload AAV remains uncertain with conflicting reports. Based on retrospective observational data, some studies suggest no association, while others report a higher frequency of new cases in summer months and winter months alike with postulation as to the potential reasons (94–96).

1.3.4 Silica

Silica exposure is known to increase the risk of developing various autoimmune disorders. Its strong association as an independent risk factor for AAV has been investigated and corroborated by several case-controls studies (88,97–99). A subsequent met-analysis found that any history of previous silica exposure resulted in a significantly higher likelihood for developing disease (OR 2.56 95% CI 1.51-4.36) (100). This remained unchanged when evaluated according to the clinical disease phenotype. The exact mechanism of silica induced disease is not well understood, but several theories have been proposed, including the role of silica in lymphocyte stimulation and the release of lysosome enzymes such as PR3 and MPO (101).

1.3.5 Drug induced disease

Various culprit agents of drug induced AAV have been identified, including prophythouracil, hydralazine, minocycline, allopurinol, penicillamine and levamisole-contaminated cocaine (102,103). Time between drug exposure and symptom onset can be quite variable and disease typically resolves following drug cessation (102,104). Some cases will require immunosuppressive therapy depending on the severity of presentation. Casting doubt on this as a coincidental association is a prospective study by Hyon *et al* which evaluated ANCA seroconversion amongst rheumatology patients in three separate randomised controls trials for minocycline, sulfasalazine and penicillamine. Their results found no induction of ANCA seroconversion following drug exposure(105). Nevertheless, cases of prophythouracil and levamisole-contaminated cocaine are widely reported in the literature.

The association of prophythouracil with the formation of ANCA and disease has been shown in several case series (104,106,107). Patients typically displayed anti-MPO positivity or dual positivity with a predominant anti-MPO titre (104,107,108). In vitro studies have eluded to the mechanism of disease, suggesting that prophythouracil accumulates in neutrophils and binds to MPO to induce a structural change which may prompt ANCA formation (109). Others have also identified abnormal conformation and impaired degradation of NETs secondary to prophythouracil, with subsequent MPO-ANCA associated AAV in a rodent model (110). Levamisole can often be found as a contaminant in cocaine with a strong association with disease. Patients with levamisole exposure can display a varied immune response ranging from an anti-PR3 predominance to dual positivity, a discordance between immunofluorescence and ELISA as well as a range of antibody positivity (103,111–113).

1.3.6 Infection

Micro-organisms exhibiting molecular mimicry for the MPO or PR3 autoantigens are capable of triggering disease. The most commonly implicated micro-organism is *Staphylococcus aureus* (*S. aureus*), with several studies finding that chronic nasal carriage is associated with a higher relapse rate in patients with GPA; a clinical disease phenotype which often displays destructive sinonasal lesions as a prominent feature (114–116). The mechanism of *S. aureus* induced immunopathogenesis is suggested by the presence of a peptide bearing close homology to the amino acid sequence of a restricted epitope in the middle and terminal c portion of cPR3, with cross reactivity

to PR3 (117,118). In addition, several genetic loci of *S. aureus* have been associated with AAV and in vitro study has suggested that the cytosine-phosphate-guanine motif in the promoter regions of *S. aureus* DNA may be the trigger for ANCA production (119,120).

Although more commonly associated with anti-PR3 AAV, cases of anti-MPO mediated disease have been reported in *S. aureus* endocarditis (121). Supporting this, the *S. aureus* peptide 5-phosphogluconate dehydrogenase found in bacterial plasmids has recently been shown to be homologous to the immunodominant MPO T-cell epitope, inducing anti-MPO autoreactivity and disease in a mouse model (122).

1.4 Clinical manifestation of disease

AAV can be considered on the basis of its clinical presentation. In 1994, the Chapel Hill Consensus conference (CHCC) developed a nomenclature for the systemic vasculitides according to the distribution of vessel size involved with definitions based on agreed expert opinion (Figure 3) (123). In 2012 this was revised to reflect recent advances in the field of vasculitis. AAV was defined as a necrotising group of vasculitis with few or no immune deposits on tissue histology, with a predominance for small blood vessel and a general association with detectable circulating ANCA (124). Four main clinical presentations are grouped under this term; GPA, eosinophilic granulomatosis with polyangiitis (EGPA), microscopic polyangiitis (MPA) and single-organ AAV such as renal limited disease (124). The definitions for each of these is shown in Table 1. GPA is more commonly associated with PR3-ANCA, with a roughly equal predominance of MPO-ANCA for MPA, EGPA and renal limited disease (125,126). Up to 50% of EGPA cases are ANCA negative (126) and of the small subpopulation with PR3 associated EGPA, patients tend to display a GPA phenotype with cutaneous manifestations and pulmonary nodules as opposed to the higher frequency of asthma and peripheral neuropathy more commonly seen in MPO and ANCA negative disease (127). In 2018 an addendum was made to the 2012 CHCC nomenclature with standardised definitions and descriptors for the cutaneous component of disease (128).

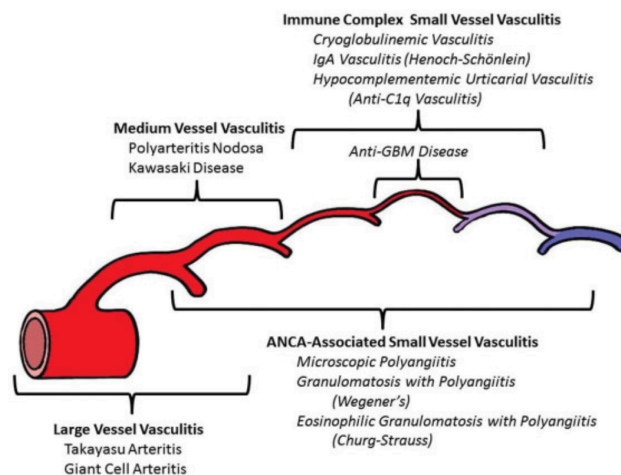


Figure 3 - Distribution of vessel involvement by large vessel vasculitis, medium vessel vasculitis, and small vessel vasculitis (taken from - Jennette JC, Falk RJ, Bacon PA, N. B, Cid MC, Ferrario L., et al. 2012 Revised International Chapel Hill Consensus Conference Nomenclature of Vasculitides. *Arthritis Rheum.* 2012;65(1):1–11)

Currently the Diagnostic and Classification Criteria in Vasculitis (DCVAS) study is underway which seeks to develop a new criterion for systemic vasculitis that can be used in clinical practice and trials. In 2019 the DCVAS group released an abstract proposing a draft revised classification criteria for the three clinical syndromes of AAV; GPA, EGPA and MPA (129). The criteria groups certain clinical findings diagnostic criteria to differentiate these three groups from one another with a high degree of specificity and sensitivity (Table 2). It also recognises the emergence of interstitial lung disease as a feature of MPA, which can occur in the absence of other organ system involvement and carries and two to four-fold increased mortality rate (130).

The clinicopathologic phenotypes of GPA and MPA remain poor predictors of the natural history of disease compared with the predictive capacity of the ANCA, which is arguably a more important distinction to make. This is supported by Lyons *et al* who identified a genetic difference between GPA and MPA, but more importantly demonstrated that associations with the particular genes were more strongly associated with ANCA specificity rather than clinical diagnosis (84).

Table 1 - Definitions for AAV clinical presentations adopted by the international Chapel Hill Consensus Conference 2012

ANCA-associated vasculitis (AAV)	Necrotizing vasculitis, with few or no immune deposits, predominantly affecting small vessels (i.e., capillaries, venules, arterioles, and small arteries), associated with myeloperoxidase (MPO) ANCA or proteinase 3 (PR3) ANCA. Not all patients have ANCA. Add a prefix indicating ANCA reactivity, e.g., MPO-ANCA, PR3-ANCA, ANCA- negative.
Granulomatosis with polyangiitis (Wegener’s) (GPA)	Necrotizing granulomatous inflammation usually involving the upper and lower respiratory tract, and necrotizing vasculitis affecting predominantly small to medium vessels (e.g., capillaries, venules, arterioles, arteries and veins). Necrotizing glomerulonephritis is common.
Eosinophilic granulomatosis with polyangiitis (Churg-Strauss) (EGPA)	Eosinophil-rich and necrotizing granulomatous inflammation often involving the respiratory tract, and necrotizing vasculitis predominantly affecting small to medium vessels, and associated with asthma and eosinophilia. ANCA is more frequent when glomerulonephritis is present.
Microscopic polyangiitis (MPA)	Necrotizing vasculitis, with few or no immune deposits, predominantly affecting small vessels (i.e., capillaries, venules, or arterioles). Necrotizing arteritis involving small and medium arteries may be present. Necrotizing glomerulonephritis is very common. Pulmonary capillaritis often occurs. Granulomatous inflammation is absent.
Single-organ AAV	Vasculitis in arteries or veins of any size in a single organ that has no features that indicate that it is a limited expression of a systemic vasculitis. The involved organ and vessel type should be included in the name (e.g., cutaneous small vessel vasculitis, testicular arteritis, central nervous system vasculitis). Vasculitis distribution may be unifocal or multifocal (diffuse) within an organ.

(taken from - Jennette JC, Falk RJ, Bacon PA, N. B, Cid MC, Ferrario L., et al. 2012 Revised International Chapel Hill Consensus Conference Nomenclature of Vasculitides. *Arthritis Rheum.* 2012;65(1):1–11)

Table 2 - Draft Classification criteria for the ANCA-associated vasculitides

Draft Classification criteria for the ANCA-associated vasculitides					
This criteria set is for use when a diagnosis of small or medium vessel vasculitis has been made					
Granulomatosis with polyangiitis (GPA)		Microscopic polyangiitis with polyangiitis (MPA)		Eosinophilic granulomatosis w	
• Bloody nasal discharge, ulcers, crusting, congestion, or blockage, or septal defect/perforation	+3	• Pauci-immune glomerulonephritis	+3	• Obstructive airways disease	
• Cartilaginous involvement*	+2	• Bloody nasal discharge, ulcers, crusting, congestion, or blockage, or septal defect/perforation	-3	• Nasal polyps	
• Conductive or sensorineural hearing loss	+1	• pANCA or MPO-antibody positive	+6	• Mononeuritis multiplex o	
• Pauci-immune glomerulonephritis	+1	• Fibrosis or ILD on chest imaging	+3	• Eosinophil count $\geq 1 \times 10^9/L$	
• cANCA or PR3-antibody positive	+5	• cANCA or PR3-antibody positive	-1	• Extravascular eosinophil inflammation/eosinophil	
• pANCA or MPO-antibody positive	-1	• Eosinophil count $\geq 1 \times 10^9/L$	-4	• cANCA or PR3-antibody p	
• Eosinophil count ≥ 1	-4			• Microscopic hematuria	
• Granuloma, extravascular granulomatous inflammation, or giant cells on biopsy	+2				
• Nodules, mass, or cavitation on chest imaging	+2				
• Inflammation, consolidation, or effusion of the nasal/ paranasal sinuses on imaging	+1				
Total score ≥ 5 needed for classification of GPA		Total score ≥ 6 needed for classification of MPA		Total score ≥ 5 needed for c	
Sensitivity 93%, Specificity 94%		Sensitivity 87%, Specificity 96%		Sensitivity 88%, Sp	

*Cartilaginous involvement: Any of inflamed ear or nose cartilage, hoarse voice/stridor, endobronchial involvement, or saddle nose

(taken from - Robson J, Grayson P, Ponte C, Suppiah R, Craven A, Khalid S, et al. Classification criteria for the ANCA-associated Vasculitides. Rheumatology. 2019;58(2):109–10)

1.5 Epidemiology

The peak incidence of disease has previously been reported as 65-74 years (131,132), while another study evaluating data from an overlapping timeline in a different geographical population identified the highest incidence in those aged ≥ 75 years (133). Both emphasise the increased incidence of disease with advancing age.

During the initial years following the first described cases by Davies *et al* in 1982, there was limited epidemiological data available with a low incidence rate of disease reported at the time (134–136). Two initial ten-year retrospective studies that followed collated data from the mid 1980s to the mid 1990s amongst UK cohorts, reporting a disease incidence of 4–9.7 per million/year with an annual prevalence of 19.8 per million (131,137). Using UK data from the general practice research database, a subsequent 15-year study from 1990-2005 identified a stable annual disease incidence of 8.1 per million, but an increase in the annual prevalence from 28.8 per million in 1990 to 64.8 million in 2005 (132). Until recently, data from numerous studies in varying regions have demonstrated an annual incident rate of 13-20/million, which has remained largely unchanged over the past 20 years (134). The initial incremental rise in the incident rate likely reflects the introduction of routine ANCA testing and increased physician awareness over a significant rise in the number of true incident cases. Alongside this the prevalence rate has increased, with most recent estimates of 46-184/million, reflecting improved patient survival in line with advancement in treatment strategies (134).

Berti *et al* have since reported a 20 -year population based study from 1996-2015 in an American cohort from Olmsted County Minnesota, with adjustment of the incident rate to the 2010 US white population. Based on 58 incident cases and 44 prevalent cases over the 20-year period, they identified a higher annual incident rate of 33 per million (3.3/100 000) and prevalence of 421 per million/year (42.1/100 000) which remained relatively stable over the study period (138). In keeping with previous studies, gender distribution was similar and nearly all

patients were Caucasian; although the latter may reflect the limited number of reported studies in predominantly non-Caucasian population cohorts and genetic susceptibility (132,134,139). Based on ANCA serotype, incident cases of MPO-ANCA were higher. Subgroup analysis according to clinical phenotype found a similar incident rate for GPA and MPA. In contrast, previously a geographic variation in clinical phenotype has been observed, with MPA being more common in southern Europe and GPA more common in northern Europe (140). However, this observation was not mirrored by other studies in other northern European countries with a comparable incident rate for GPA and MPA found (133). As expected the EGPA was less common.

Berti *et al* have since reported on the epidemiology and ANCA-associated glomerulonephritis (AAGN) in the same population and time period, with an incidence of 2.0/100 000 per year and overall prevalence of 35/100 000 (141). The mortality risk in patients with renal involvement was higher than those with extra-renal disease only, which mirrors findings from previous studies (141,142).

Amongst European and South East Asian cohorts, the presence of seronegative pauci-immune glomerulonephritis has previously been reported in up to 30% of cases (137,143,144). More recent studies report a more conservative rate of 7-12% (145–147). This may reflect improvements in assay sensitivity over the years, but it is also worth noting that these figures are reflective of South East Asian and Mexican cohorts only. In comparison, up to 54% of patients with limited extra-renal disease are ANCA negative and as an overall group, up to 42% of those with a history of ANCA positivity have undetectable circulating ANCA at the time of relapsing disease (148–153).

1.6 Treatment

Current standard remission-induction therapy for organ or life threatening AAV centres around the use of glucocorticoids in conjunction with either cytotoxic therapy using cyclophosphamide or B-cell depleting therapy with agents such as Rituximab. For less severe non-organ threatening disease a limited course of glucocorticoids alongside an anti-metabolite agent such as methotrexate or mycophenolic acid can be used (154). Previous convention continued maintenance therapy for two years, but recent trial evidence supports prolonged maintenance immunosuppression for up to four years, with a higher relapse rate (OR 5.96 95% CI 2.58 – 13.77) and poorer renal survival in patients stopping therapy earlier (155). Prolonged therapy was not associated with a significantly increased adverse event rate, although a comparative analysis of cumulative steroid treatment in each arm was not available; a factor which is known to contribute to long term treatment related morbidity (156,157). The following section will discuss the evidence base guiding current remission-induction and remission-maintenance therapy, as well as certain adjuvant treatment options.

1.6.1 Remission induction therapy

1.6.1.1 Glucocorticoids

Glucocorticoids exert an anti-inflammatory and immunosuppressive action through regulation of gene transcription. The glucocorticoid receptor has been identified as a DNA binding protein which acts to downregulate the expression of pro-inflammatory cytokines such as IL-2, IL-6, IFN- γ and TNF- α , as well as upregulate anti-inflammatory cytokines such as IL-10 (158). The downstream effect of this induces lymphocyte apoptosis and reduced expression of cell adhesion molecules, which alongside reduced vasodilation and vascular permeability will reduce T-cell migration to sites of inflammation (158). The transrepressive effect of glucocorticoids appears to work within eighteen hours of administration, with sustained action up until at least seventy-two hours (159). Currently, glucocorticoids remain a cornerstone of AAV remission-induction therapy while other induction agents take effect.

The use of glucocorticoid therapy in AAV stems from a case series of 10 patients in the late 1970s with idiopathic rapidly progressive glomerulonephritis (RPGN) (160). Patients received 1g of intravenous methylprednisolone/day for seven days, followed by a reducing course of prednisolone starting at 80mg/day. Virtually no justification was provided for the dosing regimen used and at the time the authors acknowledged that the side effect profile of treatment was worse than disease. Nonetheless, at a time when other therapeutic options were limited, this treatment strategy was adopted by two small observational studies that followed, which also drew on data from a case series of lupus nephritis and transplant rejection (161,162). This formed the basis for steroid therapy in AAV and evolved to resemble the dosing protocol adopted for co-administration in subsequent trials of new induction agents and clinical practice; methylprednisolone 1g /day for three consecutive days followed by 60-80mg/day prednisolone with dose taper.

The use of steroid therapy has been associated with significant treatment related morbidity and mortality. Data from randomised control trials (RCT) has found that the mortality rate and incident rate of serious infection is highest within the initial few months of remission induction therapy (163,164). This is thought to reflect the contributing impact of concomitant high dose steroids within the first three months. Follow up data from four landmark trials undertaken by the European Vasculitis Society (EUVAS) sought to determine long term treatment and disease related damage. Of the 467 patients included, 55% had data on glucocorticoid use with a mean duration of 3.3 years. Significant treatment-related damage occurred secondary to steroids which increased over time (156). A further study by the same group specifically looked at glucocorticoid related treatment damage at seven years follow up. Higher levels of damage were independently associated with glucocorticoid use which increased with duration (OR 1.26 per 12 months of use, 95% CI 1.03 – 1.53) (157). This is compounded by relapsing disease and increased cumulative glucocorticoid exposure often required. Attempts have been made to minimise steroid exposure by utilising a combination of cyclophosphamide and rituximab with rapid dose taper of steroids to zero within two weeks (165). Initial reports found comparable outcomes to previous standard therapy, but with reduced rate of glucocorticoid related adverse events. However, the study was small, observational in

nature, lacked long term follow up data and did not include those with a serum creatinine greater than 500 µmol/L, dialysis dependence or diffuse alveolar haemorrhage. Furthermore, the option of dual therapy with rituximab and cyclophosphamide is not widely accessible within our current healthcare system.

Data evaluating outcomes on the use of methylprednisolone is scarce with only two studies to date offering any meaningful insight on this. Chanouzas *et al* recently published a multicentre retrospective observation study determining outcomes according to methylprednisolone use in patients presenting with severe renal impairment. This did not identify any benefit of intravenous methylprednisolone for patient survival, renal survival or 12-month relapse rates, but did confirm a higher rate of treatment related adverse effects (infection: HR 2.7, 95% CI 1.4-5.3) (diabetes: HR 6.33, 95% CI 1.94-20.63) (166). A study by McGregor *et al* identified similar findings in a subgroup analysis of 101 patients who received methylprednisolone and 46 who did not (167).

PEXIVAS is a large multinational landmark RCT that confirmed the dose of oral steroids currently used in standard remission-induction regimes can safely be reduced (59). At three and six months, the cumulative dose of oral steroids was 44% and 60% lower than current standard therapy, respectively. The trial was adequately powered and demonstrated non-inferiority of the reduced dose regime against the primary composite outcome of death from any cause or end-stage kidney disease. This was associated with a reduced rate of severe infections at one year (incident rate ratio 0.69, 95% CI 0.52-0.93). The only other trial evaluating oral glucocorticoid dosing during remission induction therapy for AAV is the recently published LoVAS study (168,169). This compared a reducing regimen of prednisolone starting at 1mg/kg vs. 0.5mg/kg alongside rituximab in a Japanese population with non-severe disease. No difference in the 6 month remission rate was identified, but a higher adverse event rate occurred in the high dose group (168). When considering both the PEXIVAS and LoVAS trials, it is interesting there was a marked difference in their typical cumulative dose of oral glucocorticoids, with 2240mg and 952mg being used respectively. Although, it was noting that the LoVAS study population was much smaller with only 140 patients, was representative of a specific demographic group and had a shorter follow up period compared to PEXIVAS.

A case can therefore be made for the discontinuation of intravenous methylprednisolone from current practice alongside the reduced dosing regimen of prednisolone outlined by PEXIVAS in an attempt to improve patient outcomes. However, the study data evaluating methylprednisolone was based on a high dose oral prednisolone and patients in the PEXIVAS trial still received up to 3g of intravenous methylprednisolone. In view of this and the pharmacogenetics of glucocorticoids, it may be reasonable to continue with a markedly reduced single dose of methylprednisolone, such as 250mg. The duration of steroids will be discussed further down in the section on remission-maintenance therapy, but it is clear that there is further scope for refinement of current therapy. A multi-targeted approach with emerging adjuvant therapies is likely to play a key role in facilitating future steroid avoidance strategies.

1.6.1.2 Cyclophosphamide

Cyclophosphamide is an alkylating agent. Its active metabolite of phosphoramidate mustard adds an alkyl group to guanine base strands, resulting in interstrand and intrastrand crosslinking. The resulting damage to DNA is irreversible, causing apoptosis of dividing lymphocytes. In the late 1970s, Fauci *et al* was one of the first studies to demonstrate a role for cyclophosphamide in systemic vasculitis in a cohort review (170). Several small underpowered RCTs that followed in the late 1990s compared continuous oral therapy against pulsed intravenous dosing, which suggested similar remission rates and patient outcomes amongst the two arms (171–173). However, the higher cumulative dose with continuous oral therapy did confer a better sustained long term remission rates, but was associated with a higher rate of leukopaenia and infections (171,172). More definitive data came from the landmark CYLOPS trial in 2009. This confirmed no difference in the absolute remission rate or time to remission between the two groups. The median cumulative dose of cyclophosphamide was higher in the oral treatment group (15.9g vs. 8.2g; P 0.001), which was associated with a significantly higher rate of leukopaenia (174). Five year follow up data did identify a lower relapse rate with oral therapy (HR 0.50, 95% CI 0.26 to 0.93), but there was no difference in patient or renal survival (175). In view of this and the higher rate of adverse effects with oral therapy, pulsed intravenous cyclophosphamide with dose adjustment for age and renal function has been adopted into mainstream practice.

1.6.1.3 B-cell depleting therapy

Confirmation of the pathogenic role of ANCA and the central role of B-cells in this process provides a strong basis for therapy with B-cell depleting agents such as rituximab. Rituximab is a chimeric anti-CD20 monoclonal antibody that binds to CD20-expressing B-cells to induce complement and antibody mediated cell cytotoxicity. Its use as an effective treatment strategy for remission-induction has been well established. RAVE and RITUXVAS were two randomised control trials that both demonstrated non-inferiority to cyclophosphamide as the previous standard of care, with the former also identifying superiority of rituximab in relapsing disease (176,177). Recent data from the RITZAREM trial supports the effectiveness of Rituximab in relapsing disease, irrespective of whether patients previously had cyclophosphamide (79% cases) or rituximab (36% cases) (178). Sustained remission rates at 12months in both the RAVE and RITUXVAS trials were 76% and 64% respectively with no significant difference in the adverse event rate amongst the various treatment arms (176,177).

All patients included both the RAVE and RITUXVAS trials were ANCA positive at the time of treatment, with limited published data to support the use of rituximab in the absence of detectable circulating ANCA. Smith *et al* reported a single centre experience evaluating fixed interval maintenance dosing of rituximab. Amongst their cohort, 41 patients with relapsing or refractory disease were ANCA negative at the time of rituximab treatment with no difference in remission rates according to ANCA serology (153). Similarly, two other cohort studies have demonstrated the successful use of rituximab in limited extra-renal disease with negative ANCA serology (179,180). The effectiveness of rituximab in the absence of detectable circulating antibody prompts reconsideration of its predominant mode of action in such cases. One possibility is the presence of a novel autoantibody as previously discussed. The second is attenuation of disease beyond that of reduced autoantibody

production. As previously outlined, B-cell T-cell cross talk plays a key role in immune dysregulation and pathogenesis. Rituximab has been shown to induce T-cell depletion through downregulation of B-cell cytokine release and its antigen presenting function, which may be the mechanism through which a beneficial therapeutic effect is seen in the absence of circulating autoantibody in pauci-immune small vessel vasculitis (181).

In cases of disease that remain refractory to anti-CD20 therapy with rituximab, treatment with ofatumumab might be a viable option. The CD20 molecule is a transmembrane protein that exhibits two extracellular loops; one small and one large (182). When bound by anti-CD20 monoclonal antibodies, CD20 fails to internalise and remains expressed on the B cell membrane, facilitating complement-mediated cell cytotoxicity (182). Rituximab binds to an epitope found on the large extracellular loop of CD20 and changes or internalisation of this have been attributed to instances of rituximab-resistant B-cell lymphomas (182,183). Ofatumumab binds to an epitope that encompasses both the small and large loops of CD20, and in such cases has been used with good effect (182,184,185). More recently ofatumumab has been used in a case series of patients with relapsing and new onset pauci-immune small vessel vasculitis with good therapeutic response, warranting future evaluation as a potential treatment strategy in resistant disease or rituximab intolerance (186). An additional therapeutic option may be the antagonism of B-cell activating factor with belimumab, impeding B-cell survival and maturation. The efficacy of belimumab has been demonstrated in other autoimmune diseases such as systemic lupus erythematosus (SLE) and combined therapy with rituximab has been proposed in patients with AAV (187–189).

1.6.1.4 Combination therapy: B-cell depletion & Cyclophosphamide

Results with monotherapy using either rituximab or cyclophosphamide alongside glucocorticoids yields excellent results, as seen in multiple randomised control trials and clinical practice. In the setting of severe disease cyclophosphamide may be preferable over rituximab with a larger body of evidence, faster time to action, direct effect on both B and T cells as well as better long term sustained remission rates with a higher cumulative dose. However the question remains, can better results be attained with a combined approach. This becomes more pertinent when considering the severe end of the disease spectrum with potential multi-organ system failure and death or the need for drastic steroid avoidance.

The combined use of cyclophosphamide and rituximab has been around for some time with original trial evidence from RITUXVAS (177). The trial two arms consisted of cyclophosphamide (CYCLOPS dosing protocol) and steroids or rituximab 4 x 375mg/m² alongside 2 x 15mg/kg cyclophosphamide and steroids. As RITUXVAS included those with more severe disease, including dialysis dependence, this approach was adopted for rituximab as it was unclear at the time if rituximab alone would be sufficient for this cohort against the established standard of care. In contrast, although the RAVE study was a larger trial and included those with pulmonary haemorrhage, it excluded anyone with a serum creatinine >354 µmol/L (176). As reflected by recent KDIGO guidelines, when considering the evidence, both should be used in this context amongst severe disease cohorts as an equal alternative to cyclophosphamide monotherapy (190).

Published in 2019, both McAdoo *et al* and Pepper *et al* applied this combined approach with a higher cumulative dose of cyclophosphamide for the purpose of severe disease and steroid avoidance respectively (165,191). Both are single centre, observational and relatively small studies which need to be taken into account when considering them. McAdoo *et al* provided five year follow up data of Rituximab 2g with cyclophosphamide 3-3.75g in a propensity score matched study design against EUVAS data using the CYCLOPS regimen (191). Both cohorts used high dose prednisone of 1mg/kg with a tapering regimen to 5mg OD over 6 months. The study excluded those with severe disease, i.e a serum creat >500 µmol/L, dialysis dependence and diffuse alveolar haemorrhage. In the absence of steroid minimisation or severe disease, its appeal in this context may be less compared to standard of care. Nevertheless, the combined approach had a lower risk of ESRD, death and relapse with no significant safety concern. The paper by Pepper *et al* applied a similar induction regimen and study design, again in a non-severe disease cohort, but with a much more rapid steroid withdrawal over two weeks (165). The regimen was as effective as standard of care with no significant safety concerns. Follow up was limited to year, but the study highlights the combined approach, with the additional low cumulative dosing of cyclophosphamide facilitating a steroid sparing effect.

In a more recent study, McAdoo's group applied the combined regimen plus plasma exchange in a severe disease cohort. Limited analysis against a historical cohort treated with cyclophosphamide was provided, but the study did identify superior outcomes (192). High dose oral prednisolone was used at 1mg/kg with a tapering regime to 5mg OD over 5-6 months.

When evaluating therapeutic options there is a potential signal from PEXIVAS that rituximab may take longer to work (193). This may have previously led to the view that a higher dose and duration of steroids at induction might be needed to support its use, however this was not borne out in the recent LoVAS trial (168). Nevertheless, when considering the severe spectrum of disease and the priority to achieve fast remission, the potential longer time to action with rituximab would add support to additional cyclophosphamide in this setting.

Care should clearly be individualised to the patient with no one size fits all strategy, but the above factors help to highlight the following. Firstly, when considering severe disease, treatment options include cyclophosphamide or rituximab in addition to 2 x 500mg cyclophosphamide as standard of care. Secondly, when considering the more extreme end of the severe life/multi-organ threatening disease spectrum the priority is switching off disease and the recent data published by McaDoo's group suggests that the combined approach may offer a viable option. The difference from standard of care in this context is the cumulative dose exposure of cyclophosphamide which can be continually assessed depending on the risk-benefit profile, giving anywhere from 1-3g. Finally, when anticipating the need for steroid avoidance the dual approach offers a viable alternative and based on the current published data the full 3g of cyclophosphamide would be need to be used to ensure sufficient steroid sparing cover. There is no current evidence for this approach in severe disease. Caution should be adopted if withdrawing steroids so rapidly in such cases without a viable adjuvant such as C5a inhibition. Further trials on combination

therapy are needed and a multi-targeted approach with emerging adjuvant therapies is likely to play a key role in facilitating future steroid avoidance strategies.

1.6.1.5 Mycophenolic acid

Mycophenolic acid (MPA) is a reversible inhibitor of inosine-5-monophosphate dehydrogenase, which ultimately acts to inhibit de-novo purine synthesis required for nucleotide base formation, reducing T and B cell proliferation. It can either be administered in the form of mycophenolate sodium or its prodrug mycophenolate mofetil (MMF). Two initial small RCTs compared 1-2g/day of MMF with monthly dosing of cyclophosphamide for induction-remission in patients with non-severe renal disease (194,195). Their findings found MMF to be an equally effective treatment, however both studies had a short follow up period of 6 months only and both were only representative of Chinese cohorts.

The recently published MYCYC trial demonstrated non-inferiority of MMF against cyclophosphamide in the remission-induction of AAV in cases of moderate or severe disease, with no meaningful difference in the adverse event rate (196). This places MMF as a viable alternative agent in cases where cyclophosphamide or rituximab are either contraindicated, or in the case of rituximab, potentially unavailable due to cost. The MYCYC trial was an adequately powered, multinational study, but it should be noted that its findings cannot be applied to patients presenting with life threatening disease, rapidly declining renal function or an estimated glomerular filtration rate (eGFR) < 15 ml/min/1.73m². Furthermore, MMF was associated a higher relapse rate, a finding that is mirrored by other trials evaluating its use for remission-maintenance therapy (197).

1.6.1.6 Methotrexate

Methotrexate applies its immunosuppressive action through the disruption of DNA synthesis by exerting an antifolate action through the competitive inhibition dihydrofolate reductase, as well as downregulating T and B cell function. The NORAM trial randomised patients with to receive either 2mg/kg/day oral cyclophosphamide or 20-25 mg/week oral methotrexate. Non-inferiority of methotrexate in achieving remission at 6 months, however several caveats restrict its use in mainstream practice (164). Firstly, methotrexate should only be used in patients with mild disease and appears suboptimal in patients with pulmonary involvement. The NORAM trial only included patients with creatinine < 150 µmol/L and those without organ threatening disease. Even amongst this cohort it was still identified that patients with a higher index of disease activity and those with pulmonary disease took a longer time to achieve remission. Secondly, methotrexate was associated with a significantly higher relapse rate (RR 0.57, 95% CI 0.34-0.96) and thirdly the antifolate action of methotrexate limits co-administration of co-trimoxazole which is a useful adjuvant in managing upper respiratory tract disease. Subsequent follow up data confirmed less effective disease control with methotrexate (198).

1.6.1.7 Complement system inhibition

Recognising the role of the alternative complement pathway in the amplification loop of disease, there has been significant interest in the inhibition of the complement system to attenuate disease activity; in particular C5a-

inhibition with substantial recent advances made in this area. Two C5a receptors are present on the neutrophil cell surface; the CD88 activating receptor and the anti-inflammatory C5a-like receptor (C5L2). CCX168, also known as avacopan, is a compound that is capable of binding to and inhibiting CD88. The CLEAR trial was a multicentre phase II RCT evaluating the safety and efficacy of avacopan in new or relapsing AAV when administered orally at a dose of 30mg twice daily (199). The primary end point was a $\geq 50\%$ reduction in the Birmingham Vasculitis Activity Score by week 12 with patients divided into three treatment arms; i) prednisolone 60mg/day only, ii) prednisolone 20mg/day plus avacopan and iii) avacopan only. Non-inferiority was demonstrated in both avacopan groups with the end point being reached in 70%, 86% and 81% of patients in each group respectively (199). This raised the exciting possibility that avacopan could safely reduce or replace steroids all together in the treatment of AAV with no increased adverse events.

Advocate is a phase III international trial that randomised 331 patients to receive either avacopan or prednisolone in addition to current standard therapy of either cyclophosphamide or four infusion of rituximab at a dose of 375mg/m² followed by azathioprine (200). A graphic of the study design and treatment regimens is shown in Figure 4. Results demonstrated non-inferiority of avacopan for remission at six months (72.3% vs 70.1%, $p < 0.0001$) and superiority for sustained remission rates at 12 months (65.7% vs. 54.9%, $p = 0.0066$) (201). The safety profile was similar between the two arms, although the prednisolone group clearly had a significantly higher glucocorticoid toxicity index. Both health related quality of life and renal function was better amongst patients treated with avacopan, although the change in eGFR between the two groups did not reach significance. While encouraging, these results need to be considered with the constraints of several potential limiting factors. In view of the study design, beyond five months avacopan is compared against the absence of any continued steroid therapy. The duration of oral glucocorticoids as part of remission maintenance therapy is discussed further in section 1.6.2.1, but given that the current published body of evidence favours continued low dose prednisolone for 12 months, the result of superior sustained remission rates with avacopan in this context may be unsurprising. Furthermore, over the 52 week treatment period the avacopan cohort still had a reasonable degree of glucocorticoid exposure with nearly equitable mean total intravenous and oral use between the two arms beyond the protocol specific prednisolone study medication; 379.5 ± 553.66 mg vs. 480.8 ± 825.79 mg and 885.8 ± 1329.08 mg vs. 868.1 ± 1501.08 mg respectively (200). The study also excluded those with severe disease; eGFR < 15 mls/min/1.73m² and diffuse alveolar haemorrhage. Nevertheless, avacopan heralds a new era in the management of AAV with safe steroid cessation at five months. When combined with the low dose oral steroid regime proposed by PEXIVAS, this is likely to result in markedly improved patient outcomes. The mainstream use of avacopan will depend on its final cost and requires evaluation beyond 12 months as well as its role for further potential steroid avoidance.

InflaRx is a monoclonal antibody that acts to inhibit C5a. It is currently undergoing phase II study, also with the hope of replacing steroid therapy in AAV (NCT03895801). However, its need for intravenous administration, dosing schedule and associated cost may make it a less appealing option compared to avacopan.

In vitro studies have demonstrated the renin exhibits as much activity as C3-convertase on the alternative complement pathway, cleaving C3 to C3b (202). Administration of aliskiren, a direct renin inhibitor, blocked this activity with reduced production of C3b (202). As renin activity is higher in renal tissue, the use of aliskiren could offer a potential adjuvant therapy, reducing alternative complement pathway activation and therefore disease activity for those with renal involvement secondary to AAV. This would also provide the added prognostic benefits of the anti-proteinuric and an anti-hypertensive effects of direct renin inhibition, while potentially avoiding the significant immunosuppressive implications of systemic inhibition of C3 activation. Reports of glucocorticoid free induction therapy using eculizumab, a C5-blocking monoclonal antibody, is limited to a single case report (203).

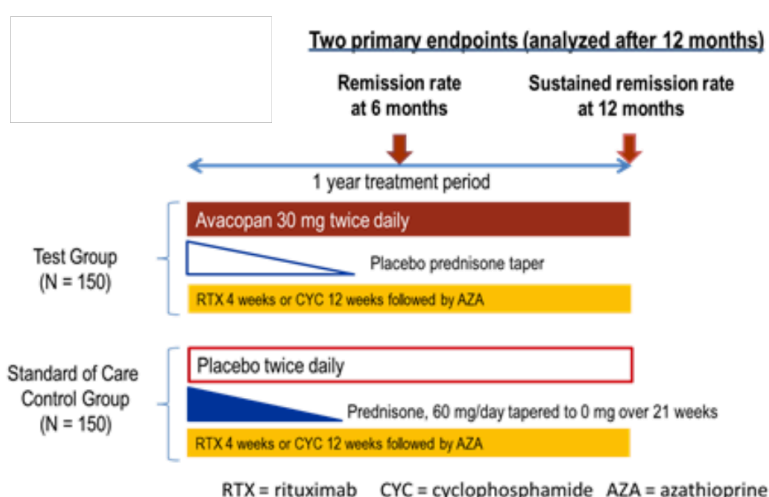


Figure 4 - Graphic of the study design and treatment regimens (taken from - Merkel P, Jayne D, Harigai M, Schall T, Bekker P, Potarca A, et al. 326. a Randomized Phase 3 Trial Evaluating the Safety and Efficacy of Avacopan in Patients With New or Relapsing Anca-Associated Vasculitis. Rheumatology. 2019;58(Supplement_2):2-4)

1.6.1.8 Anti-IL5 monoclonal antibodies

Mepolizumab is an anti-IL-5 monoclonal antibody that reduces blood eosinophil count. Amongst patients with relapsing or refractory EGPA, the use of mepolizumab vs. placebo in addition to standard care demonstrated superior initial and sustained remission rates in the MIRRA trial (204,205). This could facilitate reduced dosing of glucocorticoids. Benralizumab is another anti-IL-5 monoclonal antibody that has drawn attention. The MANDARA trial is a randomised, double blind, multicentre phase three trial that is currently ongoing comparing benralizumab with mepolizumab in cases of relapsing or refractory EGPA (NCT04157348).

1.6.1.9 Intravenous immunoglobulins

The basis of intravenous immunoglobulin therapy (IVIg) in AAV is to inhibit ANCA-induced neutrophil activation through the potential presence of anti-idiotypic antibodies. A recent meta-analysis of nine studies identified improvement in disease activity following administration of IVIg (206). However, amongst other limitations, the majority of studies included were observational. The only RCT of IVIg in AAV to date suggests that any beneficial effect is not maintained beyond three months, with a higher rate of potential mild side effects and no difference in the cumulative dose of immunosuppression (207). As such, the use of IVIg may be considered as a useful short

term adjuvant therapy where other treatment options are restricted and in cases of severe, refractory or life threatening disease.

1.6.2 Remission maintenance therapy

1.6.2.1 Glucocorticoids

In the context of monotherapy with either cyclophosphamide, rituximab or an oral anti-proliferative agent, the current duration and intensity of oral glucocorticoids in the in the remission maintenance phase of treatment varies amongst clinicians. Study data tends to consider either six or twelve months therapy.

In 2012, McGregor *et al* undertook a retrospective study comparing relapse rates according to steroid therapy at six months (167). Patients were divided into three groups; 0mg, 5mg/day or >5mg/day. No statistically significant difference in relapse rates was observed amongst these groups, but continued therapy beyond six months was associated by a higher rate of diabetes mellitus and infection. This may favour stopping prednisolone at six months, but should be considered within the following caveat; patients with dialysis dependence at presentation, treatment resistant disease and those who died at six months were excluded from the study.

RAVE was a multicentre RCT of 197 patients comparing glucocorticoids alongside either rituximab or cyclophosphamide. The primary outcome was complete remission and successful taper of prednisolone to 0mg by six months. Although non-inferiority of the rituximab was demonstrated, 42% of patients still failed to achieve the primary outcome (176). This may favour continued prednisolone beyond 6 months, although it could be considered that the study cohort was high risk or future disease flares anyway with 50% of the trial cohort consisting of patients with relapsing disease. Subsequently, the higher relapse rate observed with steroid cessation at five months in the more recent advocate trial lends further support to a longer duration of glucocorticoids in the absence of an effective alternative such as avacopan (208).

Early steroid withdrawal alongside single agent remission induction therapy was explored by Miloslavsky *et al* (209). This was a prospective single centre non-randomised study evaluating steroid withdrawal at eight weeks in the context of rituximab therapy. The remission rate at six months was comparable to findings of the RAVE study with fewer adverse events, but relapse rates were higher (30% vs 7%) (209). These relapses were more likely in patients with severe disease at presentation, weakening any case for such early steroid withdrawal in the absence of dual concomitant therapy with cyclophosphamide and rituximab (165). Although as previously discussed, this treatment strategy requires further trial study and may not be widely accessible.

Walsh *et al* undertook a metaanalysis on the effect of the duration of glucocorticoid therapy on relapse rates (210). Included studies were grouped according to glucocorticoid target dose; i) 'no glucocorticoid withdrawal' with a target dose of 5 – 7.5 mg prednisone/day, ii) 'early glucocorticoid withdrawal' with steroid withdrawal before 12 months and iii) 'late glucocorticoid withdrawal' with therapy only stopped after 12 months. Differences in the

steroid regime was the most significant factor accounting for the between group differences in relapse rates. A higher relapse rate was observed amongst those stopping steroids before 12 months (48%; 95% CI 38-58%, $p < 0.001$), with no significant difference between stopping therapy after 12 months or continuing low dose therapy beyond this time point (27%; 95% CI 16-39% and 14%; 95% CI 10-19%, respectively, $p = 0.13$) (210). Taking these findings in conjunction with those of more recent studies and the risks associated with prolonged treatment exposure, current evidence would support continued low dose prednisolone for up to 12 months, particularly in high risk patients.

1.6.2.2 Anti-proliferative agents

Azathioprine inhibits purine synthesis required DNA replication in proliferative leucocytes. Given the inherent risks of prolonged cyclophosphamide exposure, the landmark CYCAZAREM trial sought to determine if this could be substituted for azathioprine for maintenance of disease remission (211,212). It found that azathioprine was equally effective in maintaining sustained remission at 18 months follow up and may be safer than oral cyclophosphamide. Patients are typically converted to azathioprine at three to six-months post remission-induction therapy. This practice is not associated with poorer patient outcomes compared to later conversion at twelve months following prolonged oral cyclophosphamide therapy, with five year follow up data from the CYCAZAREM trial finding no significant difference in the rate of death, end stage kidney disease (ESRD), malignancies or relapse rate according (213).

Other oral antiproliferative agents have been assessed. The IMPROVE trial compared MMF with azathioprine. MMF was inferior to azathioprine with a higher relapse rate (HR 1.69, 95% CI 1.06-2.70), although there was no difference in the rate of adverse events, renal function, proteinuria and vasculitis damage index between the two groups (197). Based on this, MMF is generally considered for patients who are unable to tolerate other maintenance agents such as rituximab, azathioprine and methotrexate, or where their use is not ideal, particularly in the case of the latter.

In 2002 Keller *et al* undertook a retrospective study of 71 patients using methotrexate 0.3mg/kg/week for maintenance therapy; a high relapse rate was observed (214). A large RCT was then undertaken in 2008 comparing azathioprine 2mg/kg/day and methotrexate 25mg/week for 12 months following remission induction therapy with cyclophosphamide (215). Both agents were equally effective for maintenance therapy with no significant difference in relapse rates or adverse events. A further trial in 2017 randomised patients to either methotrexate 0.3 mg/kg/week or oral cyclophosphamide 1.5mg/kg/day up to 12 months (216). Patients with severe renal impairment were not included. Again outcomes did not differ between the two groups, reaffirming the safe use of methotrexate for remission maintenance therapy in mild disease.

There is no trial comparing MMF and methotrexate. However, given the similar efficacy of methotrexate to azathioprine and that azathioprine is superior to MMF, methotrexate could be considered superior to MMF although there is no direct evidence to support this.

Leflunamide inhibits the mitochondrial enzyme dihydroorotate dehydrogenase which ultimately acts to inhibit DNA synthesis in rapidly dividing cells, such as lymphocytes. There is only one small trial guiding its use, comparing leflunamide 30mg/day with methotrexate 20mg/week (217). The trial data was limited as a significantly higher relapse rate with methotrexate led to premature termination of the study. Aside from this, leflunamide has a considerable side effect profile and was associated with a higher rate of adverse events including peripheral neuropathy, leucopaenia and hypertension (217).

1.6.2.3 Anti-TNF α

In theory, anti-TNF α therapy should be effective in attenuating disease activity by reducing neutrophil priming and auto-antigen expression. The WGET study is the only trial assessing anti-TNF α therapy in AAV, comparing etanercept with placebo for remission-maintenance in patients receiving induction therapy with cyclophosphamide or methotrexate (14). Etanercept did not confer any benefit for sustained remission rates and any continued enthusiasm for its use was tapered by concerns of an increased rate of solid organ malignancies with ($P=0.01$).

1.6.2.4 Rituximab

An initial trial suggested that a single dose of rituximab was non-inferior to continuous conventional immunosuppression with azathioprine at 18 months for sustained disease remission (218). Nevertheless, other studies have shown that relapses are more frequent following a single dose of rituximab, with only 39% of patients remaining relapse free following initial dosing amongst the RAVE study cohort (176). Other retrospective study has observed that relapses tend to occur at 6-10 months post initial treatment, supporting the need for maintenance therapy (219).

The MAINRITSAN trial compared 6 monthly rituximab of 500mg versus azathioprine 2mg/kg/day for remission maintenance therapy (220). A significantly higher relapse rate was observed with azathioprine (HR 6.61, 95% CI 1.56 to 27.96) (220). The superiority of rituximab for sustained remission was maintained on five year follow up data with major relapse-free survival rates of 49.4% (95% CI 38.0% to 64.3%) and 71.9% (95% CI 61.2% to 84.6%) ($p=0.003$) for rituximab and azathioprine respectively (221). The exact dosing regime and duration of continued rituximab remained a key question.

The MAINRITSAN 2 trial compared fixed schedule-dosing of rituximab 500mg every six months against individually tailored treatment according to B-cell repopulation, ANCA reappearance or a large rise in ANCA titre over 18 months (222). It found no significant differences in relapse rates and fewer infusions given in the individually tailored arm, with implications for cost. However, there are several concerns when considering this data. Follow up is limited to two years. Although not statistically significant, the relapse rate was higher in the tailored treatment arm compared to the fixed-schedule group, which might yield a significant difference on long term follow up of a larger cohort. Secondly the biomarkers used to guide tailored therapy remain an imperfect marker

of disease activity and their use remains controversial. Substantiating this, amongst all relapses in the trial, half occurred despite depletion of circulating B cells.

MAINRITSAN 3 was recently published and was undertaken as a follow up study of the original MAINRITSAN 2 trial cohort (223). It assessed a second phase of maintenance therapy from 18 months onwards to determine duration of rituximab. Rituximab 500mg every 6 months for a further 24 months was compared against a placebo treatment arm, revealing superior relapse free survival with intervention; 96% (95% CI 95-100%) and 74% (95% CI 63-88%) in the rituximab and placebo groups respectively, with a hazard ratio for relapse of 7.5 (95% CI 1.67-33.7) with discontinuation of rituximab (223). The benefit of prolonged maintenance therapy with rituximab beyond two years mirrors the findings of the remain trial (155).

Considering the potential for B-cell reconstitution at six months post therapy and the risk of relapse that can be associated with this, the RITAZAREM trial evaluated a different fixed dosing regimen of 4 monthly rituximab dosing versus azathioprine 2mg/kg/day (201). If the hazard ratio for relapse across all time points was significant by 5%, it also sought to consider the hazard ratios during treatment and the follow up period separately to assess the risk of treatment cessation after two years and help determine optimal duration. Currently the full published results are pending, but similar to the MAINRITSAN trial, presented data shows that rituximab was superior to azathioprine in preventing disease relapse with a preliminary overall hazard ratio estimate of 0.36 (95% CI 0.23-0.57) and a during-treatment hazard ratio estimate of 0.30 (95% CI 0.15-0.60) (201).

Rituximab is the most superior maintenance agent with an optimal maintenance dosing regimen of 500mg every four to six months. Current funding may restrict its duration to two years and patients may only be on it in the event of previous relapse or contraindication to cyclophosphamide for remission induction therapy. The next most superior agent is azathioprine or methotrexate, although arguably the former is preferable as methotrexate has limited trial follow up data, may be restricted in more severe renal impairment and will restrict adjuvant use of septrin in ENT disease. MMF is the most inferior agent, but would facilitate co-administration of septrin and may be favourable over methotrexate in patients with more severe renal impairment where azathioprine is contraindicated or not tolerated.

1.6.3 Adjuvant therapy

1.6.3.1 Plasma exchange

Intended as an adjuvant therapy in cases of severe disease, plasma exchange (PLEX) is used with the premise of removing circulating autoantibodies in an effort to attenuate disease activity while standard remission induction therapy takes effect. Findings from early RCTs evaluating its potential role in AAV were limited. The included sample size of patients was typically small with a non-homogenous disease cohort and varying treatment regimens (224–227). Results differed amongst these studies, with only modest benefit demonstrated for renal survival at best and no significant impact on mortality. The MEPEX trial was an RCT of 137 patients with biopsy proven pauci-immune glomerulonephritis and a serum creatinine > 500 µmol/L (163). Little basis was provided

for choosing this serum creatinine. Patients were randomised to receive standard therapy at the time of oral cyclophosphamide and prednisolone with either seven sessions of PLEX or a total dose of 3g intravenous methylprednisolone. At three months 69% of patients in the PLEX group were alive and dialysis independent compared to only 49% in the methylprednisolone group. At 12 months PLEX was associated with a 24% risk reduction of ESRD only, however this was not maintained on five year follow up with no sustained benefit of therapy (163,228). Analysis of patients with diffuse alveolar haemorrhage (DAH) was restricted due to the small size of this subgroup. Based on the MEPEX trial, it became mainstream in clinical practice to undertake PLEX for patients with DAH, dialysis dependence, a serum creatinine >500 µmol/L or rapidly progressive renal impairment.

In 2011 a meta-analysis suggested that PLEX may reduce the composite outcome of death or ESRD, but lacked the optimum information to reliably conclude its use (229). To identify a 25% relative risk reduction of this endpoint it was calculated that a further RCT of 500 patients would be needed to demonstrate at least a modest benefit of PLEX in AAV (229). This is only applicable to patients with renal impairment as previous included studies did not include DAH. The PEXIVAS trial was designed to fill this data gap.

PEXIVAS is the largest RCT in the field of AAV to date, including 704 patients across numerous countries (59). In addition to the evaluation of reduced dose glucocorticoid therapy previously outlined, PEXIVAS also sought to determine the role of PLEX as an adjuvant to standard therapy in patients with DAH or acute kidney injury. The latter included patients with an eGFR <50 mls/min/1.73m². The study was adequately powered and identified no added benefit of PLEX on the primary composite end point of death from any cause or ESRD (HR 0.8, 95% CI 0.65-1.13) (59). One potential counterpoint to this finding is the lack of biopsy data presented and the inability to determine the degree of chronicity of renal impairment amongst patients. It has been previously suggested that those with more active inflammatory lesions and minimal scarring would benefit the most for adjuvant PLEX therapy (230). This study was based on prospective data with renal histology from the MEPEX cohort and publication prior to the final trial. It did not undertake a direct subgroup analysis of the effect of PLEX according to histology, only general determinants of renal outcomes in the overall cohort according to biopsy findings. Amongst the 100 patients with biopsy data in the published MEPEX trial, the degree of cellular crescents was similar amongst both groups (PLEX: 90.8 ± 57.2 %, Non-PLEX: 90.4 ± 49.1%) with equally moderate interstitial fibrosis and tubular atrophy and no demonstrable long lasting benefit of therapy (163,228). As such, the potential benefit of PLEX in any such group is likely to be small and unlikely to be of any significance. Further supporting this, a recent large retrospective cohort study benefiting from propensity score matching has since identified no benefit of PLEX on the six month remission rate, twelve month relapse rate or overall rate of ESRD and/or death in patients with severe renal impairment (eGFR < 30 mls/min/1.73m²) (231). With biopsy data available in 90% of cases, this lack of treatment efficacy did not appear to be contingent on any potential chronicity with 36.7% exhibiting mixed disease, 24.6% crescentic, 19.6% focal and only 19.1% sclerotic.

A further potential criticism of PEXIVAS is that the time to resolution of DAH and the direct associated mortality rate is not reported as the trial was not designed to assess these specific outcomes. PEXIVAS included 191 patients

with DAH; 130 with severe disease and 61 non-severe. Severe DAH was defined as oxygen saturation \leq 85% breathing ambient air or whilst on mechanical ventilation. Unpublished presented data demonstrates a slightly higher mortality rate in the absence of PLEX (31% vs 28.4%), however this was not statistically significant and subgroup analysis of the trial data amongst these patients did not show any significant added benefit of PLEX on the primary composite endpoint. It is also worth noting that the subgroup of patients with DAH was larger than the entire MEPEX trial which has previously defined current therapy. Similarly, a previous retrospective study of 73 patients with DAH secondary to severe AAV demonstrated no benefit of PLEX in addition to standard remission induction therapy (232).

PEXIVAS is an adequately powered study providing robust and generalizable data. Its findings and the limited evidence base that precedes it suggests no effective role for PLEX in pauci-immune glomerulonephritis or DAH. However, given the limited trial data in regards to the latter, a case can be made for physician discretion and its continued role in severe/hypoxic DAH. A recently published updated systematic review and meta-analysis provides some further clarity on the role of PLEX in AAV (233). This utilised data from nine trials including 1060 patients with a median follow-up of three years. No significant effect on all-cause mortality was identified at 12 months (RR 0.90, 95% CI 0.64-1.27) or long term follow up (RR 0.93, 95% CI 0.73 to 1.19). This was irrespective of the presence or absence of DAH; RR 0.94 (95% CI 0.36-2.45) vs. RR 0.89 (95% CI, 0.01-92), respectively (p=0.45). Similarly, the use of PLEX had no significant impact on remission rates (RR 1.01, 95% CI 0.89-1.15) or risk of disease relapse (RR 0.92, 95% CI 0.32-2.67).

When considering its potential role in renal disease, there was a demonstrable reduced risk of ESRD at 12 months (RR 0.62, 95% CI 0.39-0.98), although this was not sustained at three year follow up (RR 0.79, 95% CI 0.58-10.8) (233). The clinical application of PLEX for this indication requires judicious consideration when taking into account the potential increased risk of infection. In the recent meta-analysis patients were categorised into four risk groups according to serum creatinine at presentation: low risk (creatinine \leq 200 μ mol/L), low-moderate risk (creatinine >200- 300 μ mol/L), moderate-high risk (creatinine >300- 500 μ mol/L), and high risk (creatinine >500 μ mol/L or requiring dialysis) (233). Detailed below in Table 3 is the risk reduction for ESRD and increased infection risk with PLEX at one year. The risk of serious infection increased in line with poorer renal function at presentation and may be higher in dialysis dependent patients given their need for central venous access, although data in this subgroup is not provided. Further analysis suggested that additional trial randomisation would be unlikely to alter their overall findings.

Table 3: Risk reduction for end stage renal disease (ESRD) and increased infection risk at 12 months post plasma exchange

Risk group (serum creatinine $\mu\text{mol/L}$)	Risk reduction for ESRD at 1 year	Increased risk of serious infection at 1 year
Low risk (≤ 200)	0.08%	2.7%
Low-Moderate ($>200-300$)	2.1%	4.9%
Moderate-High ($>300-500$)	4.6%	8.6%
High (>500 or on dialysis)	16%	13.5%

(Adapted from - Walsh M, Collister D, Zeng L, Merkel PA, Pusey CD, Guyatt G, et al. The effects of plasma exchange in patients with ANCA-associated vasculitis: an updated systematic review and meta-analysis. *Bmj.* 2022;e064604)

Based on the published evidence and the value placed on the risk reduction of ESRD vs. avoidance of serious infection, a recent practice guideline that accounted for patient views stated the following; a) weak recommendation for immunosuppression plus PLEX for patients who are at moderate-high or high risk of ESRD at one year, b) weak recommendation for immunosuppression alone in cases of isolated DAH (234). However, it is worth noting that the patient survey used to help inform this was limited to four patients and one carer. Additionally, the author panel may not reflect wider expert views and data within the meta-analysis may remain limited, with all studies other than PEXIVAS and MEPEX consisting of a small sample size, short follow up period, a non-homogenous treatment group and differing treatment protocols.

When considered against the risk of serious infection, the resource requirements of PLEX, the often prolonged hospital stay that ensues and the potential logistical difficulties in renal biopsy and treatment administration it can often cause, the marginal gain with a risk reduction for ESRD of 4.6% vs. an 8.6% increased risk of infection amongst patients with a serum creatinine of 300-500 $\mu\text{mol/L}$ could be considered unsatisfactory. Indeed, it is acknowledged that the increased risk of infection associated PLEX may offset any benefit for patient survival and account for the discordant effect between PLEX and all-cause mortality (233). The risk trade-off for a serum creatinine >500 $\mu\text{mol/L}$ may be more acceptable with a risk reduction for ESRD of 16%, but with an 13.5% increased risk of infection, careful patient selection is needed. Taking recent data into account, as well as wider updated guidelines including updated KDIGO and the American Society for Apheresis (190,235), the following may therefore be reasonable treatment threshold for PLEX; a serum creatinine approaching >500 $\mu\text{mol/L}$, a disease trend rapidly approaching this, dialysis dependence, relapsing disease with limited baseline residual renal function and clinically severe/hypoxic DAH. The role of PLEX in AAV outside of renal or pulmonary disease remains unanswered.

Immunoadsorption and lymphocytapheresis both have a very limited evidence base with no meaningful benefit of intervention from the data available (236,237).

1.6.3.2 Anti-microbial agents

Recognising that the chronic nasal carriage of *S. aureus* may predispose patients to an increased rate of relapse, antimicrobial therapy may mitigate this risk. Several studies have demonstrated the use of co-trimoxazole (septrin) as an independent factor associated with sustained remission in patients with upper respiratory tract disease (238–240). Similarly, topical mupirocin may be of benefit in eradication therapy in confirmed case of *S. aureus* to reduce the risk of relapse (241).

Aside from its role in remission maintenance, the prophylactic use of co-trimoxazole reduces the frequency of severe infections in patients treated with rituximab, particularly respiratory tract infections (242).

1.6.3.3 Anti-fibrotic agents

Nintedanib and pifernidone are two antifibrotic medications that are currently licenced for the treatment of idiopathic pulmonary fibrosis (243). Nintedanib is an intracellular tyrosine kinase inhibitor, resulting in the downregulation of platelet derived growth factor receptor, fibroblast growth factor receptor and vascular endothelial growth factor receptor (243). Whereas pifernidone reduces fibroblast proliferation and inhibits collagen production mediated by transforming growth factor beta (243). Both agents ultimately act to slow the rate of progression of pulmonary fibrosis with a reduced rate of decline in forced vital capacity. More recently the efficacy of nintedanib has been shown across a broader range of progressive interstitial lung disease (ILD), including autoimmune mediated disease (244). Pifernidone has also shown promising results in case reports of rheumatoid arthritis associated ILD (245). These findings have prompted consideration as to whether such agents could offer an additional treatment strategy in ILD secondary to AAV. The first pilot study is currently underway, trialling pifernidone as an adjuvant therapy in anti-MPO AAV ILD, including those without other systemic features of disease (NCT03385668).

1.6.4 Novel therapeutic targets

Given its key role in NET formation and pathogenesis, MPO autoantigen inhibition may offer a potential treatment target. AZM198 is an orally administered myeloperoxidase inhibitor. Initial in vitro study found that its use led to reduced neutrophil degranulation, NET formation and endothelial damage (18). Subsequent in vivo assessment using a murine model, as well as evaluation of renal biopsy samples from AAV patients, confirmed that the use of AZM198 was associated with better renal function, reduced proteinuria and reduced glomerular inflammation (18). This finding may provide an adjuvant treatment in patients with pauci-immune glomerulonephritis.

As previously outlined, one way in which the Th17 T-cell subset helps mediate disease is by inducing the expression of the chemokine receptor CXCL5 within renal tubules (53). Upregulation of CXCL5 has been shown in patients with ANCA-associated glomerulonephritis and its inhibition may therefore help attenuate disease by reducing neutrophil recruitment and the production of pro-inflammatory cytokines.

1.7 Diagnosis & Disease Activity

Despite the advent of highly effective treatment strategies with transformed patient outcomes, the nature of AAV remains one of relapsing disease and their recurrent use is not without risk. Treatment related toxicity now poses the greatest risk to patient morbidity and mortality, of which cumulative glucocorticoid exposure is a major contributing factor (1,156,157). Predicting and gauging the presence of relapsing AAV is currently hampered by the lack of a practical and reliable marker of disease. The consequence of this risks potentially undertreated disease and resulting organ damage or over exposure to therapy and adverse effects of therapy. The following section discusses current and potential candidate markers of disease activity. Figure 5 outlines the required stages in biomarker development and Table 4 provides a summary of the current and prospective non-invasive biomarkers in AAV.

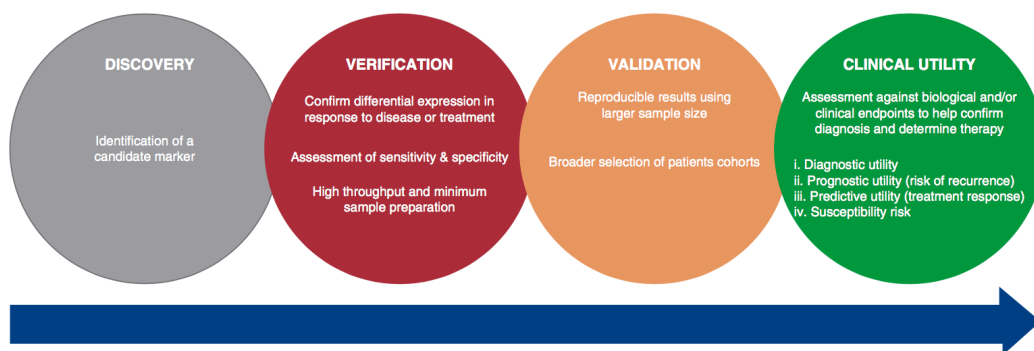


Figure 5: The required stages of biomarker development

1.7.1 Histopathology

The application of histopathology to help assess disease activity is restricted by the impracticality and inherent risks of serial biopsies, the potential low diagnostic yield contingent on biopsy site and that sample attainment is not always feasible depending on the organ system affected. The most commonly biopsied site in clinical practice include renal, sinonasal, cutaneous and peripheral nerves.

The presence of renal involvement and dialysis dependence is associated with a higher risk of death (141,246). Renal biopsy remains the ideal gold standard for establishing a diagnosis of pauci-immune glomerulonephritis, with specific histopathological findings predictive of clinical outcomes. Key histopathological findings are shown in Figure 6. In 2010, Berden *et al* proposed and validated a pathological classification system based on four key variables; focal disease ($\geq 50\%$ normal glomeruli), crescentic disease ($\geq 50\%$ cellular crescents), sclerotic disease ($\geq 50\%$ globally sclerotic glomeruli) and mixed disease with no predominant lesion (247). This was predictive of renal prognosis at five year follow up, with a higher degree of renal survival in patients with focal disease and worst amongst those in the sclerotic group. Numerous studies have since validated this finding, but varied in their reported class discrepancy between crescentic and mixed disease (248). Emerging from these studies was the importance of the percentage of normal glomeruli as a significant predictor of renal survival, as well as the degree

of tubulointerstitial disease (249–252). T-cell mediated tubulitis and as expected a higher degree of interstitial fibrosis and tubular atrophy (IFTA) are associated with poorer renal outcomes, with the degree of IFTA increasing in parallel with the degree of glomerular scarring (250–252). Two scoring systems have since been proposed, incorporating extraglomerular features of histopathology and renal function. The Mayo Chronicity Score utilises glomerulosclerosis, IFTA and arteriosclerosis with more scarring and a higher score predictive of poorer renal recovery (141). Recognising the importance of unaffected glomeruli and tubulointerstitial damage, the ANCA renal risk score utilises a graded score for IFTA, proportion and normal glomeruli and renal function at diagnosis to accurately predict the risk of ESRD, although patients who died were excluded from the validation study which may have impacted these findings (253).

A recent study sought to validate the Berden classification system and ANCA renal risk score in a retrospective cohort study with ten year follow up data, followed by meta-analysis for the former. Both the cohort and meta-analysis results found no significant difference in ESRD between mixed and crescentic disease (248). ANCA renal risk score did correlate with rate of ESRD amongst the reported cohort (248). When considering the implications of such scoring systems, their use is only applicable in renal limited disease with further research needed to provide clinical context of the risk vs. benefit of treatment to identify those at greater risk of treatment related harm.

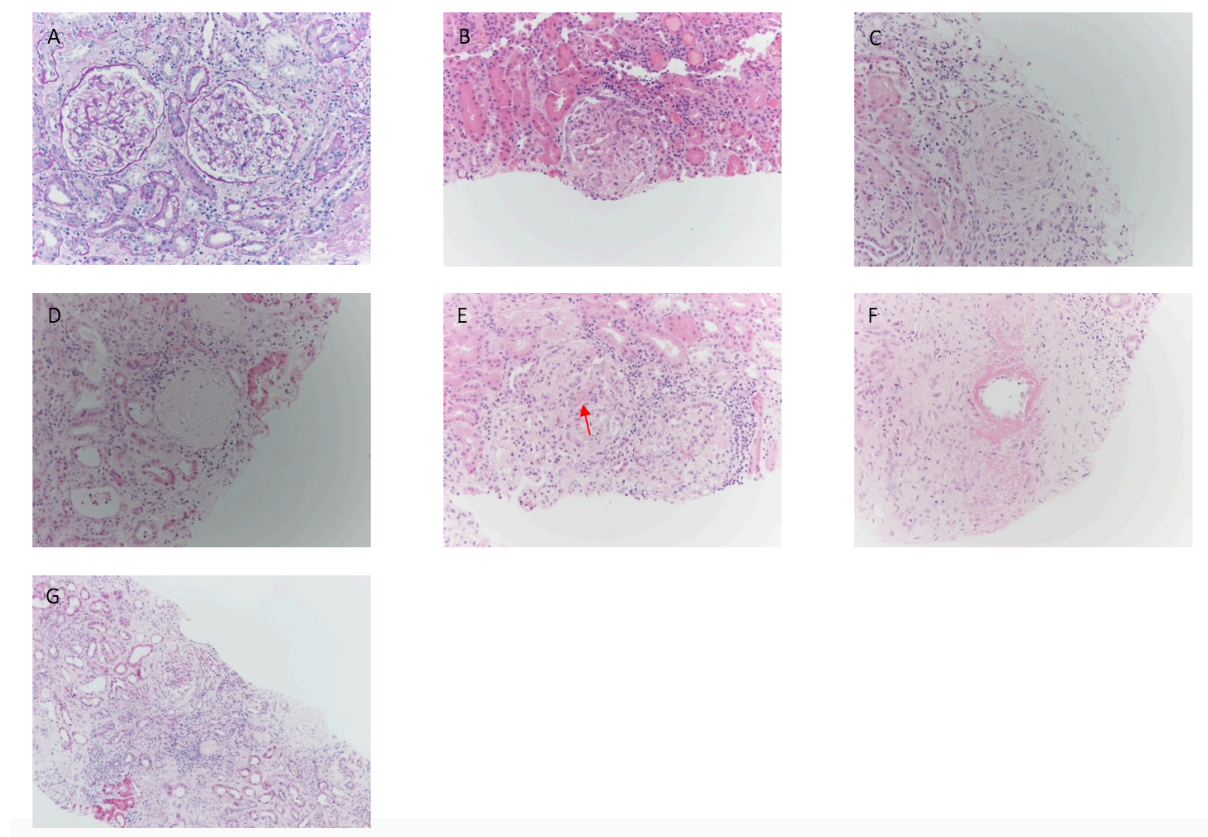


Figure 6: Pathology of ANCA-associated glomerulonephritis: light microscopy (images taken from archived biopsy samples of patients consented for participation in the studies presented in this thesis) – **A)** Normal glomerulus, **B)** Cellular crescent, **C)** Fibrocellular crescent, **D)** Fibrous crescent, **E)** Necrotising glomerulonephritis (red arrow), **F)** Vessel wall necrosis, **G)** Interstitial fibrosis & tubular atrophy. (A - periodic acid-Schiff stain, B, C, D, E, F and G – Hematoxylin-eosin stain)

The reported diagnostic yield from lung biopsies varies from 50-90% (254,255) with a very low pick up rate from transbronchial biopsies of only 7% (211,256). Similarly, sinonasal biopsies are of limited value, with pathological findings only identified in up to 50% of cases (257–260). These tend to be non-specific and unhelpful and determining the diagnosis or altering clinical management, particularly in the absence of other parameters such as positive ANCA serology.

Cutaneous signs secondary to AVV are common amongst all three major clinical phenotypes of disease and tend to be associated with more severe systemic disease (261). Lesions occur in 30-50% of cases, mainly comprising of pretechieae and purpura (261–263). Biopsy of these lesions are often diagnostic, typically demonstrating leukocytoclastic vasculitis with fibrinoid necrosis or granulomatous inflammation, the yield of which increases if the sample is taken from the most tender, prominent lesions with extension into the subcutis (263–266). Despite this and ease of accessibility, data from the DCVAS suggests that skin biopsy in AAV remains underutilised (261).

Data on ANCA-associated vasculitis neuropathy (VN) is limited. DCVAS provides the largest reported cohort to date from 269 patients, identifying an incidence rate 28% (267). ANCA-associated VN was most commonly observed in patients with EGPA, occurring in up to 65% of cases. Its presence in MPA and GPA was far less frequent at approximately 20% (267). The biopsy rate amongst these patient groups was only 12%, of which only 53% were diagnostic. As such, a diagnosis of ANCA-associated VN is often supported by other clinical parameters including nerve conduction studies, which typically show low amplitude response and reduced conduction velocities (268).

1.7.2 Imaging

In the absence of histological confirmation of disease, imaging can be used as a surrogate marker of disease where radiological findings are in keeping with the clinical presentation (124). Computerised tomography (CT) is commonly used to evaluate disease and is best described in patients with respiratory tract disease.

The most commonly reported radiological features of pulmonary disease include nodules, cavitating lesions, and bronchial wall thickening (254,255,269,270). Features are often bilateral and subpleural or peribronchovascular in distribution (271). However, restricting the findings from these studies is their small sample size, retrospective design and lack of adequate control groups. Furthermore, the radiological features described are not specific to vasculitis and can often be observed in other conditions such as malignancy or rheumatoid nodules. The interpretation of such findings becomes more challenging in the context of ANCA negative disease, as well as the evaluation of new lesions on follow up scans given the associated risk of malignancy and infection with immunosuppressive therapy. Repeated exposure to ionising radiation also limits the use of serial imaging for disease monitoring.

Over recent years the development of ILD as a subtype of ANCA-associated lung disease has become increasingly recognised, with a more robust literature base reporting its prevalence and characteristic radiological findings. The exact pathophysiology of ANCA-associated ILD remains unclear, with recurrent episodes subclinical intra-alveolar haemorrhage suggested as a potential cause (130). Studies mostly reflect French and Japanese cohorts

with ILD occurring in up to 66% of patients with ANCA-associated lung disease; the majority of which are anti-MPO positive and exhibit an MPA disease phenotype (272–274). High resolution CT findings typically include bilateral ground glass opacities with a usual interstitial pneumonia pattern of disease and a predilection for the lower lobes (274–278). Less commonly a non-specific interstitial pneumonia pattern may be observed (277).

The findings and distribution of disease on sinonasal imaging with CT is not well established, with reported studies limited to retrospective case series. Amongst these, commonly observed findings include mucosal thickening, bony destruction, septal perforation and osteoneogenesis (279–282). Similar findings have been observed on magnetic resonance imaging (MRI) (282,283). Yet, these features lack specificity and can be difficult to differentiate from other causes of chronic rhinosinusitis. Only one prior study has taken into account previous surgery, identifying this as a risk factor for neo-osteogenesis and more severe features of chronic rhinosinusitis (284). It is unclear if this represents a group of patients with more severe underlying vasculitic disease or the sequelae of surgery as a compounding factor. In the absence of surgery, bony destruction is present in up to 60% of cases (284). The selection bias of presented cases in these studies, small sample size and lack of adequate control groups limits any conclusion that can be drawn from them and any findings need to be interpreted in the context of clinical suspicion. A recent large retrospective cohort study evaluated time dependent changes by reviewing patients with three or more sinonasal CT scans, each a minimum of twelve months apart with comparison against a control group of patients without known rhinosinusitis (285). This found that the combination of the global osteitis score and diameter ratio measurement allowed the distribution and severity of disease to be monitored (285). When evaluating ophthalmic masses, the presence of sinonasal symptoms and the associated described radiological findings on CT imaging is highly suggestive of AAV (286).

The potential role of flurodeoxyglucose positron emission tomography CT (FDG PET-CT) is well established in large vessel vasculitis, but is not well reported in SVV. From the studies available, data suggests that it may offer superior delineation of respiratory tract lesions compared to unenhanced CT, as well as guiding potential biopsy site selection and determining treatment response. Nonetheless, findings remain non-specific (287–289).

1.7.3 ANCA

The diagnostic value of ANCA in the context of clinical symptoms is well established, yet its role in the prediction of relapsing disease and correlation with disease severity remains debatable. Given the evidence supporting its key role in pathogenesis, it would be expected that the presence of detectable circulating ANCA would present an inherent risk factor for relapse, however this is not always reflected in practice. Numerous studies have attempted to delineate the role of serial ANCA monitoring, with varying results and a lack of consensus on reported outcomes. The subsequent discordance between ANCA serology and disease activity limits any advocacy for its use as a reliable biomarker.

Early retrospective studies supported the relationship between ANCA and disease activity, however their sensitivity and positive predictive value for relapse remained relatively low at 23-28%, proposing its use when

taken into account with other clinical parameters (290–294). An initial systematic review in 2006 attempted to provide more insight on the topic, but was unable to undertake a meta-analysis and offer any meaningful conclusion due to the considerable method heterogeneity and suboptimal design of most studies for the assessment of test accuracy (295). A subsequent meta-analysis by Tomassen *et al*, which was more stringent in its study selection, identified a modest association at best for persisting ANCA positivity or rising titres with the risk of relapse (296). Several studies with more longitudinal data, including follow up data from large RCTs, have since corroborated earlier findings that persistent ANCA positivity, ANCA reappearance and the presence of anti-PR3 antibodies are risk factors for relapsing disease (189,221,297–300). Data from the Mainritsan trial identified a hazard ratio of 2.04 (95% CI 1.06-3.91) for relapse in anti-PR3 associated disease and a recent Japanese study observed an odds ratio of 26.2 (95% CI 82-101) for relapse with anti-MPO reappearance (221,301). Similarly, seronegativity post remission induction therapy is associated with a longer relapse free survival period (189,297). The positive predictive value of detectable ANCA and disease relapse increases when combined with the clinical index of suspicion for active disease (302).

The relevance of a change in ANCA titre on the risk of relapse and disease severity remains more controversial. A single Italian study has correlated a rise in anti-MPO and anti-PR3 titre with changes in Birmingham Vasculitis Activity Score 3 (BVAS), however the sample size was small with application of a non-standardised ELISA kit (303). Elsewhere a rise in ANCA titre has been observed in cases of relapsing disease, but its positive predictive value remains modest at best with other studies equally showing no association with disease activity (149,292,299,300,304–307). Crucially, amongst these studies persisting ANCA positivity or a rise in titre occurred in up to 50% of patients with no subsequent relapse and up to 30% of those with active disease had undetectable circulating ANCA (298,299,304).

Ultimately it is the presence of seronegative disease and positivity in the absence of disease that limits the use of ANCA as a functional and infallible biomarker. As previously outlined, the reported rate of seronegative pauci-immune glomerulonephritis varies from 12-30%, with up to 54% of patients with limited extra-renal disease and a significant proportion of relapsing disease exhibiting undetectable circulating ANCA (137,143,152,153,144–151). Circulating ANCA has also been detected in individuals without any known history of vasculitic disease. Two case-control studies confirmed positive ANCA serology from biobank samples of asymptomatic individuals up to nineteen years prior to disease onset (308,309). In this context it is possible that these individuals might have been lacking the ‘second hit’ required for disease at the time of sample collection. Similarly anti-PR3 and anti-MPO positivity have been detected in healthy individuals and other diagnoses including inflammatory bowel disease, liver disease, rheumatic disease and infection such as tuberculosis (61,310,311). The presence of anti-MPO ANCA in healthy individuals may represent differing epitope specificity (61).

1.7.4 B-cell population & Cytokines

Recognising the pivotal role of B-cells in pathogenesis through autoantibody production and B-cell T-cell cross talk, B-cell repopulation following targeted therapy has the potential to predict relapsing disease. Data from observational studies suggests that incomplete B-cell depletion and B-cell repopulation post rituximab is associated with a significantly higher relapse rate (297,312). Supporting this, follow up data from the RITUXVAS trial observed that B-cell repopulation accompanied all cases of relapsing disease (313). However, the trial was not powered to draw any significant conclusion from this subgroup and follow up data from several other larger trials did not corroborate this finding. Amongst the RAVE patient cohort, B-cell count did not predict relapse with disease occurring despite undetectable CD19+ B-cells in the vast majority of relapsing cases and the presence of B-cell detectability in quiescent disease (300). Similarly data from both the Mainritsan and Mainritsan 2 trials found that CD19+ B-cell reconstitution was not predictive of relapse (220,222). Confirmation of the tenuous association of B-cell population with disease activity comes from a case report by Ferraro *et al* that demonstrated relapsing disease with B-cells present in tissue sites of active disease despite peripheral depletion in serum (314). As such, B-cell depletion should not provide reassurance of a reduced risk of disease flare and repopulation may indicate a potential risk of relapse when taken into account with other clinical parameters.

B-cell subset populations that have drawn interest include regulatory B-cells (Bregs), such as CD5+ B-cells. The CD5 protein acts to attenuate any activating signals from the B-cell receptor, downregulating B-cell activity. Measurement of Bregs showed initial promise, with a lower CD5+ B-cell count correlating with active disease, while maintaining a normal count may confer a longer relapse free survival period (315). The suggestion being that its level could be used guide treatment intensity and risk stratification. Data from the RAVE study cohort observed a similar findings, but subsequent analysis found that serial measurement of CD5+ B-cell count was not predictive of disease relapse, severity or treatment failure (316).

Key cytokines may offer another predictive tool of relapsing disease. As previously described, BAFF is important for B-cell maturation and survival, potentially facilitating autoimmune B-cell tolerance. Krumbholz *et al* initially exhibited elevated levels in active disease, with a corresponding fall post treatment (55). Following this Nagai *et al* identified a positive correlation of BAFF with ANCA titres and active disease (57). Conversely, of the few studies evaluating the predictive value of BAFF, work by both Bader *et al* and Sanders *et al* found no association with disease activity and a potential inverse correlation with ANCA titre, bringing into questions its role in autoantibody production (56,317). Following remission induction therapy, assessment of other cytokines has found lower levels of anti-inflammatory cytokines such as IL-10 and increased levels of proinflammatory IL-6 may signal a higher risk of relapse; particularly anti-PR3 associated disease with renal and respiratory tract disease in the case of the latter (56,318). Indicators of T-cell activation have also been found with elevated levels of soluble IL-2 receptors and CD30 in active disease, but further study is required to elicit their potential role as a biomarker of disease activity (56).

A panel of other inflammatory cytokines and proteins have been prospectively evaluated from patients enrolled in the RAVE trial at presentation and six months post remission. This benefited from a large sample size with standardised data collection and identified three candidate markers; the B-lymphocyte chemoattractant chemokine (C-X-C motif) ligand 13 (CXCL13), matrix metalloproteinase 3 (MMP-3) which is an enzyme involved in the breakdown of extracellular matrix and tissue inhibitor of metalloproteinase inhibitor 1 (TIMP-1). These distinguished active disease from remission with an AUC >0.8 and likelihood ratio of 4.3-4.6, warranting future assessment (319).

1.7.5 Complement

Alternative pathway complement activation is fundamental for the development of disease. In line with this, tissue deposition of cleavage products C3d, C3c and Bb have been associated with more severe renal inflammation with a higher proportion of cellular crescents, IFTA and a poor renal function at diagnosis (28,30,31). In light of this Gou *et al* set out to determine the significance of complement activation products in urine as a biomarker of renal disease activity. In doing so they found that urinary levels of Bb, C3a, C5a and soluble C5b-9 were significantly higher in active disease compared to remission, in addition to Bb in effect providing a surrogate marker of renal histopathology with the urinary level inversely correlating with the percentage of normal glomeruli (30). As the application of this finding is restricted to renal limited disease, the same group subsequently demonstrated that the plasma level of these complement degradation products were significantly higher amongst patients with active multisystem disease (320). Several retrospective studies have since analysed circulating levels of C3 and their relation to patient outcomes; a low level is present in up to 35% of patients at the time of initial diagnosis with a higher likelihood of more severe disease and poorer renal function at presentation (321,322). This has also demonstrated some prognostic value with a lower circulating level of C3 associated with a poor renal and patient survival (323–325). However, a recent metanalysis concluded that although higher plasma levels of factor B, C5a and C5b-9 were associated with active AAV compared to patients in remission and healthy controls, this was only observed in a proportion of patients and persistently raised levels were also observed despite successful remission-induction therapy (326). Furthermore, there was no correlation of these degradation products with BVAS, renal function or proteinuria and changes in plasma C3a levels was of no significance. These findings potentially limit the use of the complement system in plasma as an accurate biomarker to distinguish active from quiescent multisystem disease. Nevertheless, circulating and particularly urinary markers of alternative complement pathway activation holds promise. Studies assessing their use in relapsing disease remain lacking and their role as a functional biomarker of disease activity requires further study.

In 2015 a study by Chen *et al* concluded that plasma levels of complement factor H (CFH), a negative regulator of the alternative complement pathway, were lower in patients with active disease and inversely correlated with renal function, renal inflammation and BVAS (327). An *in vitro* study by the same group supported the hypothesis that higher CFH inhibited ANCA-induced neutrophil activation with reduced functional activity in patients with active disease (328). This raises the question whether or not a subgroup of patients have a predisposition to disease due to an abnormality affecting CFH, such as the presence of C3 nephritic factor, complement factor H

related proteins, anti-CFH antibodies or a congenital deficiency in CFH. Measurement of circulating levels of CFH may help identify those patients who may be more susceptible to disease and subsequent future potential relapse.

1.7.6 Inflammatory markers

Traditional inflammatory markers such as erythrocyte sedimentary rate (ESR) and C-reactive protein (CRP) may rise in line with active disease, however they remain non-specific for AAV with limited clinical use (37,319,329). A large cross-sectional study of the BVAS provides further confirmation of this (330). BVAS is a validated quantitative clinical tool to help assess disease severity. In this study poor correlation was shown between BVAS and CRP, demonstrating the limited role of such inflammatory markers in assessing disease activity (330). Other inflammatory markers such as calprotectin, hepcidin and procalcitonin have also been evaluated, but face the same limitation (37,331–336).

The presence of C3a and C5a receptor on activated platelets and their function in disease propagation has drawn attention to their level as a potential gauge of disease activity. Willeke 2015 suggested that platelets correlate with disease, with significantly higher counts observed in active AAV compared to remission and infection (37). Nonetheless, there was an irregularity in their findings with raised levels in patients with multisystem disease, but relatively lower levels in those with severe disease. Park *et al* also sought to assess the correlation of platelets with disease in a retrospective study using the platelet:lymphocyte ratio (337). In doing so they found that a value >272 was an independent predictor of severe disease, particularly amongst patients with renal and pulmonary disease, although this small study was unable to account for confounding factors and the impact of comorbidities on their significance (337). Along similar lines, Ahn *et al* looked at the neutrophil:lymphocyte (N:L) ratio at diagnosis to estimate disease activity and prognosis, with patients exhibiting a ratio >5.9 presenting with more severe disease and a higher frequency of future relapse (338). Application of the N:L ratio is needed in larger prospective studies to determine their reliability.

Neutrophil gelatinase-associated lipocalin (NGAL) provides a marker of neutrophil degranulation with a significantly higher level found at the time of diagnosis and relapsing AAV compared to remission (339). NGAL has also been extensively investigated as a potential early predictor of acute kidney injury and as with all of the inflammatory markers discussed in this section, if employed its use should be interpreted alongside an array of other clinical parameters to help inform an assessment current disease activity.

More direct indices of vascular damage have been investigated. Analysis of circulating necrotic endothelial cells yielded promising results with higher levels in ANCA-associated glomerulonephritis compared to remission and control groups, although its intensive resource requirements may have restricted clinical application (340). Investigation of angiopoietin 2 was of limited clinical utility, failing to discriminate disease activity following clinically successful treatment or to predict relapses (341).

1.7.7 Urinary proteins

In 2004 Tam *et al* undertook a prospectively study evaluating urinary monocyte chemoattractant protein-1 (uMCP-1) as a non-invasive assessment tool of renal vasculitis (342). In doing so, significantly elevated levels were found amongst patients with active or persistent renal vasculitis compared to those in remission or non-renal disease. This correlated with upregulated macrophage infiltration in severely inflamed glomeruli. A corresponding fall in uMCP-1 was seen following successful treatment. Several subsequent studies have since validated this finding, confirming that levels of uMCP-1 reflects disease activity in renal vasculitis and may also indicate the presence of subclinical glomerulonephritis (343–345). One study has assessed the role of serum MCP-1 in a mixed cohort of systemic vasculitis with higher levels seen in those with active disease (346).

CD163 is expressed on monocytes and macrophages, functioning as a scavenger receptor for the haemoglobin-haptoglobin complex. It also provides a surrogate marker of cell activity with cleavage to soluble CD163 (sCD163) in a proinflammatory state. In a rodent model of disease, O'Reilly *et al* detected higher levels from urine in small vessel vasculitis compared to other glomerular pathologies on glomerular microdissection and mRNA analysis (347). They subsequently undertook human study with noticeably higher levels present in urine samples from patients with active disease compared to remission and other control groups; results that were confirmed by internal and external validation cohorts. This well conducted study identified a high sensitivity and specificity of sCD163 for active disease with a likelihood ratio of 20.8 (347). sCD163 offers a promising non-invasive biomarker, though its use is limited to renal vasculitis with potential elevation in the context of infection. Evaluation of urinary sCD163 with serial renal biopsy data has since demonstrated a high degree of correlation with fibrinoid necrosis and cellular crescents in those with both de-novo and relapsing active ANCA-associated glomerulonephritis compared to remission and healthy controls (348). This also lends support to the position that serial comparative analysis of non-invasive biomarkers and histopathology in renal vasculitis is potentially feasible and arguably needed as the ideal reference standard when determining their clinical utility in predicting outcomes and disease recurrence (349,350).

Moran *et al* combined uMCP-1 in urinary sCD163 positive patients, with a 97.9% specificity and positive likelihood ratio of 19.2 for relapsing disease in the presence of new onset proteinuria, subject to pre-test probability (351). Both urinary proteins offer a promising non-invasive candidate biomarker that could be translated into clinical practice, though their use is limited to renal vasculitis with potential elevation in the context of infection.

1.7.8 mRNA

Considering the role of epigenetics in AAV, with genetic variance in autoantigen membrane expression as a risk factor for disease, MPO and PR3 mRNA have been proposed as a candidate biomarkers. Alcorta *et al* was the first study describe mRNA expression in AAV following a genome wide expression study from circulating leukocytes in a heterogenous group of renal diseases (352). Variation in autoantigen gene expression has since been confirmed as a risk factor for disease through histone depletion, hypomethylation and impaired transcriptional repression due to reduced RUNX3 at the MPO and PRTN3 gene loci. Jones *et al* confirmed this link by investigating the DNA

methyltransferase 1 (DNMT1) gene expression required for DNA methylation and downregulation autoantigen expression. In doing so they found that the degree of DNMT1 mRNA positively correlated with DNA methylation and negatively correlated with PRTN3 and MPO gene expression (83). As such, a reduction in DNMT1 mRNA and DNA hypomethylation was associated with active disease and predicted a higher risk of relapse (HR 4.55, 95% CI 2.09 – 9.91), while patients exhibiting increased DNA methylation at the PRTN3 promoter in remission had a greater likelihood of a longer relapse free survival period (83). Contrary to this, Kurz *et al* concluded that elevated leucocyte PR3 mRNA was not predictive of relapsing disease, although this may reflect the transrepressive effect of concurrent glucocorticoid therapy (353).

In 2010, McKinney *et al* quantified the gene expression profiles from purified leukocytes amongst patients with active AAV to prospectively predict the risk future relapse (354). In doing so, they identified that transcriptional profiling of CD8⁺ T-cells with overexpression of mRNA encoding proteins for IL7 receptor pathway, T-cell receptor signalling and expanded CD8⁺ T-cell memory population identified a poorer prognosis (354). This finding has the potential for translation to clinical practice and requires validation in a prospective study with longitudinal data.

1.7.9 Metabolomics

Metabolomics enables the quantitative analysis of the substrates and products of metabolism to directly reflect the biochemical activity within a cell, biofluid or tissue. It includes the study of molecules within the range of 150-1500 daltons such as lipids, amino acids and fatty acids, with variation in the metabolomic profile reflective of changes in the underlying biochemical composition caused by physiological processes or pathological states. Its use complements other analytical techniques of biological systems including proteomics, transcriptomics and genomics and can be used to define biomarkers of disease and treatment response. Metabolomics has been applied in the early detection of drug induced nephrotoxicity prior to changes in histopathology and more recently in autoimmune disease including vasculitis (355–357). Using nuclear magnetic resonance (NMR) spectroscopy with partial least square (PLS) discriminate analysis, a distinctive metabolomic profile was identified in patients with active Takayasu's arteritis compared to controls (356). A larger study that followed corroborated this finding, with good discrimination of patients with active disease from those in remission and a subsequent change in the metabolomic spectra following treatment (357). Key metabolites associated with active disease included increased choline metabolites, low density lipoproteins, N-acetyl glycoproteins (NAG) and glucose.

Studies applying metabolomics in AAV are limited. In 2016 Al-Ani *et al* analysed the urinary metabolomic profile in a rodent model of disease using NMR spectroscopy (358). In doing so they identified a distinctive metabolomic profile in active disease compared to control groups on partial least square (PLS) discriminate analysis. This resolved following disease remission with subsequent recurrence in relapsing disease. A large patient cohort study by the same group yielded similar results using liquid chromatography mass spectrometry, with raised urinary myo-inositol and hypocitraturia present in active disease and a ratio of the two closely associated with active renal vasculitis (358). A study by Gupta *et al* has since evaluated the metabolomic profile in serum amongst AAV patients, identifying a metabolomic profile that was specific to active disease with good separation from

control groups that included Takyasu's arteritis and systemic lupus erythematosus (359). The metabolomic spectra was characterised by raised NAG, low/very low density lipoproteins, choline and glycerophosphocholine, whereas glucose and amino acids were reduced compared to control groups. The role of metabolomics as a robust and relatively non-invasive biomarker of disease activity in AAV merits further study, but its associated costs may limit its potential application.

1.7.10 Biospectroscopy

Biospectroscopy provides a novel and low cost surrogate technique of determining the metabolomic profile of a sample through one of two primary spectroscopic techniques; attenuated total reflection Fourier-transform infrared (ATR-FTIR) spectroscopy and Raman spectroscopy (360). Both offer a non-destructive and label free means of quantitatively delineating the biochemical and structural information of a sample without the need for prior fixation. Underpinning this is the principle that all chemical bonds present within a component molecule exhibit a periodic vibrational mode. The internal vibrational energy will vary according to the bond present and their interaction with light, determined by the presence of a dipole moment, will detect these changes to facilitate their assessment through spectrochemical analysis (360). ATR-FTIR utilises infrared radiation. Chemical bonds that exhibit a vibrational pattern in the dipole moment are active within the infrared (IR) spectral range and according to the bonds present, a unique spectral pattern will arise according to the degree of IR absorption that occurs following exposure to mid-IR radiation (360,361). The spectral range of 900-1800 cm^{-1} contains wavenumber variables representative of key chemical bonds present in lipids, proteins, carbohydrates, nucleic acid and glycogen to reflect particular cellular activity (360). Raman spectroscopy centres on the interaction of a chemical bond with photons and the change in molecular polarisation determined by inelastic scattering. Inelastic scattering refers to a frequency shift, where the radiation emitted is higher or lower than the initial absorbed radiation (360). Only a small proportion of incident photons will exhibit this and the frequency shift that occurs will be reflective of the vibrational mode present in the bond, resulting in a spectral fingerprint that is characteristic of the chemical composition of the analysed sample.

Irrespective of the modality used, biochemical changes caused by disease will result in a unique spectral fingerprint that is representative of the underlying pathophysiological state. Advancements in instrumentation and standardised chemometric analysis have enabled the successful application of biospectroscopy across numerous areas of medicine using a range of biofluids and tissue samples with studies in oncology, neurodegenerative disease, rheumatic disease, lymphocyte subsets, cytokine monitoring and nephrology (360,361,370–379,362,380–383,363–369). Its use in the field of vasculitis is emerging with one previous study by Yu *et al* using ATR-FTIR to identify potential urinary biomarkers in an animal model of crescentic glomerulonephritis and patients with ANCA-associated glomerulonephritis (384). This identified the 1545 cm^{-1} spectral marker as a key wavenumber variable, increasing in intensity in line the degree of glomerular injury and subsiding following treatment. In parallel, the intensity of 1033 cm^{-1} was inversely related with the degree of fibrosis. These findings suggest that ATR-FTIR could be used as a fast, innovative method of monitoring disease

progression and treatment response in renal vasculitis. The promising use of biopsepectroscopy to provide a robust biomarker of disease activity in AAV that can be readily translated to clinical practice requires further study.

Table 4: Summary of current and prospective non-invasive biomarkers in ANCA-associated vasculitis

Biomarker	Source	Organ System	Comment
ANCA	Serum	Multisystem disease	<ul style="list-style-type: none"> • Diagnostic value in the context of clinical symptoms is well established. • Persistent ANCA positivity, ANCA reappearance and the presence of anti-proteinase 3 antibodies are risk factors for relapsing disease. • Discordance with serology and disease activity with seronegative disease and positivity in the absence of disease restricts its use as a reliable biomarker.
Anti-LAMP2 Ab	Serum	Multisystem disease	<ul style="list-style-type: none"> • Initial studies suggested a potential role in pathogenesis and association with disease activity, although these findings were not corroborated in subsequent study.
Anti-tissue plasminogen Ab	Serum	Multisystem disease	<ul style="list-style-type: none"> • Associated with ANCA seropositivity and a higher degree of acute inflammatory renal lesions. • Validation studies are required as well as determination of its prognostic and predictive utility.
CD19+ B-cell population	Serum	Multisystem disease	<ul style="list-style-type: none"> • Conflicting data on the prognostic utility of B-cell reconstitution from follow up data of several large trials. • Relapsing disease can occur despite peripheral B-cell depletion with B-cells present in tissue sites of active disease. • B-cell depletion should not provide reassurance of a reduced relapse risk and repopulation may indicate susceptibility when taken into account with other clinical parameters.
Cytokines	Serum	Multisystem disease	<ul style="list-style-type: none"> • CXCL-13, TIMP-1 & MMP-3 each distinguish active disease from remission with a high degree of accuracy. Further validation study is required to assess their use. • Conflicting data exists of the association of BAFF with disease activity. • Conflicting data exists on the association of Bregs, such as CD5+ B-cells, with disease activity and its prognostic utility.
T-cells	Serum	Multisystem disease	<ul style="list-style-type: none"> • T-cell activity is associated with disease activity with elevated levels of IL-2 and CD30 with further validation study and assessment of its clinical utility required.
ESR & acute phase proteins	Serum	Multisystem disease	<ul style="list-style-type: none"> • ESR & acute phase proteins including CRP, calprotectin, hepcidin, procalcitonin remain non-specific for active AAV with limited clinical use.
N:L & P:L ratio	Plasma	Multisystem disease	<ul style="list-style-type: none"> • Both the N:L & P:L ratio are potential predictors of disease severity, but both require larger prospective study.
NGAL	Serum	Multisystem disease	<ul style="list-style-type: none"> • Higher levels of NGAL are associated with relapsing disease, but remains non-specific and should be cautiously interpreted.
Endothelial cells	Plasma	Multisystem disease	<ul style="list-style-type: none"> • Circulating necrotic endothelial cells offer a direct indices of vascular damage with a high degree of correlation in active ANCA-associated vasculitis, although intensive resource requirements limit its clinical application and validation study.
Angiopietin 2	Plasma	Multisystem disease	<ul style="list-style-type: none"> • Limited ability to distinguish active from quiescent disease or predict relapse.
Complement	Serum	Multisystem disease	<ul style="list-style-type: none"> • Higher plasma concentrations of alternative complement pathway degradation products in active disease. Prospective study is required with assessment in relapsing disease.
	Urine	Renal Limited disease	<ul style="list-style-type: none"> • Higher urinary degradation products associated with active renal vasculitis, with urinary Bb inversely correlated with the percentage or normal glomeruli. These results require validation study.

mRNA	Plasma	Multisystem disease	<ul style="list-style-type: none"> • Autoantigen gene expression is a risk factor for disease through histone depletion, hypomethylation & impaired transcriptional repression. Lower levels of DNMT1 mRNA & subsequent DNA hypomethylation is associated with active disease and a higher risk of relapse. • CD8+ T-cell transcriptional profile is predictive of relapsing disease. • Further prospective validation studies of gene expression profiles are required.
MCP-1	Urine	Renal limited disease	<ul style="list-style-type: none"> • Prospective validation studies have demonstrated a positive association of urinary MCP-1 levels with active renal vasculitis, with a corresponding fall following remission-induction therapy. Evaluation of its clinical utility now required.
Soluble CD163	Urine	Renal limited disease	<ul style="list-style-type: none"> • Higher urinary levels of soluble CD163 cleaved from macrophages and monocytes conferred a high sensitivity and specificity for active renal vasculitis compared to remission. This correlates with the degree of inflammatory lesions on histopathology in both new and relapsing ANCA-associated glomerulonephritis. Potential elevation can occur in infection with study of its clinical utility required.
Metabolomics	Serum	Multisystem disease	<ul style="list-style-type: none"> • Active vasculitis is associated with a distinctive metabolomic profile of raised N-acetyl glycoproteins, low/very low density lipoproteins, choline and glycerophosphocholine, whereas glucose and amino acids were reduced compared to control groups.
	Urine	Renal Limited disease	<ul style="list-style-type: none"> • Raised urinary myo-inositol and hypocitraturia is present in active disease and a ratio of the two closely associated with active renal vasculitis. Validation study and evaluation in relapsing disease required. • Further study of metabolomics is warranted, although associated costs may limit its potential application.
Biospectroscopy	Urine	Renal limited disease	<ul style="list-style-type: none"> • Biospectroscopy offers a novel and low cost surrogate technique of determining a samples metabolomic profile. One study observed the 1545 cm^{-1} spectral band increasing in intensity in line with glomerular inflammation and treatment response. 1033 cm^{-1} was inversely related with the degree of fibrosis.

1.8 Hypothesis, Aims & Objectives

The advent of increasingly effective treatment strategies for AAV over the past three decades has been accompanied by a rising disease prevalence. The absence of a reliable biomarker to detect relapsing or persistent disease represents a significant unmet clinical need, risking increasing morbidity and mortality from suboptimal disease control or unnecessary patient exposure to potentially harmful therapy. This thesis aim to test the hypothesis that biospectroscopy can be applied to the field of AAV to provide a fast, non-invasive and effective biomarker of disease activity.

Specific aims of the study are as follows:

- I. To apply ATR-FTIR and Raman spectroscopy to plasma, serum and urine samples in order to accurately distinguish active disease from remission

- II. Classify and compare attained spectra from biofluids to relevant control groups

- III. To apply Raman spectroscopy to renal tissue with differentiation of acquired spectral data according to histological classification and comparative analysis against the spectra attained from paired urine samples at the time of biopsy; thereby determining their potential use as a non-invasive surrogate marker of histological activity in renal vasculitis, in effect providing a liquid biopsy.

Chapter 2: Materials & Methods

2.1 Patients & ethics

Over a fourteen-month period from February 2019 to March 2020, paired blood and urine samples were collected from consecutive patients with active AAV and those in disease remission for analysis by ATR-FTIR and Raman spectroscopy. For the purpose of renal tissue analysis by Raman spectroscopy, consecutive patients with active AAGN and those in disease remission were recruited between February and August 2019. For those in disease remission at the time of recruitment, where available archived renal tissue samples taken at the time of initial diagnosis and held by the tissue bank at Royal Preston Hospital were obtained. For those patients with active disease at the time of recruitment, renal tissue samples along with paired urine samples taken immediately prior to renal biopsy were collected.

The active disease cohort consisted of patients with new presentation or relapsing disease. The definition of AAV as outlined by the 2012 Chapel Hill Consensus Conference was used. As the histological confirmation of disease is often not a viable diagnostic tool in the context of extra-renal disease and a reference standard test with a sufficient degree of sensitivity and specificity is lacking in such cases, the index test of ATR-FTIR spectroscopy and Raman spectroscopy were evaluated in the context of this widely used criterion as reference standard for clinical diagnosis. Patients who did not meet this criterion, who were aged <18 years, unable to provide consent or exhibited dual positivity with anti-glomerular basement membrane disease were excluded. Disease remission was defined as a BVAS of 0. A significant difference in the spectral data amongst patients with and without active AAV was the primary outcome of interest. As this study is applying a novel and previously untested technology to this patient group a sample size could not be calculated. All participants were registered with the Department of Renal Medicine regional vasculitis service at Lancashire Teaching Hospitals NHS Foundation Trust, UK. Informed written consent was obtained prior to enrolment in accordance with study approval from the Health Research Authority, Cambridge South Research Ethics Committee (REC reference 18/EE/0194) and the Research and Development team in the Centre for Health Research and Innovation at Lancashire Teaching Hospitals NHS Foundation Trust. All enrolled participants were recorded on the Edge clinical research management system. All collected clinical data was pseudonymised and recorded separately using Microsoft Excel (Microsoft Corporation, USA). Data was held on computers in Lancashire Teaching Hospitals NHS Foundation Trust, with appropriate access control in place. All experiments were carried out in accordance with the relevant guidelines and regulations.

The following clinical data was collected at baseline assessment; demographics, clinical presentation, BVAS, histological evaluation of renal biopsies by a renal pathologist and salient laboratory results including ANCA serotype were applicable, serum creatinine, haemoglobin, white cell count, lymphocyte count, neutrophil count, platelet count, CRP, ESR and urine protein creatinine ratio (uPCR). Urine samples were sent for microscopy and culture to determine the presence of bacteriuria and its potential impact as a confounding factor on spectroscopic analysis. For patients with active disease, further biofluid samples were collected following successful remission induction therapy where possible for comparative analysis. Control groups for biofluid analysis included

membranous nephropathy, minimal change disease, IgA nephropathy, acute kidney injury (AKI) in the context of infection and healthy individuals. Participants in the healthy control group were not known to have renal impairment and had a normal dipstick urinalysis.

Recorded histological data included the assigned Berden classification (focal: $\geq 50\%$ normal glomeruli, crescentic: $\geq 50\%$ cellular crescents, sclerotic: $\geq 50\%$ globally sclerotic glomeruli and mixed: no predominant lesion) (6), the percentage of normal glomeruli (N0 $>25\%$, N1 10-25%, N2 $< 10\%$), the severity of IFTA (T1 $>25\%$, T0 $\leq 25\%$) and the presence of interstitial infiltrate, necrotising glomerular lesions, extra-glomeruli arteritis and vessel wall necrosis. The percentage of normal glomeruli and degree of IFTA was assessed according to the grading scale applied by Brix *et al* in the ANCA renal risk score (12).

2.2 Biofluid sample collection & preparation

Samples from participants with active disease were taken in both the outpatient clinic and acute in-patient setting. All remission and disease control samples were taken in the outpatient clinic. Healthy control samples were attained from individuals working in the hospital outside of the laboratory setting. Whole blood samples were collected in ethylenediaminetetraacetic acid (EDTA) and serum separator tubes. All blood and urine samples were centrifuged at 3000 rpm, 4°C for 10 minutes. The resulting plasma, serum and supernatant urine were collected in 0.5ml Eppendorf tubes and stored on site at -80°C. When required for experimentation samples were thawed at room temperature, after which 30 μ l aliquots were placed on IR-reflective aluminium coated FisherBrand slides and left to air dry for a minimum of 2 hours prior to spectroscopic analysis.

2.3 Tissue sample collection & preparation

Following their initial acquisition and departmental assessment, formalin-fixed paraffin-embedded tissue blocks were retrieved from the tissue bank at Royal Preston Hospital. To ensure close correlation between histopathology reports and spectroscopic measurements, contiguous sections of 10 μ m thickness were used from each tissue block. After sections had been cut and placed on IR-reflective aluminium coated FisherBrand™ slides, all samples were deparaffinised according to local protocols using xylene and ethanol in order to avoid any potential impact on the spectral data obtained.

2.4 ATR-FTIR spectral acquisition from biofluids

ATR-FTIR spectra were attained using a Bruker Tensor 27 FTIR spectrometer with Helios ATR attachment (Bruker Optics Ltd, Coventry UK), operated by OPUS 6.5 software. The sample area was defined by the diamond crystal internal reflective element, approximately 250 μ m by 250 μ m. Spectra were acquired from 10 locations on each sample; five central and five peripheral to help minimise any potential bias. Parameters for spectral acquisition consisted of 32 scans per location, 8 cm^{-1} spectral resolution with 2x zero-filling and 6mm aperture setting, yielding a data spacing of 4 cm^{-1} over 4000-400 cm^{-1} spectral range. The diamond crystal was cleaned with distilled water,

dried with Kimwipes and a background absorption spectra was taken at the start of each new sample analysis to account for atmospheric conditions.

2.5 Raman spectral acquisition from biofluid & renal tissue samples

Spectral data was attained using a Renishaw InVia Raman spectrometer in conjunction with a charge-coupled device and Leica confocal microscope (Renishaw pls UK). This system utilised a 200-mW laser diode at a wavelength of 785 nm with a grating of 1200 lines/mm. Renishaw WiRE™ was used to control data acquisition. The spectral range was set between 400 – 2000 cm^{-1} with a 1 cm^{-1} spectral resolution and extended grading scale.

For biofluid samples ten individual spectral points were taken per sample over a randomly selected acquisition area of 250 x 125 μm using 20x magnification, with 10% laser power and an exposure time of 10 seconds. Within each acquisition area four spectral points were taken along the superior horizontal plane, four along the inferior horizontal plane and two in the middle. Before measuring each sample batch, a Renishaw® silicon reference was measured to ensure signal consistence, where the resulting silicon peak signal centred at 520 cm^{-1} was consistently observed, thus indicating no spectral shift over time.

For tissue mapping spectral data was obtained over the entirety of a 1000 x 500 μm acquisition area, using 5 x magnification, 100% laser power, exposure time of 0.1 seconds with 5 x 5 steps in high confocality and spectral centre of 1300 cm^{-1} . Three select regions of interest where the highest number of glomeruli were visible within the acquisition area were analysed from each sample. For comparative analysis of tissue and urine samples one representative mean spectrum was subsequently generated per sample for later use in the analysis.

2.6 Spectral pre-processing

All spectral data were imported into MATLAB R2014b environment (MathWorks Inc., USA) for pre-processing and subsequent multivariate analysis. Following upload, three-dimensional (3D) Raman mapping images were unfolded into two-dimensional (2D) structures containing n rows (number of spectra) and m columns (number of wavenumbers).

Pre-processing consists of mathematical techniques employed to the raw spectral data to remove or reduce contributions of signals that are not related to the analyte target property or to the sample discrimination, hence, reducing chemically irrelevant variations in order to improve the accuracy and precision of qualitative and quantitative analyses (360). Initially raw spectral data attained by Raman spectroscopy was evaluated for anomalous spectra or biased patterns through a Hotelling's T^2 versus Q residuals chart (360). No outlier was identified, hence, no spectra were excluded from the analysis. Raw Raman spectral data was then cut between the 900 -1800 cm^{-1} spectral range with application of Savitzky-Golay 2nd order derivative (51 window points, 2nd order polynomial) smoothing to correct for random noise.

Herein, all raw spectral data attained by both Raman spectroscopy and ATR-FTIR were pre-processed by automatic weighted least squares (AWLS) baseline correction and vector normalisation to correct for baseline distortions and physical difference between samples (362).

2.7 Multivariate analysis

In order to identify any natural clustering patterns or trends in the data, principal component analysis (PCA) was used for initial exploratory analysis through 2D PCA plot scores on principal components (PCs) 1 and 2 (385). PCA is a multivariate technique of exploratory analysis and data reduction, in which the original variables such as spectral wavenumbers are reduced to a few number of PCs responsible for the majority of the original data variance. Each PC is composed of scores and loadings. The scores represent the variance on sample direction, thus being used to identify similarity/dissimilarity patterns between the samples. Whereas the loadings represent the variance on the variable direction, thus being used to identify possible spectral markers responsible for the patterns observed on the scores plot.

2.7.1 Chemometric models for analysis of biofluids

For biofluid sample analysis, partial least squares discriminant analysis (PLS-DA) was employed for supervised classification, differentiating the spectral data according to the experimental classes. Prior to model construction by partial PLS-DA, the pre-processed data are mean-centred. All models were trained and tested with pre-processed data only.

PLS-DA is an established chemometric technique based on a PLS decomposition of the dataset (18). In PLS, the dataset is decomposed into a few latent variables (LVs) responsible for maximizing the covariance between the spectral data and the response information, which in this case is the disease category. Then, a straight line that divides the projected classes' spaces is delineated maximizing the classes separation (386). Following this, the pre-processed data were split into training and test (external validation) sets using the Morais-Lima-Martin algorithm (363). The training set consisted of 60% of the samples for model construction, with the optimisation step of defining the number of LVs for PLS-DA via venetian blind cross-validation to prevent overfitting. The remaining 40% of samples were used as the test set for blind predictive modelling to evaluate the classification systems performance. The spectral replicas per sample were averaged prior to model construction so the model was constructed on a sample-basis, hence, with no overlap of samples between the training and test sets.

2.7.2 Chemometric models for comparative analysis of tissue & urine samples

For comparative analysis of tissue and urine samples, in each model the spectral data from both tissue and urine samples was segregated according to the presence of recorded histological data to generate the experimental classes of the assigned Berden classification (focal, crescentic, sclerotic and mixed) (247), the percentage of normal glomeruli (N0 >25%, N1 10-25%, N2 <10%), the severity of IFTA (T1 >25%, T0 ≤25%) and the presence of interstitial infiltrate, necrotising glomerular lesions, extra-glomerular arteritis and vessel wall necrosis. A lower

proportion of normal glomeruli indicates greater disease burden with their composition guiding the degree of acute disease vs. chronicity. A higher burden of IFTA and sclerosed glomeruli represent chronic damage, whereas the remaining lesions described are indicative of active disease. An experimental class according to ANCA seropositivity and in positive cases ANCA serotype were also generated. For each, the total data obtained were used to build the models, without dividing samples by selection methods due to the limited sample availability in certain classes. The models were evaluated using the venetian blinds cross-validation method. Analysis of the spectral mean was used as the test set for blind predictive modelling. These test samples are independent from training data as they are not used in the model training process and are considered new data to the model. The overall performance of each discriminant analysis algorithm was then compared.

The discriminant analysis algorithms of principal component analysis linear discriminant analysis (PCA-LDA), PLS-DA, support vector machines (SVM) and genetic algorithm linear discriminant analysis (GA-LDA) were applied to the pre-processed data for supervised classification. Models were constructed using the PLS Toolbox and Classification Toolbox graphical user interface of the Milano Chemometrics group (387). For supervised classification by PLS-DA the dataset was broken down into a few LVs responsible for maximizing the covariance between the spectral data and the response information, which in this the case is the histological or serological category. The number of latent variables was determined by the leave-one-out type cross-validation to prevent overfitting. The key distinguishing spectral peaks were then identified using the PLS-DA coefficient. While PCA and PLS perform a reduction in the number of original variables generating another set of variables, the genetic algorithm (GA) selects the most important variables based on a selection, recombination and mutation of a set of the original variables. Thus, its main objective is to reduce the number of variables, taking advantage of not changing the type of variable and original information according to an adjustment function. The GA routine was carried out during 100 generations with 200 chromosomes each. Mutation and crossover probabilities were adjusted to 10% and 60% respectively. The best solution set for this algorithm is based on the fitness value. The adjustment function is calculated as the inverse of the cost function G , which can be defined as follows:

$$G = \frac{1}{N_V} \sum_{n=1}^{N_V} g_n \quad (1)$$

Where N_V is the number of validation samples and g_n is defined as follows:

$$g_n = \frac{r^2(x_n, m_{I(n)})}{\min_{I(m) \neq I(n)} r^2(x_n, m_{I(m)})} \quad (2)$$

Where the numerator is the squared Mahalanobis distance between object x_n of class index $I(n)$ and the sample mean $m_{I(n)}$ of its true class; and the denominator is the squared Mahalanobis distance between object $x(n)$ and the centre of the closest wrong class.

The classifiers used here were LDA and SVM. LDA is based on the Mahalanobis distance between samples and considers that all classes have a similar variance structure, building a model based on pooled covariance matrix. The input data used for LDA are scores obtained via PCA. The LDA classifier, non-Bayesian form, can be obtained by the following equation for a sample i in a given class k :

$$L_{ik} = (\mathbf{x}_i - \bar{\mathbf{x}}_k)^T \mathbf{C}_{\text{pooled}}^{-1} (\mathbf{x}_i - \bar{\mathbf{x}}_k) \quad (3)$$

Where \mathbf{x}_i is a vector with variables for sample i ; $\bar{\mathbf{x}}_k$ is the mean of class k ; and $\mathbf{C}_{\text{pooled}}$ is the pooled covariance matrix between the classes.

SVM is a machine learning technique that uses the kernel transformation (388). This projects data in a non-linear fashion into a feature dimension to provide the radial basis function (RBF) and classify samples according to a linear threshold. This has the advantage of being able to adjust for different data distributions to provide a more powerful discriminant analysis but may carry a higher risk of overfitting. The RBF is calculated as follows:

$$k(\mathbf{x}_i, \mathbf{z}_j) = \exp(-\gamma \|\mathbf{x}_i - \mathbf{z}_j\|^2) \quad (4)$$

Where \mathbf{x}_i and \mathbf{z}_j are sample measurements vectors, and γ is a tuning parameter that controls the RBF width. In the RBF function, the γ parameter was set to 1. The SVM classification is obtained by the following equation:

$$f(x) = \text{sign}(\sum_{i=1}^{N_{SV}} \alpha_i y_i k(\mathbf{x}_i, \mathbf{z}_j) + b) \quad (5)$$

Where N_{SV} is the number of support vectors; α_i is the Lagrange multiplier; y_i is the class membership, ranging from -1 to +1; $k(\mathbf{x}_i, \mathbf{z}_j)$ is the kernel function and b is the bias parameter. The parameters used were obtained through an internal validation dataset.

2.8 Model validation

Calculation of accuracy, sensitivity, specificity, G-scores and F-scores for the test set was used for model validation. Accuracy represents the total number of samples correctly classified, considering true and false negatives. The proportion of disease remission and active disease samples correctly classified represents the sensitivity and specificity respectively. The G-score is a metric that is used to evaluate the models performance independent of class size, whereas the F-score measures a models performance considering imbalanced data (389). The statistical parameters presented can be calculated as follows:

$$AC(\%) = \left(\frac{TP+TN}{TP+FP+TN+FN} \right) \times 100$$

$$SENS(\%) = \left(\frac{TP}{TP+FN} \right) \times 100$$

$$\text{SPEC}(\%) = \left(\frac{\text{TN}}{\text{TN} + \text{FP}} \right) \times 100$$

$$\text{F-score} = \frac{2 \times \text{SENS} \times \text{SPEC}}{\text{SENS} + \text{SPEC}}$$

$$\text{G-score} = \sqrt{\text{SENS} \times \text{SPEC}}$$

Where FN stands for false negative, FP for false positive, TP for true positive, TN for true negative, AC for accuracy, SENS for sensitivity, SPEC for specificity, Fs for F-score and Gs for G-Score. Herein, although both were derived from the same experiment, the test samples are independent from the training samples. The validation performance depicted here are ideal for small datasets in order to have a good approximation of the real blind performance (360). For a further model validation it would be necessary to realise a second experiment with completely new samples in order to assess the blind model performance.

2.9 Correlation with clinical variables

Correlation between the pre-processed spectra attained by ATR-FTIR and individual clinical variables was evaluated by PLS regression (for continuous variables) and PLS-DA (for categorical variables). PLS and PLS-DA models were built using cross-validation. The association between spectra and a clinical variable was evaluated by assessing the determination coefficient (R^2) and root mean square error of cross-validation (RMSECV). Clinical parameters for which the R^2 was low, or RMSECV elevated, were considered to have poor correlation with the spectral data.

Chapter 3: Results

3.1 Study population

3.1.1 Biofluid samples

One hundred and eight participants were enrolled; 25 with active disease (AD), 38 in disease remission (DR), 10 with membranous nephropathy (MM), five with minimal change disease (MCD), 10 with IgA nephropathy, 10 with pre-renal AKI in the context of infection and 10 healthy controls (HC). Descriptive baseline characteristics for the active and remission disease cohorts are shown in Table 5. Amongst these two groups, overall mean age was 66 ± 11.9 years with no significant gender predominance. The majority were Caucasian, with only one South-Asian participant in the remission cohort. Baseline characteristics for the disease control groups are outlined in Appendix 1 (A1), Supplementary Information (SI) Table S1. All cohort samples were analysed by ATR-FTIR spectroscopy, whereas only those with active AAV, disease remission and healthy control were analysed by Raman spectroscopy.

The AD cohort was comprised of 80% (n=20) newly diagnosed cases and 5 (n=20%) patients with relapsing disease. Amongst this group 16% (n=4) had undetectable circulating ANCA, 68% (n=17) had multisystem disease and of the remaining 32% (n=8) with single organ disease, 4 were renal limited, 3 were limited to ear nose and throat disease and one had ophthalmic disease. Amongst the remission cohort 52% (n=20) had persisting positive ANCA serology despite clinically quiescent disease. Overall two patients died, both in the AD cohort and both due to infection. No patients were lost to follow up. Following successful remission induction therapy, paired remission samples were collected from 14 patients in the AD cohort for comparative analysis. Amongst this group the majority (n=13) were ANCA positive at initial diagnosis, of which six remained ANCA positive at the time of paired remission sample collection. Inclusive of these patients, of the total number of number of remission samples included for analysis, 50% (n=26) had detectable circulating ANCA despite clinically quiescent disease.

Table 5: Characteristics of study population at the time of enrolment for biofluid analysis		
	Active Disease (n=25)	Disease Remission (n=38)
Mean Age (SD)	64 \pm 11.9	67 \pm 11.9
Sex		
Male	12/25 (48%)	20/38 (53%)
Female	13/25 (52%)	18/38 (47%)
Median serum creatinine ($\mu\text{mol/L}$)	216 (347-132)	122 (174-94)
Mean eGFR (mls/min/1.73m ²)	22 (48-8)	47 (65-29)
Newly diagnosed disease	20/25 (80%)	-
Relapsing disease	5/25 (20%)	-
ANCA serotype		
MPO	9/25 (36%)	6/38 (16%)
PR3	12/25 (48%)	14/38 (37%)
Negative	4/25 (16%)	18/38 (47%)

BVAS	16 ±9.6	0
Organ involvement		
Constitutional signs or symptoms	15/25 (60%)	-
Mucous membranes / Ophthalmic	6/25 (24%)	-
Cutaneous	1/25 (4%)	-
ENT	12/25 (48%)	-
Respiratory	6/25 (24%)	-
Cardiovascular	1/25 (4%)	-
Gastrointestinal	0	-
Renal	18/25 (72%)	-
Neurological	5/25 (20%)	-
Multisystem disease	17/25 (68%)	-
Renal limited	4/25 (16%)	-
Other Laboratory Salient Laboratory Results:		
Mean Haemoglobin (g/L)	100 ± 28.3	130 ± 13.4
Mean White cell count (10 ⁹ /L)	9 ± 3.7	7.2 ± 2.2
Mean Lymphocyte count (10 ⁹ /L)	1.2 ± 0.7	1.3 ± 0.6
Mean Neutrophil count (10 ⁹ /L)	7 ± 3.6	5.1 ± 2.2
Mean Platelet count (10 ⁹ /L)	309 ± 143.5	270 ± 80.6
Median CRP (mg/L)	42 (64.8-4.8)	2.6 (5.3-1.2)
Median ESR (mm/hr)	42 (80.5-9)	12 (19.8-5)
Median ESR (mm/hr)	42 (80.5-9)	12 (19.8-5)
Mean serum albumin (g/L)	34.7 ±7.3	44.4 ±2.9
Mean serum total protein (g/L)	62 ± 9.8	67.1 ± 4.7
Co-morbidities		
Ischaemic heart disease	1 (4%)	4 (11%)
Congestive cardiac failure	0	1 (3%)
Cerebrovascular disease	1 (4%)	2 (5%)
Hypertension	5 (20%)	18 (47%)
Peripheral vascular disease	0	1(3%)
Diabetes Mellitus	2 (8%)	3 (8%)
Chronic pulmonary disease	6 (24%)	5 (13%)
Chronic liver disease	0	0
Connective tissue disease	1 (4%)*	0
Malignancy	2 (8%)**	1 (3%)*
Immunosuppression		
None	8 (26%)	7 (18%)
Prednisolone****	14 (56%)	15 (39%)
Methylprednisolone	7 (28%)	0
Rituximab within the preceding 6 months	1 (4%)	13 (34%)
Cyclophosphamide	2 (8%)	2 (5%)
Azathioprine	0	6 (16%)
Mycophenolate	0	4 (11%)
Methotrexate	0	1 (3%)

eGFR, estimated glomerular filtration rate; ANCA, anti-neutrophil cytoplasmic autoantibody; MPO, myeloperoxidase; PR3, proteinase-3; ESR, erythrocyte sedimentary rate; CRP, C-reactive protein

*One case of rheumatoid arthritis in remission, **One case of non-metastatic prostate cancer in remission & one case of colonic tubular adenoma, ***One case of non-melanoma skin cancer, **** Amongst the remission cohort a daily dose of prednisolone ≥5mg was considered significant

3.1.2 Renal tissue & paired urine samples

Over the 6-month study period 28 patients were recruited; 11 with new presentation AAGN and 17 currently in disease remission. One patient was excluded due to the development of dual positivity with anti-glomerular basement autoantibodies. Table 6 outlines the characteristics of the overall study population. Recently processed and archived renal tissue samples taken at the time of active disease were obtained for all remaining 27 participants, with paired urine samples prior to biopsy in all ten cases of newly presenting AAGN.

Amongst those participants with a paired urine sample at the time of renal biopsy (n=10), mean age was 63 ± 7.6 with 80% (n=8) female predominance, median serum creatinine of $282 \mu\text{mol/L}$ (IQR 447-201) and 90% (n=9) seropositivity; four with anti-MPO and five with anti-PR3 associated disease. The mean number of glomeruli per biopsy sample was 19 ± 9 , with a distribution of disease of 50% (n=5) focal, 40% (n=4) mixed and 10% (n=1) crescentic according to the Berden classification system (247). The proportion of samples with >25% normal glomeruli (grade N0) was 70% (n=7) and 30% (n=3) exhibited <10% (grade N2) normal glomeruli. A similar distribution for IFTA was seen; 70% (n=7) $\leq 25\%$ (grade T0) and 30% (n=3) >25% (grade T1). The observed frequency of necrotising glomerular lesions and interstitial infiltrate were 30% (n=3). For extra-glomerular arteritis and vessel wall necrosis 20% (n=2) were affected. The median uPCR and urine white cell count was 89 mg/mmol (IQR 258-63) and $31 \times 10^9/\text{L}$ (IQR 34-27) respectively. None of the collected urine samples displayed any bacterial growth.

Table 6: Characteristics of study population at the time of enrolment for renal tissue analysis	
	AAGN (n=27)
Mean Age (SD)	63 ± 10
Sex	
Male	15/27 (55.6%)
Female	12/27 (44.4%)
Median serum creatinine at biopsy ($\mu\text{mol/L}$)	215 (338-164)
Median eGFR at biopsy ($\text{mls/min}/1.73\text{m}^2$)	22 (33-12)
ANCA serotype at biopsy	
MPO	12/27 (44.4%)
PR3	12/27 (44.4%)
Negative	3/27 (11.1%)
Mean number of glomeruli per biopsy sample	20 ± 9
Berden classification	
Focal	15/27(55.6%)
Crescentic	3/27 (11.1%)
Sclerosed	0
Mixed	9/27 (33.3%)
Normal glomeruli	
N0 (> 25%)	21/27 (77.8%)
N1 (10-25%)	2/27 (7.4%)
N2 (<10%)	4/27 (14.8%)
IFTA	
T0 ($\leq 25\%$)	20/27 (74.1%)
T1 (>25%)	7/27(25.9%)
Necrotising glomerular lesions	16/27 (29.3%)
Interstitial infiltrate	10/27 (37%)
Extra-glomerular arteritis	5/27 (18.5%)
Vessel wall necrosis	4/27 (14.8%)

ANCA, anti-neutrophil cytoplasmic autoantibody; MPO, myeloperoxidase; PR3, proteinase-3; IFTA, interstitial fibrosis

3.2 Biofluid sample analysis by ATR-FTIR spectroscopy

3.2.1 Spectral data and classification models

ATR-FTIR spectrochemical interrogation of plasma samples yielded the highest degree of accuracy for discrimination between AD and DR, followed by serum and urine sample analysis respectively. Plasma sample data is presented below, with serum and urine datasets provided in A1 SI.

Figures 7a and 7b show the raw and pre-processed IR absorption spectra attained from plasma samples between the 900-1800 cm^{-1} spectral range for participants with AD and DR. Spectra initially appear to overlap. Given that a vast majority of constituent biomolecules present in plasma will be common to most individuals, this would be expected. Following second order differentiation to resolve overlapping peaks, multivariate analysis using PCA exhibits good separation between AD and DR on PC2 direction (Figure 7c). A subsequent supervised classification model using PLS-DA was undertaken (Figure 7d). In this process 60% of samples with known categories of either AD or DR were used as a training set to generate the classification model, with cross validation to prevent overfitting and blind assessment of the remaining 40% of samples to test the models predictive performance. The receiver operating characteristic (ROC) curve (Figure 7e) demonstrates excellent ability of ATR-FTIR spectroscopy to distinguish between AD and DR using this classification system with an area under the curve of 0.901. This predictive classification model is shown in Table 7, with 100% sensitivity (F-score 92.3%) for DR and 85.7% specificity (F-score 92.3%) for correctly identifying AD.

Following successful remission induction therapy, analysis of paired remission samples revealed similar findings with good ability to discriminate AD and DR; PLS-DA AUC >0.9 (Figure 8) and 100% sensitivity (F-score 75%) for DR on predictive modelling (Table 8). There is a high level of accuracy in distinguishing AD from healthy controls (Figure 9b, 9c and Table 9). On PCA scores of HC and DR, there was no clear segregation pattern between the two groups on PC2 direction following removal three outlier spectra from the HC cohort (Figure 9e). Subsequent analysis of all participants in disease remission (n=52), inclusive of those in remission at the time of study enrolment (n=38) and paired remission samples (n=14), confirmed excellent separation of spectral data from all control groups (see A1 SI, Figure S2e, 2f and Table S2). There was equally good separation of AD from all control groups (see A1 SI, Figure S2b, 2c and Table S2).

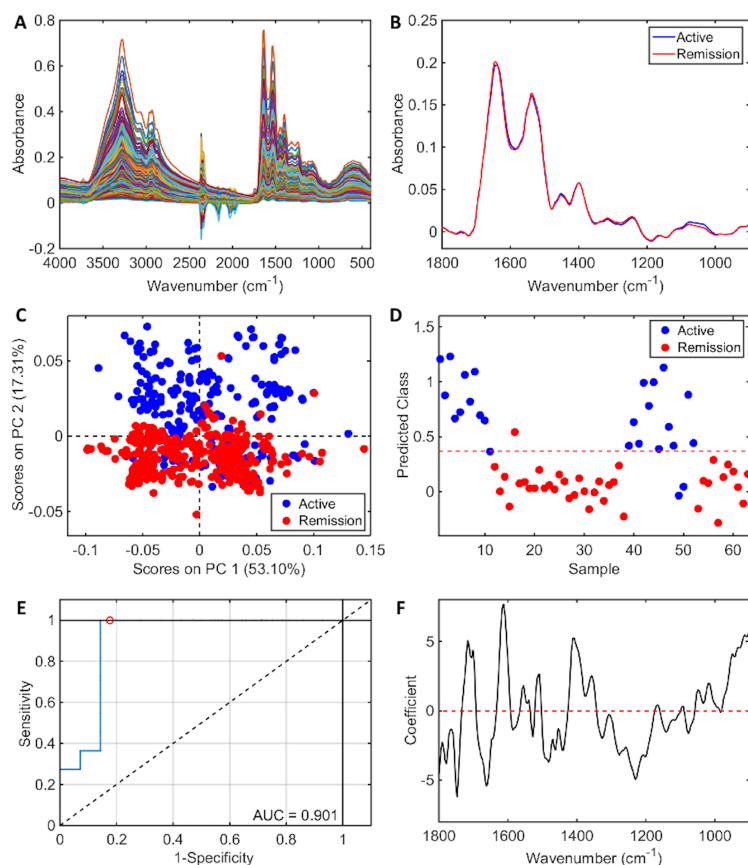


Figure 7: ATR-FTIR spectral classification of active disease vs. disease remission for plasma samples - (A) Raw spectral data (B) Pre-processed spectra (C) PCA scores plot (D) PLS-DA discriminant function graph (E) ROC curve for PLS-DA (F) PLS-DA coefficients for identification of spectral biomarkers

Table 7: Classification parameters for plasma samples in active disease (AD) vs. disease remission (DR)				
AD vs. DR	Accuracy (%)	Sensitivity (%)	Specificity (%)	F-Score (%)
Training (5 LVs)	93.6	96.3	90.9	93.5
Cross-validation	91.7	92.6	90.9	91.7
Test	92.8	100	85.7	92.3

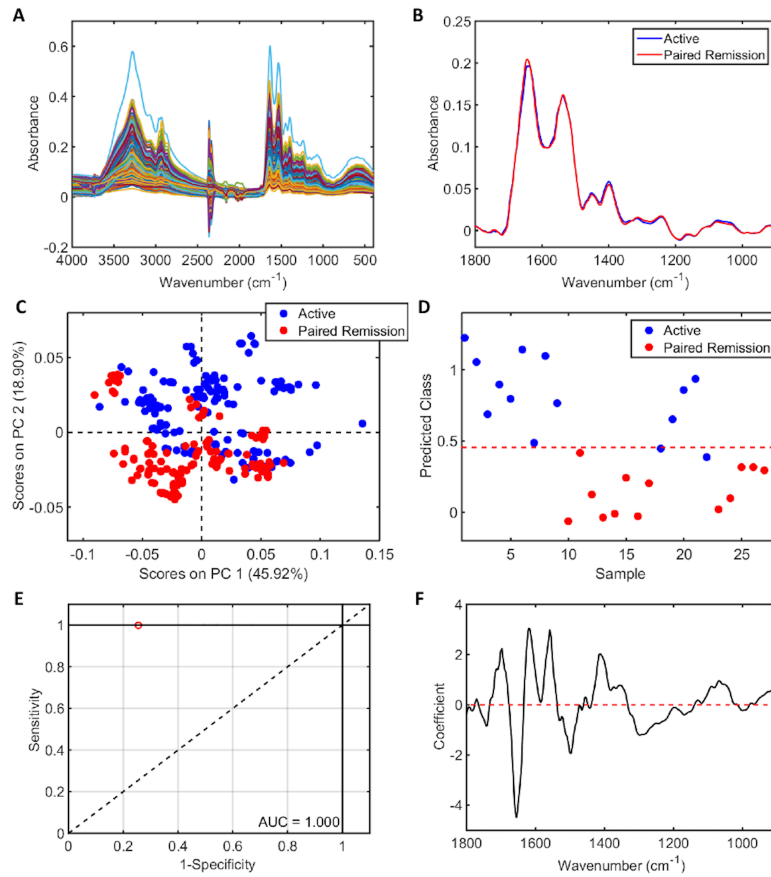


Figure 8: ATR-FTIR spectral classification of active disease vs. paired remission for plasma samples following successful remission induction therapy - (A) Raw spectral data (B) Pre-processed spectra (C) PCA scores plot (D) PLS-DA discriminant function graph (E) ROC curve for PLS-DA (F) PLS-DA coefficients for identification of spectral biomarkers

Table 8: Classification parameters for plasma samples in active disease (AD) vs. paired remission (PR)				
AD vs. PR	Accuracy (%)	Sensitivity (%)	Specificity (%)	F-Score (%)
Training (2 LVs)	100	100	100	100
Cross-validation	82.6	87.5	77.8	82.4
Test	80.0	100	60.0	75.0

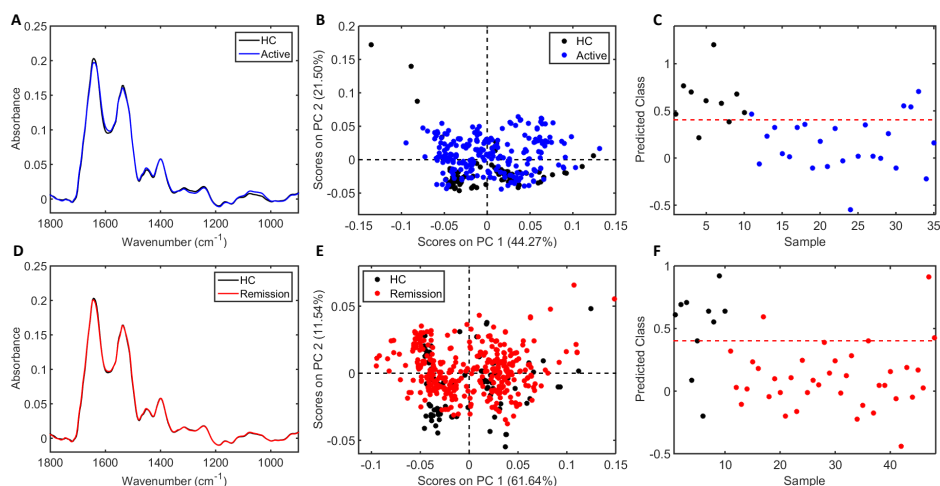


Figure 9: ATR-FTIR spectral classification of healthy controls (HC) vs. active disease (AD) & healthy controls (HC) vs. disease remission (DR) for plasma samples – (A) Average pre-processed spectral points for HC (n=100) & patients with AD (n=250) (B) PCA scores plot for HC & AD (C) PLS-DA discriminant function graph for classification of HC & AD using cross validation (D) Average pre-processed spectral points for HC (n=100) & DR (n=380) (E) PCA scores plot for HC & DR (F) PLS-DA discriminant function graph for classification of HC & DR using cross validation

Table 9: Classification parameters for plasma samples in healthy controls (HC) vs. active disease (AD) and disease remission (DR)

	Accuracy (%)	Sensitivity (%)	Specificity (%)	F-Score (%)
HC vs. AD				
Training (4 LVs)	94.0	88.0	100	93.6
Cross-validation	82.0	84.0	80.0	82.0
HC vs. DR				
Training (3 LVs)	92.3	94.7	90.0	92.3
Cross-validation	81.0	92.1	70.0	79.5

3.2.2 Correlation with clinical parameters

The correlation between ATR-FTIR spectral data for plasma and relevant clinical variables amongst those with AD is shown in Table 10. Based on the R^2 , other than serum albumin and total protein, there is no demonstrable significant correlation shown and the ability of ATR-FTIR spectroscopy to accurately discriminate between AD and DR was independent of organ system involvement, detectable circulating ANCA, ANCA titre in cases of seropositive disease, renal function, commonly used markers of inflammation and other salient laboratory results. There was no significant correlation between spectral data and BVAS, a validated and widely applied clinical assessment tool of disease severity. Correlation between ATR-FTIR spectral data for plasma and relevant clinical variables amongst those with DR is shown in A1 SI Table S3. This confirmed no significant findings. The sensitivities and specificities provided in both tables only relates to the ability to separate the two groups. It was not possible to calculate these respective values for age, BVAS ANCA titre and other routine salient laboratory results, as these are variables with defined numerical values for which discriminatory algorithms could not be executed.

Treatment data at the time of sample collection is outlined in Table 5. The varied distribution of therapy provided the opportunity to tentatively determine the impact of immunosuppression on spectral analysis independently of the effects of disease activity. Of the 56% (n=14) of patients in the AD cohort and 39% (n=15) in the DR cohort on prednisolone, the median daily dose was 40 mg (IQR 60-20) and 5 mg (IQR 10-5) respectively. Neither dosing regimens accounted for any difference in data variance (see A1 SI, Figures S3 & S4). Similarly, rituximab exposure up to six months prior to sample collection did not influence spectral analysis in the DR cohort (see A1 SI, Figure S5). Meaningful subgroup analysis evaluating the impact of methylprednisolone, cyclophosphamide, azathioprine, methotrexate and mycophenolate were not feasible owing to the limited sample size of each subgroup.

Table 10: Comparative analysis between clinical variables and ATR-FTIR spectral data from plasma samples

Active disease	Sensitivity of clinical variable	Specificity of clinical variable	Coefficients of determination (R ²)
Age	-	-	0.01
Gender	0.75	0.77	0.29
BVAS	-	-	0.19
Organ involvement:			
Constitutional signs or symptoms	0.60	0.60	0.00
Mucous Membrane / Ophthalmic	0.58	0.50	0.12
Cutaneous	0.83	1.00	0.02
ENT	0.39	0.67	0.14
Respiratory	0.58	0.50	0.02
Cardiovascular	1.00	1.00	0.00
Renal	1.00	0.94	0.52
Neurological	0.50	0.20	0.04
ANCA Positivity	0.67	0.75	0.06
ANCA Serotype			
MPO	0.44	0.50	0.00
PR3	0.67	0.38	0.01
Negative	0.75	0.71	0.02
ANCA titre	-	-	0.12
Serum creatinine (µmol/L)	-	-	0.27
eGFR(mls/min/1.73m²)	-	-	0.45
Haemoglobin	-	-	0.51
White cell count	-	-	0.51
Lymphocyte count	-	-	0.24
Neutrophil count	-	-	0.52
Platelet count	-	-	0.08
CRP	-	-	0.18
ESR	-	-	0.29
Serum albumin	-	-	0.86
Total protein	-	-	0.65

ENT, ear nose and throat; ANCA, anti-neutrophil cytoplasmic autoantibody; MPO, myeloperoxidase; PR3, proteinase-3; BVAS, Birmingham vasculitis activity score; eGFR, estimated glomerular filtration rate; ESR, erythrocyte sedimentary rate; CRP, C-reactive protein

3.2.3 Key spectral biomarkers

Key distinguishing peaks can be identified amongst the spectral data in each model based on PLS-DA coefficients. The wavenumber-variables responsible for largest between group differences provide biomarker extraction through the chemical bond they represent, which in turn can be associated with a particular cellular activity. Amongst AD and HC cohorts, wavenumber-variables 1612 cm^{-1} (adenine vibration in DNA) and 1040 cm^{-1} (symmetric PO_2^- stretching in RNA/DNA) were both higher in AD, whereas 1540 cm^{-1} (protein Amide II β -sheet) was higher in HC (Figure 10).

Notable wave-number variables characterising AD from DR and their potential corresponding chemical bonds are outlined in Table 11. Noteworthy peaks for AD were in the $1620 - 1716\text{ cm}^{-1}$ range, representing nucleobase functional group expression as the main contributors; 1620 cm^{-1} (base carbonyl stretching and ring breathing mode of nucleic acids), 1698 cm^{-1} ($\text{C}_2=\text{O}$ guanine), 1701 cm^{-1} ($\nu(\text{C}=\text{O})$ thymine) and 1716 cm^{-1} ($\nu(\text{C}=\text{O})$ DNA/RNA). Lipid (1748 cm^{-1} , 1778 cm^{-1}) and protein functional groups at the Amide I (1662 cm^{-1}) and Amide II (1481 cm^{-1}) bands were associated with disease remission.

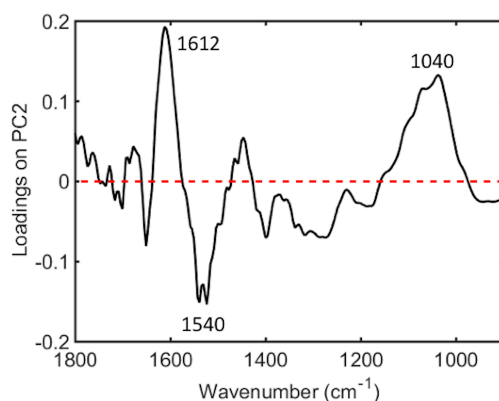


Figure 10: Main band differences for healthy controls (HC) vs. active disease (AD) using PCA loadings on PC2 from plasma samples - 1612 cm^{-1} (higher in AD, adenine vibration in DNA), 1540 cm^{-1} (higher in HC, protein Amide II β -sheet), 1040 cm^{-1} (higher in AD, symmetric PO_2^- stretching in RNA/DNA).

Table 11: Potential spectral biomarkers for distinguishing active disease and disease remission using plasma samples based on the PLS-DA coefficients (ν = stretching; δ = bending)

Wavenumber (cm ⁻¹)	Tentative assignment	Influence on AD
1778	ν (C=C) lipids	↓
1748	ν (C=C) lipids	↓
1716	ν (C=O) DNA/RNA	↑
1701	ν (C=O) thymine	↑
1662	Amide I	↓
1509	In-plane δ (CH) phenyl ring	↑
1481	Amide II	↓
1408	δ (CH ₃)	↑
1358	ν (C-O), δ (CH), δ (NH)	↑
1230	ν_{as} (PO ₂ ⁻)	↓
948	Phosphodiester region (collagen and glycogen)	↑
914	Phosphodiester region (collagen and glycogen)	↑
1698	C ₂ =O guanine	↑
1654	C=O, C=N, N-H of adenine, thymine, guanine, cytosine	↓
1620	Base carbonyl stretching and ring breathing mode of nucleic acids	↑
1558	Ring base mode	↑
1415	CH deformation	↑

3.3 Biofluid sample analysis by Raman spectroscopy

3.3.1 Spectral data & classification models

Spectral data from plasma and serum samples demonstrated equal efficacy in distinguishing active disease from remission. Figures 11A-1B & 12A-2B show the raw and average pre-processed data within the 900 – 1800 cm⁻¹ spectral range from plasma and serum samples respectively. Savitzky-Golay smoothing, baseline correction and vector normalisation was performed to reduce spectral interferences, such as noise and baseline distortions, hence highlighting the analytical information used to identify key discriminatory spectrochemical signatures. Following this, initial data exploration without prior sample knowledge showed reasonable separation between AD and DR amongst both biofluids (Figures 11C & 12C). Application of discriminant analysis through PLS-DA algorithm and subsequent blind predictive modelling of the remaining pre-processed data demonstrated excellent cluster separation and outstanding ability to distinguish between to AD and DR (Figures 11D & 12D). The diagnostic ability of this classification model is evident with an F-score of 80% for plasma (specificity 93.3%, sensitivity 70%, AUC 0.95) and 80% for serum (specificity 80%, sensitivity 80%, AUC 0.92) (Tables 12 & 13). Similar findings were observed following successful remission induction therapy and comparative analysis of paired remission samples (Figures 13 & 14, Tables 14 & 15). Discriminatory analysis showed excellent ability to distinguish healthy controls from both AD and DR cohorts (AUC 1) [see Appendix 2 (A2) SI; Figures 1 & 3, Tables 1 & 2].

Spectral data attained from urine samples are shown in A2 SI with overall poor ability to differentiate between active and quiescent disease, as well as healthy controls. This may have been contributed to in part by the presence of renal vasculitis in only 75% (n=18) of participants with active disease, of which only 60% (n=15) were able to provide a urine sample for analysis.

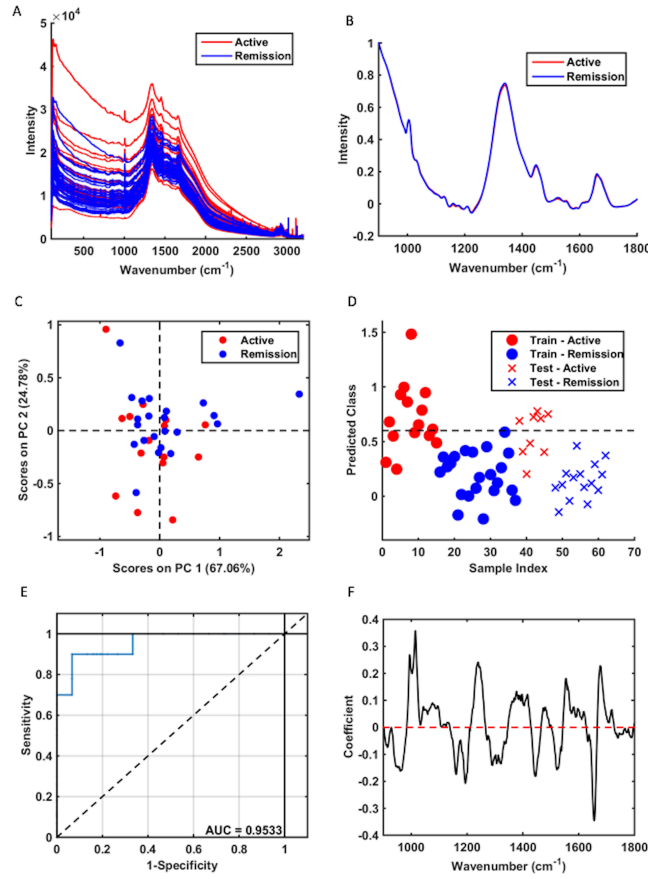


Figure 11: Raman spectral data for classification of active disease vs. disease remission for plasma samples - (A) Raw spectral data (B) Average pre-processed spectra (C) PCA scores plot (D) PLS-DA discriminant function graph (E) ROC curve for PLS-DA (F) PLS-DA coefficients for identification of spectral biomarkers.

Table 12: Classification parameters for plasma samples in active disease (AD) vs. disease remission (DR)

AD vs. DR	Accuracy (%)	Sensitivity (%)	Specificity (%)	G-Score (%)	F-Score (%)
Training (3 LVs)	88.8	86.7	90.9.	88.8	88.8
Cross-validation	78.7	80	77.3	78.6	78.6
Test	81.7	70	93.3	80.8	80

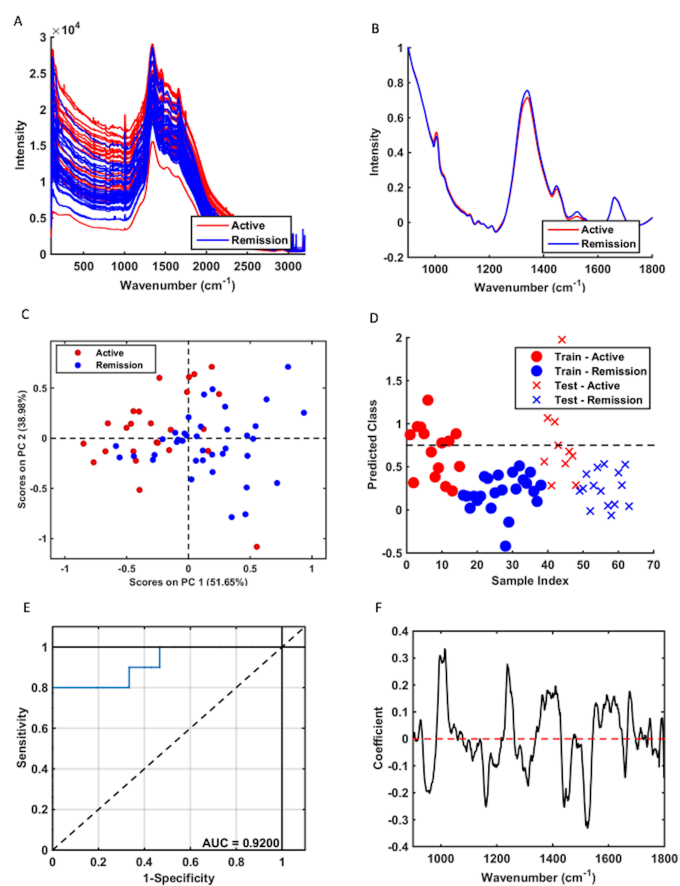


Figure 12: Raman spectral data for classification of active disease vs. disease remission for serum samples - (A) Raw spectral data (B) Average pre-processed spectra (C) PCA scores plot (D) PLS-DA discriminant function graph (E) ROC curve for PLS-DA (F) PLS-DA coefficients for identification of spectral biomarkers.

Table 13: Classification parameters for serum samples in active disease (AD) vs. disease remission (DR)

AD vs. DR	Accuracy (%)	Sensitivity (%)	Specificity (%)	G-Score (%)	F-Score (%)
Training (3 LVs)	84.5	73.3	95.7	83.8	83
Cross-validation	71.3	60	82.6	70.4	69.5
Test	80	80	80	80	80

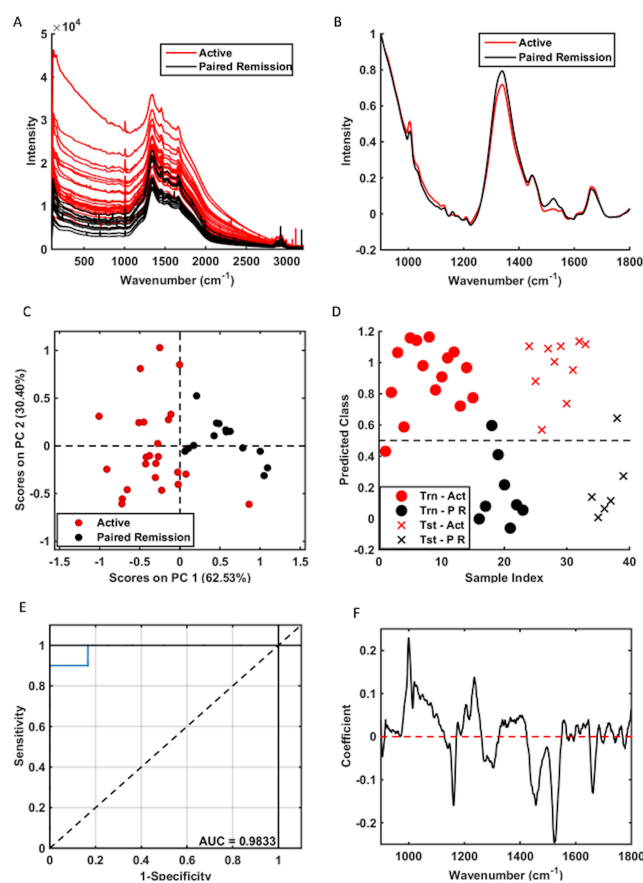


Figure 13: Raman spectral data for classification of active disease vs. paired remission for plasma samples following successful remission induction therapy - (A) Raw spectral data (B) Pre-processed spectra (C) PCA scores plot (D) PLS-DA discriminant function graph (E) ROC curve for PLS-DA (F) PLS-DA coefficients for identification of spectral biomarkers.

Table 14 Classification parameters for plasma samples in active disease (AD) vs. paired remission (PR)

AD vs. PR	Accuracy (%)	Sensitivity (%)	Specificity (%)	G-Score (%)	F-Score (%)
Training (3 LVs)	90.4	93.3	87.5	90.4	90.3
Cross-validation	87.1	86.7	87.5	87.1	87.1
Test	91.7	100	83.3	91.3	90.9

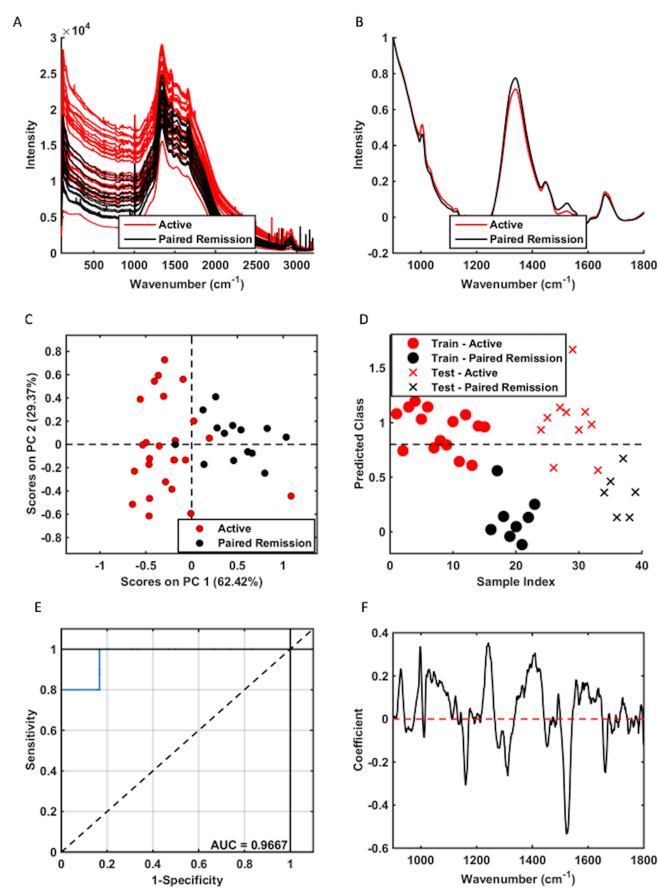


Figure 14: Raman spectral data for classification of active disease vs. paired remission for serum samples following successful remission induction therapy - (A) Raw spectral data (B) Pre-processed spectra (C) PCA scores plot (D) PLS-DA discriminant function graph (E) ROC curve for PLS-DA (F) PLS-DA coefficients for identification of spectral biomarkers.

Table 15: Classification parameters for serum samples in active disease (AD) vs. paired remission (PR)					
AD vs. PR	Accuracy (%)	Sensitivity (%)	Specificity (%)	G-Score (%)	F-Score (%)
Training (3 LVs)	93.8	100	87.5	93.5	93.3
Cross-validation	87.1	86.7	87.5	87.1	87.1
Test	91.7	100	83.3	91.3	90.9

3.3.2 Key discriminating spectral bands

Key wavenumber variables responsible for AD and DR class separation for both plasma and serum are shown in Figures 15 and 16 respectively. This was attained following a combination of the difference-between-mean spectrum of AWLS baseline corrected pre-processed data with the PCA loadings on PC1 amongst the two groups. For plasma samples the key distinguishing peaks responsible for the largest between group differences were 1015 cm^{-1} (carbohydrates peak for solids), 1678 cm^{-1} (bound and free nicotinamide adenine dinucleotide) and 1446 cm^{-1} (CH_2 bending mode for proteins and lipids, CH_2 deformation). The former two were higher amongst those with AD, whereas 1446 cm^{-1} was associated with DR. Notable wavenumber variables for DR in serum were 1311 cm^{-1} (CH_3/CH_2 twisting or bending mode of lipid/collagen), 1441 cm^{-1} (CH_2 scissoring and CH_3 bending in lipids), 1524 cm^{-1} (carotenoid). The only characterising spectral peak for AD in serum was 1659 cm^{-1} (Amide I vibration collagen-like proteins, Amide C=O stretching absorption for the α -folded polypeptide films).

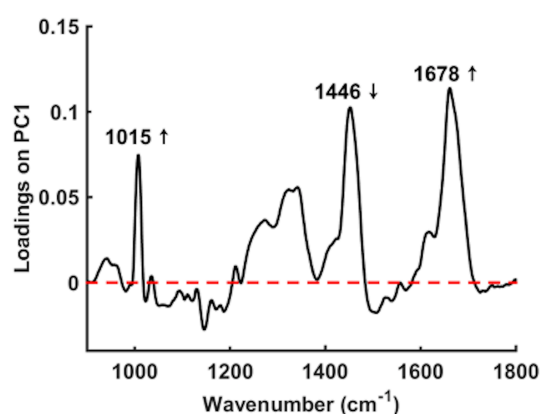


Figure 15: Main band differences for active disease (AD) vs. disease remission (DR) using PCA loadings on PC1 from plasma samples – 1015 cm^{-1} (higher in AD, carbohydrates peak for solids), 1446 cm^{-1} (higher in DR, CH_2 bending mode for proteins and lipids, CH_2 deformation), 1678 cm^{-1} (higher in AD, bound and free NADH).

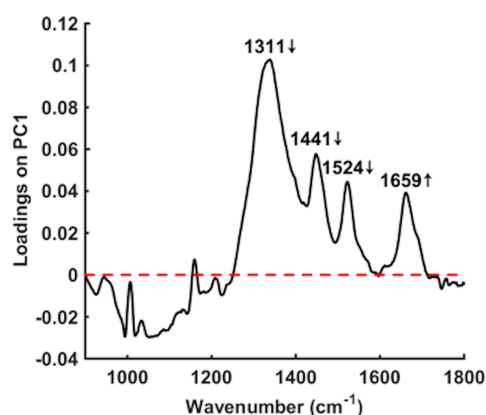


Figure 16: Main band differences for active disease (AD) vs. disease remission (DR) using PCA loadings on PC1 from serum samples – 1311 cm^{-1} (higher in DR, CH_3/CH_2 twisting or bending mode of lipid/collagen), 1441 cm^{-1} (higher in DR, CH_2 scissoring and CH_3 bending in lipids), 1524 cm^{-1} (higher in DR, carotenoid), 1659 cm^{-1} (higher in AD, amide I vibration collagen like proteins, amide C=O stretching absorption for the α -folded polypeptide films).

3.4 Renal tissue & paired urine sample analysis by Raman spectroscopy

3.4.1 Spectral data & classification models: all renal tissue samples

For the three spectra obtained from each sample image, one representative mean spectrum was generated per sample. As such, there are a total of 81 spectra for the 27-sample cohort and consequently 27 representative mean spectra. The total raw spectra, total pre-processed spectra and average pre-processed spectral data for the overall study population are shown in Figures 17a, 17b and 17c respectively. For the construction of supervised classification models both the total raw spectra and pre-processed spectra were used as training data with known categories according to each experimental class. Following cross-validation using the leave-one-out approach, the mean spectral data was applied as the test set for blind predictive modelling to validate the classification systems performance. In this construct, the cross-validation data is the most significant result that should be considered, representing the models ability correctly predict new data based on the existing knowledge obtained from any training data. This process helps to mitigate any potential overfitting. Due to the unbalanced sample size distribution amongst all four Berden classes, comparative analysis was only feasible between focal (n=15) and mixed (n=9) disease. Similarly, evaluation of normal glomeruli was undertaken as a sample distribution of those with >25% normal glomeruli (group N0) (n=21) vs. those exhibiting <25% normal glomeruli (groups N1 & N2) (n=6).

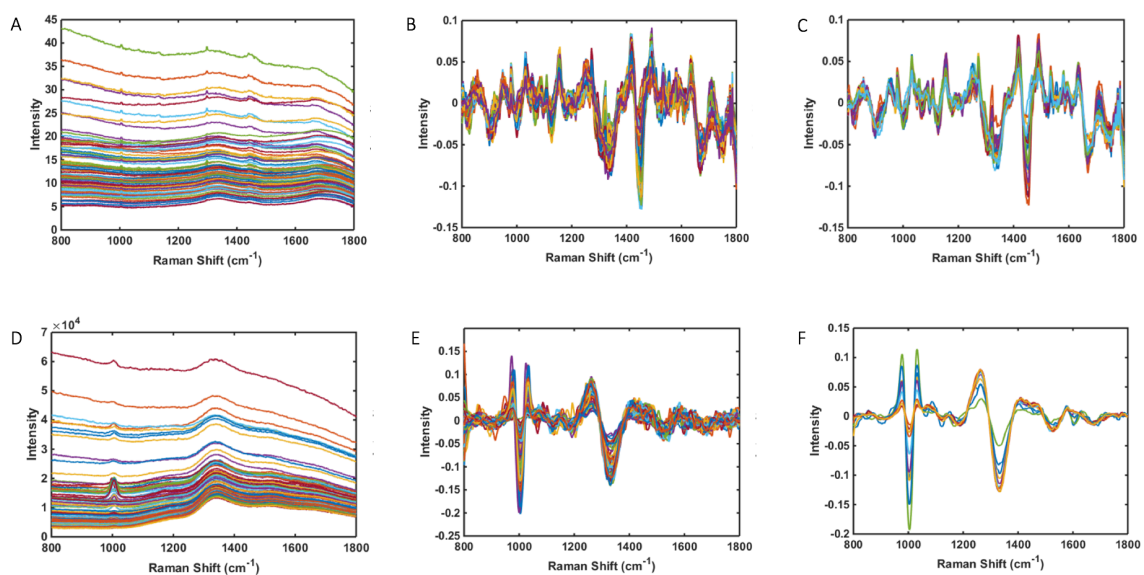


Figure 17: Raman spectral data - (A) Total raw spectra for all tissue samples (n=81) **(B)** Total pre-processed spectra for all tissue samples (n=81) **(C)** Average pre-processed spectra for all tissue samples (n=27) **(D)** Total raw spectra for paired urine samples (n=100) **(E)** pre-processed spectra for paired urine samples (n=100) **(F)** Average pre-processed spectra paired urine tissue samples (n=10)

PLS-DA discriminant function graphs and the classification model performance according to histological data for all renal biopsy samples are shown in Figure 18 and Table 16 respectively. The mean Raman spectral data for each histological group is shown in Figure 19. The spectral profiles for necrotising glomerular lesions, interstitial infiltrate and IFTA yielded the most accurate results. This is evident with an F-score 95% for >25% IFTA (sensitivity 100%, specificity 90%, area under ROC 0.98), 100% for necrotising glomerular lesions (sensitivity 100%, specificity 100%, area under ROC 1) and 100% for interstitial infiltrate (sensitivity 100%, specificity 100%, area under ROC 0.97). The predictive performance in distinguishing focal from mixed disease, >25% normal glomeruli and the presence of vessel wall necrosis was limited with a sensitivity of <60% in each model. Similarly, the discriminant model for ANCA was not significant with a sensitivity of only 56% in seropositive cases.

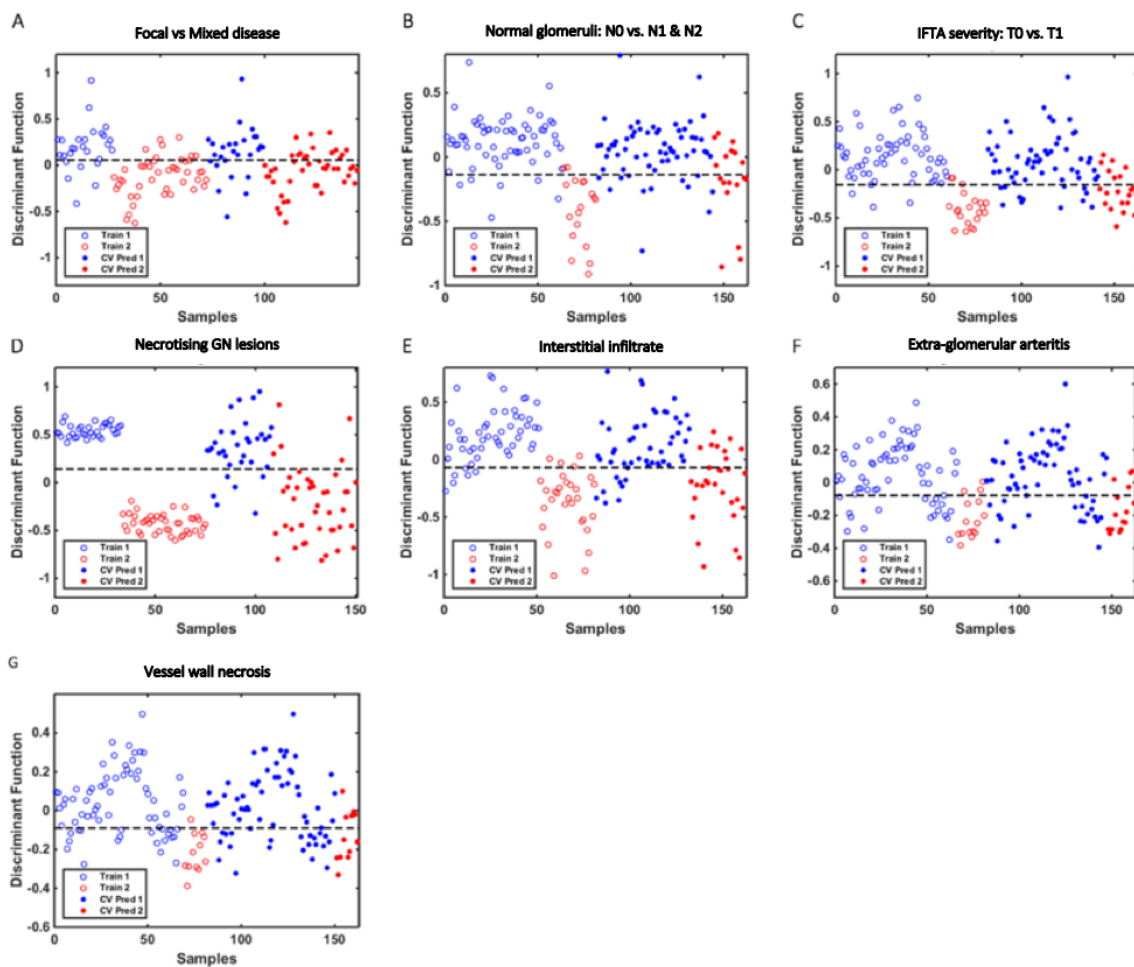


Figure 18: PLS-DA discriminant function graphs for the classification of histological data using spectral data from all tissue samples with corresponding receiver operating characteristic curve data. Train 1 and Train 2 represent training sample data for each histological group. CV Pred 1 and CV Pred 2 represent test sample data for each histological group analysed by the cross-validation (CV) prediction process: **(A)** Mixed vs. focal disease (train 1 & CV Pred 1 vs. train 2 & CV Pred 2) area under ROC 0.85 **(B)** Normal glomeruli N0 vs. N1 & N2 (train 1 & CV Pred 1 vs. train 2 & CV Pred 2) area under ROC 0.96 **(C)** Interstitial fibrosis and tubular atrophy (IFTA) severity T0 vs. T1 (train 1 & CV Pred 1 vs. train 2 & CV Pred 2) area under ROC 0.98 **(D)** Necrotising glomerular (GN) lesions absent vs. present (train 1 & CV Pred 1 vs. train 2 & CV Pred 2) area under ROC 1 **(E)** Interstitial infiltrate absent vs. present (train 1 & CV Pred 1 vs. train 2 & CV Pred 2) area under ROC 0.97 **(F)** Extraglomerular arteritis absent vs. present (train 1 & CV Pred 1 vs. train 2 & CV Pred 2) area under ROC 0.89 **(G)** Vessel wall necrosis absent vs. present (train 1 & CV Pred 1 vs. train 2 & CV Pred 2) area under ROC 0.92

Table 16: Classification model performance according to histological data for renal biopsy samples (n=27)

Presence of histological features as an experimental class	Best Discriminate Model	Spectral data	Accuracy (%)	Sensitivity (%)	Specificity (%)	F-Score (%)	G-Score (%)
Berden classification: Focal vs. Mixed	PLS-DA (3 LVs)	Training: TPS	81	82	78	80	80
		CV: TPS	75	80	67	73	73
		Test: MPS	69	69	70	69	69
Normal Glomeruli: N0 vs. N1&N2	PLS-DA (3 LVs)	Training: TPS	90	89	90	89	89
		CV: TPS	77	56	83	67	68
		Test: MPS	93	83	95	89	89
IFTA: T0 vs. T1	PLS-DA (3 LVs)	Training: TPS	91	86	93	89	89
		CV: TPS	78	67	82	74	74
		Test: MPS	93	100	90	95	95
Necrotising glomerular lesions	PLS-DA (8 LVs)	Training: TPS	100	100	100	100	100
		CV: TPS	87	88	85	86	86
		Test: MPS	100	100	100	100	100
Interstitial Infiltrate	PLS-DA (3 LVs)	Training: TPS	88	87	88	87	87
		CV: TPS	80	73	84	78	78
		Test: MPS	100	100	100	100	100
Extra-glomerular arteritis	PLS-DA (2 LVs)	Training: TPS	74	80	73	76	76
		CV: TPS	72	67	73	70	70
		Test: MPS	78	100	73	84	85
Vessel Wall Necrosis	PLS-DA (2 LVs)	Training: TPS	74	92	71	80	81
		CV: TPS	69	58	71	64	64
		Test: MPS	81	100	78	88	88

Berden classification, Focal: $\geq 50\%$ normal glomeruli, Mixed: no predominant lesion; Normal glomeruli, N0 $>25\%$, N1 10-25%, N2 $< 10\%$; IFTA, interstitial fibrosis & tubular atrophy, T1 $>25\%$, T0 $\leq 25\%$; PLS-DA, partial least squares discriminant analysis; LVs, latent variables; TPS, total processed spectra; MPS, mean processed spectra, CV; cross-validation

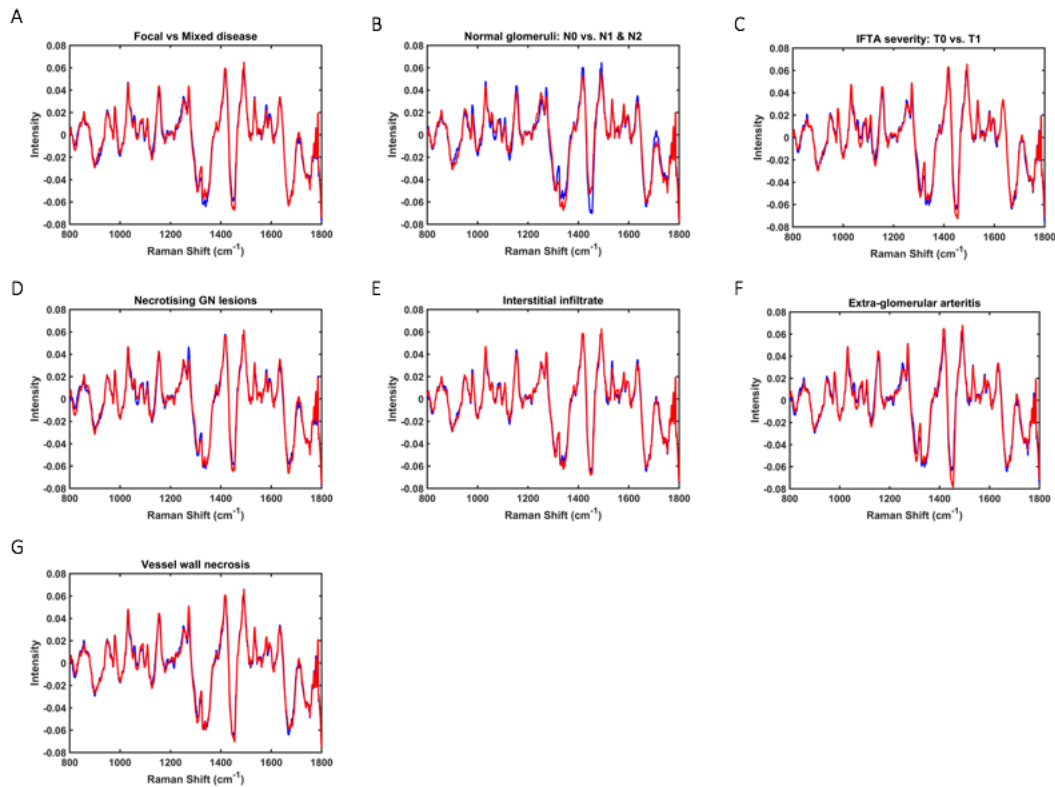


Figure 19: Mean Raman spectral data for each histological group – (A) focal vs. mixed disease, (B) proportional of normal glomeruli, (C) severity of interstitial fibrosis and tubular atrophy (IFTA), (D) presence of necrotising glomerular (GN) lesions, (E) presence of interstitial infiltrate, (F) presence of extra-glomerular arteritis, (G) presence of vessel wall necrosis.

3.4.2 Spectral data & classification models: comparative results for tissue & paired urine samples

Based on the findings observed in the overall cohort, a comparative subgroup analysis was undertaken amongst those with a paired urine sample at the time of renal biopsy (n=10). This sought to determine if equally good discrimination for necrotising glomerular lesions, interstitial infiltrate and >25% IFTA could be demonstrated in both biosamples. For the three spectra obtained from each tissue sample, one representative mean spectrum was generated per sample resulting in a total of 30 spectra and 10 representative mean spectra for the subgroup. Ten individual spectral points were obtained from each urine sample, generating a total of 100 spectra and 10 representative average spectra. Findings are shown in Table 17 and exhibit limited accuracy in distinguishing the presence of each category in urine on blind predictive modelling with a sensitivity <60% and F-score <65% for each. Subgroup model data for normal glomeruli, Berden classification, vessel wall necrosis and extra-glomerular arteritis are not presented in view of their suboptimal performance in tissue analysis amongst the overall cohort.

Table 17: Classification model performance according to histological data: comparative results for paired tissue & urine samples (n=10)

Presence of histological features as an experimental class	Sample	Best Discriminate Model	Spectral data	Accuracy (%)	Sensitivity (%)	Specificity (%)	F-Score (%)	G-Score (%)
Presence of IFTA: T0 vs. T1	Tissue	PLS-DA (6 LVs)	Training: TPS	100	100	100	100	100
			CV: TPS	83	67	90	77	78
			Test: MPS	100	100	100	100	100
	Urine	PLS-DA (10 LVs)	Training: TPS	100	100	100	100	100
			CV: TPS	66	57	70	63	63
			Test: MPS	100	100	100	100	100
Presence of Necrotising glomerular lesions	Tissue	PLS-DA (3 LVs)	Training: TPS	100	100	100	100	100
			CV: TPS	87	78	90	84	84
			Test: MPS	100	100	100	100	100
	Urine	PLS-DA (4 LVs)	Training: TPS	93	93	93	93	93
			CV: TPS	67	53	73	61	62
			Test: MPS	100	100	100	100	100
Presence of Interstitial Infiltrate	Tissue	PLS-DA (6 LVs)	Training: TPS	100	100	100	100	100
			CV: TPS	90	89	90	89	89
			Test: MPS	100	100	100	100	100
	Urine	PLS-DA (10 LVs)	Training: TPS	99	97	100	98	98
			CV: TPS	72	53	80	64	65
			Test: MPS	100	100	100	100	100

IFTA, interstitial fibrosis & tubular atrophy, T1 >25%, T0 ≤ 25%; PLS-DA, partial least squares discriminant analysis; LVs, latent variables; TPS, total processed spectra; MPS, mean processed spectra, CV; cross-validation

3.4.3 Key discriminating spectral biomarkers: tissue & paired urine samples

Based on PLS-DA coefficients, the key distinguishing spectral peaks and wavenumber assignments identified for necrotising glomerular lesions, interstitial infiltrate and IFTA in the subgroup of paired tissue and urine samples are shown in Figure 20. Peaks associated with necrotising glomerular lesions in tissue were 1680 cm^{-1} (C=O, stretching vibrations of cortisone), 1443 cm^{-1} (CH₂ bending mode of proteins & lipids CH₂ deformation), 1539 cm^{-1} (amide carbonyl group vibrations & aromatic hydrogens) (390). The only corresponding peak seen in urine was reflective of cortisone (1716 cm^{-1} , C=O of cortisone), which is not specific to this type of lesion (390). Although peaks representative of increased collagen deposition were seen in urine for IFTA, which would be anticipated (1247 cm^{-1} , amide III collagen assignment), this was not observed in tissue (390). Similarly, parallel biochemical activity for interstitial infiltrate was not seen between the two biosamples. Figure 21 demonstrates the key wavenumber variables for these same experimental classes amongst the overall cohort of 27 tissue samples.

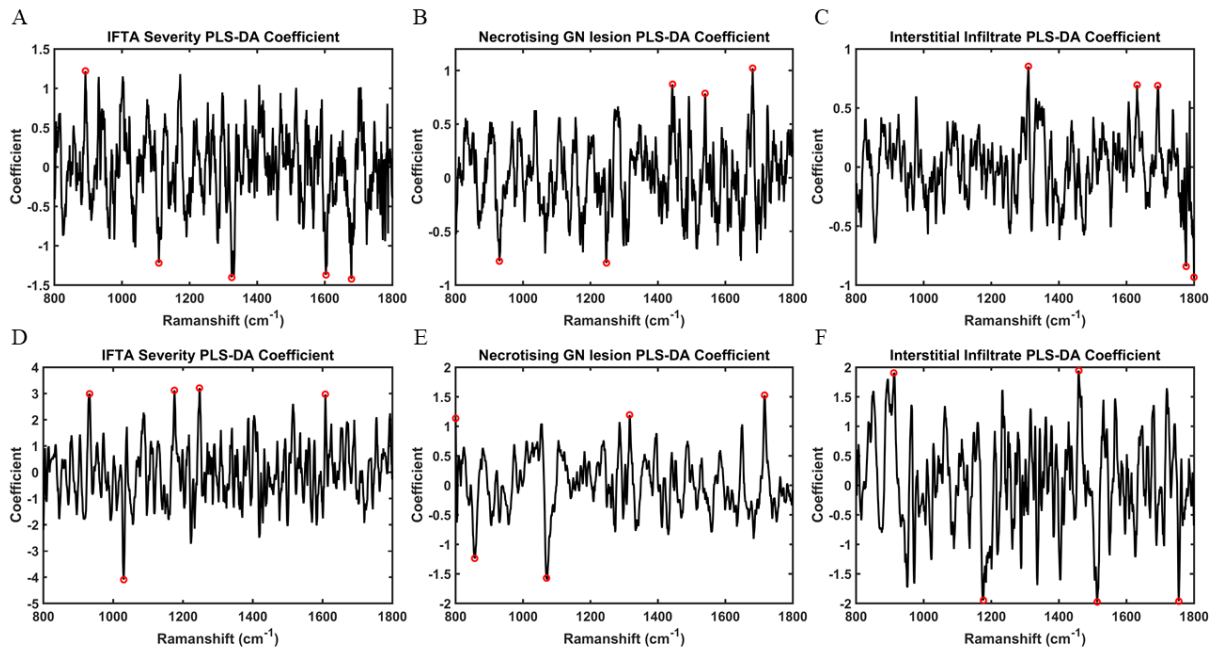


Figure 20: PLS-DA coefficients for identification of spectral biomarkers in tissue and corresponding paired urine samples (n=10) – (A) Wavenumber variables associated with interstitial fibrosis & tubular atrophy (IFTA) in tissue samples – 891.92 cm^{-1} (saccharide band) **(B)** Wavenumber variables associated with necrotising glomerular (GN) lesions in tissue samples - 1680 cm^{-1} (C=O, stretching vibrations of cortisone), 1443 cm^{-1} (CH₂ bending mode of proteins & lipids CH₂ deformation), 1539 cm^{-1} (amide carbonyl group vibrations & aromatic hydrogens) **(C)** Wavenumber variables associated with interstitial infiltrate in tissue samples – 1309 cm^{-1} (CH₃/CH₂ twisting or bending mode of lipid & collagen), 1631 cm^{-1} (amide I), 1692 cm^{-1} (amide) **(D)** Wavenumber variables associated with interstitial fibrosis & tubular atrophy (IFTA) in paired urine samples - 1247 cm^{-1} (amide III collagen assignment), 1175 cm^{-1} (cytosine, guanine), 932 cm^{-1} (proline, hydroxyproline), 1607 cm^{-1} (C=C phenylalanine, tyrosine) **(E)** Wavenumber variables associated with necrotising glomerular (GN) lesions in paired urine samples - 1716 cm^{-1} (C=O of cortisone), 1316 cm^{-1} (guanine), 800 cm^{-1} (phosphate ion interactions) **(F)** Wavenumber variables associated with interstitial infiltrate in paired urine samples – 1458 cm^{-1} (nucleic acid), 911 cm^{-1} (glucose)

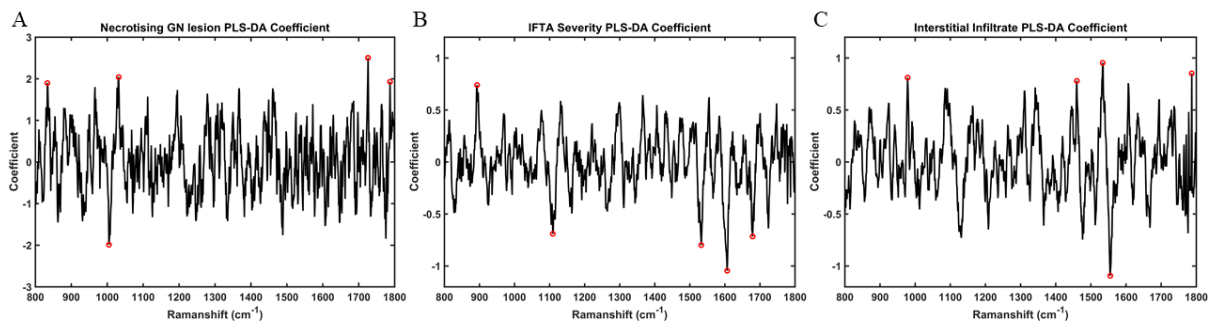


Figure 21: PLS-DA coefficients for identification of spectral biomarkers from tissue samples (n=27) – (A) Wavenumber variables associated with necrotising glomerular (GN) lesions: 1726 cm^{-1} (C=O stretching vibrations of cortisone), 1031 cm^{-1} (C-H in-plane bending mode of phenylalanine), 833 cm^{-1} (asymmetric O-P-O stretching of tyrosine), 1787 cm^{-1} (C=O stretching vibrations of cortisone) **(B)** Wavenumber variables associated with interstitial fibrosis & tubular atrophy (IFTA): 893 cm^{-1} (phosphodiester deoxyribose) **(C)** Wavenumber variables associated with interstitial infiltrate: 1533 cm^{-1} (amide carbonyl group vibrations and aromatic hydrogens), 1787 cm^{-1} (C=O stretching vibrations of cortisone), 978 cm^{-1} (C-C stretching in β -sheet proteins), 1459 cm^{-1} (deoxyribose).

Chapter 4: Discussion

Currently a reliable biomarker of disease activity in AAV is lacking. This can leave treating clinicians in a precarious position, unsure of the presence of relapsing or persistent disease when considering the need to reintroduce or escalate immunosuppression. This risks treatment related harm or unimpeded disease activity and associated ensuing organ damage in the absence of therapy. The presented biofluid study provides the first evidence that biospectroscopy has the potential to provide an accurate biomarker of active disease and treatment response in multisystem AAV. To our knowledge this is the first study of its kind, in which we demonstrate its novel use as a quantitative method to distinguish active from quiescent disease with a high degree of sensitivity and specificity. This was applicable both in renal and extra-renal disease irrespective of current ANCA serology. In this exploratory work, we also demonstrate for the first time that biospectroscopy offers a potential novel method of machine learning with automated computational detection of AAGN disease activity in renal biopsy specimens. This was demonstrated with the ability of spectral data to distinguish the presence histological lesions indicative of chronic damage and active disease with a high degree of accuracy, inclusive of IFTA, interstitial infiltrate and necrotising glomerulonephritis.

Histological evaluation of renal biopsy samples remains the optimum method for diagnosing disease, but certain challenges remain. Key histological findings such as IFTA and interstitial infiltrate are potentially subject to inter-observer variability, with important prognostic implications of the former. As such, there remains scope for adjuvant techniques to complement and aid current tissue analysis. Moreover, given the inherent procedural risks, serial renal biopsies for histological confirmation of active disease is not practical and in the context of extra-renal disease, a tissue biopsy is often not feasible and typically has a low diagnostic yield (391). Current approaches in clinical practice use two main biomarkers to help predict potential relapse; ANCA and B-cell population, however their clinical utility remains limited. Persisting ANCA positivity, ANCA reappearance and anti-PR3 associated disease have been associated with a higher rate of relapse (189,290,294,297), but despite this a significant proportion of de-novo and relapsing disease occurs in the absence of detectable circulating ANCA (137,143,144,152,153), particularly amongst patients with extra-renal disease (148). The significance of rising titres also remains debateable (296,300). Moreover, ANCA positivity has been shown to occur in healthy individuals (61,308,392) as well as other systemic illnesses (310), further restricting its use. Similarly, while B-cell repopulation following targeted therapy with rituximab has been associated with relapsing disease (220,297,313), follow up data from other large trials has not corroborated this finding (222,300) and active disease has been shown to occur with B-cell activity in tissue despite depletion in serum (314). Amongst other potential biomarker tools, urinary sCD163 and uMCP-1 have both demonstrated significant promise, with higher levels of both associated with active AAGN (342–345,347,348). Furthermore, combination of the two has yielded a high specificity and positive likelihood ratio for relapsing disease (351). However, any potential role of urinary sCD163 and uMCP-1 remains limited to renal vasculitis, with a robust non-invasive biomarker of multisystem disease still lacking. Other potential biomarkers including novel autoantibodies, autoantigen gene expression, serum

cytokines and degradation products of the alternative complement pathway have either failed to be validated or require further investigation (393).

A limited number of studies have successfully applied metabolomics as a potential candidate biomarker for disease activity in vasculitis. Its use in Takayasu's arteritis has been evaluated, demonstrating good ability to distinguish active from quiescent disease, with acute phase protein associated NAG as the key discriminating metabolite (356,357). Al-Ani *et al* analysed the urinary metabolomic profile in cases of renal limited AAV, demonstrating good discriminatory capacity with hypocitraturia and raised levels of myo-inositol associating with active disease (358). Nuclear magnetic resonance based metabolomics has since been applied to AAV in serum with similar diagnostic potential and in line with those studies undertaken in Takayasu's arteritis, one of the metabolites characterising active disease was NAG (359). However, despite these promising results, further research into the use and clinical application of metabolomics is often hindered by the associated costs.

The use of biospectroscopy offers a surrogate technique for metabolomics. It provides the ability to optically characterise the biomolecular changes associated with disease. The unique spectrochemical fingerprint generated is representative of the chemical bonds present within any given biosample and can be considered akin to the samples metabolomic profile. In doing so, the cellular activity unique to any given pathological state can be characterised. Two key analytical techniques are available, IR spectroscopy and Raman spectroscopy. Both benefit from being fast, low cost and reagent-free with minimal sample preparation required and the potential for automated clinical laboratory use. Additionally, technological improvements and advancements in chemometric analysis over the past decade have enabled a high throughput of large datasets with increasing investigation of its potential application in renal medicine.

When considering the novel application of biospectroscopy in AAV as an innovative candidate for the development of a functional biomarker of disease activity, both potential modalities require consideration. Both have the potential for automation and translation into clinical practice, although Raman may have two key advantages; it is not constrained by the need for sample uniformity or potential need for dilution to avoid saturation and there is no potential risk of interference from water. However, fluorescence can cause interference with attainment of spectrochemical data when using Raman spectroscopy. This would not be a factor when using ATR-FTIR spectroscopy, which also has the potential to detect target analytes at lower concentrations.

Yu *et al* used ATR-FTIR spectroscopy to analyse urine samples from rodent models of inflammatory glomerulonephritis, as well as a limited number of patients with ANCA positive pauci-immune glomerulonephritis to determine renal inflammation and injury (384). Several key characteristic spectral markers were identified that correlated with the progression and severity of disease. In particular, both the 1545 cm^{-1} and 1033 cm^{-1} wavenumber intensity correlated with disease severity in the rodent model, with normalisation to baseline following treatment with dexamethasone. However, the 1545 cm^{-1} band intensity increased with declining renal function amongst both patients with active disease and those in remission, failing to discriminate between the

two groups. The 1545 cm^{-1} band was also present in the murine model of lupus nephritis, suggesting that it may not be specific to vasculitis, instead reflecting glomerular inflammation and damage. Nonetheless, these original findings demonstrated the potential application of ATR-FTIR spectra from urine as marker of disease activity in patients with ANCA positive renal limited disease.

The use of Raman spectroscopy in the field of AAV remained completely untested until this presented body of work, although its application as a candidate biomarker of disease activity has been evaluated in other autoimmune diseases. In 2011, Caralho *et al* determined the spectrochemical fingerprint of rheumatoid arthritis compared to healthy controls, identifying superior diagnostic ability of Raman spectroscopy when compared to rheumatoid factor and CRP with 92% accuracy (sensitivity 88%, specificity 96%) (394).

4.1 Biofluid sample analysis by ATR-FTIR spectroscopy

In order to detect differences between patients with active disease and those in clinical remission, we employed ATR-FTIR to extract spectral data from three key biofluids; plasma, serum and urine. Using unsupervised learning where spectra are classified without any prior sample knowledge, overall category separation using PCA was good in both plasma and serum samples. On subsequent blind predictive modelling of known and unknown spectral profiles with PLS-DA, our findings demonstrated that plasma was the most accurate biofluid for discriminating between the two categories, correctly identifying active disease in 85.7% of cases and 100% of those in remission. This finding was independent of ANCA serology with 16% of patients in the AD cohort having undetectable circulating ANCA and 53% of patients having persistent ANCA positivity despite disease remission. Parallel findings were also seen in the AD cohort where paired remission samples were attained; demonstrating that not only can ATR-FTIR spectroscopy be used as a biomarker of active disease, but it could also be applied help determine treatment response. Our results were also applicable to both renal and non-renal disease with the majority of patients in the AD cohort having multisystem disease and no demonstrable correlation of discriminating spectral data with organ system involvement. The lack of any significant correlation between the spectral data and currently used clinical markers including ANCA, CRP and ESR is unsurprising as the latter are all known to have a limited association with disease activity. Similarly, the absence of any significant correlation with BVAS suggests that the application of ATR-FTIR spectroscopy may only be used to identify active disease and not disease severity. Group separation on PCA plot of spectral data attained from urine may have been restricted as not all included patients had renal involvement and of those who did, a urine sample could not be attained from three patients.

Several key wavenumber-variables associated with active disease from plasma samples were of particular interest, namely 1620 cm^{-1} , 1698 cm^{-1} , 1701 cm^{-1} and 1716 cm^{-1} which are all associated increased nucleic acid expression. This may reflect the known genetic contribution to disease susceptibility and epigenetic factors of disease activity, with reduced DNA methylation of MPO and PRTN3 resulting in increased autoantigen expression and disease activity (81,83,84). Alternatively, recognising the role of nuclear extracellular traps (NETs) in disease pathogenesis, this this finding may simply reflect increased free cell DNA as a result of NET remnants and apoptotic cells (17–20). Protein groups at the Amide I (1662 cm^{-1}) and Amide II (1481 cm^{-1}) bands were associated

with disease remission. This may be a reflection of plasma protein abundance in the acute phase of illness with slightly lower trend in serum albumin observed in active disease (34.7 ± 7.3 g/L) compared to disease remission (44.4 ± 2.9 g/L). However, the R^2 for both serum albumin and total protein did not confirm a positive correlation with spectral data amongst the disease remission cohort, but trended towards significance in active disease leaving the relevance of this result unclear. Mean serum total protein was largely similar between the two groups; 62 ± 9.8 g/L vs. 67.1 ± 4.7 g/L. Mass spectrometric analysis could be applied in future study to help correlate the ATR-FTIR spectral pattern with potential key compositional properties.

4.2 Biofluid sample analysis by Raman spectroscopy

In our study of Raman spectroscopy, good separation between active AAV and quiescent disease was observed on applying unsupervised learning with PCA to serum and plasma sample spectral data. Further investigation with validation testing using PLS-DA blind predictive modelling of the remaining 40% of samples yielded excellent results, with robust models and statistically significant discrimination of the two groups. In this model the diagnostic accuracy for active disease was 81.7% for plasma samples, with 70% sensitivity for disease remission and 93.3% specificity for active disease (F-score 80%, AUC 0.95). Similar results were attained from serum samples. With only 32% of patients exhibiting single organ disease and an overall mean BVAS of 16 ± 9.6 , this suggests that our findings are independent of the organ system affected and that this classification model is applicable to multisystem disease of varying clinical severity. Furthermore, given the absence of detectable circulating ANCA in 16% of patients with active disease and persisting seropositivity in 50% of overall remission samples, this indicates that the spectral data attained is independent of ANCA status with potential application in ANCA negative disease. The shift in the spectral profile following successful remission induction therapy, with accurate characterisation of disease remission indicates that the spectrochemical fingerprint attained can also be used to help determine treatment response.

Notable discriminating wavenumber variables for active disease were 1015 cm^{-1} and 1678 cm^{-1} from plasma and 1659 cm^{-1} from serum. The key chemical bonds and biomolecular changes represented by these included increased collagen synthesis, carbohydrate activity and NADH, which plays an essential role in cellular metabolism. These are reflective of the increased metabolic activity that would be expected in a proinflammatory state of active disease and subsequent organ damage. This is not dissimilar to the metabolomic profile characterising active AAV in the previous metabolomic study by Gupta *et al* with elevated levels of NAG (359).

4.3 Renal tissue & paired urine sample analysis by Raman spectroscopy

The clinical application of machine learning is an evolving area of interest. In a recent study, based on tissue staining with Masson trichrome and periodic acid-Schiff, Ginley *et al* applied machine learning algorithms to digital images in order to reliably identify IFTA and glomerulosclerosis in cases of diabetic nephropathy and renal transplant specimens (395). In recent years infrared spectroscopy has been successfully used to detect early biochemical variations that may precede histological changes seen in diabetic nephropathy amongst both native and transplant renal biopsy samples (375–377). The same modality has also been applied in a large study by

Vuiblet *et al* to correctly quantify interstitial fibrosis and inflammation in renal transplant biopsies with >90% accuracy and good correlation with clinical outcomes (378). Whereas the complementary method of Raman microspectroscopy has been investigated and validated as a viable technique to distinguish malignant renal tissue from both healthy parenchyma and benign disease (396,397), as well as successful tumour staging using spectra from surface-enhanced Raman scattering (398).

We applied Raman spectroscopy to unstained renal tissue samples from patients with histopathology reports consistent with AAGN. The resulting spectral data was able to correctly identify the presence of necrotising glomerular lesions, interstitial infiltrate and IFTA with a high degree of diagnostic accuracy on blind predictive modelling. The wavenumber-variables responsible for largest between group differences for the former two were associated with increased amino acid and cortisone activity, whereas IFTA tended to be associate with increased nucleic acid expression. The poor performance of the classification models according to the Berden classification system, presence of vessel wall necrosis and the proportion of normal glomeruli likely reflects the limited sample distribution amongst these groups.

The aim of the subgroup analysis was to determine if the spectral data from urine could potentially be used as a surrogate for renal biopsy. The premise being that the biomolecular signature obtained from urine could characterise and reflect histological findings at a given time point. To address this question, the histological categories associated with good discriminatory function in the initial spectral analysis of the entire study cohort were evaluated in those tissue samples with a corresponding paired urine sample at the time of biopsy. These categories included necrotising glomerular lesions, interstitial infiltrate and IFTA. Using the same chemometric methodology, there was limited performance in the models ability to reliably discriminate the presence of these categories in urine with a poor sensitivity in each group. This may have resulted from the limited sample size in each category amongst the subgroup and the possibility of insufficient training data. Taking this into account, it should not dissuade further research in this area. As previously outlined, excellent results have been obtained from the spectrochemical interrogation of other biofluids including plasma and serum, demonstrating both infrared and Raman spectroscopy as a viable non-invasive candidate biomarker tool of disease activity in AAV. Additionally, in the present study it is worth noting that there was some similarity in the key distinguishing spectral peaks between the two biological samples, with increased protein and cortisone expression observed in both tissue and urine for necrotising glomerular lesions. As would be expected, notable biomolecular changes in urine for IFTA were representative of increased collagen synthesis, although this was not observed in tissue samples. One consideration is that the difference in the spectral acquisition method used for tissue and urine samples may account for the lack of consistency between spectral profiles obtained and the metabolic activities they represent. However, this would require a larger-sized and longitudinal temporal study to elucidate. It is also very possible that different profiles of spectral biomarkers present themselves depending on sample type.

4.4 Study limitations & future work

Although our results are encouraging they should be considered within the context of its primary limitation; despite taking measures to avoid the risk of overfitting, the risk of bias from insufficient training data remains a potential factor in this phase one study for biomarker discovery. Nevertheless, this should be weighed against the rigorous analytical approach taken and the previously untested application of biospectroscopy as an innovative means of addressing a significant unmet clinical need amongst a rare disease cohort. A larger future phase two validation study is required to provide sufficient longitudinal training data and prevent bias from small sample size. Based on known outcomes, machine-learning using forward feature extraction algorithms could then be used to construct prediction models based on extracted spectral features. Such features would also lend novel insight into evolving mechanisms of action. We calculate that the optimal sample size for validation of biosamples analysis would be 199 samples (79 active and 120 remission cases) for a power of 80%. For the optimal sample size we used a Fisher's exact test considering the spectral proportion of active and remission cases, which is roughly 0.4:0.6 (Figure 22). Given the rare nature of disease, such a timely study would be feasible using existing biobanks from previous large randomised control trials in the field, with samples from various disease time points alongside current standard diagnostic methods.

A second limitation to consider is the control groups used in the analysis of biofluids with ATR-FTIR. Although good separation of active disease from all control groups was seen, other than AKI with systemic infection, disease control groups were otherwise restricted to renal limited pathology. Any future study of biospectroscopy as a biomarker of multisystem AAV would benefit from inclusion of controls with other systemic inflammatory conditions, such as systemic lupus erythematosus or rheumatoid arthritis to help evaluate its clinical utility further.

Similarly, when considering tissue and paired urine sample analysis, aside from sample size, one potential limiting factor is the absence of control groups. However, this is not essential herein with a factorial-based design determining the presence or absence of a feature in a cohort displaying a range of histological variation that is common amongst patients with AAGN. A further limitation is the lack of assigned variables to novel biomolecules reported in the literature. In our study all experimental categories from tissue samples were based on known key histological variables. Promising non-invasive biomarkers of disease activity in AAGN include uMCP-1, urinary sCD163 and degradation products of the complement cascade (30,31,342–345,347,399). Each has been shown to correlate well with disease activity, in addition to an associated upregulation of macrophage infiltration in inflamed glomeruli with higher levels of uMCP-1 and the presence fibrinoid necrosis and cellular crescents with sCD163 (342,348). Tissue depositions of alternative pathway cleavage products including C3d, C3c and Bb have been associated with a higher degree of cellular crescents and IFTA. This was mirrored in urine with higher levels of C3a, C5a and soluble C5b-9 present in active disease, as well as higher urinary levels of Bb correlating with a lower proportion of normal glomeruli (30). Any future study evaluating the role of biospectroscopy in AAGN would benefit from assay and analysis of these potential biomarkers with spectral data. In addition to offering a potentially cheaper and faster surrogate technique for their detection, their analysis may also help resolve the current lack of concordance in the spectral profiles between the two biosamples. Other potential areas of

research include the application of forward feature extraction algorithms to construct prediction outcome models based extracted spectral features, as well as correlation of spectral data with imaging mass spectrometry to aid in the delineation of any potential biomarkers.

Considering other areas of future work, when applying Raman spectroscopy to our pre-specified biofluids, identification of the spectral changes directly associated with levels NADH and NAG is difficult to ascertain in the milieu of a biological sample with Raman spectroscopy alone and is beyond the scope of this current study. An approach of immunolabelling pioneered by Hodges *et al* using surface-enhanced Raman spectroscopy coupled with cationic gold-conjugated antibodies could be undertaken in future work to directly target these tentative biomarkers (400).

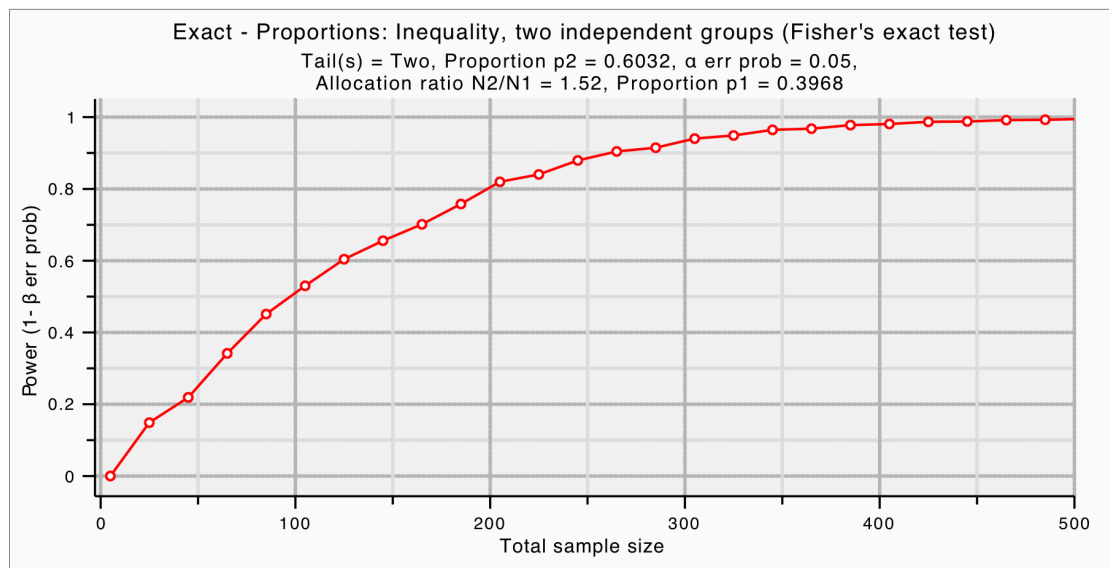


Figure 22: Power test based on a Fisher's exact test (two-tails, error probability = 0.05) showing the power varying the total sample size of active and remission cases.

4.5 Summary

The absence of a functional biomarker that accurately correlates with disease activity in AAV represents a significant clinical need. The translation of biospectroscopy into clinical practice is feasible. Portable handheld devices are currently in use in non-medical fields (401). Coupled with the integration of chemometric algorithms, minimal sample requirements and label free preparation means that both ATR-FTIR and Raman spectroscopy offer a potential low cost, fast, automated near-patient test to complement current clinical practice and help identify patients with active disease.

Our findings demonstrate that both ATR-FTIR and Raman spectroscopy offer a novel means of distinguishing active multisystem AAV from quiescent disease using plasma and serum samples, independent of ANCA status.

As well as aiding diagnosis, this may facilitate early intervention and tailored maintenance therapy to help improve patient outcomes, particularly in seronegative disease. Furthermore biospectroscopy has the potential to offer a robust tool for machine learning and standardised automated detection of disease activity in AAGN. Its application enables the simultaneous analysis of a broad spectrum of biomolecules, providing an adjuvant technique for biomarker extraction and additional potential insight into the molecular mechanism of disease. Our pilot study highlights the potential for spectral profiles to be used as a non-invasive surrogate marker of histological changes in order to aid disease monitoring and guide patient care. These findings warrants further research and require validation in a larger study, with longitudinal data and comparison against a wider range of renal pathology and autoimmune disease.

Chapter 5: General Discussion & Study Overview

Despite impressive advancements in the therapeutic strategies for AAV over the past 30 years, the continued lack of a reliable non-invasive biomarker of disease activity remains a clinical challenge when determining the presence of persistent or relapsing disease. Although several prospective candidate markers are on the horizon, they either require further validation study, evaluation of their clinical utility or only remain applicable to renal limited disease. Amongst them, promising results have been shown in the field of metabolomics, but its practical translation into clinical practice remains limited by the associated costs. Biospectroscopy offers a low cost surrogate technique to elicit a samples metabolomic profile through the interaction of light with the chemical bonds that make its constituent molecules. The resulting spectral data attained from this innovative approach has the potential to be uniquely representative of the biochemical changes that occur with a given disease state. Despite impressive results in other medical disciplines, prior to this body of work only one previous study has applied biospectroscopy in vasculitis with encouraging results identified from urine in patients with renal limited disease. This thesis aimed to determine if biospectroscopy could be applied to the field of multisystem AAV as a fast, non-invasive and robust biomarker of disease activity. In doing so, we applied both ATR-FTIR spectroscopy and Raman spectroscopy to plasma, serum, urine and tissue samples in order to i) accurately distinguish active disease from remission in the afore mentioned biofluids, ii) classify and compare any attained spectra to relevant control groups and iii) acquire spectral data from renal tissue samples with differentiation according to key histological findings, followed by a comparative subgroup analysis against the spectra attained from paired urine samples at the time of biopsy to determine potential use as a non-invasive surrogate marker of histological activity in renal vasculitis, in effect providing a liquid biopsy. The schematic of the thesis structure is shown in Figure 23.

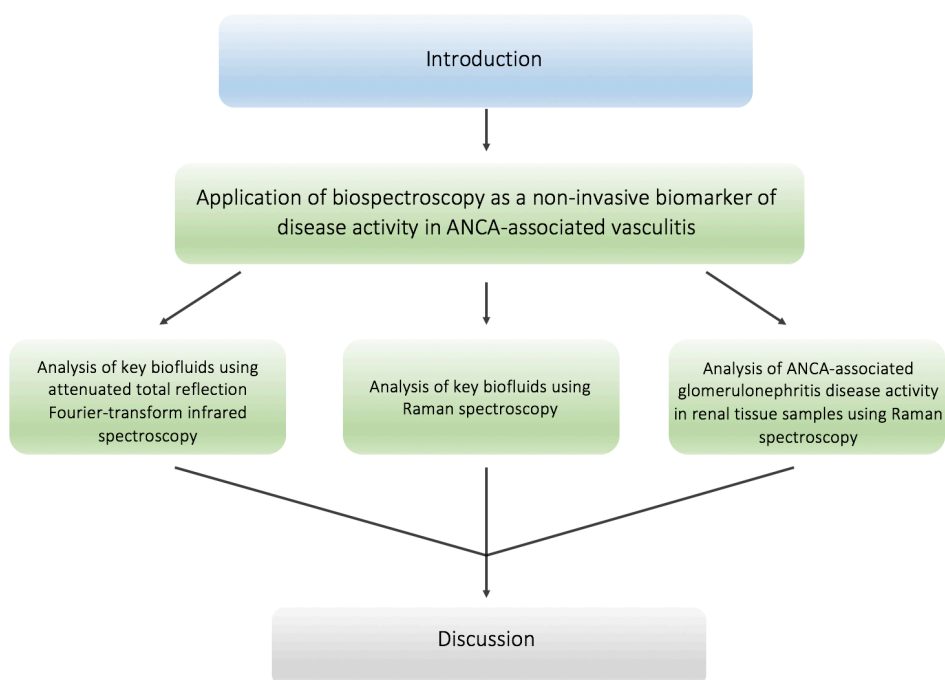


Figure 23: Schematic of thesis structure

We initially sought to determine the potential role of ATR-FTIR in distinguishing active from quiescent disease in AAV amongst the three key biofluids of plasma, serum and urine. As a part of this preliminary work, one hundred and eight participants were recruited; 25 with active disease, 38 in disease remission, 10 with membranous nephropathy, five with minimal change disease, 10 with IgA nephropathy, 10 with pre-renal AKI in the context of infection and 10 healthy controls. This exploratory study confirmed that plasma was the most favourable biofluid for spectrochemical analysis, discriminating between the two groups with up to 93% accuracy on blind predictive modelling following supervised learning using 60% of the sample cohort: F-score 92.3% (sensitivity 100% for disease remission, specificity 85.7% for active disease, AUC 0.901). This was independent of the organ system affected, ANCA serology, renal function and other key salient laboratory results.

Similarly, spectral data exhibited excellent segregation from all control groups and was unaffected by immunosuppressive therapy where treatment data was sufficient to enable meaningful principle component score plot analysis. The spectral data attained from urine may have been less favourable as not all participants with active AAV had renal involvement and of those who did, a urine sample could not be attained from three patients due to anuria at presentation. Where repeat plasma samples could be attained from participants following successful remission induction therapy, equally good group separation was seen between active disease and remission in this subgroup, indicating the potential application of ATR-FTIR to also help gauge treatment response: F-score 75% (sensitivity 100% for disease remission, specificity 60% for active disease, AUC 0.9). In active disease, the biochemical signature identified by the key distinguishing wavenumber-variables were representative of increased nucleic acid expression. This may have reflected the known genetic and epigenetic factors contributing to disease activity through increased autoantigen expression, or alternatively the increased free cell DNA that results from nuclear extracellular traps and cell apoptosis that occurs during pathogenesis. The latter is potentially more likely.

Using the same sample cohort of participants with AAV, we then went on to confirm the ability of Raman spectroscopy to correctly classify active disease from remission with outstanding accuracy from both plasma and serum; F-score 80% for plasma (specificity 93.3%, sensitivity 70%, AUC 0.95) and 80% for serum (specificity 80%, sensitivity 80%, AUC 0.92). Parallel findings were again seen on analysis of paired remission samples; F-score 90.9% (specificity 83.3% and sensitivity 100%) in both plasma and serum, with an AUC of 0.98 and 0.97 respectively. Key discriminating wave-number variables for active disease were indicative of the increased metabolic activity that would be anticipated in a proinflammatory state and ensuing organ damage with upregulation of collagen synthesis, carbohydrate activity and NADH identified. This mirrors the findings of previous studies evaluating the application of metabolomics in serum amongst patient with AAV.

Both studies benefited from fast, reagent free analysis with minimal sample requirements. In conjunction with the application of advanced chemometric modelling and the scope for automation, biospectroscopy offers a viable and effective biomarker tool to distinguish the presence active disease in AAV. This can readily be implemented into clinical practice with scope for the development of a near patient test. When considering the

two modality options, they are not directly interchangeable with key differences present. Raman spectroscopy more readily lends itself to automation, but remains more time consuming out of the two, is potentially subject to interference by fluorescence and certain compounds are not Raman active. In contrast, IR spectroscopy is less liable to signal interference, is capable of measuring target analytes at lower concentrations and any concerns of water interference can be mitigated through the use of ATR-FTIR spectroscopy. Additionally, a better understanding of band assignments is available with more extensive spectral libraries. Although sample uniformity is more essential in infrared spectroscopy with direct contact of the sensor with the sample needed, overall the afore mentioned considerations potentially make ATR-FTIR a more appealing option out of the two.

Despite the analytical approach taken with measures to avoid overfitting, the risk of bias from insufficient training data and lack of controls with a wider range of other systemic inflammatory conditions limits our findings. Following on from this phase one proof of concept work, a larger phase two validation study is required with longitudinal data. Based on the latter, forward feature extraction algorithms could be applied to construct prediction models of clinical outcomes based on key spectral features. Other additional areas of future research include the role of immunolabelling using surface-enhanced Raman spectroscopy coupled with cationic gold-conjugated antibodies to directly target and identify the spectral changes associated with a potential biomarker.

The final study explored the use of Raman spectroscopy as means of machine learning with automated computational detection of AAGN disease activity in unstained renal tissue samples. When evaluated against key histological features of disease, spectral data was able to accurately detect the presence of >25% IFTA (sensitivity 100%, specificity 90%, AUC 0.98, F-score 95%), necrotising glomerular lesions (sensitivity 100%, specificity 100%, AUC 1, F-score 100%) and interstitial infiltrate (sensitivity 100%, specificity 100%, AUC 0.97, F-score 100%). Other characteristic lesions of vessel wall necrosis, the proportion of normal glomeruli and sample separation according to the Berden classification system did not perform well on blind predictive modelling. The restricted findings amongst these groups may be attributable to the limited sample distribution in each category. Subsequent subgroup analysis to determine if the biochemical signature from urine could offer a non-invasive tool to characterise the histological findings at a given time point using paired tissue and urine samples was disappointing. Again, this likely reflects the limited sample size and more significant results may be seen with further training data. Nevertheless, we demonstrated that biospectroscopy can be applied to AAGN to provide reproducible and objective automated quantification of histological findings. Further research in this field would benefit from prediction models of clinical outcomes based on extracted spectral features, assigned variables to novel biomarker molecule reported in the literature; including uMCP-1, urinary sCD163 and degradation product of the complement cascade, as well as correlation of spectral data with imaging mass spectrometry to help identify any potential biomarkers and any implications on the current understood pathogenesis. The use of ATR-FTIR also requires study with the potential to generate very high resolution chemical images.

This body of work is the first to demonstrate that biospectroscopy has the potential to provide a low cost, robust and reliable biomarker of disease activity in multisystem AAV, with scope to help determine treatment response and offer automated detection of histological lesions associated with chronic damage and acute disease. This

novel approach could help the move towards more individualised treatment strategies, reducing the risk of suboptimal disease control or unnecessary therapy. Future research is required to validate these findings and explore its clinical utility, with further potential for new insights into the molecular mechanism of disease through biomarker extraction and comparative biofluid analysis as a non-invasive surrogate for renal biopsy.

References

1. Little MA, Nightingale P, Verburch CA, Hauser T, De Groot K, Savage C, et al. Early mortality in systemic vasculitis: Relative contribution of adverse events and active vasculitis. *Ann Rheum Dis*. 2010;69(6):1036–43.
2. Falk RJ, Terrell RS, Charles LA, Jennette JC. Anti-neutrophil cytoplasmic autoantibodies induce neutrophils to degranulate and produce oxygen radicals in vitro. *Proc Natl Acad Sci U S A*. 1990;87(11):4115–9.
3. Charles LA, Caldas MLR, Falk RJ, Terrell RS, Jennette JC. Antibodies against granule proteins activate neutrophils in vitro. *J Leukoc Biol*. 1991;50(6):539–46.
4. Xiao H, Heeringa P, Hu P, Liu Z, Zhao M, Aratani Y, et al. Antineutrophil cytoplasmic autoantibodies specific for myeloperoxidase cause glomerulonephritis and vasculitis in mice. *J Clin Invest*. 2002;110(7):955–63.
5. Little MA, Smyth CL, Yadav R, Ambrose L, Cook HT, Nourshargh S, et al. Antineutrophil cytoplasm antibodies directed against myeloperoxidase augment leukocyte-microvascular interactions in vivo. *Blood*. 2005;106(6):2050–8.
6. Davies DJ, Moran JE, Niall JF, Ryan GB. Segmental necrotising glomerulonephritis with antineutrophil antibody: Possible arbovirus aetiology? *Br Med J*. 1982;285(6342):606.
7. Van Der Woude FJ, Rasmussen N, Lobatto S, Wiik A, Permin H, van Es LA, et al. Autoantibodies against neutrophils and monocytes: tool for diagnosis and marker of disease activity in Wegener's granulomatosis. *Lancet*. 1985;23(1):425–9.
8. Falk RJ, Jennette JC. Anti-neutrophil Cytoplasmic Autoantibodies With Specificity for Myeloperoxidase in Patients with Systemic Vasculitis and Idiopathic Necrotising and Crescentic Glomerulonephritis. *NEJM*. 1988;318(25):1651–7.
9. Niles JL, McCluskey RT, M A, Arnaout A. Wegner's Granulomatosis Autoantigen is a Novel Neutrophil Serine Proteinase. *Blood*. 1989;74(6):1888–93.
10. Ewert BH, Jennette JC, Falk RJ. Anti-myeloperoxidase antibodies stimulate neutrophils to damage human endothelial cells. *Kidney Int*. 1992;41(2):375–83.
11. Kettritz R, Jennette JC, Falk RJ. Crosslinking of ANCA-Antigens Stimulates Superoxide Release by Human Neutrophils. *J Am Soc Nephrol*. 1997;8(3):386–94.
12. Little MA, Bhangal G, Smyth CL, Nakada MT, Cook HT, Nourshargh S, et al. Therapeutic effect of anti-TNF- α antibodies in an experimental model of anti-neutrophil cytoplasm antibody-associated systemic vasculitis. *J Am Soc Nephrol*. 2006;17(1):160–9.
13. Little MA, Al-Ani B, Ren S, Al-Nuaimi H, Leite M, Alpers CE, et al. Anti-proteinase 3 anti-neutrophil cytoplasm autoantibodies recapitulate systemic vasculitis in mice with a humanized immune system. *PLoS One*. 2012;7(1).
14. The Wegener's Granulomatosis Etanercept Trial (WGET) Research Group. Etanercept plus standard therapy for Wegener's granulomatosis. *N Engl J Med*. 2005;352(4):351–61.
15. Schlieben DJ, Korbet SM, Kimura RE, Schwartz MM, Lewis EJ. Pulmonary-renal syndrome in a newborn with placental transmission of ANCA. *Am J Kidney Dis*. 2005;45(4):758–61.

16. Brinkmann V, Reichard U, Goosmann C, Fauler B, Uhlemann Y, Weiss DS, et al. Neutrophil Extracellular Traps Kill Bacteria. *Science* (80-). 2004;303(5663):1532–5.
17. Björnsdóttir H, Welin A, Michaëlsson E, Osla V, Berg S, Christenson K, et al. Neutrophil NET formation is regulated from the inside by myeloperoxidase-processed reactive oxygen species. *Free Radic Biol Med*. 2015;89:1024–35.
18. Antonelou M, Michaëlsson E, Evans RDR, Wang CJ, Henderson SR, Walker LSK, et al. Therapeutic myeloperoxidase inhibition attenuates neutrophil activation, anca-mediated endothelial damage, and crescentic GN. *J Am Soc Nephrol*. 2020;31(2):350–64.
19. Kessenbrock K, Krumbholz M, Schönemmarck U, Back W, Wolfgang L, Werb Z, et al. Netting neutrophils in autoimmune small-vessel vasculitis. *Nat Med*. 2010;15(6):623–5.
20. Abreu-Velez AM, Smith JG, Howard MS. Presence of neutrophil extracellular traps and antineutrophil cytoplasmic antibodies associated with vasculitides. *N Am J Med Sci*. 2009;1(6):309–13.
21. Xiao H, Schreiber A, Heeringa P, Falk RJ, Jennette JC. Alternative complement pathway in the pathogenesis of disease mediated by anti-neutrophil cytoplasmic autoantibodies. *Am J Pathol*. 2007;170(1):52–64.
22. Huugen D, Van Esch A, Xiao H, Peutz-Kootstra CJ, Buurman WA, Tervaert JWC, et al. Inhibition of complement factor C5 protects against anti-myeloperoxidase antibody-mediated glomerulonephritis in mice. *Kidney Int*. 2007;71(7):646–54.
23. Wang H, Wang C, Zhao MH, Chen M. Neutrophil extracellular traps can activate alternative complement pathways. *Clin Exp Immunol*. 2015;181(3):518–27.
24. Schreiber A, Xiao H, Jennette JC, Schneider W, Luft FC, Kettritz R. C5a receptor mediates neutrophil activation and ANCA-induced glomerulonephritis. *J Am Soc Nephrol*. 2009;20(2):289–98.
25. Xiao H, Dairaghi DJ, Powers JP, Ertl LS, Baumgart T, Wang Y, et al. C5a receptor (CD88) blockade protects against MPO-ANCA GN. *J Am Soc Nephrol*. 2014;25(2):225–31.
26. Hao J, Meng LQ, Xu PC, Chen M, Zhao MH. P38MAPK, ERK and PI3K signaling pathways are involved in C5a-Primed neutrophils for ANCA-Mediated activation. *PLoS One*. 2012;7(5):1–10.
27. Hao J, Chen M, Zhao MH. Involvement of protein kinase C in C5a-primed neutrophils for ANCA-mediated activation. *Mol Immunol*. 2013;54(1):68–73.
28. Chen M, Xing GQ, Yu F, Liu G, Zhao MH. Complement deposition in renal histopathology of patients with ANCA-associated pauci-immune glomerulonephritis. *Nephrol Dial Transplant*. 2009;24(4):1247–52.
29. Xing GQ, Chen M, Liu G, Heeringa P, Zhang JJ, Zheng X, et al. Complement activation is involved in renal damage in human antineutrophil cytoplasmic autoantibody associated pauci-immune vasculitis. *J Clin Immunol*. 2009;29(3):282–91.
30. Gou SJ, Yuan J, Wang C, Zhao MH, Chen M. Alternative complement pathway activation products in urine and kidneys of patients with ANCA-associated GN. *Clin J Am Soc Nephrol*. 2013;8(11):1884–91.
31. Hilhorst M, Van Paassen P, Van Rie H, Bijnens N, Heerings-Rewinkel P, Van Breda Vriesman P, et al. Complement in ANCA-associated glomerulonephritis. *Nephrol Dial Transplant*. 2015;32(8):1302–13.
32. Kambas K, Chrysanthopoulou A, Vassilopoulos D, Apostolidou E, Skendros P, Girod A, et al. Tissue factor expression in neutrophil extracellular traps and neutrophil derived microparticles in antineutrophil

- cytoplasmic antibody associated vasculitis may promote thromboinflammation and the thrombophilic state associated with the disease. *Ann Rheum Dis*. 2014;73(10):1854–63.
33. Huber-Lang M, Sarma JV, Zetoune FS, Rittirsch D, Neff TA, McGuire SR, et al. Generation of C5a in the absence of C3: A new complement activation pathway. *Nat Med*. 2006;12(6):682–7.
 34. Ritis K, Doumas M, Mastellos D, Micheli A, Giaglis S, Magotti P, et al. A Novel C5a Receptor-Tissue Factor Cross-Talk in Neutrophils Links Innate Immunity to Coagulation Pathways. *J Immunol*. 2006;177(7):4794–802.
 35. Martel C, Cointe S, Maurice P, Matar S, Ghitescu M, Thérout P, et al. Requirements for membrane attack complex formation and anaphylatoxins binding to collagen-activated platelets. *PLoS One*. 2011;6(4):1–12.
 36. Del Conde I, Cruz MA, Zhang H, López JA, Afshar-Kharghan V. Platelet activation leads to activation and propagation of the complement system. *J Exp Med*. 2005;201(6):871–9.
 37. Willeke P, Kümpers P, Schlüter B, Limani A, Becker H, Schotte H. Platelet counts as a biomarker in ANCA-associated vasculitis. *Scand J Rheumatol*. 2015;44(4):302–8.
 38. Stassen PM, Derks RPH, Kallenberg CGM, Stegeman CA. Venous thromboembolism in ANCA-associated vasculitis - Incidence and risk factors. *Rheumatology*. 2008;47(4):530–4.
 39. Merkel PA, Lo GH, Holbrook JT, Tibbs AK, Allen NB. Article Brief Communication : High Incidence of Venous Thrombotic Events among Patients with Wegener Granulomatosis : The Wegener ' s Clinical. *Ann Intern Med*. 2005;142:620–6.
 40. Isaacs B, Gapud EJ, Antiochos B, Seo P, Geetha D. Venous Thrombotic Events in ANCA-Associated Vasculitis: Incidence and Risk Factors. *Kidney360*. 2020;1(4):258–62.
 41. Zöller B, Li X, Sundquist J, Sundquist K. Risk of pulmonary embolism in patients with autoimmune disorders: A nationwide follow-up study from Sweden. *Lancet*. 2012;379(9812):244–9.
 42. Allenbach Y, Seror R, Pagnoux C, Teixeira L, Guilpain P, Guillevin L. High frequency of venous thromboembolic events in Churg-Strauss syndrome, Wegener's granulomatosis and microscopic polyangiitis but not polyarteritis nodosa: A systematic Retrospective Study on 1130 patients. *Ann Rheum Dis*. 2009;68(4):564–7.
 43. Jennette JC, Falk RJ. Pathogenesis of antineutrophil cytoplasmic autoantibody-mediated disease. *Nat Rev Rheumatol*. 2014;10(8):463–73.
 44. Martinez Valenzuela L, Bordinon Draibe J, Fulladosa Oliveras X, Bestard Matamoros O, Cruzado Garrit JM, Torras Ambrós J. T-lymphocyte in ANCA-associated vasculitis: what do we know? A pathophysiological and therapeutic approach. *Clin Kidney J*. 2019;12(4):503–11.
 45. Rimbart M, Hamidou M, Braudeau C, Puéchal X, Teixeira L, Caillon H, et al. Decreased numbers of blood dendritic cells and defective function of regulatory T cells in antineutrophil cytoplasmic antibody-associated vasculitis. *PLoS One*. 2011;6(4).
 46. Morgan MD, Day CJ, Piper KP, Khan N, Harper L, Moss PA, et al. Patients with Wegener's granulomatosis demonstrate a relative deficiency and functional impairment of T-regulatory cells. *Immunology*. 2010;130(1):64–73.

47. Abdulahad WH, Van Der Geld YM, Stegeman CA, Kallenberg CGM. Persistent expansion of CD4+ effector memory T cells in Wegener's granulomatosis. *Kidney Int.* 2006;70(5):938–47.
48. Abdulahad WH, Stegeman CA, Van Der Geld YM, Doornbos-Van Der Meer B, Limburg PC, Kallenberg CGM. Functional defect of circulating regulatory CD4+ T cells in patients with Wegener's granulomatosis in remission. *Arthritis Rheum.* 2007;56(6):2080–91.
49. Katz Y, Nadiv O, Beer Y. Interleukin-17 Enhances Tumor Necrosis Factor α -Induced Synthesis of Interleukins 1, 6, and 8 in Skin and Synovial Fibroblasts: A Possible Role as a "Fine-Tuning Cytokine" in Inflammation Processes. *Arthritis Rheum.* 2001;44(9):2176–84.
50. Fossiez F, Djossou O, Chomarat P, Flores-Romo L, Ait-Yahia S, Maat C, et al. T cell interleukin-17 induces stromal cells to produce proinflammatory and hematopoietic cytokines. *J Exp Med.* 1996;183(6):2593–603.
51. Nogueira E, Hamour S, Sawant D, Henderson S, Mansfield N, Chavele KM, et al. Serum IL-17 and IL-23 levels and autoantigen-specific Th17 cells are elevated in patients with ANCA-associated vasculitis. *Nephrol Dial Transplant.* 2010;25(7):2209–17.
52. Popa ER, Stegeman CA, Bos NA. Differential B- and T-cell activation in Wegener's granulomatosis. *J Allergy Clin Immunol.* 1999;103(5):885–94.
53. Disteldorf EM, Krebs CF, Paust HJ, Turner JE, Nouailles G, Tittel A, et al. CXCL5 drives neutrophil recruitment in TH17-mediated GN. *J Am Soc Nephrol.* 2014;26(1):55–66.
54. Iking-Konert C, Vogl T, Prior B, Wagner C, Sander O, Bleck E, et al. T lymphocytes in patients with primary vasculitis: Expansion of CD8+ T cells with the propensity to activate polymorphonuclear neutrophils. *Rheumatology.* 2008;47(5):609–16.
55. Krumbholz M, Specks U, Wick M, Kalled SL, Jenne D, Meinel E. BAFF is elevated in serum of patients with Wegener's granulomatosis. *J Autoimmun.* 2005;25(4):298–302.
56. Sanders JSF, Huitma MG, Kallenberg CGM, Stegeman CA. Plasma levels of soluble interleukin 2 receptor, soluble CD30, interleukin 10 and B cell activator of the tumour necrosis factor family during follow-up in vasculitis associated with proteinase 3-antineutrophil cytoplasmic antibodies: Associations with di. *Ann Rheum Dis.* 2006;65(11):1484–9.
57. Nagai M, Hirayama K, Ebihara I, Shimohata H, Kobayashi M, Koyama A. Serum levels of BAFF and APRIL in myeloperoxidase anti-neutrophil cytoplasmic autoantibody-associated renal vasculitis: Association with disease activity. *Nephron - Clin Pract.* 2011;118(4):339–46.
58. Scapini P, Nardelli B, Nadali G, Calzetti F, Pizzolo G, Montecucco C, et al. G-CSF-stimulated neutrophils are a prominent source of functional BlyS. *J Exp Med.* 2003;197(3):297–302.
59. Walsh M, Merkel PA, Peh C-A, Szpirt WM, Puéchal X, Fujimoto S, et al. Plasma Exchange and Glucocorticoids in Severe ANCA-Associated Vasculitis. *N Engl J Med.* 2020;382(7):622–31.
60. Tateyama K, Kodama S, Kishibe K, Harabuchi Y, Suzuki M. A novel strategy with combined assays for detection of anti-neutrophil cytoplasmic antibody (ANCA) in clinically ANCA-negative granulomatosis with polyangiitis patients. *J Otolaryngol Japan.* 2017;121(8):1131–2.
61. Roth AJ, Ooi JD, Hess JJ, Van Timmeren MM, Berg EA, Poulton CE, et al. Epitope specificity determines

- pathogenicity and detectability in anca-associated vasculitis. *J Clin Invest*. 2013;123(4):1773–83.
62. Kelley JM, Monach PA, Ji C, Zhou Y, Wu J, Tanaka S, et al. IgA and IgG antineutrophil cytoplasmic antibody engagement of Fc receptor genetic variants influences granulomatosis with polyangiitis. *Proc Natl Acad Sci U S A*. 2011;108(51):20736–41.
 63. Kain R, Matsui K, Exner M, Binder S, Schaffner G, Somner EM, et al. A Novel Class of Autoantigens of Anti-neutrophil Cytoplasmic Antibodies in Necrotizing and Crescentic Glomerulonephritis: The Lysosomal Membrane Glycoprotein h-lamp-2 in Neutrophil Granulocytes and a Related Membrane Protein in Glomerular Endothelial Cell. *J ex*. 1995;181(February).
 64. Kain R, Exner M, Brandes R, Ziehermayr R, Alderson CA, Davidovits A, et al. Molecular mimicry in pauci-immune focal necrotizing glomerulonephritis. *Nat Med*. 2008;14(10):1088–96.
 65. Kain R, Tadema H, McKinney EF, Benharkou A, Brandes R, Peschel A, et al. High prevalence of autoantibodies to hLAMP-2 in anti-neutrophil cytoplasmic antibody-associated vasculitis. *J Am Soc Nephrol*. 2012;23(3):556–66.
 66. Peschel A, Basu N, Benharkou A, Brandes R, Brown M, Dieckmann R, et al. Autoantibodies to hLAMP-2 in ANCA-negative pauci-immune focal necrotizing GN. *J Am Soc Nephrol*. 2014;25(3):455–63.
 67. Roth AJ, Brown MC, Smith RN, Badhwar AK, Parente O, Chung HC, et al. Anti-LAMP-2 antibodies are not prevalent in patients with antineutrophil cytoplasmic autoantibody glomerulonephritis. *J Am Soc Nephrol*. 2012;23(3):545–55.
 68. Richard Kitching AR, Holdsworth SR, Ploplis VA, Plow EF, Collen D, Carmeliet P, et al. Plasminogen and plasminogen activators protect against renal injury in crescentic glomerulonephritis. *J Exp Med*. 1997;185(5):963–8.
 69. Berden AE, Nolan SL, Morris HL, Bertina RM, Erasmus DD, Hagen EC, et al. Anti-plasminogen antibodies compromise fibrinolysis and associate with renal histology in ANCA-associated vasculitis. *J Am Soc Nephrol*. 2010;21(12):2169–79.
 70. Hao J, Wang C, Gou SJ, Zhao MH, Chen M. The association between anti-plasminogen antibodies and disease activity in ANCA-associated vasculitis. *Rheumatol (United Kingdom)*. 2014;53(2):300–6.
 71. Bautz DJ, Preston GA, Lionaki S, Hewins P, Wolberg AS, Jia JY, et al. Antibodies with dual reactivity to plasminogen and complementary PR3 in PR3-ANCA vasculitis. *J Am Soc Nephrol*. 2008;19(12):2421–9.
 72. Mendoza CE, Brant EJ, McDermott ML, Froment A, Hu Y, Hogan SL, et al. Elevated Microparticle Tissue Factor Activity Differentiates Patients With Venous Thromboembolism in Anti-neutrophil Cytoplasmic Autoantibody Vasculitis. *Kidney Int Reports*. 2019;4(11):1617–29.
 73. Göçeroğlu A, Grenmyr E, Berden AE, Hagen EC, Bunch D, Sommarin Y, et al. Anti-plasminogen antibodies in ANCA-associated vasculitis: An optimized anti-plasminogen assay. *PLoS One*. 2018;13(11):1–10.
 74. Nagao T, Suzuki K, Utsunomiya K, Matsumura M, Saiga K, Wang PC, et al. Direct activation of glomerular endothelial cells by anti-moesin activity of anti-myeloperoxidase antibody. *Nephrol Dial Transplant*. 2011;26(9):2752–60.
 75. Suzuki K, Suzuki K, Nagao T, Itabashi M, Hamano Y, Sugamata R, et al. A novel autoantibody against moesin in the serum of patients with MPO-ANCA-associated vasculitis. *Nephrol Dial Transplant*. 2014;29(6):1168–

- 77.
76. Damianovich M, Gilburd B GJ et al. Pathogenic role of anti-endothelial cell antibodies in vasculitis. An idiotypic experimental model. *J Immunol.* 1996;156:4946–51.
77. Cong M, Chen M, Zhang JJ, Hu Z, Zhao MH. Anti-endothelial cell antibodies in antineutrophil cytoplasmic antibodies negative pauci-immune crescentic glomerulonephritis. *Nephrology.* 2008;13(3):228–34.
78. Schreiber A, Busjahn A, Luft FC, Kettritz R. Membrane expression of proteinase 3 is genetically determined. *J Am Soc Nephrol.* 2003;14(1):68–75.
79. Schreiber A, Luft FC, Kettritz R. Membrane proteinase 3 expression and ANCA-induced neutrophil activation. *Kidney Int.* 2004;65(6):2172–83.
80. Yang JJ, Pendergraft WF, Alcorta DA, Nachman PH, Hogan SL, Thomas RP, et al. Circumvention of normal constraints on granule protein gene expression in peripheral blood neutrophils and monocytes of patients with antineutrophil cytoplasmic autoantibody-associated glomerulonephritis. *J Am Soc Nephrol.* 2004;15(8):2103–14.
81. Ciavatta DJ, Yang JJ, Preston GA, Badhwar AK, Xiao H, Hewins P, et al. Epigenetic basis for aberrant upregulation of autoantigen genes in humans with ANCA vasculitis. *J Clin Invest.* 2010;120(9):3209–19.
82. Jaenisch R, Bird A. Epigenetic regulation of gene expression: How the genome integrates intrinsic and environmental signals. *Nat Genet.* 2003;33(3S):245–54.
83. Jones BE, Yang J, Muthigi A, Hogan SL, Hu Y, Starmer J, et al. Gene-specific DNA methylation changes predict remission in patients with ANCA-associated vasculitis. *J Am Soc Nephrol.* 2016;28(4):1175–87.
84. Lyons PA, Rayner TF, Trivedi S, Holle JU, Watts RA, Jayne DRW, et al. Genetically distinct subsets within ANCA-associated vasculitis. *N Engl J Med.* 2012;367(3):214–23.
85. Lane SE, Watts RA, Bentham G, Innes NJ, Scott DGI. Are environmental factors important in primary systemic vasculitis? A case-control study. *Arthritis Rheum.* 2003;48(3):814–23.
86. Willeke P, Schlüter B, Sauerland C, Becker H, Reuter S, Jacobi A, et al. Farm exposure as a differential risk factor in ANCA-associated vasculitis. *PLoS One.* 2015;10(9):1–12.
87. Stamp LK, Chapman PT, Francis J, Beckert L, Frampton C, Watts RA, et al. Association between environmental exposures and granulomatosis with polyangiitis in Canterbury, New Zealand. *Arthritis Res Ther.* 2015;17(1):1–8.
88. Hogan SL, Cooper GS, Savitz DA, Nylander-French LA, Parks CG, Chin H, et al. Association of silica exposure with anti-neutrophil cytoplasmic autoantibody small-vessel vasculitis: A population-based, case-control study. *Clin J Am Soc Nephrol.* 2007;2(2):290–9.
89. Haubitz M, Woywodt A, De Groot K, Haller H, Goebel U. Smoking habits in patients diagnosed with ANCA associated small vessel vasculitis. *Ann Rheum Dis.* 2005;64(10):1500–2.
90. Basu, N, Mohammad A, Watts RA, Gatenby P, Flores-Suarez LF, Mahr A. The effect of smoking on the clinical expression of anca-associated vasculitis. *Arthritis Rheum.* 2013;65:S1192–3.
91. McDermott G, Fu X, Stone JH, Wallwork R, Zhang Y, Choi HK, et al. Association of Cigarette Smoking with Antineutrophil Cytoplasmic Antibody-Associated Vasculitis. *JAMA Intern Med.* 2020;180(6):870–6.
92. Sessa A, Meroni M, Battini G, Vaccari M, Giordanol F, Torri Tarelli L. Cigarette smoking and pauci-immune

- extracapillary glomerulonephritis with anca-associated idiopathic systemic vasculitis: A retrospective study. *Contrib Nephrol.* 2000;130:103–8.
93. Benarous L, Terrier B, Puéchal X, Dunogué B, Cohen P, Le Jeune C, et al. Tobacco differentially affects the clinical-biological phenotypes of ANCA-associated vasculitides. *Clin Exp Rheumatol.* 2015;33(2):116–21.
 94. Koldingsnes W, Nossent H. Epidemiology of Wegener’s granulomatosis in northern Norway. *Arthritis Rheum.* 2000;43(11):2481–7.
 95. Draibe J, Rodó X, Fulladosa X, Martínez-Valenzuela L, Diaz-Encarnación M, Santos L, et al. Seasonal variations in the onset of positive and negative renal ANCA-associated vasculitis in Spain. *Clin Kidney J.* 2018;11(4):468–73.
 96. Mahr A, Artigues N, Coste J, Aouba A, Pagnoux C, Guillevin L. Seasonal variations in onset of Wegener’s granulomatosis: Increased in summer? [3]. *J Rheumatol.* 2006;34(4):889–90.
 97. Hogan SL, Satterly KK, Dooley MA, Nachman PH, Jennette JC, Falk RJ. Silica exposure in anti-neutrophil cytoplasmic autoantibody-associated glomerulonephritis and Lupus nephritis. *J Am Soc Nephrol.* 2001;12(1):134–42.
 98. Rihova Z, Maixnerova D, Jancova E, Pelcova D, Bartunkova J, Fenclova Z, et al. Silica and asbestos exposure in ANCA-associated vasculitis with pulmonary involvement. *Ren Fail.* 2005;27(5):605–8.
 99. Beaudreuil S, Lasfargues G, Laureiere L, Ghoul Z tl, Fourquet F, Longuet C, et al. Occupational exposure in ANCA-positive patients : A case-control study. *Kidney Int.* 2005;67:1961–6.
 100. Gómez-Puerta JA, Gedmintas L, Costenbader KH. The association between silica exposure and development of ANCA-associated vasculitis: Systematic review and meta-analysis. *Autoimmun Rev.* 2013;12(12):1129–35.
 101. Tervaert JWC, Stegeman CA, Kallenberg CG. Silicon exposure and vasculitis. *Curr Opin Rheumatol.* 1998;10:12–7.
 102. Holder SM te., Joy MS, Falk RJ. Cutaneous and systemic manifestations of drug-induced vasculitis. *Ann Pharmacother.* 2002;36(1):130–47.
 103. McGrath MM, Isakova T, Rennke HG, Mottola AM, Laliberte KA, Niles JL. Contaminated cocaine and antineutrophil cytoplasmic antibody-associated disease. *Clin J Am Soc Nephrol.* 2011;6(12):2799–805.
 104. Yu F, Chen M, Gao Y, Wang S xia, Zou W zhong, Zhao M hui, et al. Clinical and Pathological Features of Renal Involvement in Propylthiouracil-Associated ANCA-Positive Vasculitis. *Am J Kidney Dis.* 2007;49(5):607–14.
 105. Choi HK, Slot MC, Pan G, Weissbach CA, Niles JL, Merkel PA. Evaluation of antineutrophil cytoplasmic antibody seroconversion induced by minocycline, sulfasalazine, or penicillamine. *Arthritis Rheum.* 2000;43(11):2488–92.
 106. Choi HK, Merkel PA, Walker AM, Niles JL. Drug-associated antineutrophil cytoplasmic antibody-positive vasculitis: Prevalence among patients with high titers of antimyeloperoxidase antibodies. *Arthritis Rheum.* 2000;43(2):405–13.
 107. Visavachaipan N, Ong-Ajyooth L, Chanchairujira T, Parichatikanond P, Choensuchon B. Clinical features

- and outcomes in patient with antineutrophil cytoplasmic autoantibody-Positive glomerulonephritis associated with propylthiouracil treatment in Siriraj Hospital. *J Med Assoc Thai.* 2010;93(SUPPL 1):139–46.
108. Morita S, Ueda Y, Eguchi K. Anti-Thyroid Drug-Induced ANCA-Associated Vasculitis: A Case Report and Review of the Literature. *Endocr J.* 2000;47(4):467–70.
 109. Jiang X, Khursigara G, Rubin RL. Transformation of lupus-inducing drugs to cytotoxic products by activated neutrophils. *Science (80-).* 1994;266(5186):810–3.
 110. Nakazawa D, Tomaru U, Suzuki A, Masuda S, Hasegawa R, Kobayashi T, et al. Abnormal conformation and impaired degradation of propylthiouracil-induced neutrophil extracellular traps: Implications of disordered neutrophil extracellular traps in a rat model of myeloperoxidase antineutrophil cytoplasmic antibody-associated vasculiti. *Arthritis Rheum.* 2012;64(11):3779–87.
 111. Trimarchi M, Gregorini G, Facchetti F, Morassi ML, Manfredini C, Maroldi R, et al. Cocaine-induced midline destructive lesions: Clinical, radiographic, histopathologic, and serologic features and their differentiation from Wegener granulomatosis. *Medicine (Baltimore).* 2001;80(6):391–404.
 112. Graft J, Lynch K, Yeh CL, Tarter L, Richman N, Nguyen T, et al. Purpura, cutaneous necrosis, and antineutrophil cytoplasmic antibodies associated with levamisole-adulterated cocaine. *Arthritis Rheum.* 2011;63(12):3998–4001.
 113. Friedman DR, Wolfsthal SD. Cocaine-Induced Pseudovasculitis. *Mayo Clin Proc.* 2005;80(5):671–3.
 114. Stegeman CA, Cohen Tervaert JW, Sluiter WJ, Manson WL, De Jong PE, Kallenberg CGM. Association of chronic nasal carriage of *Staphylococcus aureus* and higher relapse rates in Wegener granulomatosis. *Ann Intern Med.* 1994;120(1):12–7.
 115. Laudien M, Gadola SD, Podschun R, Hedderich J, Paulsen J, Reinhold-Keller E, et al. Nasal carriage of *Staphylococcus aureus* and endonasal activity in Wegener’s granulomatosis as compared to rheumatoid arthritis and chronic rhinosinusitis with nasal polyps. *Clin Exp Rheumatol.* 2010;28(1 SUPPL. 57):51–5.
 116. Salmela A, Rasmussen N, Tervaert JWC, Jayne DRW, Ekstrand A. Chronic nasal *Staphylococcus aureus* carriage identifies a subset of newly diagnosed granulomatosis with polyangiitis patients with high relapse rate. *Rheumatol (United Kingdom).* 2017;56(6):965–72.
 117. Pendergraft WF, Preston GA, Shah RR, Tropsha A, Carter CW, Jennette JC, et al. Autoimmunity is triggered by cPR-3(105-201), a protein complementary to human autoantigen proteinase-3. *Nat Med.* 2003;10(1):72–9.
 118. Hewins P, Belmonte F, Charles Jennette J, Falk RJ, Preston GA. Longitudinal studies of patients with ANCA vasculitis demonstrate concurrent reactivity to complementary PR3 protein segments cPR3m and cPR3C and with no reactivity to cPR3N. *Autoimmunity.* 2011;44(2):98–106.
 119. Glasner C, De Goffau MC, Van Timmeren MM, Schulze ML, Jansen B, Tavakol M, et al. Genetic loci of *Staphylococcus aureus* associated with anti-neutrophil cytoplasmic autoantibody (ANCA)-associated vasculitides. *Sci Rep.* 2017;7(1):1–9.
 120. Tadema H, Abdulhad WH, Lepse N, Stegeman CA, Kallenberg CGM, Heeringa P. Bacterial DNA motifs trigger ANCA production in ANCA-associated vasculitis in remission. *Rheumatology.* 2011;50(4):689–96.

121. Miranda-Fillooy JA, Veiga JA, Juarez Y, Gonzalez-Juanatey C, Gonzalez-Gay MA, Garcia-Porrúa C. Microscopic polyangiitis following recurrent *Staphylococcus aureus* bacteremia and infectious endocarditis. *Clin Exp Rheumatol*. 2006;24(6):705–6.
122. Ooi JD, Jiang JH, Eggenhuizen PJ, Chua LL, van Timmeren M, Loh KL, et al. A plasmid-encoded peptide from *Staphylococcus aureus* induces anti-myeloperoxidase nephritogenic autoimmunity. *Nat Commun*. 2019;10(1).
123. Jennette JC, Falk RJ, Andrassy K, Bacon PA, Churg J, Gross WL, et al. Nomenclature of Systemic Vasculitides. *Arthritis Rheum*. 1994;37(2):187–92.
124. Jennette JC, Falk RJ, Bacon PA, N. B, Cid MC, Ferrario L., et al. 2012 Revised International Chapel Hill Consensus Conference Nomenclature of Vasculitides. *Arthritis Rheum*. 2012;65(1):1–11.
125. Hagen EC, Daha MR, Hermans J, Andrassy K, Csernok E, Gaskin G, et al. Diagnostic value of standardized assays for anti-neutrophil cytoplasmic antibodies in idiopathic systemic vasculitis. *Kidney Int*. 1998;53(3):743–53.
126. Sable-Fourtassou R, Cohen P, Mahr A, Pagnoux C, Mouthon L, Jayne D, et al. Antineutrophilic Cytoplasmic Antibodies and the Churg-Stauss Syndrome. *Ann Intern Med*. 2008;143(3):632–8.
127. Papo M, Sinico RA, Venhoff N, Urban M, Iudici M, Mahrhold J, et al. Significance of PR3-ANCA positivity in eosinophilic granulomatosis with polyangiitis (Churg-Strauss). *Rheumatology*. 2020;00:1–6.
128. Sunderkötter CH, Zelger B, Chen KR, Requena L, Piette W, Carlson JA, et al. Nomenclature of Cutaneous Vasculitis: Dermatologic Addendum to the 2012 Revised International Chapel Hill Consensus Conference Nomenclature of Vasculitides. *Arthritis Rheumatol*. 2018;70(2):171–84.
129. Robson J, Grayson P, Ponte C, Suppiah R, Craven A, Khalid S, et al. Classification criteria for the ANCA-associated vasculitides. *Rheumatology*. 2019;58(2):109–10.
130. Sebastiani M, Manfredi A, Vacchi C, Cassone G, Faverio P, Cavazza A, et al. Epidemiology and management of interstitial lung disease in ANCA-associated vasculitis. *Clin Exp Rheumatol*. 2020;38(2):221–31.
131. Watts RA, Lane SE, Bentham G, Scott DGI. Epidemiology of systemic vasculitis: A ten-year study in the United Kingdom. *Arthritis Rheum*. 2000;43(2):414–9.
132. Watts RA, Al-Taiar A, Scott DGI, MacGregor AJ. Prevalence and incidence of Wegener’s granulomatosis in the UK general practice research database. *Arthritis Care Res*. 2009;61(10):1412–6.
133. Mohammad AJ, Jacobsson LTH, Westman KWA, Sturfelt G, Segelmark M. Incidence and survival rates in Wegener’s granulomatosis, microscopic polyangiitis, Churg-Strauss syndrome and polyarteritis nodosa. *Rheumatology*. 2009;48(12):1560–5.
134. Watts RA, Mahr A, Mohammad AJ, Gatenby P, Basu N, Flores-Suárez LF. Classification, epidemiology and clinical subgrouping of antineutrophil cytoplasmic antibody (ANCA)-associated vasculitis. *Nephrol Dial Transplant*. 2015;30:i14–22.
135. Andrews M, Edmunds M, Campbell A, Walls J, Feehally J. Systemic vasculitis in the 1980s - Is there an increasing incidence of Wegener’s granulomatosis and microscopic polyarteritis? *J R Coll Physicians Lond*. 1990;24(4):284–8.
136. Knight A, Ekblom A, Brandt L, Askling J. Increasing incidence of Wegener’s granulomatosis in Sweden,

- 1975-2001. *J Rheumatol.* 2006;33(10):2060–3.
137. Hedger N, Stevens J, Drey N, Walker S, Roderick P. Incidence and outcome of pauci-immune rapidly progressive glomerulonephritis in Wessex, UK: A 10-year retrospective study. *Nephrol Dial Transplant.* 2000;15(10):1593–9.
138. Berti A, Cornec D, Crowson CS, Specks U, Metteson EL. The epidemiology of ANCA associated vasculitis in Olmsted County, Minnesota (USA): a 20 year population-based study. *Arthritis Rheumatol.* 2017;69(12):2338–50.
139. Watts RA, MacGregor AJ, Mackie SL. HLA allele variation as a potential explanation for the geographical distribution of granulomatosis with polyangiitis. *Rheumatol (United Kingdom).* 2015;54(2):359–62.
140. Watts RA, Lane SE, Scott DI, Koldingsnes W, Nossent H, Gonzalez-Gay MA, et al. Epidemiology of vasculitis in Europe. *Ann Rheum Dis.* 2001;60(12):1156–7.
141. Berti A, Cornec-Le Gall E, Cornec D, Casal Moura M, Matteson EL, Crowson CS, et al. Incidence, prevalence, mortality and chronic renal damage of anti-neutrophil cytoplasmic antibody-associated glomerulonephritis in a 20-year population-based cohort. *Nephrol Dial Transplant.* 2018;34(9):1508–17.
142. de Joode AAE, Sanders JSF, Stegeman CA. Renal survival in Proteinase 3 and Myeloperoxidase ANCA-associated systemic Vasculitis. *Clin J Am Soc Nephrol.* 2013;8(10):1709–17.
143. Chen M, Yu F, Wang SX, Zou WZ, Zhao MH, Wang HY. Antineutrophil cytoplasmic autoantibody-negative pauci-immune crescentic glomerulonephritis. *J Am Soc Nephrol.* 2007;18(2):599–605.
144. Hung PH, Chiu YL, Lin WC, Chiang WC, Chen YM, Lin SL, et al. Poor renal outcome of antineutrophil cytoplasmic antibody negative pauci-immune glomerulonephritis in Taiwanese. *J Formos Med Assoc.* 2006;105(10):804–12.
145. Kim HW, Kim JW, Im CH, Shin KC, Lee EY, Lee EB, et al. The clinicopathologic characteristics of granulomatosis with polyangiitis (Wegener's): A retrospective study of 45 patients in Korea. *Mod Rheumatol.* 2013;23(5):864–71.
146. Lee SW, Yu MY, Baek SH, Ahn SY, Kim S, Na KY, et al. Long-term prognosis of anti-neutrophil cytoplasmic antibody-negative renal vasculitis: Cohort study in Korea. *J Korean Med Sci.* 2016;31(4):542–6.
147. Córdova-Sánchez BM, Mejía-Vilet JM, Morales-Buenrostro LE, Loyola-Rodríguez G, Uribe-Urbe NO, Correa-Rotter R. Clinical presentation and outcome prediction of clinical, serological, and histopathological classification schemes in ANCA-associated vasculitis with renal involvement. *Clin Rheumatol.* 2016;35(7):1805–16.
148. Holle JU, Gross WL, Holl-Ulrich K, Ambrosch P, Noelle B, Both M, et al. Prospective long-term follow-up of patients with localised Wegener's granulomatosis: Does it occur as persistent disease stage? *Ann Rheum Dis.* 2010;69(11):1934–9.
149. Kemna MJ, Damoiseaux J, Austen J, Winkens B, Peters J, Van Paassen P, et al. ANCA as a predictor of relapse: Useful in patients with renal involvement but not in patients with nonrenal disease. *J Am Soc Nephrol.* 2015;26(3):537–42.
150. Stone JH. Limited versus severe Wegener's granulomatosis: Baseline data on patients in the Wegener's granulomatosis etanercept trial. *Arthritis Rheum.* 2003;48(8):2299–309.

151. Wojciechowska J, Kręćicki T. Clinical characteristics of patients with granulomatosis with polyangiitis and microscopic polyangiitis in ENT practice: a comparative analysis. *Acta Otorhinolaryngol Ital.* 2018;38(6):517–27.
152. Morgan MD, Szeto M, Walsh M, Jayne D, Westman K, Rasmussen N, et al. Negative anti-neutrophil cytoplasm antibody at switch to maintenance therapy is associated with a reduced risk of relapse. *Arthritis Res Ther.* 2017;19(1):1–7.
153. Smith RM, Jones RB, Guerry MJ, Laurino S, Catapano F, Chaudhry A, et al. Rituximab for remission maintenance in relapsing antineutrophil cytoplasmic antibody-associated vasculitis. *Arthritis Rheum.* 2012;64(11):3760–9.
154. Yates M, Watts RA, Bajema IM, Cid MC, Crestani B, Hauser T, et al. EULAR/ERA-EDTA recommendations for the management of ANCA-associated vasculitis. *Ann Rheum Dis.* 2016;75(9):1583–94.
155. Karras A, Pagnoux C, Haubitz M, De Groot K, Puechal X, Tervaert JWC, et al. Randomised controlled trial of prolonged treatment in the remission phase of ANCA-associated vasculitis. *Ann Rheum Dis.* 2017;76(10):1662–8.
156. Robson J, Doll H, Suppiah R, Flossmann O, Harper L, Höglund P, et al. Damage in the ANCA-associated vasculitides: Long-term data from the European Vasculitis Study Group (EUVAS) therapeutic trials. *Ann Rheum Dis.* 2013;74(1):177–84.
157. Robson J, Doll H, Suppiah R, Flossmann O, Harper L, Höglund P, et al. Glucocorticoid treatment and damage in the anti-neutrophil cytoplasm antibody-associated vasculitides: Long-term data from the European Vasculitis Study Group trials. *Rheumatol (United Kingdom).* 2014;54(3):471–81.
158. Coutinho AE, Chapman KE. The anti-inflammatory and immunosuppressive effects of glucocorticoids, recent developments and mechanistic insights. *Mol Cell Endocrinol.* 2011;335(1):2–13.
159. Jin JY, Almon RR, Dubois DC, Jusko WJ. Modeling of corticosteroid pharmacogenomics in rat liver using gene microarrays. *J Pharmacol Exp Ther.* 2003;307(1):93–109.
160. O’neill WM, Etheridge WB, Bloomer HA. High-Dose Corticosteroids: Their Use in Treating Idiopathic Rapidly Progressive Glomerulonephritis. *Arch Intern Med.* 1979;139(5):514–8.
161. Bolton K, Couser WG. Intravenous pulse methylprednisolone therapy of acute primary crescentic rapidly progressive glomerulonephritis. *Am J Med.* 1979;66:495–502.
162. Bolton K, Sturgill B. Methylprednisolone Therapy for Acute Crescentic Rapidly Progressive Glomerulonephritis. *Am J Nephrol.* 1989;9:368–75.
163. Jayne DRW, Gaskin G, Rasmussen N, Abramowicz D, Ferrario F, Guillevin L, et al. Randomized trial of plasma exchange or high-dosage methylprednisolone as adjunctive therapy for severe renal vasculitis. *J Am Soc Nephrol.* 2007;18(7):2180–8.
164. De Groot K, Rasmussen N, Bacon PA, Tervaert JWC, Feighery C, Gregorini G, et al. Randomized trial of cyclophosphamide versus methotrexate for induction of remission in early systemic antineutrophil cytoplasmic antibody-associated vasculitis. *Arthritis Rheum.* 2005;52(8):2461–9.
165. Pepper RJ, McAdoo SP, Moran SM, Kelly D, Scott J, Hamour S, et al. A novel glucocorticoid-free maintenance regimen for anti-neutrophil cytoplasm antibody-associated vasculitis. *Rheumatology*

- (Oxford). 2019;58(2):260–8.
166. Chanouzas D, McGregor JAG, Nightingale P, Salama AD, Szpirt WM, Basu N, et al. Intravenous pulse methylprednisolone for induction of remission in severe ANCA associated Vasculitis: A multi-center retrospective cohort study. *BMC Nephrol*. 2019;20(1):1–8.
 167. McGregor JAG, Hogan SL, Hu Y, Jennette CE, Falk RJ, Nachman PH. Glucocorticoids and relapse and infection rates in anti-neutrophil cytoplasmic antibody disease. *Clin J Am Soc Nephrol*. 2012;7(2):240–7.
 168. Furuta S, Nakagomi D, Kobayashi Y, Hiraguri M, Sugiyama T, Amano K, et al. Effect of reduced-dose vs high-dose glucocorticoids added to rituximab on remission induction in anca-associated vasculitis: A randomized clinical trial. *JAMA - J Am Med Assoc*. 2021;325(21):2178–87.
 169. Xiao Y, Guyatt G, Zeng L, RW Jayne D, A Merkel P, AC Siemieniuk R, et al. Comparative efficacy and safety of alternative glucocorticoids regimens in patients with ANCA-associated vasculitis: a systematic review. *BMJ Open*. 2022;12(2):e050507.
 170. Fauci AS, Katz P, Haynes BF, Wolff SM. Cyclophosphamide Therapy of Severe Systemic Necrotizing Vasculitis. *N Engl J Med*. 1979;301(5):235–8.
 171. Adu D, Pall A, Luqmani RA, Richards NT, Howie AJ, Emery P, et al. Controlled trial of pulse versus continuous prednisolone and cyclophosphamide in the treatment of systemic vasculitis. *QJM - Mon J Assoc Physicians*. 1997;90(6):401–9.
 172. Haubitz M, Schellong S, Göbel U, Schurek HJ, Schaumann D, Koch KM, et al. Intravenous pulse administration of cyclophosphamide versus daily oral treatment in patients with antineutrophil cytoplasmic antibody-associated vasculitis and renal involvement: A prospective, randomized study. *Arthritis Rheum*. 1998;41(10):1835–44.
 173. Guillevin L, Cordier JF, Lhote F, Cohen P, Jarrousse B, Royer I, et al. A prospective, multicenter, randomized trial comparing steroids and pulse cyclophosphamide versus steroids and oral cyclophosphamide in the treatment of generalized Wegener's granulomatosis. *Arthritis Rheum*. 1997;40(12):2187–98.
 174. Groot K De, Harper L, Jayne DRW, Felipe L, Suarez F, Gregorini G. Pulse Versus Daily Oral Cyclophosphamide for Induction of Remission. *Ann Intern Med*. 2009;150(8):670–80.
 175. Harper L, Morgan MD, Walsh M, Hoglund P, Westman K, Flossmann O, et al. Pulse versus daily oral cyclophosphamide for induction of remission in ANCA-associated vasculitis: Long-term follow-up. *Ann Rheum Dis*. 2011;71(6):955–60.
 176. Stone JH, Merkel PA, Spiera R, Seo P, Langford C, Hoffman G, et al. Rituximab versus Cyclophosphamide for ANCA-Associated Vasculitis. *N Engl J Med*. 2010;363:221–32.
 177. Jones RB, Tervaert JWC, Hauser T, Luqmani R, Morgan MD, Peh C-A, et al. Rituximab versus Cyclophosphamide in ANCA-Associated Renal Vasculitis. *N Engl J Med*. 2010;363(3):211–20.
 178. Smith RM, Jones RB, Specks U, Bond S, Nodale M, Aljayyousi R, et al. Rituximab as therapy to induce remission after relapse in ANCA-associated vasculitis. *Ann Rheum Dis*. 2019;79(9):1243–9.
 179. Martinez Del Pero M, Chaudhry A, Jones RB, Sivasothy P, Jani P, Jayne D. B-cell depletion with rituximab for refractory head and neck Wegener's granulomatosis: A cohort study. *Clin Otolaryngol*. 2009;34(4):328–35.

180. Keogh KA, Wylam ME, Stone JH, Specks U. Induction of remission by B lymphocyte depletion in eleven patients with refractory antineutrophil cytoplasmic antibody-associated vasculitis. *Arthritis Rheum.* 2005;52(1):262–8.
181. Mélet J, Mulleman D, Goupille P, Ribourtout B, Watier H, Thibault G. Rituximab-induced T cell depletion in patients with rheumatoid arthritis: Association with clinical response. *Arthritis Rheum.* 2013;65(11):2783–90.
182. Uchiyama S, Suzuki Y, Otake K, Yokoyama M, Ohta M, Aikawa S, et al. Development of novel humanized anti-CD20 antibodies based on affinity constant and epitope. *Cancer Sci.* 2010;101(1):201–9.
183. Robak T, Robak E. New anti-CD20 monoclonal antibodies for the treatment of B-cell lymphoid malignancies. *BioDrugs.* 2011;25(1):13–25.
184. Czuczman MS, Fayad L, Delwail V, Cartron G, Jacobsen E, Kuliczowski K, et al. Ofatumumab monotherapy in rituximab-refractory follicular lymphoma: Results from a multicenter study. *Blood.* 2012;119(16):3698–704.
185. Matasar MJ, Czuczman MS, Rodriguez MA, Fennessy M, Shea TC, Spitzer G, et al. Ofatumumab in combination with ICE or DHAP chemotherapy in relapsed or refractory intermediate grade B-cell lymphoma. *Blood.* 2013;122(4):499–506.
186. McAdoo SP, Bedi R, Tarzi R, Griffith M, Pusey CD, Cairns TD. Ofatumumab for B cell depletion therapy in ANCA-associated vasculitis: A single-centre case series. *Rheumatol (United Kingdom).* 2016;55(8):1437–42.
187. Furie R, Petri M, Zamani O, Cervera R, Wallace DJ, Tegzová D, et al. A phase III, randomized, placebo-controlled study of belimumab, a monoclonal antibody that inhibits B lymphocyte stimulator, in patients with systemic lupus erythematosus. *Arthritis Rheum.* 2011;63(12):3918–30.
188. Navarra S V., Guzmán RM, Gallacher AE, Hall S, Levy RA, Jimenez RE, et al. Efficacy and safety of belimumab in patients with active systemic lupus erythematosus: A randomised, placebo-controlled, phase 3 trial. *Lancet.* 2011;377(9767):721–31.
189. McClure ME, Wason J, Gopaluni S, Tieu J, Smith RM, Jayne DR, et al. Evaluation of PR3-ANCA Status after Rituximab for ANCA-Associated Vasculitis. *J Clin Rheumatol.* 2019;25(5):217–23.
190. Rovin BH, Adler SG, Barratt J, Bridoux F, Burdge KA, Chan TM, et al. KDIGO 2021 Clinical Practice Guideline for the Management of Glomerular Diseases. *Kidney Int.* 2021;100(4):S1–276.
191. Mcadool SP, Medjeral-Thomas N, Gopaluni S, Tanna A, Mansfield N, Galliford J, et al. Long-term follow-up of a combined rituximab and cyclophosphamide regimen in renal anti-neutrophil cytoplasm antibody-associated vasculitis. *Nephrol Dial Transplant.* 2019;34(1):63–73.
192. Galati K, Edwards H, Prendecki M, Cairns TD, Condon M, Galliford J, et al. Combination treatment with rituximab, low-dose cyclophosphamide and plasma exchange for severe antineutrophil cytoplasmic antibody-associated vasculitis. *Kidney Int.* 2021;100:1316–24.
193. Walsh M, Merkel PA, Peh CA, Szpirt WM, Puechal X, Fujimoto S, et al. Plasma exchange and glucocorticoids in severe ANCA-associated vasculitis (supplementary file). *N Engl J Med.* 2020;382(7):622–31.
194. Hu W, Liu C, Xie H, Chen H, Liu Z, Li L. Mycophenolate mofetil versus cyclophosphamide for inducing

- remission of ANCA vasculitis with moderate renal involvement. *Nephrol Dial Transplant*. 2008;23(4):1307–12.
195. Han F, Liu G, Zhang X, Li X, He Q, He X, et al. Effects of mycophenolate mofetil combined with corticosteroids for induction therapy of microscopic polyangiitis. *Am J Nephrol*. 2011;33(2):185–92.
196. Jones RB, Hiemstra TF, Ballarin J, Blockmans DE, Brogan P, Bruchfeld A, et al. Mycophenolate mofetil versus cyclophosphamide for remission induction in ANCA-associated vasculitis: A randomised, non-inferiority trial. *Ann Rheum Dis*. 2019;1–7.
197. Hiemstra TF, Walsh M, Mahr A, Savage CO, De Groot K, Harper L, et al. Mycophenolate mofetil vs azathioprine for remission maintenance in antineutrophil cytoplasmic antibody-associated vasculitis: A randomized controlled trial. *JAMA - J Am Med Assoc*. 2010;304(21):2381–8.
198. Faurischou M, Westman K, Rasmussen N, De Groot K, Flossmann O, Höglund P, et al. Long-term outcome of a randomized clinical trial comparing methotrexate to cyclophosphamide for remission induction in early systemic antineutrophil cytoplasmic antibody-associated vasculitis. *Arthritis Rheum*. 2012;64(10):3472–7.
199. Jayne DRW, Bruchfeld AN, Harper L, Schaefer M, Venning MC, Hamilton P, et al. Randomized trial of C5a receptor inhibitor avacopan in ANCA-associated vasculitis. *J Am Soc Nephrol*. 2017;28(9):2756–67.
200. Jayne DRW, Merkel PA, Schall TJ, Bekker P. Supplementary Appendix: Avacopan for the Treatment of ANCA-Associated Vasculitis. *N Engl J Med*. 2021;384(7):599–609.
201. Merkel P, Jayne D, Harigai M, Schall T, Bekker P, Potarca A, et al. Randomized Phase 3 Trial Evaluating the Safety and Efficacy of Avacopan in Patients With New or Relapsing Anca-Associated Vasculitis. *Rheumatology*. 2019;58(Supplement_2):2–4.
202. Békássy ZD, Kristoffersson AC, Rebetz J, Tati R, Olin AI, Karpman D. Aliskiren inhibits renin-mediated complement activation. *Kidney Int*. 2018;94(4):689–700.
203. Ribes D, Belliere J, Piedrafita A, Faguer S. Glucocorticoid-free induction regimen in severe ANCA-associated vasculitis using a combination of rituximab and eculizumab. *Rheumatol (United Kingdom)*. 2019;58(12):2335–7.
204. Wechsler ME, Akuthota P, Jayne D, Khoury P, Klion A, Langford CA, et al. Mepolizumab or placebo for eosinophilic granulomatosis with polyangiitis. *N Engl J Med*. 2017;376(20):1921–32.
205. Steinfeld J, Bradford ES, Brown J, Mallett S, Yancey SW, Akuthota P, et al. Evaluation of clinical benefit from treatment with mepolizumab for eosinophilic granulomatosis with polyangiitis. *J Allergy Clin Immunol*. 2019;143(6):2170–7.
206. Shimizu T, Morita T, Kumanogoh A. The therapeutic efficacy of intravenous immunoglobulin in anti-neutrophilic cytoplasmic antibody-associated vasculitis: A meta-analysis. *Rheumatol (United Kingdom)*. 2020;59(5):959–67.
207. Jayne DRW. Intravenous immunoglobulin for ANCA-associated systemic vasculitis with persistent disease activity. *Qjm*. 2000;93(7):433–9.
208. Jayne DRW, Merkel PA, Schall TJ, Bekker P. Avacopan for the Treatment of ANCA-Associated Vasculitis. *N Engl J Med*. 2021;384(7):599–609.

209. Miloslavsky EM, Niles JL, Wallace ZS, Cortazar FB, Fernandes A, Laliberte K, et al. Reducing glucocorticoid duration in ANCA-associated vasculitis: A pilot trial. *Semin Arthritis Rheum*. 2018;48(2):288–92.
210. Walsh M, Merkel P, Mahr A, Jayne D. The effects of duration of glucocorticoid therapy on relapse rate in anti-neutrophil cytoplasm antibody associated vasculitis: A meta-analysis. *Arthritis care*. 2010;62(8):1166–73.
211. Hoffman GS, Kerr GS, Leavitt RY, Hallahan CW, Lebovics RS, Travis WD, et al. Wegener granulomatosis: An analysis of 158 patients. *Ann Intern Med*. 1992;116(6):488–98.
212. Jayne D, Rasmussen N, Andrassy K, Bacon P, Tervaert JWC, Dadoniené J, et al. A randomized trial of maintenance therapy for vasculitis associated with antineutrophil cytoplasmic autoantibodies. *N Engl J Med*. 2003;349(1):36–44.
213. Walsh M, Faurschou M, Berden A, Flossmann O, Bajema I, Hoglund P, et al. Long-term follow-up of cyclophosphamide compared with azathioprine for initial maintenance therapy in anca-associated vasculitis. *Clin J Am Soc Nephrol*. 2014;9(9):1571–6.
214. Reinhold-Keller E, Fink COE, Herlyn K, Gross WL, de Groot K. High rate of renal relapse in 71 patients with Wegener’s granulomatosis under maintenance of remission with low-dose methotrexate. *Arthritis Rheum*. 2002;47(3):326–32.
215. Pagnoux C, Mahr A, Hamidou MA, Boffa J-J, Ruivard M, Ducroix J-P, et al. Azathioprine or methotrexate maintenance for ANCA-associated vasculitis. *N Engl J Med*. 2008;360(13):1358–9.
216. Maritati F, Alberici F, Oliva E, Urban ML, Palmisano A, Santarsia F, et al. Methotrexate versus cyclophosphamide for remission maintenance in ANCA-associated vasculitis: A randomised trial. *PLoS One*. 2017;12(10):1–14.
217. Metzler C, Miehle N, Manger K, Iking-Konert C, de Groot K, Hellmich B, et al. Elevated relapse rate under oral methotrexate versus leflunomide for maintenance of remission in Wegener’s granulomatosis. *Rheumatology*. 2007;46(7):1087–91.
218. Specks U, Merkel PA, Seo P, Spiera R, Langford CA, Hoffman GS, et al. Efficacy of remission-induction regimens for ANCA-associated vasculitis. *N Engl J Med*. 2013;369(5):417–27.
219. Alberici F, Smith RM, Jones RB, Roberts DM, Willcocks LC, Chaudhry A, et al. Long-term follow-up of patients who received repeat-dose rituximab as maintenance therapy for ANCA-associated vasculitis. *Rheumatol (United Kingdom)*. 2014;54(7):1153–60.
220. Guillevin L, Pagnoux C, Karras A, Khouatra C, Aumaître O, Cohen P, et al. Rituximab versus azathioprine for maintenance in ANCA-associated vasculitis. *N Engl J Med*. 2014;371(19):1771–80.
221. Terrier B, Pagnoux C, Perrodeau É, Karras A, Khouatra C, Aumaître O, et al. Long-term efficacy of remission-maintenance regimens for ANCA-associated vasculitides. *Ann Rheum Dis*. 2018;77(8):1151–7.
222. Charles P, Terrier B, Perrodeau É, Cohen P, Faguer S, Huart A, et al. Comparison of individually tailored versus fixed-schedule rituximab regimen to maintain ANCA-associated vasculitis remission: Results of a multicentre, randomised controlled, phase III trial (MAINRITSAN2). *Ann Rheum Dis*. 2018;77(8):1144–50.
223. Charles P, Samson M, Bonnotte B, Agard C, Huart A, Karras A, et al. Long-Term Rituximab Use to Maintain Remission of Antineutrophil Background : Objective : *Ann Intern Med*. 2020;173(3):179–87.

224. Pusey CD, Rees AJ, Evans DJ, Peters DK, Lockwood CM. Plasma exchange in focal necrotizing glomerulonephritis without anti-GBM antibodies. *Kidney Int.* 1991;40(4):757–63.
225. Cole E, Cattran D, Magil A, Greenwood C, Churchill D, Sutton D, et al. A Prospective Randomized Trial of Plasma Exchange as Additive Therapy in Idiopathic Crescentic Glomerulonephritis. *Am J Kidney Dis.* 1992;20(3):261–9.
226. Zäuner I, Bach D, Braun N, Krämer BK, Fünfstück R, Helmchen U, et al. Predictive value of initial histology and effect of plasmapheresis on long-term prognosis of rapidly progressive glomerulonephritis. *Am J Kidney Dis.* 2002;39(1):28–35.
227. Szpirt WM, Heaf JG, Petersen J. Plasma exchange for induction and cyclosporine A for maintenance of remission in Wegener’s granulomatosis clinical randomized controlled trial. *Nephrol Dial Transplant.* 2010;26(1):206–13.
228. Walsh M, Casian A, Flossmann O, Westman K, Höglund P, Pusey C, et al. Long-term follow-up of patients with severe ANCA-associated vasculitis comparing plasma exchange to intravenous methylprednisolone treatment is unclear. *Kidney Int.* 2013;84(2):397–402.
229. Walsh M, Catapano F, Szpirt W, Thorlund K, Bruchfeld A, Guillevin L, et al. Plasma exchange for renal vasculitis and idiopathic rapidly progressive glomerulonephritis: a meta-analysis. *Am J Kidney Dis.* 2011;57(4):566–74.
230. De Lind Van Wijngaarden RAF, Hauer HA, Wolterbeek R, Jayne DRW, Gaskin G, Rasmussen N, et al. Clinical and histologic determinants of renal outcome in ANCA-associated vasculitis: A prospective analysis of 100 patients with severe renal involvement. *J Am Soc Nephrol.* 2006;17(8):2264–74.
231. Moura MC, Irazabal M V., Eirin A, Zand L, Sethi S, Borah BJ, et al. Efficacy of rituximab and plasma exchange in antineutrophil cytoplasmic antibody-associated vasculitis with severe kidney disease. *J Am Soc Nephrol.* 2020;31(11):2688–704.
232. Cartin-Ceba R, Diaz-Caballero L, Al-Qadi MO, Tryfon S, Fervenza FC, Ytterberg SR, et al. Diffuse Alveolar Hemorrhage Secondary to Antineutrophil Cytoplasmic Antibody-Associated Vasculitis: Predictors of Respiratory Failure and Clinical Outcomes. *Arthritis Rheumatol.* 2016;68(6):1467–76.
233. Walsh M, Collister D, Zeng L, Merkel PA, Pusey CD, Guyatt G, et al. The effects of plasma exchange in patients with ANCA-associated vasculitis: an updated systematic review and meta-analysis. *Bmj.* 2022;e064604.
234. Zeng L, Walsh M, Guyatt GH, Siemieniuk RAC, Collister D, Booth M, et al. Plasma exchange and glucocorticoid dosing for patients with ANCA-associated vasculitis: a clinical practice guideline. *Bmj.* 2022;e064597.
235. Balogun RA, Sanchez AP, Klingel R, Witt V, Aqui N, Meyer E, et al. Update to the ASFA guidelines on the use of therapeutic apheresis in ANCA-associated vasculitis. *J Clin Apher.* 2020;35(5):493–9.
236. Stegmayr BG, Almroth G, Berlin G, Fehrman I, Kurkus J, Norda R, et al. Plasma exchange or immunoadsorption in patients with rapidly progressive crescentic glomerulonephritis: A Swedish multi-center study. *Int J Artif Organs.* 1999;22(2):81–7.
237. Furuta T, Hotta O, Yusa N, Horigome I, Chiba S, Taguma Y. Lymphocytapheresis to treat rapidly progressive

- glomerulonephritis: A randomised comparison with steroid-pulse treatment. *Lancet*. 1998;352(9123):203–4.
238. Reinhold-Keller E, De Groot K, Rudert H, Nölle B, Heller M, Gross WL. Response to trimethoprim/sulfamethoxazole in Wegener's granulomatosis depends on the phase of disease. *QJM - Mon J Assoc Physicians*. 1996;89(1):15–23.
239. Zycinska K, Wardyn A, Zielonka TM, Krupa R, Lukas W. Co-trimoxazole and the prevention of relapses of PR3-ANCA positive vasculitis with pulmonary involvement. *Eur J Med Res*. 2009;14:265–7.
240. Stegeman CA, Tervaert JWC, Jong PE, M KG. Trimethoprim-Sulfamethoxazole (Co-trimoxazole) for the prevention of relapses of Wegener's granulomatosis. *N Engl J Med*. 1996;335:16–20.
241. Zycinska K, Wardyn KA, Zielonka TM, Demkow U, Traburzynski MS, Systemic P, et al. Chronic crusting, nasal carriage of *Staphylococcus aureus* and relapse rate in pulmonary Wegener's granulomatous inflammation of the upper and lower respiratory tract. *Journal of physiology & pharmacology*. 2008;825–31.
242. Kronbichler A, Kerschbaum J, Gopaluni S, Tieu J, Alberici F, Jones RB, et al. Trimethoprim-sulfamethoxazole prophylaxis prevents severe/life-threatening infections following rituximab in antineutrophil cytoplasm antibody-associated vasculitis. *Ann Rheum Dis*. 2017;1440–7.
243. Collins BF, Raghu G. Antifibrotic therapy for fibrotic lung disease beyond idiopathic pulmonary fibrosis. *Eur Respir Rev*. 2019;28(153).
244. Flaherty KR, Wells AU, Cottin V, Devaraj A, Walsh SLF, Inoue Y, et al. Nintedanib in progressive fibrosing interstitial lung diseases. *N Engl J Med*. 2019;381(18):1718–27.
245. Cassone G, Sebastiani M, Vacchi C, Cerri S, Salvarani C, Manfredi A. Pirfenidone for the treatment of interstitial lung disease associated to rheumatoid arthritis: a new scenario is coming? *Respir Med Case Reports*. 2020;30(March):0–5.
246. Flossmann O, Berden A, De Groot K, Hagen C, Harper L, Heijl C, et al. Long-term patient survival in ANCA-associated vasculitis. *Ann Rheum Dis*. 2011;70(3):488–94.
247. Berden AE, Ferrario F, Hagen EC, Jayne DR, Jennette JC, Joh K, et al. Histopathologic classification of ANCA-associated glomerulonephritis. *J Am Soc Nephrol*. 2010;21(10):1628–36.
248. van Daalen EE, Wester Trejo MAC, Göçeroglu A, Ferrario F, Joh K, Noël LH, et al. Developments in the histopathological classification of ANCA-associated glomerulonephritis. *Clin J Am Soc Nephrol*. 2020;15(8):1103–11.
249. Hilhorst M, Wilde B, Van Breda Vriesman P, Van Paassen P, Tervaert JWC. Estimating renal survival using the ANCA-associated GN classification. *J Am Soc Nephrol*. 2013;24(9):1371–5.
250. Berden AE, Jones RB, Erasmus DD, Walsh M, Noël LH, Ferrario F, et al. Tubular lesions predict renal outcome in antineutrophil cytoplasmic antibody-associated glomerulonephritis after rituximab therapy. *J Am Soc Nephrol*. 2012;23(2):313–21.
251. Quintana LF, Pérez NS, De Sousa E, Rodas LM, Griffiths MH, Solé M, et al. ANCA serotype and histopathological classification for the prediction of renal outcome in ANCA-associated glomerulonephritis. *Nephrol Dial Transplant*. 2014;29(9):1764–9.

252. Chen YX, Xu J, Pan XX, Shen PY, Li X, Ren H, et al. Histopathological classification and renal outcome in patients with antineutrophil cytoplasmic antibodies-associated renal vasculitis: A study of 186 patients and meta analysis. *J Rheumatol*. 2017;44(3):304–13.
253. Brix SR, Noriega M, Tennstedt P, Vettorazzi E, Busch M, Nitschke M, et al. Development and validation of a renal risk score in ANCA-associated glomerulonephritis. *Kidney Int*. 2018;94(6):1177–88.
254. Ikeda S, Arita M, Misaki K, Kashiwagi Y, Ito Y, Yamada H, et al. Comparative investigation of respiratory tract involvement in granulomatosis with polyangiitis between PR3-ANCA positive and MPO-ANCA positive cases: A retrospective cohort study. *BMC Pulm Med*. 2015;15(1):1–11.
255. Gómez-Gómez A, Martínez-Martínez MU, Cuevas-Orta E, Bernal-Blanco JM, Cervantes-Ramírez D, Martínez-Martínez R, et al. Pulmonary Manifestations of Granulomatosis With Polyangiitis. *Reumatol Clínica (English Ed)*. 2014;10(5):288–93.
256. Schnabel A, Holl-Ulrich K, Dalhoff K, Reuter M, Gross WL. Efficacy of transbronchial biopsy in pulmonary vasculitides. *Eur Respir J*. 1997;10(12):2738–43.
257. Diamantopoulos II, Jones NS. The investigation of nasal septal perforations and ulcers. *J Laryngol Otol*. 2001;115(7):541–4.
258. Murray A, McGarry GW. The clinical value of septal perforation biopsy. *Clin Otolaryngol Allied Sci*. 2000;25(2):107–9.
259. Tsuzuki K, Fukazawa K, Takebayashi H, Hashimoto K, Sakagami M. Difficulty of diagnosing Wegener's granulomatosis in the head and neck region. *Auris Nasus Larynx*. 2009;36(1):64–70.
260. Borner U, Landis BN, Banz Y, Villiger P, Ballinari P, Caversaccio M, et al. Diagnostic value of biopsies in identifying cytoplasmic antineutrophil cytoplasmic antibody-negative localized Wegener's granulomatosis presenting primarily with sinonasal disease. *Am J Rhinol Allergy*. 2012;26(6):475–80.
261. Micheletti RG, Chiesa Fuxench Z, Craven A, Watts RA, Luqmani RA, Merkel PA. Cutaneous Manifestations of Antineutrophil Cytoplasmic Antibody-Associated Vasculitis. *Arthritis Rheumatol*. 2020;0–3.
262. Marzano AV, Raimondo MG, Berti E, Meroni PL, Ingegnoli F. Cutaneous Manifestations of ANCA-Associated Small Vessels Vasculitis. *Clin Rev Allergy Immunol*. 2017;53(3):428–38.
263. Zycinska K, Wardyn K, Zielonka TM, Nitsch-osuch A, Smolarczyk R. Cutaneous Changes: An Initial Manifestation of Pulmonary Wegener's Granulomatosis. *Respir Regul - Clin Adv [Internet]*. 2012;755:307–10.
264. Chen KR, Carlson JA. Clinical approach to cutaneous vasculitis. *Am J Clin Dermatol*. 2008;9(2):71–92.
265. Tan JA, Dehghan N, Chen W, Xie H, Esdaile JM, Avina-Zubieta JA. Mortality in ANCA-associated vasculitis: A meta-analysis of observational studies. *Ann Rheum Dis*. 2017;76(9):1566–74.
266. Chen KR. Skin involvement in ANCA-associated vasculitis. *Clin Exp Nephrol*. 2012;17(5):676–82.
267. Bischof A, Jaeger VK, Hadden RDM, Luqmani RA, Pröbstel AK, Merkel PA, et al. Peripheral neuropathy in antineutrophil cytoplasmic antibody-associated vasculitides: Insights from the DCVAS study. *Neuro Immunol neuroinflammation*. 2019;6(6).
268. Collins MP, Periquet MI. Isolated vasculitis of the peripheral nervous system. *Clin Exp Rheumatol*. 2008;26(3 SUPPL. 49):118–30.

269. Cordier J-F, Valeyre D, Guillevin L, Loire R, Brechot J-M. Pulmonary Wegener's Granulomatosis * A Clinical and Imaging Study of 77 Cases. *Chest*. 1990;97(4):906–12.
270. Seo JB, Im JG, Chung JW, Song JW, Goo JM, Park JH, et al. Pulmonary vasculitis: The spectrum of radiological findings. *Br J Radiol*. 2000;73(875):1224–31.
271. Lee KS, Kim TS, Fujimoto K, Moriya H, Watanabe H, Tateishi U, et al. Thoracic manifestation of Wegener's granulomatosis: CT findings in 30 patients. *Eur Radiol*. 2003;13(1):43–51.
272. Hirayama K, Kobayashi M, Usui J, Arimura Y, Sugiyama H, Nitta K, et al. Pulmonary involvements of anti-neutrophil cytoplasmic autoantibody-associated renal vasculitis in Japan. *Nephrol Dial Transplant*. 2015;30:i83–93.
273. Yamagata M, Ikeda K, Tsushima K, Iesato K, Abe M, Ito T, et al. Prevalence and Responsiveness to Treatment of Lung Abnormalities on Chest Computed Tomography in Patients with Microscopic Polyangiitis: A Multicenter, Longitudinal, Retrospective Study of One Hundred Fifty Consecutive Hospital-Based Japanese Patients. *Arthritis Rheumatol*. 2016;68(3):713–23.
274. Comarmond C, Crestani B, Tazi A, Hervier B, Adam-Marchand S, Nunes H, et al. Pulmonary fibrosis in antineutrophil cytoplasmic antibodies (ANCA)-associated vasculitis: A series of 49 patients and review of the literature. *Med (United States)*. 2014;93(24):340–9.
275. Huang H, Wang Y xun, Jiang C guo, Liu J, Li J, Xu K, et al. A retrospective study of microscopic polyangiitis patients presenting with pulmonary fibrosis in China. *BMC Pulm Med*. 2014;14(1):1–6.
276. Ando Y, Okada F, Matsumoto S, Mori H. Thoracic Manifestation of Myeloperoxidase-Antineutrophil. 2004;28(5):710–6.
277. Maillet T, Goletto T, Beltramo G, Dupuy H, Jouneau S, Borie R, et al. Usual interstitial pneumonia in ANCA-associated vasculitis: A poor prognostic factor. *J Autoimmun*. 2020;106(July).
278. Hosoda C, Baba T, Hagiwara E, Ito H, Matsuo N, Kitamura H, et al. Clinical features of usual interstitial pneumonia with anti-neutrophil cytoplasmic antibody in comparison with idiopathic pulmonary fibrosis. *Respirology*. 2016;21(5):920–6.
279. Yang C, Talbot JM, Hwang PH. Bony Abnormalities of the Paranasal Sinuses in Patients with Wegener's Granulomatosis. *Am J Rhinol*. 2001;15(2):121–5.
280. Lohrmann C, Uhl M, Warnatz K, Kotter E, Ghanem N, Langer M. Sinonasal computed tomography in patients with Wegener's granulomatosis. *J Comput Assist Tomogr*. 2006;30(1):122–5.
281. Zycinska K, Wardyn KA, Piotrowska E, Zielonka TM, Zycinski H, Bogaczewicz A, et al. Rhinologic and sinonasal changes in PR3 ANCA pulmonary vasculitis. *Eur J Med Res*. 2010;15(2):241–3.
282. D'Anza B, Langford CA, Sindwani R. Sinonasal imaging findings in Granulomatosis with polyangiitis (Wegener granulomatosis): A systematic review. *Am J Rhinol Allergy*. 2017;31(1):16–21.
283. Muhle C, Reinhold-Keller E, Richter C, Duncker G, Beigel A, Brinkmann G, et al. MRI of the nasal cavity, the paranasal sinuses and orbits in Wegener's granulomatosis. *Eur Radiol*. 1997;7(4):566–70.
284. Grindler D, Cannady S, Batra PS. Computed tomography findings in sinonasal Wegener's granulomatosis. *Am J Rhinol Allergy*. 2009;23(5):497–501.
285. Holme SS, Moen JM, Kilian K, Haukeland H, Molberg Ø, Eggesbø HB. Development of CT-based methods

- for longitudinal analyses of paranasal sinus osteitis in granulomatosis with polyangiitis. *BMC Med Imaging*. 2019;19(1):1–11.
286. Tan LT, Davagnanam I, Isa H, Taylor SR, Rose GE, Verity DH, et al. Clinical and imaging features predictive of orbital granulomatosis with polyangiitis and the risk of systemic involvement. *Ophthalmology*. 2014;121(6):1304–9.
287. Ito K, Minamimoto R, Yamashita H, Yoshida S, Morooka M, Okasaki M, et al. Evaluation of Wegener’s granulomatosis using 18F-fluorodeoxyglucose positron emission tomography/computed tomography. *Ann Nucl Med*. 2013;27(3):209–16.
288. Ozmen O, Tatci E, Gokcek A, Koksal D, Dadali Y, Ozaydin E, et al. Integration of 2-deoxy-2-[18F] fluoro-d-glucose PET/CT into clinical management of patients with Wegener’s granulomatosis. *Ann Nucl Med*. 2013;27(10):907–15.
289. Nelson D, Johnson G, Cartin-Ceba R, Specks U. Characterization of F-18 fluorodeoxyglucose PET/CT in granulomatosis with polyangiitis. *Sarcoidosis Vasc Diffus Lung Dis*. 2016;18(32):342–52.
290. De’Oliviera J, Gaskin G, Dash A, Rees AJ, Pusey CD. Relationship between disease activity and anti-neutrophil cytoplasmic antibody concentration in long-term management of systemic vasculitis. *Am J Kidney Dis*. 1995;25(3):380–9.
291. Davenport A, Lock RJ, Wallington T. Clinical Significance of the Serial Measurement of Autoantibodies to Neutrophil Cytoplasm using a Standard Indirect Immunofluorescence Test. *Am J Nephrol*. 1995;15:201–7.
292. Kyndt X, Reumaux D, Bridoux F, Tribout B, Bataille P, Hachulla E, et al. Serial measurements of antineutrophil cytoplasmic autoantibodies in patients with systemic vasculitis. *Am J Med*. 1999;106(5):527–33.
293. Girard T, Mahr A, Noël LH, Cordier JF, Lesavre P, André MH, et al. Are antineutrophil cytoplasmic antibodies a marker predictive of relapse in Wegener’s granulomatosis? A prospective study. *Rheumatology*. 2001;40(2):147–51.
294. Hogan SL, Falk RJ, Chin H, Cai J, Jennette CE, Jennette JC, et al. Predictors of Relapse and Treatment Resistance in Antineutrophil. *Ann Intern Med*. 2005;621–32.
295. Birck R, Schmitt WH, Kaelsch IA, Van Der Woude FJ. Serial ANCA determinations for monitoring disease activity in patients with ANCA-associated vasculitis: Systematic review. *Am J Kidney Dis*. 2006;47(1):15–23.
296. Tomasson G, Grayson PC, Mahr AD, LaValley M, Merkel PA. Value of ANCA measurements during remission to predict a relapse of ANCA-associated vasculitis-a meta-analysis. *Rheumatology*. 2012;51(1):100–9.
297. Dam LS Van, Dirikgil E, Bredewold EW, Ray A, Bakker JA, Kooten C Van, et al. Proteinase-3-anti-neutrophil cytoplasmic antibodies (PR3-ANCAs) predict relapses in ANCA-associated vasculitis patients after rituximab. *Nephrol Dial Transplant*. 2020;1–10.
298. Thai LH, Charles P, Resche-Rigon M, Desseaux K, Guillevin L. Are anti-proteinase-3 ANCA a useful marker of granulomatosis with polyangiitis (Wegener’s) relapses? Results of a retrospective study on 126

- patients. *Autoimmun Rev.* 2014;13(3):313–8.
299. Fijolek J, Wiatr E, Petroniec V, Augustynowicz-Kopec E, Bednarek M, Gawryluk D, et al. Antineutrophil cytoplasmic antibodies and their relationship with disease activity and presence of staphylococcal superantigens in nasal swabs in patients having granulomatosis with polyangiitis: results of a study involving 115 patients from a single cen. *Clin Rheumatol.* 2019;38(11):3297–305.
300. Miloslavsky EM, Specks U, Merkel PA, Seo P, Langford CA, Hoffman GS, et al. Clinical Outcomes of Remission Induction Therapy for Severe Antineutrophil Cytoplasmic Antibody–Associated Vasculitis. *Arthritis Rheum.* 2013;65(9):2441–9.
301. Watanabe H, Sada KE, Matsumoto Y, Harigai M, Amano K, Dobashi H, et al. Association Between Reappearance of Myeloperoxidase–Antineutrophil Cytoplasmic Antibody and Relapse in Antineutrophil Cytoplasmic Antibody–Associated Vasculitis: Subgroup Analysis of Nationwide Prospective Cohort Studies. *Arthritis Rheumatol.* 2018;70(10):1626–33.
302. Verstockt B, Bossuyt X, Vanderschueren S, Blockmans D. There is no benefit in routinely monitoring ANCA titres in patients with granulomatosis with polyangiitis. *Clin Exp Rheumatol.* 2015;33(2):72–6.
303. Sinico RA, Radice A, Corace C, Di Toma L, Sabadini E. Value of a new automated fluorescence immunoassay (EliA) for PR3 and MPO-ANCA in monitoring disease activity in ANCA-associated systemic vasculitis. *Ann N Y Acad Sci.* 2005;1050:185–92.
304. Boomsma MM, Stegeman CA, Van Der Leij MJ, Oost W, Hermans J, Kallenberg CGM, et al. Prediction of relapses in Wegener’s granulomatosis by measurement of antineutrophil cytoplasmic antibody levels: A prospective study. *Arthritis Rheum.* 2000;43(9):2025–33.
305. Fussner LA, Hummel AM, Schroeder DR, Silva F, Cartin-Ceba R, Snyder MR, et al. Factors Determining the Clinical Utility of Serial Measurements of Antineutrophil Cytoplasmic Antibodies Targeting Proteinase 3. *Arthritis Rheumatol.* 2016;68(7):1700–10.
306. Da Silva Domingues VM, Machado B, Santos J. ANCA-positive vasculitis: Clinical implications of ANCA types and titers. *Rev Assoc Med Bras.* 2016;62(5):434–40.
307. Finkelman JD, Merkel PA, Schroeder D, Hoffman GS, Spiera R, St Clair EW, et al. Annals of Internal Medicine Article Antiproteinase 3 Antineutrophil Cytoplasmic Antibodies and Disease. *Ann Intern Med.* 2007;147:611–9.
308. Olson SW, Arbogast CB, Baker TP, Owshalimpur D, Oliver DK, Abbott KC, et al. Asymptomatic autoantibodies associate with future anti-glomerular basement membrane disease. *J Am Soc Nephrol.* 2011;22(10):1946–52.
309. Olson SW, Owshalimpur D, Yuan CM, Arbogast C, Baker TP, Oliver D, et al. Relation between asymptomatic proteinase 3 antibodies and future granulomatosis with polyangiitis. *Clin J Am Soc Nephrol.* 2013;8(8):1312–8.
310. Houben E, Bax WA, van Dam B, Slieker WAT, Verhave G, Frerichs FCP, et al. Diagnosing ANCA-associated vasculitis in ANCA positive patients. *Medicine (Baltimore).* 2016;95(40):e5096.
311. Flores-Suárez LF, Cabiedes J, Villa AR, van der Woude FJ, Alcocer-Varela J. Prevalence of antineutrophil cytoplasmic autoantibodies in patients with tuberculosis. *Rheumatology.* 2003;42(2):223–9.

312. Cartin-Ceba R, Golbin JM, Keogh KA, Peikert T, Sánchez-Menéndez M, Ytterberg SR, et al. Rituximab for remission induction and maintenance in refractory granulomatosis with polyangiitis (Wegener's): Ten-year experience at a single center. *Arthritis Rheum.* 2012;64(11):3770–8.
313. Jones RB, Furuta S, Tervaert JWC, Hauser T, Luqmani R, Morgan MD, et al. Rituximab versus cyclophosphamide in ANCA-associated renal vasculitis: 2-year results of a randomised trial. *Ann Rheum Dis.* 2015;74(6):1178–82.
314. Ferraro AJ, Smith SW, Neil D, Savage COS. Relapsed Wegener's granulomatosis after rituximab therapy - B cells are present in new pathological lesions despite persistent "depletion" of peripheral blood. *Nephrol Dial Transplant.* 2008;23(9):3030–2.
315. Bunch DOD, Mcgregor JG, Khandoobhai NB, Aybar LT, Burkart ME, Hu Y, et al. Article Decreased CD5 B Cells in Active ANCA Vasculitis and Relapse after Rituximab. *Clin J Am Soc Nephrol.* 2013;8:1–10.
316. Unizony S, Lim N, Phippard DJ, Carey VJ, Eli M, Tchao NK, et al. Peripheral CD5 + B-cells in ANCA-Associated Vasculitis. *Arthritis Rheum.* 2015;67(2):535–44.
317. Bader L, Koldingsnes W, Nossent J. B-lymphocyte activating factor levels are increased in patients with Wegener's granulomatosis and inversely correlated with ANCA titer. *Clin Rheumatol.* 2010;29(9):1031–5.
318. Berti A, Warner R, Johnson K, Cornec D, Schroeder DR, Kabat BF, et al. The association of serum interleukin-6 levels with clinical outcomes in antineutrophil cytoplasmic antibody-associated vasculitis. *J Autoimmun.* 2019;105(July).
319. Monach P, Warner R, Tomasson G, Specks U, Stone J, Ding L. Serum proteins reflecting inflammation, injury and repair as biomarkers of disease activity in ANCA-associated vasculitis. *Ann Rheum Dis.* 2013;72(8):1342–50.
320. Gou SJ, Yuan J, Chen M, Yu F, Zhao MH. Circulating complement activation in patients with anti-neutrophil cytoplasmic antibody-associated vasculitis. *Kidney Int.* 2013;83(1):129–37.
321. Choi H, Kim Y, Jung SM, Song JJ, Park YB, Lee SW. Low serum complement 3 level is associated with severe ANCA-associated vasculitis at diagnosis. *Clin Exp Nephrol.* 2019;23(2):223–30.
322. Manenti L, Vaglio A, Gnappi E, Maggiore U, Allegri L, Allinovi M, et al. Association of serum C3 concentration and histologic signs of thrombotic microangiopathy with outcomes among patients with ANCA-associated renal vasculitis. *Clin J Am Soc Nephrol.* 2015;10(12):2143–51.
323. Augusto JF, Langs V, Demiselle J, Lavigne C, Brilland B, Duveau A, et al. Low serum complement C3 levels at diagnosis of renal ANCA-associated vasculitis is associated with poor prognosis. *PLoS One.* 2016;11(7):1–12.
324. Villacorta J, Diaz-Crespo F, Acevedo M, Caverro T, Guerrero C, Praga M, et al. Circulating C3 levels predict renal and global outcome in patients with renal vasculitis. *Clin Rheumatol.* 2016;35(11):2733–40.
325. Crnogorac M, Horvatic I, Kacinari P, Ljubanovic DG, Galesic K. Serum C3 complement levels in ANCA associated vasculitis at diagnosis is a predictor of patient and renal outcome. *J Nephrol.* 2017;31(2):257–62.
326. Moiseev S, Lee JM, Zykova A, Bulanov N, Novikov P, Gitel E, et al. The alternative complement pathway in ANCA-associated vasculitis: further evidence and a meta-analysis. *Clin Exp Immunol.* 2020;202(3):394–

- 402.
327. Chen SF, Wang FM, Li ZY, Yu F, Zhao MH, Chen M. Plasma complement factor H is associated with disease activity of patients with ANCA-associated vasculitis. *Arthritis Res Ther.* 2015;17(1):1–9.
328. Chen SF, Wang FM, Li ZY, Yu F, Chen M, Zhao MH. Complement factor H inhibits anti-neutrophil cytoplasmic autoantibody-induced neutrophil activation by interacting with neutrophils. *Front Immunol.* 2018;9(MAR):1–13.
329. Liang H, Xin M, Zhao L, Wang L, Sun M, Wang J. Serum creatinine level and ESR values associated to clinical pathology types and prognosis of patients with renal injury caused by ANCA-associated vasculitis. *Exp Ther Med.* 2017;14(6):6059–63.
330. Suppiah R, Mukhtyar C, Flossmann O, Alberici F, Baslund B, Batra R, et al. A cross-sectional study of the Birmingham vasculitis activity score version 3 in systemic vasculitis. *Rheumatology.* 2011;50(5):899–905.
331. Příklad P, Hrušková Z, Konopásek P, Hladinová Z, Tesař V, Vokurka M. Serum hepcidin is increased in ANCA-associated vasculitis and correlates with activity markers. *Physiol Res.* 2018;67(6):945–54.
332. Valenzuela LM, Draibe J, Ramos MQ, Oliveras XF, Melilli E, Garrit JMC, et al. Calprotectin as a smoldering activity detection tool and renal prognosis biomarker in ANCA associated vasculitis. *PLoS One.* 2018;13(10):1–13.
333. Zycinska K, Wardyn KA, Zielonka TM, Tyszko P, Straburzynski M. Procalcitonin as an indicator of systemic response to infection in active pulmonary Wegener's granulomatosis. *J Physiol Pharmacol.* 2008;59(SUPPL. 6):839–44.
334. Brunkhorst R, Eberhardt OK, Haubitz M, Brunkhorst FM. Procalcitonin for discrimination between activity of systemic autoimmune disease and systemic bacterial infection. *Intensive Care Med Suppl.* 2000;26(2):199–201.
335. Herrmann K, Schinke S, Csernok E, Moosig F, Holle J. Diagnostic Value of Procalcitonin in ANCA-Associated Vasculitis (AAV) to Differentiate Between Disease Activity, Infection and Drug Hypersensitivity. *Open Rheumatol J.* 2015;9(1):71–6.
336. Eberhard OK, Haubitz M, Brunkhorst FM, Kliem V, Koch KM, Brunkhorst R. Usefulness of Procalcitonin for Differentiation Between Systemic Lupus Erythematosus / Systemic Antineutrophil. *Rheumatism.* 1997;40(7):1250–6.
337. Park HJ, Jung SM, Song JJ, Park YB, Lee SW. Platelet to lymphocyte ratio is associated with the current activity of ANCA-associated vasculitis at diagnosis: a retrospective monocentric study. *Rheumatol Int.* 2018;38(10):1865–71.
338. Ahn SS, Jung SM, Song JJ, Park YB, Lee SW. Neutrophil to lymphocyte ratio at diagnosis can estimate vasculitis activity and poor prognosis in patients with ANCA-associated vasculitis: A retrospective study. *BMC Nephrol.* 2018;19(1):1–7.
339. Chen M, Wang F, Zhao MH. Circulating neutrophil gelatinase-associated lipocalin: A useful biomarker for assessing disease activity of ANCA-associated vasculitis. *Rheumatology.* 2009;48(4):355–8.
340. Woywodt A, Streiber F, De Groot K, Regelsberger H, Haller H, Haubitz M. Circulating endothelial cells as markers for ANCA-associated small-vessel vasculitis. *Lancet.* 2002;361(9353):206–10.

341. Monach PA, Kümpers P, Lukasz A, Tomasson G, Specks U, Stone JH, et al. Circulating angiopoietin-2 as a biomarker in ANCA-associated vasculitis. *PLoS One*. 2012;7(1).
342. Tam FWK, Sanders JS, George A, Hammad T, Miller C, Dougan T, et al. Urinary monocyte chemoattractant protein-1 (MCP-1) is a marker of active renal vasculitis. *Nephrol Dial Transplant*. 2004;19(11):2761–8.
343. Ohlsson S, Bakoush O, Tencer J, Torffvit O, Segelmark M. Monocyte chemoattractant protein 1 is a prognostic marker in ANCA-associated small vessel vasculitis. *Mediators Inflamm*. 2009;2009(February).
344. Lieberthal JG, Cuthbertson D, Carette S, Hoffman GS, Khalidi NA, Koenig CL, et al. Urinary biomarkers in relapsing antineutrophil cytoplasmic antibody-associated vasculitis. *J Rheumatol*. 2013;40(5):674–83.
345. Jönsson N, Erlandsson E, Gunnarsson L, Pettersson Å, Ohlsson S. Monocyte chemoattractant protein-1 in antineutrophil cytoplasmic autoantibody-associated vasculitis: Biomarker potential and association with polymorphisms in the MCP-1 and the CC chemokine receptor-2 gene. *Mediators Inflamm*. 2018;2018.
346. Liu S, Li N, Zhu Q, Zhu B, Wu T, Wang G, et al. Increased Serum MCP-1 Levels in Systemic Vasculitis Patients with Renal Involvement. *J Interf Cytokine Res*. 2018;38(9):406–12.
347. O'Reilly VP, Wong L, Kennedy C, Elliot LA, O'Meachair S, Coughlan AM, et al. Urinary soluble CD163 in active renal vasculitis. *J Am Soc Nephrol*. 2016;27(9):2906–16.
348. Aendekerk JP, Timmermans SAMEG, Busch MH, Potjewijd J, Heeringa P, Damoiseaux JGMC, et al. Urinary Soluble CD163 and Disease Activity in Biopsy-Proven ANCA-Associated Glomerulonephritis. *Clin J Am Soc Nephrol*. 2020;15:CJN.07210520.
349. Hruskova Z, Honsova E, Berden AE, Rychlik I, Lanska V, Zabka J, et al. Repeat protocol renal biopsy in ANCA-associated renal vasculitis. *Nephrol Dial Transplant*. 2014;29(9):1728–32.
350. Hauer HA, Bajema IM, Hagen EC, Noël LH, Ferrario F, Waldherr Rüd, et al. Long-term renal injury in ANCA-associated vasculitis: an analysis of 31 patients with follow-up biopsies. *Nephrol Dial Transplant*. 2002;17(4):587–96.
351. Moran SM, Monach PA, Zgaga L, Cuthbertson D, Carette S, Khalidi NA, et al. Urinary soluble CD163 and monocyte chemoattractant protein-1 in the identification of subtle renal flare in anti-neutrophil cytoplasmic antibody-associated vasculitis. *Nephrol Dial Transplant*. 2018;35(2):283–91.
352. Alcorta D, Preston G, Munger W, Sullivan P, Yang JJ, Waga I, et al. Microarray studies of gene expression in circulating leukocytes in kidney diseases. *Exp Nephrol*. 2002;10(2):139–49.
353. Kurz T, Weiner M, Skoglund C, Basnet S, Eriksson P, Segelmark M. A myelopoiesis gene signature during remission in anti-neutrophil cytoplasm antibody-associated vasculitis does not predict relapses but seems to reflect ongoing prednisolone therapy. *Clin Exp Immunol*. 2014;175(2):215–26.
354. McKinney EF, Lyons PA, Carr EJ, Hollis JL, Jayne DRW, Willcocks LC, et al. A CD8+ T cell transcription signature predicts prognosis in autoimmune disease. *Nat Med*. 2010;16(5):586–91.
355. Boudonck KJ, Mitchell MW, Németh L, Keresztes L, Nyska A, Shinar D, et al. Discovery of Metabolomics Biomarkers for Early Detection of Nephrotoxicity. *Toxicol Pathol*. 2009;37(3):280–92.
356. Guleria A, Misra DP, Rawat A, Dubey D, Khetrapal CL, Bacon P, et al. NMR-Based Serum Metabolomics Discriminates Takayasu Arteritis from Healthy Individuals: A Proof-of-Principle Study. *J Proteome Res*. 2015;14(8):3372–81.

357. Jain A, Kumar D, Guleria A, Misra DP, Zanwar A, Chaurasia S, et al. NMR-Based Serum Metabolomics of Patients with Takayasu Arteritis: Relationship with Disease Activity. *J Proteome Res.* 2018;17(9):3317–24.
358. Al-Ani B, Fitzpatrick M, Al-Nuaimi H, Coughlan AM, Hickey FB, Pusey CD, et al. Changes in urinary metabolomic profile during relapsing renal vasculitis. *Sci Rep.* 2016;6:1–11.
359. Gupta L, Jain A, Ekbote GG, Mishra R. NMR based serum metabolomics revealed distinctive metabolic Patterns of ANCA- associated vasculitis. *Int J Rheum Dis.* 2019;22(S3):40–226.
360. Morais CLM, Lima KMG, Singh M, Martin FL. Tutorial: multivariate classification for vibrational spectroscopy in biological samples. *Nat Protoc.* 2020;15(7):2143–62.
361. Trevisan J, Angelov PP, Carmichael PL, Scott AD, Martin FL. Extracting biological information with computational analysis of Fourier-transform infrared (FTIR) biospectroscopy datasets: Current practices to future perspectives. *Analyst.* 2012;137(14):3202–15.
362. Morais CLM, Paraskevaidi M, Cui L, Fullwood NJ, Isabelle M, Lima KMG, et al. Standardization of complex biologically derived spectrochemical datasets. Vol. 14, *Nature Protocols.* 2019. 1546–1577 p.
363. Morais CLM, Santos MCD, Lima KMG, Martin FL. Improving data splitting for classification applications in spectrochemical analyses employing a random-mutation Kennard-Stone algorithm approach. *Bioinformatics.* 2019;35(24):5257–63.
364. Paraskevaidi M, Morais CLM, Lima K, Snowden J, Saxon J, Richardson A, et al. Differential diagnosis of Alzheimer 's disease using spectrochemical analysis of blood. *Proc Natl Acad Sci USA.* 2017;114(38):7929–38.
365. Purandare NC, Trevisan J, Patel II, Gajjar K, Mitchell AL, Theophilou G, et al. Exploiting biospectroscopy as a novel screening tool for cervical cancer: towards a framework to validate its accuracy in a routine clinical setting. *Bioanalysis.* 2013;5(21):2697–711.
366. Shaw RA, Kotowich S, Eysel HH, Jackson M, Thomson GTD, Mantsch HH. Arthritis diagnosis based upon the near-infrared spectrum of synovial fluid. *Rheumatol Int.* 1995;15(4):159–65.
367. Chen M, McReynolds N, Campbell EC, Mazilu M, Barbosa J, Dholakia K, et al. The use of wavelength modulated raman spectroscopy in label-free identification of T lymphocyte subsets, natural killer cells and dendritic Cells. *PLoS One.* 2015;10(5):1–14.
368. Kamińska A, Winkler K, Kowalska A, Witkowska E, Szymborski T, Janeczek A, et al. SERS-based Immunoassay in a Microfluidic System for the Multiplexed Recognition of Interleukins from Blood Plasma: Towards Picogram Detection. *Sci Rep.* 2017;7(1):1–11.
369. Ci XIC, Hao ZEZ, Hang GEZ, Hen SHUOC, Hao YUEZ. Analysis and classification of kidney stones based on Raman spectroscopy. *Biomed Opt Express.* 2018;9(9):4175–83.
370. Chi J, Ma Y, Weng FL, Thiessen-philbrook H, Parikh R, Du H. Surface-enhanced Raman scattering analysis of urine from deceased donors as a prognostic tool for kidney transplant outcome. 2017;13:1–14.
371. Feng S, Zhou L, Lin D, Zhao J, Guan Q, Zheng B, et al. Assessment of treatment e ffi cacy using surface-enhanced Raman spectroscopy analysis of urine in rats with kidney transplantation or kidney disease. 2019;
372. Gaipov A, Utegulov Z, Bukasov R, Turebekov D, Tarlykov P, Markhametova Z, et al. Development and

- validation of hybrid Brillouin-Raman spectroscopy for non-contact assessment of mechano-chemical properties of urine proteins as biomarkers of kidney diseases. *BMC Nephrol.* 2020;21(1):1–9.
373. Haifler M, Pence I, Sun Y, Kutikov A, Uzzo RG, Patil AMCA. Discrimination of malignant and normal kidney tissue with short wave infrared dispersive Raman spectroscopy. 2018;(July 2017):1–8.
374. Id RSS, Sullivan M, Gouldin A, Lundgren S. Spectral characteristics of urine from patients with end-stage kidney disease analyzed using Raman Chemometric Urinalysis (Rametrix). 2020;1–12.
375. De Bruyne S, Van Dorpe J, Himpe J, Van Biesen W, Delanghe S, Speeckaert MM, et al. Detection and Characterization of a Biochemical Signature Associated with Diabetic Nephropathy Using Near-infrared Spectroscopy on Tissue Sections. *J Clin Med.* 2019;8(7):1022.
376. Varma VK, Kajdacsy-Balla A, Akkina SK, Setty S, Walsh MJ. A label-free approach by infrared spectroscopic imaging for interrogating the biochemistry of diabetic nephropathy progression. *Kidney Int.* 2016;89(5):1153–9.
377. Severcan F, Bozkurt O, Gurbanov R, Gorgulu G. FT-IR spectroscopy in diagnosis of diabetes in rat animal model. *J Biophotonics.* 2010;3(8–9):621–31.
378. Vuiblet V, Fere M, Gobinet C, Birembaut P, Piot O, Rieu P. Renal graft fibrosis and inflammation quantification by an automated fourier-transform infrared imaging technique. *J Am Soc Nephrol.* 2016;27(8):2382–91.
379. Esteve E, Luque Y, Waeytens J, Bazin D, Mesnard L, Jouanneau C, et al. Nanometric Chemical Speciation of Abnormal Deposits in Kidney Biopsy: Infrared-Nanospectroscopy Reveals Heterogeneities within Vancomycin Casts. *Anal Chem.* 2020;92(11):7388–92.
380. Khan AH, Imran S, Talati J, Jafri L. Fourier transform infrared spectroscopy for analysis of kidney stones. *Investig Clin Urol.* 2018;59(1):32–7.
381. Oliver K V., Vilasi A, Maréchal A, Moochhala SH, Unwin RJ, Rich PR. Infrared vibrational spectroscopy: A rapid and novel diagnostic and monitoring tool for cystinuria. *Sci Rep.* 2016;6:1–7.
382. Grunert T, Herzog R, Wiesenhofer FM, Vychytil A, Ehling-Schulz M, Kratochwill K. Vibrational spectroscopy of peritoneal dialysis effluent for rapid assessment of patient characteristics. *Biomolecules.* 2020;10(6):1–13.
383. Roth A, Dornuf F, Klein O, Schneditz D, Hafner-Gießauf H, Mäntele W. Infrared spectroscopy in hemodialysis: Reagent-free monitoring of patient detoxification by infrared spectroscopy. *Anal Bioanal Chem.* 2012;403(2):391–9.
384. Yu MC, Rich P, Foreman L, Smith J, Yu MS, Tanna A, et al. Label Free Detection of Sensitive Mid-Infrared Biomarkers of Glomerulonephritis in Urine Using Fourier Transform Infrared Spectroscopy. *Sci Rep.* 2017;7(1):1–12.
385. Bro R, Smilde AK. Principal component analysis. *Anal Methods.* 2014;6(9):2812–31.
386. Brereton RG, Lloyd GR. Partial least squares discriminant analysis: Taking the magic away. *J Chemom.* 2014;28(4):213–25.
387. Ballabio D, Consonni V. Classification tools in chemistry. Part 1: Linear models. PLS-DA. *Anal Methods.* 2013;5:3790–8.

388. Cortes C, Vapnik V. Support-Vector Networks. *Mach Learn.* 1995;297:273–97.
389. Morais CLM, Lima K. Comparing unfolded and two-dimensional discriminant analysis and support vector machines for classification of EEM data. *Chemom Intell Lab Syst.* 2017;162:123–9.
390. Movasaghi Z, Rehman S, Rehman IU. Raman spectroscopy of biological tissues. *Appl Spectrosc Rev.* 2007;42(5):493–541.
391. Maguchi S, Fukuda S, Takizawa M. Histological findings in biopsies from patients with cytoplasmic-antineutrophil cytoplasmic antibody (cANCA)-positive Wegener’s granulomatosis. *Auris Nasus Larynx.* 2001;28(SUPPL.):53–8.
392. Cui Z, Zhao MH, Segelmark M, Hellmark T. Natural autoantibodies to myeloperoxidase, proteinase 3, and the glomerular basement membrane are present in normal individuals. *Kidney Int.* 2010;78(6):590–7.
393. Morris AD, Rowbottom AW, Martin FL, Woywodt A, Dhaygude AP. Biomarkers in ANCA-associated vasculitis: potential pitfalls and future prospects. *Kidney360.* 2021;10.34067/KID.0006432020.
394. Carvalho CS, Martin AA, Santo AME, Andrade LEC, Pinheiro MM, Cardoso MAG, et al. A Rheumatoid arthritis study using Raman spectroscopy. *Theor Chem Acc.* 2011;130(4–6):1211–20.
395. Ginley B, Jen K-Y, Han SS, Rodrigues L, Jain S, Fogo AB, et al. Automated Computational Detection of Interstitial Fibrosis, Tubular Atrophy, and Glomerulosclerosis. *J Am Soc Nephrol.* 2021;32(4):837–50.
396. Karim B, Fleureau J, Rolland D, Lavastre O, Rioux-Leclercq N, Guille Francois, et al. Raman Spectroscopy: a novel experimental approach to evaluating renal tumours. *Eur Urol.* 2010;58(4):602–8.
397. Couapel J-P, Senhadji L, Rioux-Leclercq N, Verhoest G, Lavastre O, Crevoisier R de, et al. Optical spectroscopy techniques can accurately distinguish benign and malignant renal tumours. *BJU Int.* 2013;111(6):865–71.
398. Mert S, Özbek E, Ötünçtemur A, Çulha M. Kidney tumor staging using surface-enhanced Raman scattering. *J Biomed Opt.* 2015;20(4):047002.
399. Xing GQ, Chen M, Liu G, Heeringa P, Zhang JJ, Zheng X, et al. Complement activation is involved in renal damage in human antineutrophil cytoplasmic autoantibody associated pauci-immune vasculitis. *J Clin Immunol.* 2009;29(3):282–91.
400. Hodges MD, Kelly JG, Bentley AJ, Fogarty S, Patel II, Martin FL, et al. Combining immunolabeling and surface-enhanced Raman spectroscopy on cell membranes. *ACS Nano.* 2011;5(12):9535–41.
401. De Bruyne S, Speeckaert MM, Delanghe JR. Applications of mid-infrared spectroscopy in the clinical laboratory setting. *Crit Rev Clin Lab Sci.* 2018;55(1):1–20.

Appendix 1: Supplementary Information -Distinguishing active from quiescent disease in ANCA-associated vasculitis using attenuated total reflection Fourier-transform infrared spectroscopy

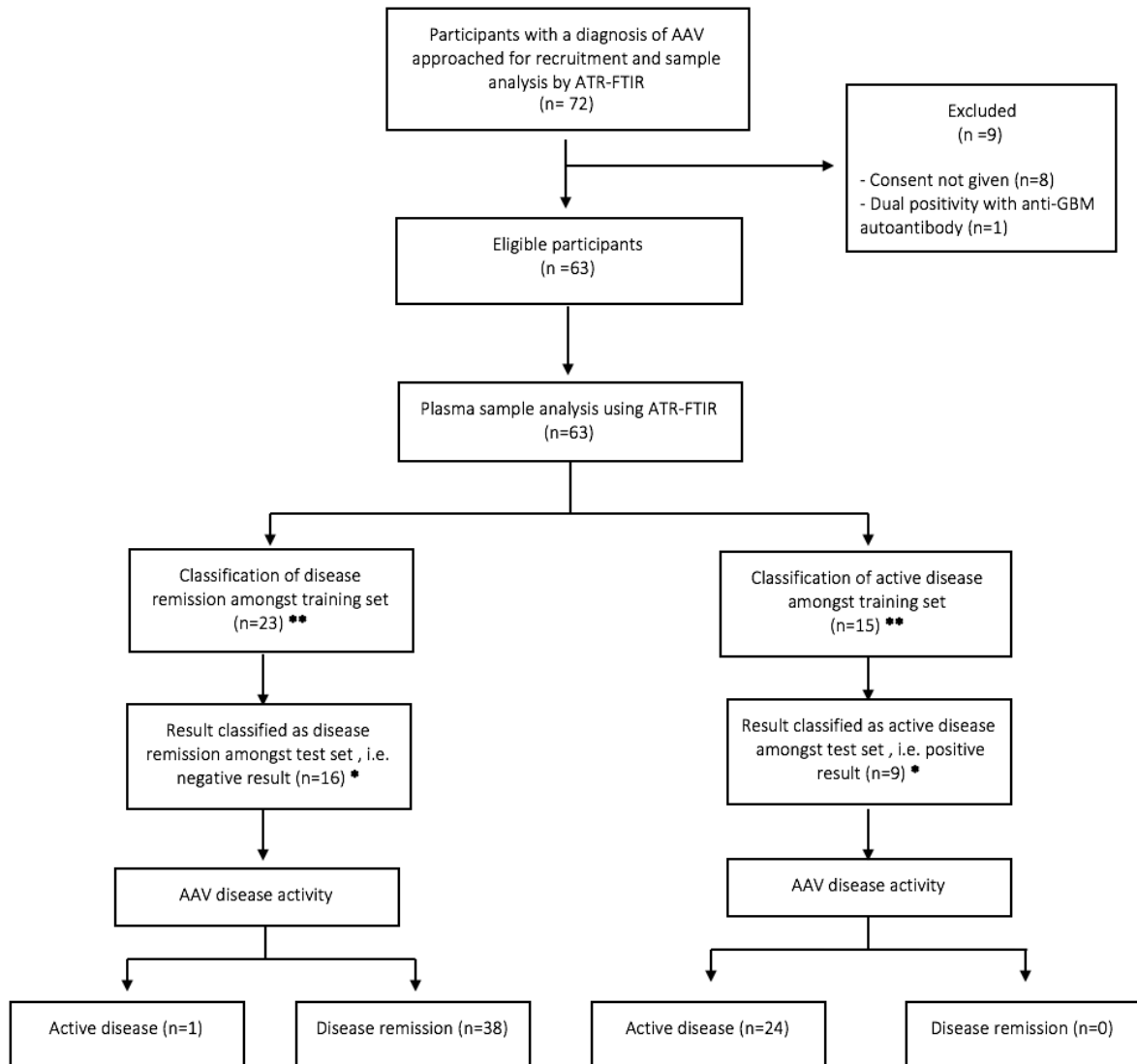


Figure S1: ANCA-associated vasculitis participant flow - AAV: ANCA-associated vasculitis, * Test set – samples used for blind predictive modelling for external validation of the classification systems performance, **Training set – samples used for model construction of classification system

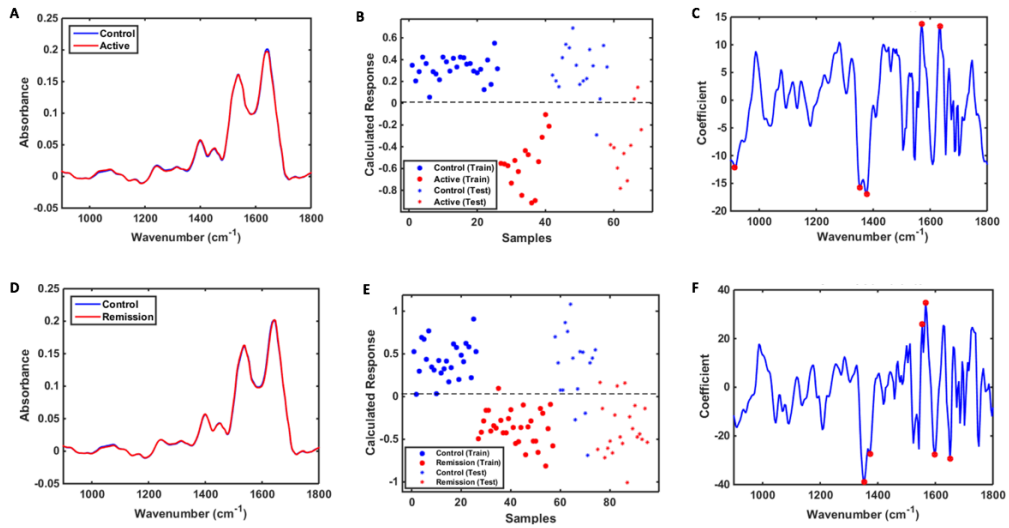


Figure S2: ATR-FTIR spectral classification of control groups (CG) vs. active disease (AD) & control groups (CG) vs. disease remission (DR) for plasma samples. CG included healthy controls and disease controls of membranous nephropathy, minimal change disease, immunoglobulin A nephropathy and acute kidney injury with infection. The DR cohort consisted of those in disease remission at the time of enrolment ($n=38$) in addition to those who achieved disease remission post enrolment following successful remission induction therapy ($n=14$) – (A) Average pre-processed spectral points for CG ($n=450$) & patients with AD ($n=250$) (B) PLS-DA discriminant function graph for classification of CG & AD using cross validation (C) PLS-DA coefficients for identification of main band differences for CG vs. AD (D) Average pre-processed spectral points for CG ($n=450$) & patients with DR ($n=520$) (E) PLS-DA discriminant function graph for classification of CG & DR using cross validation (F) PLS-DA coefficients for identification of main band differences for CG vs. DR

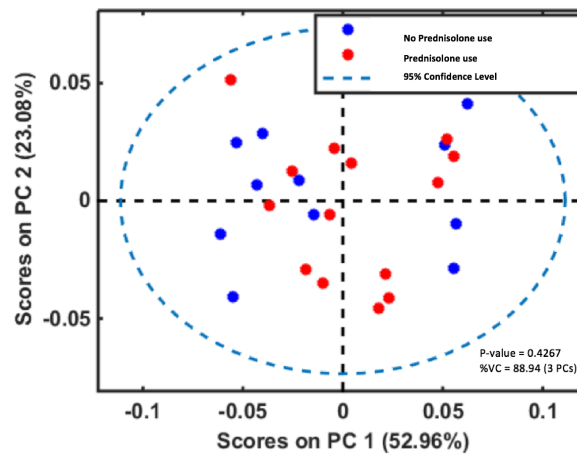


Figure S3: PCA scores plot of prednisolone use ($n=14$) vs. no prednisolone ($n=11$) use amongst the active disease cohort

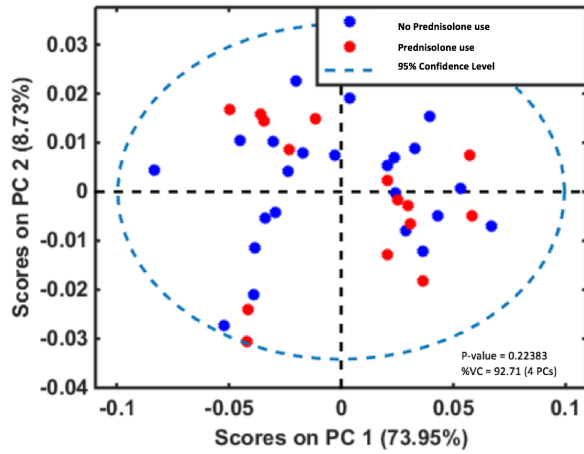


Figure S4: PCA scores plot of ≥ 5 mg/day prednisolone use (n=15) vs. no prednisolone use (n=23) amongst the disease remission cohort

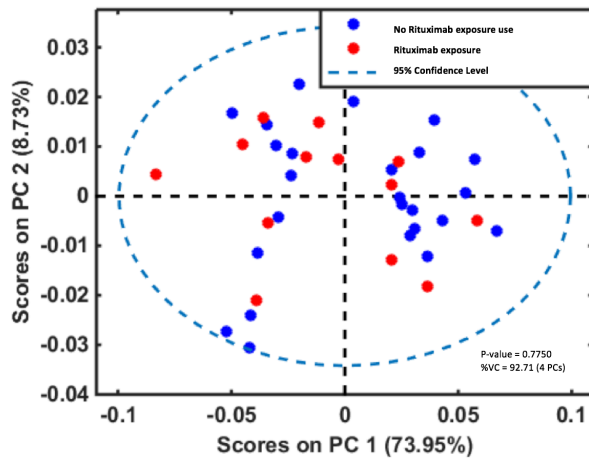


Figure S5: PCA scores plot of Rituximab exposure (n=13) vs. no Rituximab exposure (n=25) in the preceding 6 months amongst the disease remission cohort

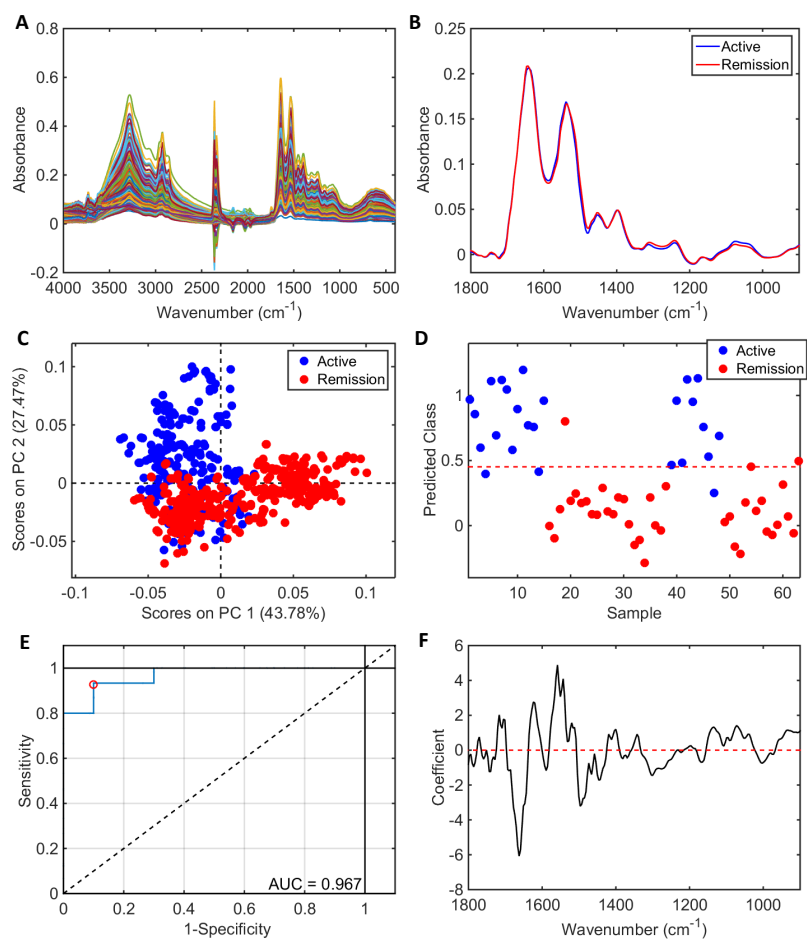


Figure S6: ATR-FTIR spectral classification of active disease vs. disease remission for serum samples - (A) Raw spectral data (B) Pre-processed spectra (C) PCA scores plot (D) PLS-DA discriminant function graph (E) ROC curve for PLS-DA (F) PLS-DA coefficients for identification of spectral biomarkers

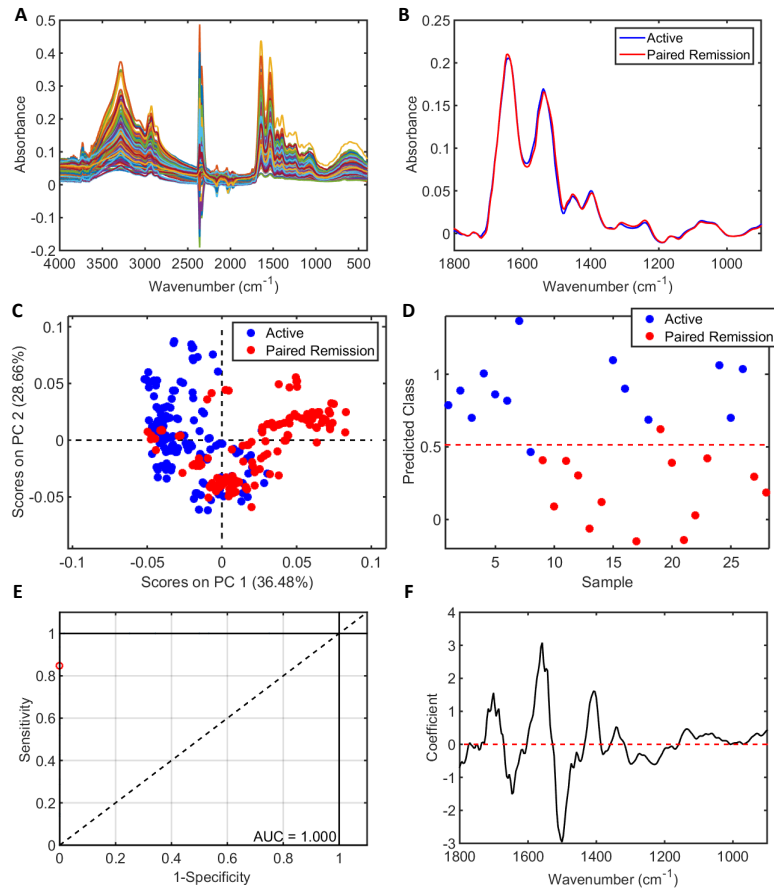


Figure S7: ATR-FTIR spectral classification of active disease vs. paired remission for serum samples following successful remission induction therapy - (A) Raw spectral data (B) Pre-processed spectra (C) PCA scores plot (D) PLS-DA discriminant function graph (E) ROC curve for PLS-DA (F) PLS-DA coefficients for identification of spectral biomarkers

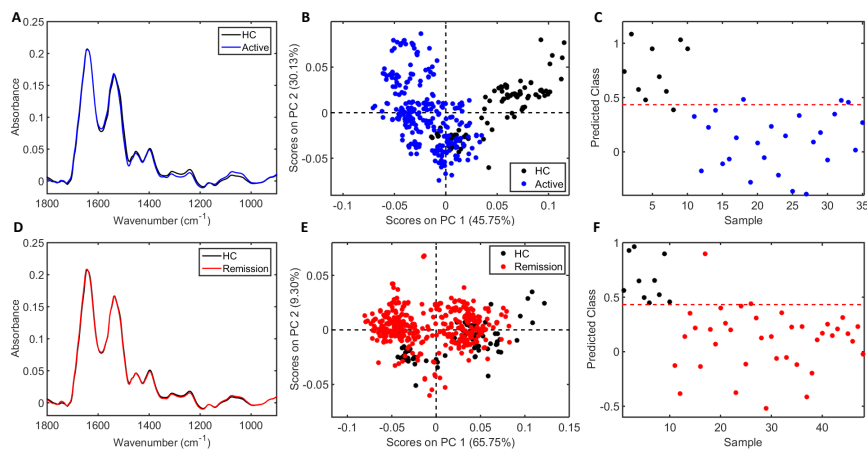


Figure S8: ATR-FTIR spectral classification of healthy controls (HC) vs. active disease (AD) & healthy controls (HC) vs. disease remission (DR) for serum samples – (A) Average pre-processed spectral points for HC (n=100) & patients with AD (n=250) (B) PCA scores plot for HC & AD (C) PLS-DA discriminant function graph for classification of HC & AD using cross validation (D) Average pre-processed spectral points for HC (n=100) & DR (n=380) (E) PCA scores plot for HC & DR (F) PLS-DA discriminant function graph for classification of HC & DR using cross validation

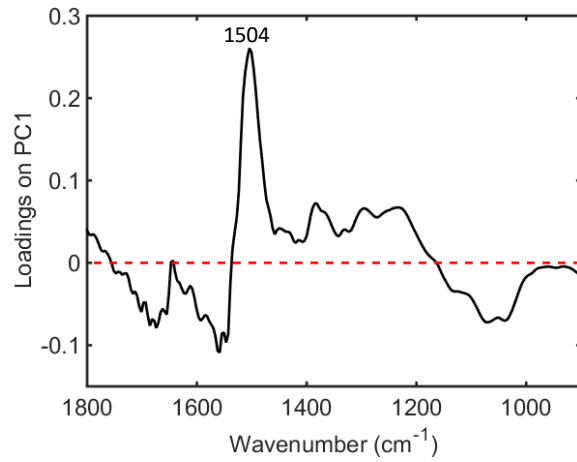


Figure S9: Main band differences for healthy controls (HC) vs. active disease (AD) using PCA loadings on PC2 from serum samples - 1504 cm^{-1} (higher in HC, Amide II).

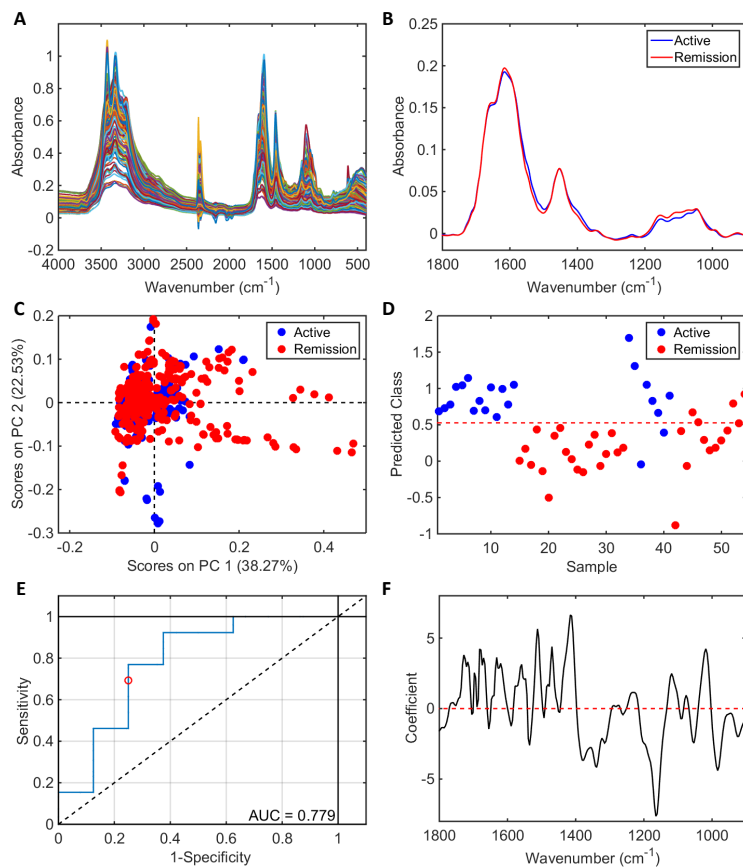


Figure S10: ATR-FTIR spectral classification of active disease vs. disease remission for urine samples - (A) Raw spectral data (B) Pre-processed spectra (C) PCA scores plot (D) PLS-DA discriminant function graph (E) ROC curve for PLS-DA (F) PLS-DA coefficients for identification of spectral biomarkers

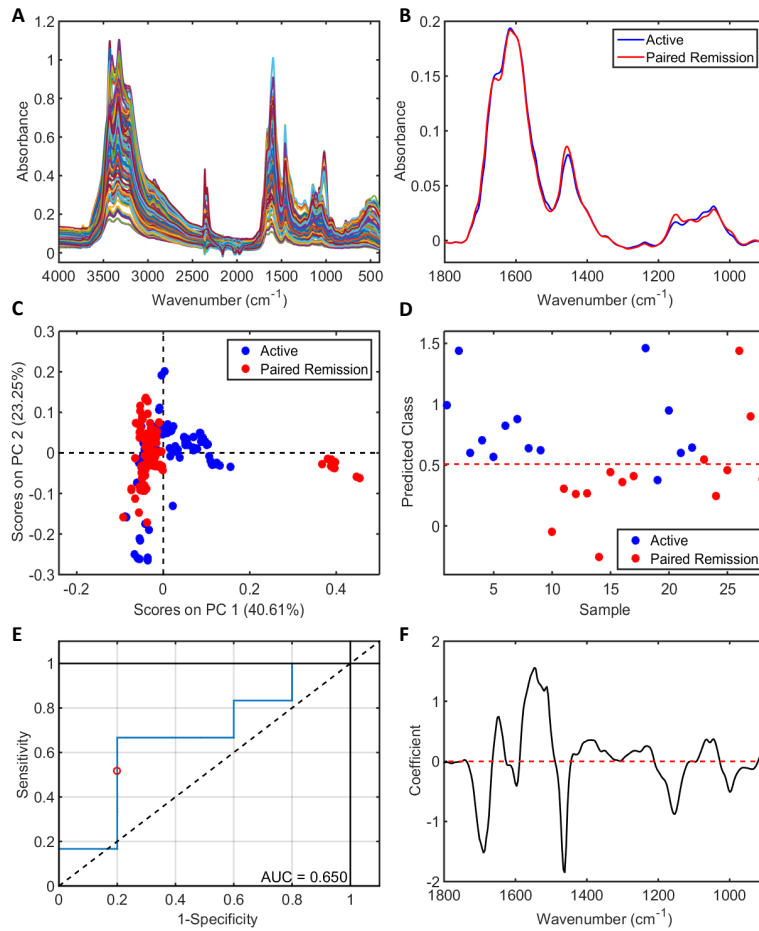


Figure S11: ATR-FTIR spectral classification of active disease vs. paired remission for urine samples following successful remission induction therapy - (A) Raw spectral data (B) Pre-processed spectra (C) PCA scores plot (D) PLS-DA discriminant function graph (E) ROC curve for PLS-DA (F) PLS-DA coefficients for identification of spectral biomarkers

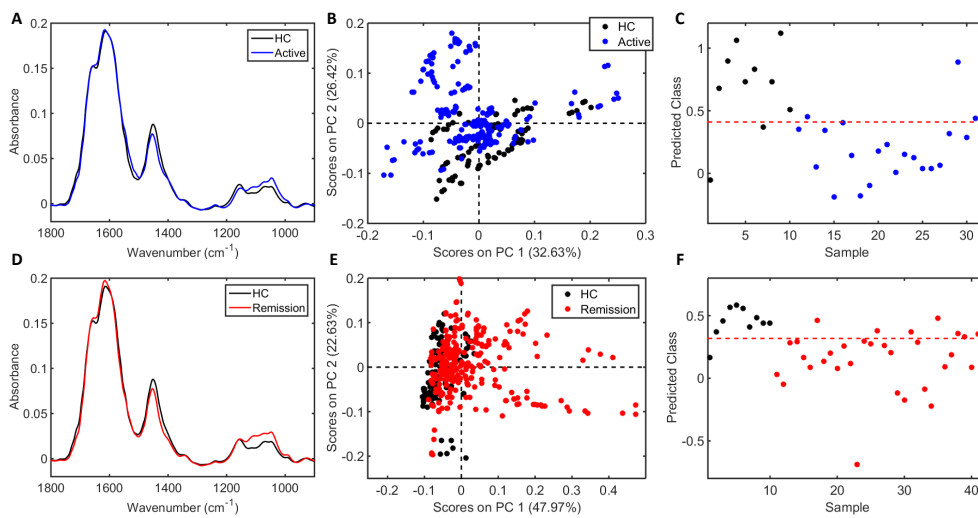


Figure S12: ATR-FTIR spectral classification of healthy controls (HC) vs. active disease (AD) & healthy controls (HC) vs. disease remission (DR) for urine samples – (A) Average pre-processed spectral points for HC (n=100) & patients with AD (n=220) (B) PCA scores plot for HC & AD (C) PLS-DA discriminant function graph for classification of HC & AD using cross validation (D) Average pre-processed spectral points for HC (n=100) & DR (n=320) (E) PCA scores plot for HC & DR (F) PLS-DA discriminant function graph for classification of HC & DR using cross validation

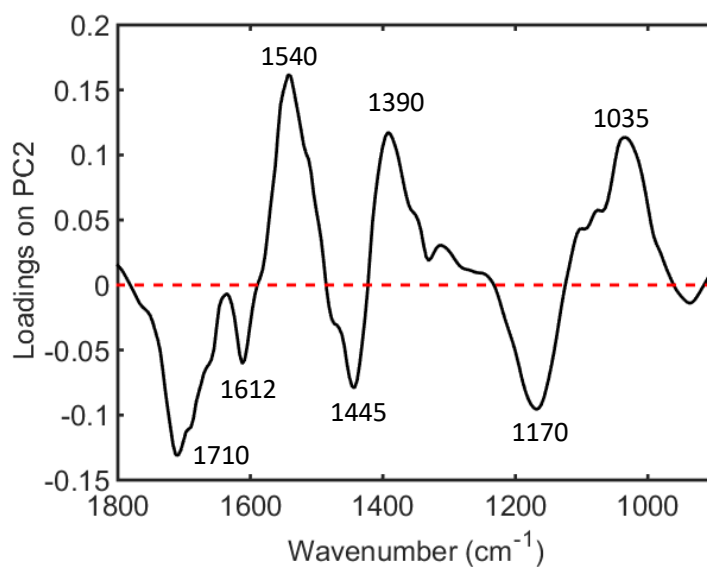


Figure S13: Main band differences for healthy controls (HC) vs. active disease (AD) using PCA loadings on PC2 from urine samples - 1710 cm⁻¹ (higher in HC, C=O thymine), 1612 cm⁻¹ (higher in HC, adenine vibration in DNA), 1540 cm⁻¹ (higher in AD, protein amide II absorption β -sheet), 1445 cm⁻¹ (higher in HC, δ (CH₂) in lipids or fatty acids), 1390 cm⁻¹ (higher in AD, CH₃ bending), 1170 cm⁻¹ (higher in HC, ν_{as} (CO-O-C)), 1035 cm⁻¹ (higher in AD, skeletal *trans* ν (C-C) of DNA).

Table S1: Characteristics of disease control groups at the time of enrolment & sample collection				
	MM (n=10)	MCD (n=5)	IgA (n=10)	AKI (n=10)
Mean Age (SD)	63 ± 9.4	50 ± 21.9	48 ± 12.9	71 ± 8.7
Sex				
Male	8	2	8	6
Female	2	3	2	4
Median serum creatinine (µmol/L)	103 (181-84)	81 (137-72)	212 (258-109)	330 (365-285)
Median eGFR (mls/min/1.73m ²)	59 (60-32)	90 (90-35)	27 (74-22)	13 (14-12)
Other Laboratory Salient Laboratory Results:				
Mean Haemoglobin (g/L)	121 ± 12.9	133 ± 14.2	128 ± 17.9	93 ± 13
Mean White cell count (10 ⁹ /L)	6 ± 2.2	9 ± 4.2	7 ± 2.4	8 ± 4.2
Mean Lymphocyte count (10 ⁹ /L)	1.7 ± 0.6	1.8 ± 0.6	1.7 ± 0.5	0.9 ± 0.5
Mean Neutrophil count (10 ⁹ /L)	4 ± 1.6	6 ± 4.3	5 ± 2.2	6 ± 3.8
Mean Platelet count (10 ⁹ /L)	258 ± 84.7	291 ± 13.7	260 ± 49.7	253 ± 95
Median CRP (mg/L)	*	*	*	83 (122-47)

MM, Membranous Nephropathy; MCD, Minimal Change Disease; IgA, Immunoglobulin A Nephropathy; AKI, Acute Kidney Injury

Table S2: Classification parameters for plasma samples for control groups (CG) vs. active disease (AD) and all disease remission (DR)				
	Accuracy (%)	Sensitivity (%)	Specificity (%)	F-Score (%)
CG vs. AD				
Training (7 LVs)	100	100	100	100
Cross-validation	93	93	92	92
Test	89	80	94	86
CG vs. DR				
Training (9 LVs)	98	97	100	98
Cross-validation	86	87	85	86
Test	84	86	82	84

Table S3: Comparative analysis between clinical variables and ATR-FTIR spectral data from plasma samples

Disease Remission	Sensitivity of clinical variable	Specificity of clinical variable	Coefficients of determination (R ²)
Age	-	-	0.03
Gender	0.55	0.61	0
ANCA Serotype			
MPO	0.61	0.2	0.06
PR3	0.21	0.8	0.02
Negative	0.67	0.53	0.01
ANCA titre	-	-	0.05
Serum creatinine (µmol/L)	-	-	0.43
eGFR(mls/min/1.73m²)	-	-	0.3
Haemoglobin	-	-	0.26
White cell count	-	-	0.01
Lymphocyte count	-	-	0
Neutrophil count	-	-	0
Platelet count	-	-	0.01
CRP	-	-	0
ESR	-	-	0.16
Serum albumin	-	-	0.1
Total Protein	-	-	0.45

Table S4: Classification parameters for serum samples in active disease (AD) vs. disease remission (DR)

AD vs. DR	Accuracy (%)	Sensitivity (%)	Specificity (%)	F-Score (%)
Training (4 LVs)	91.2	95.7	86.7	91.0
Cross-validation	91.2	95.7	86.7	91.0
Test	88.3	86.7	90.0	88.3

Table S5: Classification parameters for serum samples in active disease (AD) vs. paired remission (PR)

AD vs. PR	Accuracy (%)	Sensitivity (%)	Specificity (%)	F-Score (%)
Training (2 LVs)	95.0	100	90.0	94.7
Cross-validation	95.0	100	90.0	94.7
Test	92.8	85.7	100	92.3

Table S6: Comparative analysis between clinical variables and ATR-FTIR spectral data from serum samples			
Active disease	Sensitivity of clinical variable	Specificity of clinical variable	Coefficients of determination (R ²)
Age	-	-	0.15
Gender	0.75	0.69	0.24
BVAS	-	-	0.13
Organ involvement:			
Constitutional signs or symptoms	0.75	0.40	0.24
Mucous Membrane / Ophthalmic	0.50	0.58	0.00
Cutaneous	0.92	1.00	0.02
ENT	0.33	0.31	0.23
Respiratory	0.83	0.63	0.03
Cardiovascular	1.00	1.00	0.01
Renal	1.00	1.00	0.54
Neurological	0.40	0.65	0.00
ANCA Positivity	0.91	0.75	0.22
ANCA Serotype			
MPO	0.33	0.81	0.00
PR3	0.75	0.54	0.00
Negative	0.75	0.86	0.22
ANCA titre	-	-	0.06
Serum creatinine (µmol/L)	-	-	0.28
eGFR(mls/min/1.73m²)	-	-	0.44
Haemoglobin	-	-	0.54
White cell count	-	-	0.01
Lymphocyte count	-	-	0.21
Neutrophil count	-	-	0.04
Platelet count	-	-	0.15
CRP	-	-	0.28
ESR	-	-	0.00

ENT, ear nose and throat; ANCA, anti-neutrophil cytoplasmic autoantibody; MPO, myeloperoxidase; PR3, proteinase-3; BVAS, Birmingham vasculitis activity score; eGFR, estimated glomerular filtration rate; ESR, erythrocyte sedimentary rate; CRP, C-reactive protein

Table S7: Classification parameters for serum samples in healthy controls (HC) vs. active disease (AD) and disease remission (DR)				
	Accuracy (%)	Sensitivity (%)	Specificity (%)	F-Score (%)
HC vs. AD				
Training (3 LVs)	100	100	100	100
Cross-validation	89.0	88.0	90.0	89.0
HC vs. DR				
Training (3 LVs)	98.7	97.4	100	98.7
Cross-validation	97.3	94.7	100	97.3

Table S8: Potential spectral biomarkers for distinguishing active disease and disease remission using serum samples based on the PLS-DA coefficients (ν = stretching; δ = bending)

Wavenumber (cm ⁻¹)	Tentative assignment	Influence on Active AAV
1716	ν (C=O) DNA/RNA	↑
1704	ν (C=O) thymine	↑
1662	Amide I	↓
1623	Base carbonyl stretching and ring breathing mode of nucleic acids	↑
1558	Ring base	↑
1543	Amide II	↑
1495	ν (C=C), δ (C-H)	↓
1701	C=O guanine	↑
1646	Amide I	↓
1558	Ring base mode	↑
1500	Amide II	↓
1407	CH ₃ asymmetric deformation	↑

Table S9: Classification parameters for urine samples in active disease (AD) vs. disease remission (DR)

AD vs. DR	Accuracy (%)	Sensitivity (%)	Specificity (%)	F-Score (%)
Training (7 LVs)	100	100	100	100
Cross-validation	82.3	78.9	85.7	82.2
Test	72.1	69.2	75.0	72.0

Table S10: Classification parameters for urine samples in active disease (AD) vs. paired remission (PR)

AD vs. PR	Accuracy (%)	Sensitivity (%)	Specificity (%)	F-Score (%)
Training (2 LVs)	100	100	100	100
Cross-validation	75.7	62.5	88.9	73.4
Test	65.0	50.0	80.0	61.5

Table S11: Comparative analysis between clinical variables and ATR-FTIR spectral data from urine samples

Active disease	Sensitivity of clinical variable	Specificity of clinical variable	Coefficients of determination (R ²)
Age	-	-	0.01
Gender	0.7	0.3	0.00
BVAS	-	-	0.17
Organ involvement:			
Constitutional signs or symptoms	0.2	0.6	0.10
Mucous Membrane / Ophthalmic	0.4	0.4	0.03
Cutaneous	0.8	1.0	0.05
ENT	0.6	0.7	0.12
Respiratory	0.3	0.8	0.00
Cardiovascular	1.0	0.9	0.00
Renal	0.7	0.4	0.01
Neurological	0.2	0.9	0.01
ANCA Positivity	0.7	0.6	0.05
ANCA Serotype			
MPO	0.5	0.9	0.15
PR3	0.9	0.3	0.01
Negative	0.6	0.6	0.04
ANCA titre	-	-	0.05
Serum creatinine (µmol/L)	-	-	0.02
eGFR(mls/min/1.73m²)	-	-	0.02
Haemoglobin	-	-	0.00
White cell count	-	-	0.24
Lymphocyte count	-	-	0.00
Neutrophil count	-	-	0.32
Platelet count	-	-	0.06
CRP	-	-	0.41
ESR	-	-	0.24
uPCR	-	-	0.46
Urine white cell count	-	-	0.01
Bacterial growth			
No growth (n=19)	0.8	0.0	0.01
<i>Streptococcus agalactiae</i> (n=1)	1.0	0.9	0.00
<i>Enterococcus faecalis</i> (n=1)	1.0	0.9	0.01
Mixed growth (n=1)	1.0	0.9	0.00

ENT, ear nose and throat; ANCA, anti-neutrophil cytoplasmic autoantibody; MPO, myeloperoxidase; PR3, proteinase-3; BVAS, Birmingham vasculitis activity score; eGFR, estimated glomerular filtration rate; ESR, erythrocyte sedimentary rate; CRP, C-reactive protein; uPCR, urine protein creatinine ratio; bacterial growth n=3

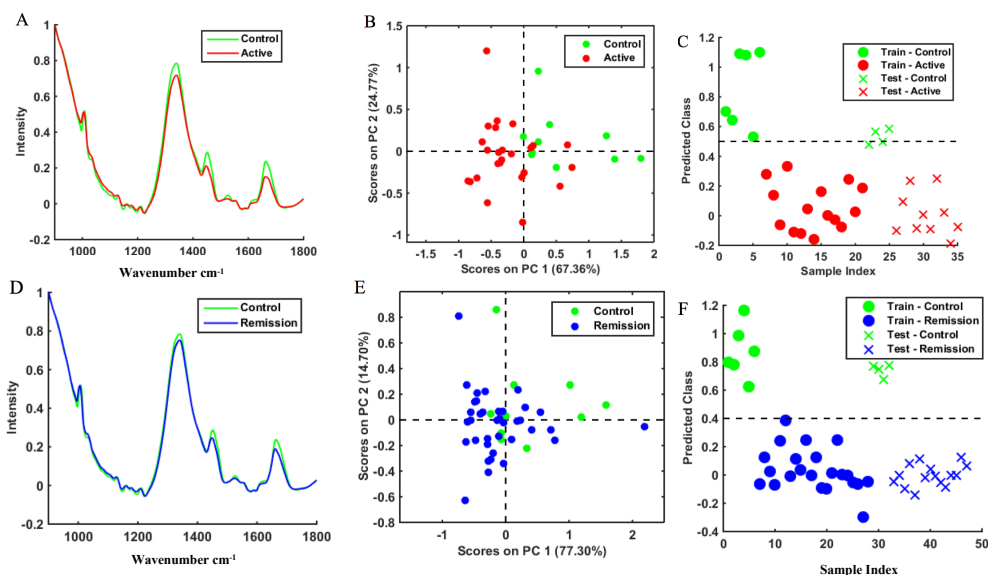
Table S12: Classification parameters for urine samples in healthy controls (HC) vs. active disease (AD) and disease remission (DR)

	Accuracy (%)	Sensitivity (%)	Specificity (%)	F-Score (%)
HC vs. AD				
Training (3 LVs)	92.7	95.5	90.0	92.7
Cross-validation	85.4	90.9	80.0	85.1
HC vs. DR				
Training (1 LVs)	84.0	78.1	90.0	83.6
Cross-validation	85.6	81.3	90.0	85.4

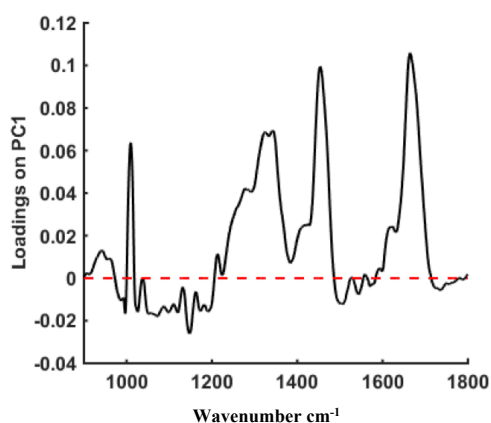
Table S13: Potential spectral biomarkers for distinguishing active disease and disease remission using urine samples based on the PLS-DA coefficients (ν = stretching; δ = bending)

Wavenumber (cm ⁻¹)	Tentative assignment	Influence on Active AAV
1728	ν (C=O)	↑
1680	Amide I	↑
1632	ν (C=C) uracil	↑
1512	In-plane δ (CH) phenyl ring	↑
1470	δ (CH ₂) methylene chains in lipids	↑
1415	δ (C-H), δ (NH), ν (C-N)	↑
1380	δ (CH ₃)	↓
1339	Collagen	↓
1164	ν (C-O) of C-OH groups of serine, threonine and tyrosine of proteins	↓
1020	DNA	↑
984	OCH ₃ polysaccharides	↓
1689	Base carbonyl stretching and ring breathing mode of nucleic acids	↓
1647	Amide I	↑
1546	Amide II of proteins	↑
1512	In-plane CH bending from phenyl rings	↑
1460	δ_{as} (CH ₃) collagen	↓
1155	C-O stretching	↓

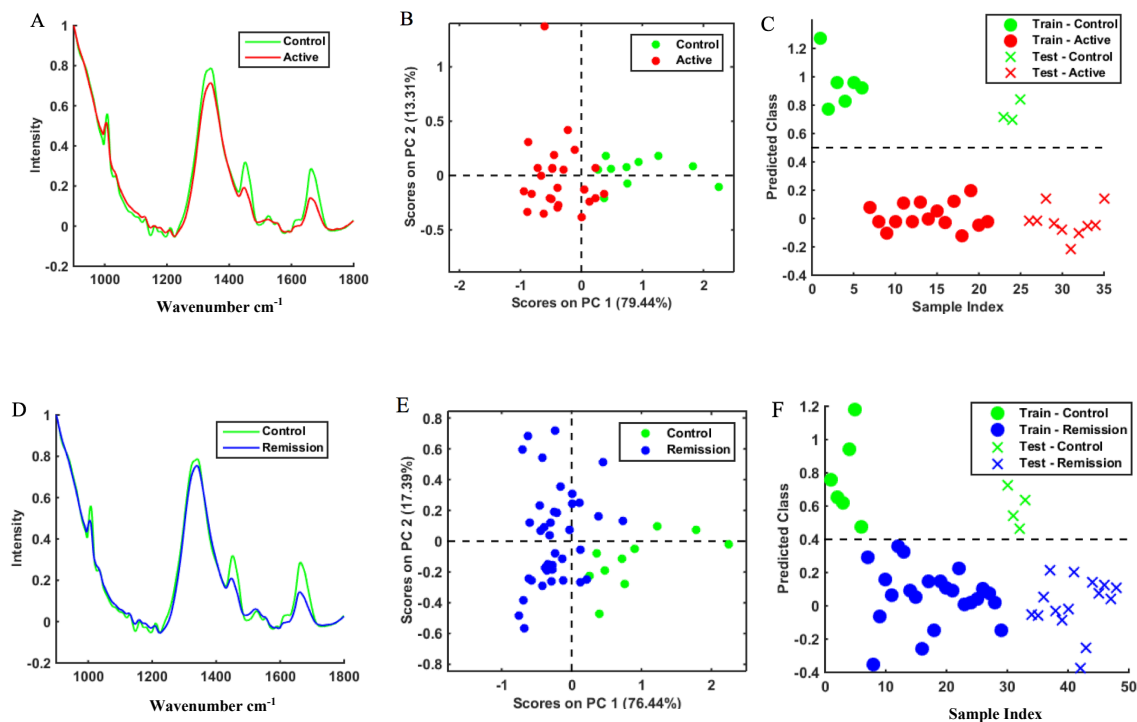
Appendix 2: Supplementary Information - A comparative analysis of different biofluids using Raman spectroscopy to determine disease activity in ANCA-associated vasculitis



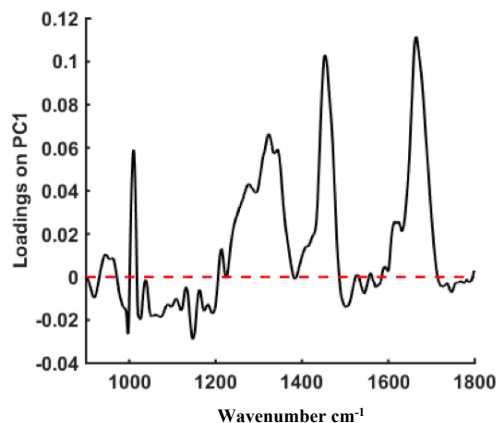
Supplementary Figure 1: ATR-FTIR spectral classification of healthy controls (HC) vs active disease (AD) & healthy controls (HC) vs disease remission (DR) for plasma samples – (A) Average pre-processed spectra for HC (n=100) & patients with AD (n=250) (B) PCA score plot for HC & AD (C) PLS-DA discriminant function graph for classification of HC & AD using cross validation (D) Average pre-processed spectra for HC (n=100) & DR (n=380) (E) PCA score plot for HC & DR (F) PLS-DA discriminant function graph for classification of HC & DR using cross validation



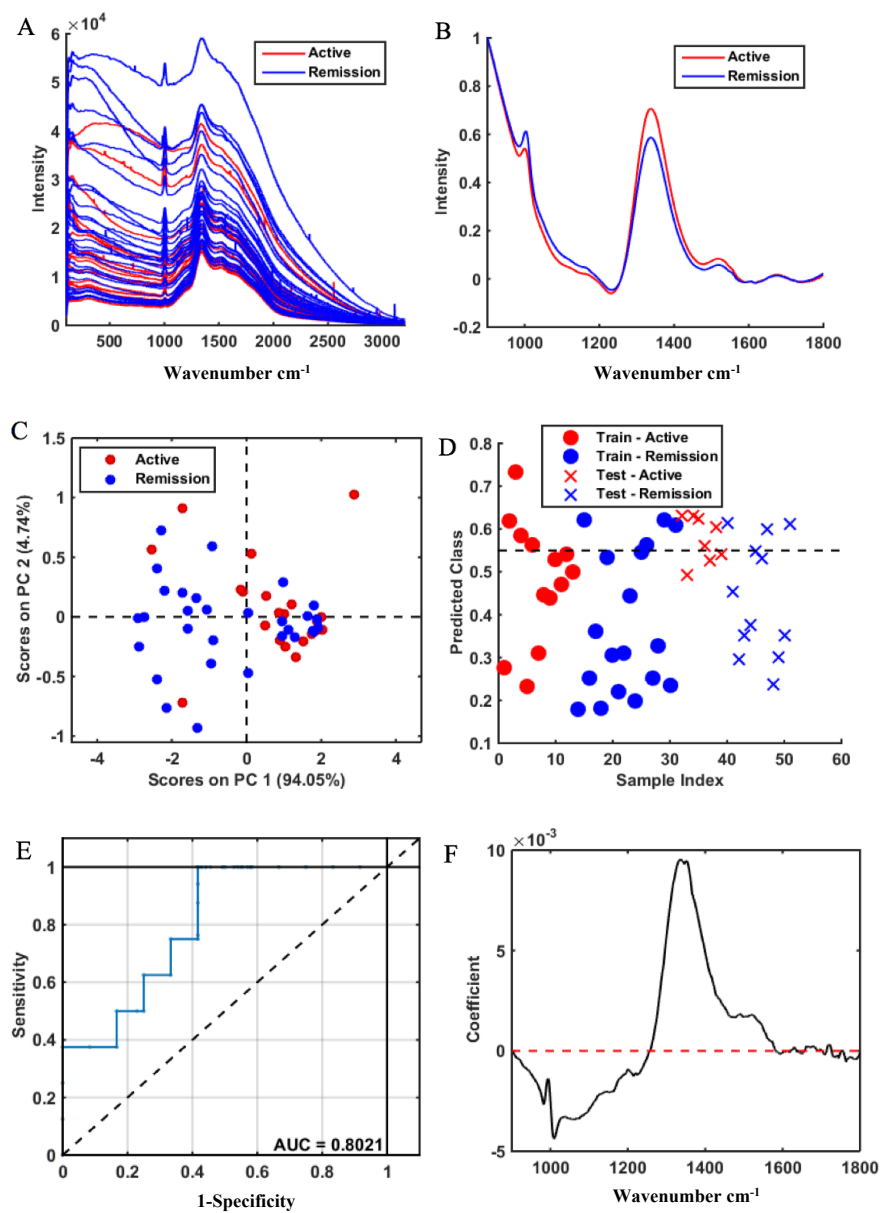
Supplementary Figure 2: Main band differences for healthy controls (HC) vs. active disease (AD) using PCA loadings on PC1 from plasma samples



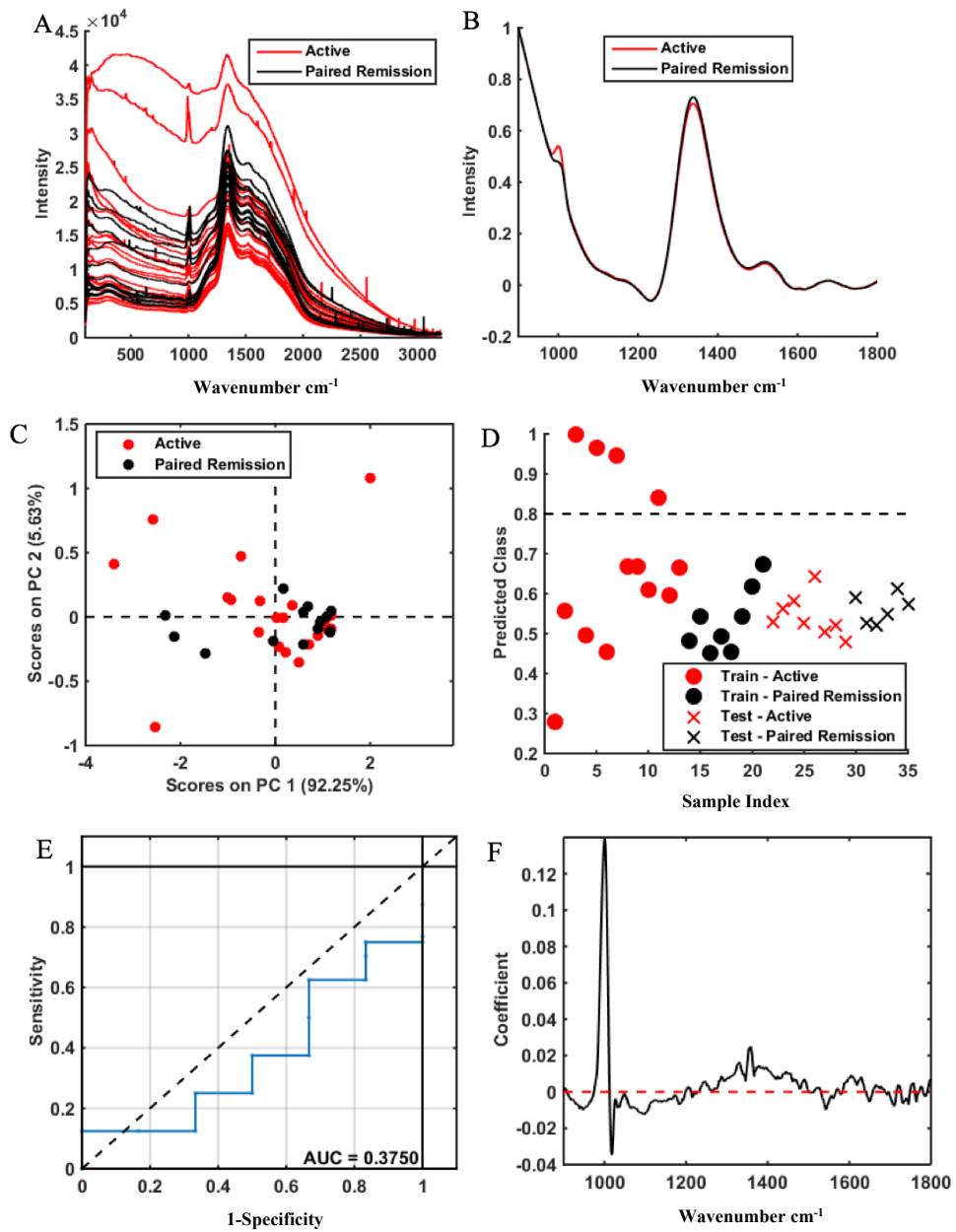
Supplementary Figure 3: ATR-FTIR spectral classification of healthy controls (HC) vs active disease (AD) & healthy controls (HC) vs disease remission (DR) for serum samples – (A) Average pre-processed spectra for HC (n=100) & patients with AD (n=250) (B) PCA score plot for HC & AD (C) PLS-DA discriminant function graph for classification of HC & AD using cross validation (D) Average pre-processed spectra for HC (n=100) & DR (n=380) (E) PCA score plot for HC & DR (F) PLS-DA discriminant function graph for classification of HC & DR using cross validation



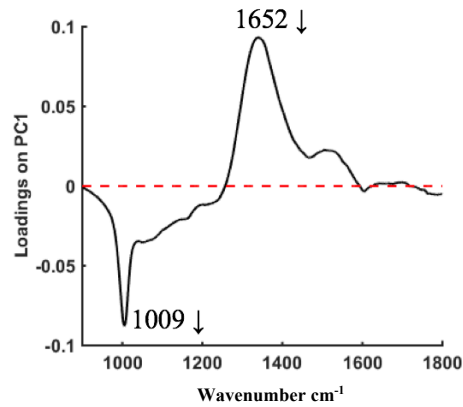
Supplementary Figure 4: Main band differences for healthy controls (HC) vs. active disease (AD) using PCA loadings on PC1 from serum samples



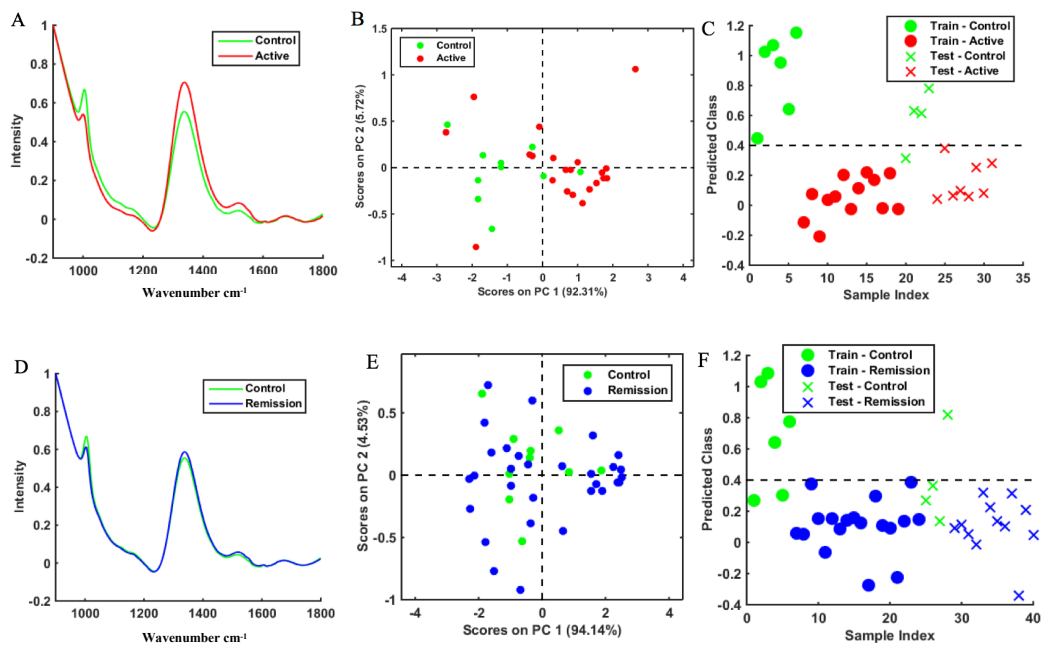
Supplementary Figure 5: Raman spectral data for classification of active disease vs. disease remission for urine samples - (A) Raw spectral data (B) Average pre-processed spectra (C) PCA scores plot (D) PLS-DA discriminant function graph (E) ROC curve for PLS-DA (F) PLS-DA coefficients for identification of spectral biomarkers



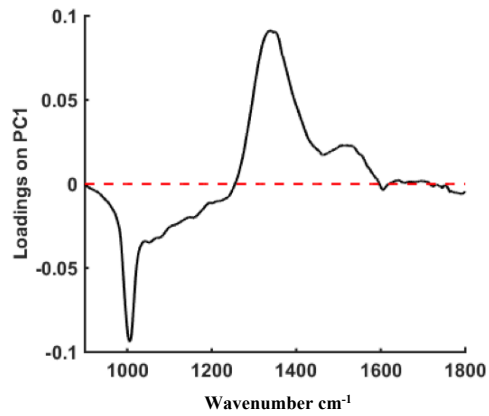
Supplementary Figure 6: Raman spectral data for classification of active disease vs. paired remission for urine following successful remission induction therapy - (A) Raw spectral data (B) Pre-processed spectra (C) PCA scores plot (D) PLS-DA discriminant function graph (E) ROC curve for PLS-DA (F) PLS-DA coefficients for identification of spectral biomarkers



Supplementary Figure 7: Main band differences for active disease (AD) vs. disease remission (DR) using PCA loadings on PC1 from urine samples – 1009 cm⁻¹ (higher in DR, phenylalanine, $\nu(\text{CO})$, $\nu(\text{CC})$, $\delta(\text{OCH})$, ring (polysaccharides, pectin), 1652 cm⁻¹ (higher in DR, lipid C=C stretch)



Supplementary Figure 8: ATR-FTIR spectral classification of healthy controls (HC) vs active disease (AD) & healthy controls (HC) vs disease remission (DR) for urine samples – (A) Average pre-processed spectra for HC (n=100) & patients with AD (n=250) (B) PCA score plot for HC & AD (C) PLS-DA discriminant function graph for classification of HC & AD using cross validation (D) Average pre-processed spectra for HC (n=100) & DR (n=380) (E) PCA score plot for HC & DR (F) PLS-DA discriminant function graph for classification of HC & DR using cross validation



Supplementary Figure 9: Main band differences for healthy controls (HC) vs. active disease (AD) using PCA loadings on PC1 from urine samples

Supplementary Table 1: Classification parameters for plasma samples in healthy controls (HC) vs. active disease (AD) and disease remission (DR)

	Accuracy (%)	Sensitivity (%)	Specificity (%)	G-Score (%)	F-Score (%)
HC vs. AD					
Training (3 LVs)	100	100	100	100	100
Cross-validation	96.7	100	93.3	96.6	96.5
Test	100	100	100	100	100
HC vs. DR					
Training (2 LVs)	100	100	100	100	100
Cross-validation	97.8	100	95.5	97.7	97.7
Test	100	100	100	100	100

Supplementary Table 2: Classification parameters for serum samples in healthy controls (HC) vs. active disease (AD) and disease remission (DR)

	Accuracy (%)	Sensitivity (%)	Specificity (%)	G-Score (%)	F-Score (%)
HC vs. AD					
Training (3 LVs)	100	100	100	100	100
Cross-validation	100	100	100	100	100
Test	100	100	100	100	100
HC vs. DR					
Training (2 LVs)	100	100	100	100	100
Cross-validation	97.9	100	95.7	97.8	97.8
Test	100	100	100	100	100

Supplementary Table 3: Classification parameters for urine samples in active disease (AD) vs. disease remission (DR)

AD vs. DR	Accuracy (%)	Sensitivity (%)	Specificity (%)	G-Score (%)	F-Score (%)
Training (1 LVs)	69	76.9	61.1	68.5	68.1
Cross-validation	69	76.9	61.1	68.5	68.1
Test	75	100	50	66.7	70.7

Supplementary Table 4: Classification parameters for urine samples in active disease (AD) vs. paired remission (PR)					
AD vs. PR	Accuracy (%)	Sensitivity (%)	Specificity (%)	G-Score (%)	F-Score (%)
Training (2 LVs)	70.7	53.8	87.5	68.6	66.6
Cross-validation	64.4	53.8	75	63.5	62.7
Test	50	0	100	0	0

Supplementary Table 5: Classification parameters for urine samples in healthy controls (HC) vs. active disease (AD) and disease remission (DR)					
	Accuracy (%)	Sensitivity (%)	Specificity (%)	G-Score (%)	F-Score (%)
HC vs. AD					
Training (5 LVs)	100	100	100	100	100
Cross-validation	91.7	83.3	100	91.3	90.9
Test	81.3	75	87.5	81	80.8
HC vs. DR					
Training (3 LVs)	77.8	66.7	88.9	77	76.2
Cross-validation	75	66.7	83.3	74.5	74.1
Test	75	50	100	66.7	70.7

Appendix 3: Health Research Authority Ethical Approval



Ymchwil Iechyd
a Gofal Cymru
Health and Care
Research Wales



Dr Adam Morris
Clinical Research Fellow
Lancashire Teaching Hospitals NHS Foundation Trust
Royal Preston Hospital
Sharoe Green Lane, North, Fulwood
Preston
PR29HT

Email: hra.approval@nhs.net
Research-permissions@wales.nhs.uk

17 August 2018

Dear Dr Morris

**HRA and Health and Care
Research Wales (HCRW)
Approval Letter**

Study title: Extraction of spectral biomarkers of ANCA-associated vasculitis applying vibrational biospectroscopy with multivariate analysis

IRAS project ID: 246059

REC reference: 18/EE/0194

Sponsor NIHR Lancashire Clinical Research Facility

I am pleased to confirm that [HRA and Health and Care Research Wales \(HCRW\) Approval](#) has been given for the above referenced study, on the basis described in the application form, protocol, supporting documentation and any clarifications received. You should not expect to receive anything further relating to this application.

How should I continue to work with participating NHS organisations in England and Wales?

You should now provide a copy of this letter to all participating NHS organisations in England and Wales, as well as any documentation that has been updated as a result of the assessment.

Following the arranging of capacity and capability, participating NHS organisations should **formally confirm** their capacity and capability to undertake the study. How this will be confirmed is detailed in the "*summary of assessment*" section towards the end of this letter.

You should provide, if you have not already done so, detailed instructions to each organisation as to how you will notify them that research activities may commence at site following their confirmation of capacity and capability (e.g. provision by you of a 'green light' email, formal notification following a site initiation visit, activities may commence immediately following confirmation by participating organisation, etc.).

It is important that you involve both the research management function (e.g. R&D office) supporting each organisation and the local research team (where there is one) in setting up your study. Contact details of the research management function for each organisation can be accessed [here](#).

How should I work with participating NHS/HSC organisations in Northern Ireland and Scotland?

HRA and HCRW Approval does not apply to NHS/HSC organisations within the devolved administrations of Northern Ireland and Scotland.

If you indicated in your IRAS form that you do have participating organisations in either of these devolved administrations, the final document set and the study wide governance report (including this letter) has been sent to the coordinating centre of each participating nation. You should work with the relevant national coordinating functions to ensure any nation specific checks are complete, and with each site so that they are able to give management permission for the study to begin.

Please see [IRAS Help](#) for information on working with NHS/HSC organisations in Northern Ireland and Scotland.

How should I work with participating non-NHS organisations?

HRA and HCRW Approval does not apply to non-NHS organisations. You should work with your non-NHS organisations to [obtain local agreement](#) in accordance with their procedures.

What are my notification responsibilities during the study?

The document "*After Ethical Review – guidance for sponsors and investigators*", issued with your REC favourable opinion, gives detailed guidance on reporting expectations for studies, including:

- Registration of research
- Notifying amendments
- Notifying the end of the study

The [HRA website](#) also provides guidance on these topics, and is updated in the light of changes in reporting expectations or procedures.

I am a participating NHS organisation in England or Wales. What should I do once I receive this letter?

You should work with the applicant and sponsor to complete any outstanding arrangements so you are able to confirm capacity and capability in line with the information provided in this letter.

The sponsor contact for this application is as follows:

Name: Kina Bennett
Tel: 01772522031
Email: Kina.Bennett@LTHTR.nhs.uk

Who should I contact for further information?

Please do not hesitate to contact me for assistance with this application. My contact details are below.

IRAS project ID	246059
-----------------	--------

Your IRAS project ID is **246059**. Please quote this on all correspondence.

Yours sincerely

Chris Kitchen
Assessor

Email: hra.approval@nhs.net

*Copy to: Dr Kina Bennett, Lancashire Teaching Hospitals NHS Foundation Trust (Sponsor
Contact and R&D Contact)*

List of Documents

The final document set assessed and approved by HRA and HCRW Approval is listed below.

<i>Document</i>	<i>Version</i>	<i>Date</i>
Copies of advertisement materials for research participants [Recruitment Poster]	1.0	15 May 2018
Covering letter on headed paper [Cover Letter]	1.0	05 August 2018
GP/consultant information sheets or letters [GP Letter - AAV Participant]	2.0	05 August 2018
GP/consultant information sheets or letters [GP Letter - Non-AAV Participant]	2.0	05 August 2018
GP/consultant information sheets or letters [GP Letter - Healthy Participant]	2.0	05 August 2018
IRAS Application Form [IRAS_Form_22052018]		22 May 2018
IRAS Checklist XML [Checklist_16082018]		16 August 2018
Letters of invitation to participant [Invitation to study]	1.0	04 April 2018
Other [answers to validation queries]		30 May 2018
Participant consent form [Consent Form - AAV Participant]	2.0	05 August 2018
Participant consent form [Consent Form - Non-AAV Participant]	2.0	05 August 2018
Participant consent form [Consent Form - Healthy Participant]	2.0	05 August 2018
Participant information sheet (PIS) [PIS - AAV Participant]	2.0	05 August 2018
Participant information sheet (PIS) [PIS - Non-AAV Participant]	2.0	05 August 2018
Participant information sheet (PIS) [PIS - Healthy Participant]	2.0	05 August 2018
Research protocol or project proposal [Research Protocol]	2.0	05 July 2018
Summary CV for Chief Investigator (CI) [CV]		
Summary CV for student		
Summary CV for supervisor (student research)		
Summary CV for supervisor (student research)		
Summary, synopsis or diagram (flowchart) of protocol in non technical language [Protocol summary (non-technical)]	1.0	15 May 2018
Validated questionnaire [BVAS]	1.0	15 May 2018

Summary of assessment

The following information provides assurance to you, the sponsor and the NHS in England and Wales that the study, as assessed for HRA and HCRW Approval, is compliant with relevant standards. It also provides information and clarification, where appropriate, to participating NHS organisations in England and Wales to assist in assessing, arranging and confirming capacity and capability.

Assessment criteria

Section	Assessment Criteria	Compliant with Standards	Comments
1.1	IRAS application completed correctly	Yes	No comments
2.1	Participant information/consent documents and consent process	Yes	No comments
3.1	Protocol assessment	Yes	No comments
4.1	Allocation of responsibilities and rights are agreed and documented	Yes	This is a non-commercial single site study taking place in the NHS where that single NHS organisation is also the study sponsor. Therefore no study agreements are expected.
4.2	Insurance/indemnity arrangements assessed	Yes	No comments
4.3	Financial arrangements assessed	Yes	No application for external funding has been made.
5.1	Compliance with the Data Protection Act and data security issues assessed	Yes	No comments
5.2	CTIMPS – Arrangements for compliance with the Clinical Trials Regulations assessed	Not Applicable	No comments
5.3	Compliance with any applicable laws or regulations	Yes	The Human Tissue Act applies.
6.1	NHS Research Ethics Committee favourable opinion	Yes	No comments

Section	Assessment Criteria	Compliant with Standards	Comments
	received for applicable studies		
6.2	CTIMPS – Clinical Trials Authorisation (CTA) letter received	Not Applicable	No comments
6.3	Devices – MHRA notice of no objection received	Not Applicable	No comments
6.4	Other regulatory approvals and authorisations received	Not Applicable	No comments

Participating NHS Organisations in England and Wales

<p><i>This provides detail on the types of participating NHS organisations in the study and a statement as to whether the activities at all organisations are the same or different.</i></p>
<p>This is a non-commercial single site study taking place in the NHS where that single NHS organisation is also the study sponsor.</p> <p>The Chief Investigator or sponsor should share relevant study documents with participating NHS organisations in England and Wales in order to put arrangements in place to deliver the study. The documents should be sent to both the local study team, where applicable, and the office providing the research management function at the participating organisation. Where applicable, the local LCRN contact should also be copied into this correspondence.</p> <p>If chief investigators, sponsors or principal investigators are asked to complete site level forms for participating NHS organisations in England and Wales which are not provided in IRAS, the HRA or HCRW websites, the chief investigator, sponsor or principal investigator should notify the HRA immediately at hra.approval@nhs.net or HCRW at Research-permissions@wales.nhs.uk. We will work with these organisations to achieve a consistent approach to information provision.</p>

Principal Investigator Suitability

<p><i>This confirms whether the sponsor position on whether a PI, LC or neither should be in place is correct for each type of participating NHS organisation in England and Wales, and the minimum expectations for education, training and experience that PIs should meet (where applicable).</i></p>
<p>A Principal Investigator is expected to be in place at the participating organisation.</p> <p>GCP training is <u>not</u> a generic training expectation, in line with the HRA/HCRW/MHRA statement on training expectations.</p>

HR Good Practice Resource Pack Expectations

IRAS project ID	246059
-----------------	--------

This confirms the HR Good Practice Resource Pack expectations for the study and the pre-engagement checks that should and should not be undertaken

For research team members that do not have existing contractual relationships with the participating organisation, Letters of Access should be in place if the activities undertaken at the NHS site involve contact with patients (e.g. to take consent), on the basis of Research passports (if University employed) or NHS to NHS confirmation of pre-engagement checks letters (if NHS employed). The pre-engagement checks should include standard DBS checks and Occupational Health Clearance. No specific pre-engagement checks are required to have taken place if the members of the research team are only accessing patients' data.

Other Information to Aid Study Set-up

This details any other information that may be helpful to sponsors and participating NHS organisations in England and Wales to aid study set-up.

The applicant has indicated that they do not intend to apply for inclusion on the NIHR CRN Portfolio.

Appendix 4: Sponsor approval



NIHR Lancashire Clinical Research Facility
 Avondale Unit
 Royal Preston Hospital
 Sharoe Green Lane, Fulwood,
 PR2 9HT

Ref: LCRF/ 01082018
 Iras: TBC

01/08/2018

Dear Dr Morris,

Extraction of spectral biomarkers of ANCA-associated vasculitis applying vibrational biospectroscopy with multivariate analysis

The application for the referenced study has been reviewed by the NIHR Lancashire Clinical Research Facility Management Team. I am pleased to confirm approval, on the basis described in the application form, protocol, supporting documentation and any clarifications made:

Approval for use of	Specifics	Time period
CRF Rooms	For use of the CRF room for patient visits	Sept 2020
CRF Nursing Staff	LCRF nurses to assist with vital signs if needed, majority completed by Dr Morris	Sept 2020
CRF Equipment	Chilled centrifuge, weighing scales, vital signs monitor	Sept 2020
Blood sampling	CRF staff to assist with venepuncture if needed, majority to be done by Dr Morris	Sept 2020
Blood processing	CRF staff to assist with sample processing if needed, majority to be done by Dr Morris	Sept 2020
Consumables	To be provided by the renal department- storage in the CRF	Sept 2020
Work area access	Dr Morris can work out of the CRF on a daily basis	Sept 2020
Emergency cover	In the unlikely event the patient requires emergency treatment – the LCRF is attached to the LTHTR trust emergency systems where medical treatment can be accessed	Sept 2020
Publications	For any trials where the LCRF has been utilised and a publication is possible we will require an acknowledgement of the NIHR LCRF. Statement should include 'The research was supported by the NIHR Lancashire Clinical Research Facility. The views expressed are those of the author(s) and not necessarily those of the NHS, the NIHR or the Department of Health'	Sept 2020

Yours Sincerely,



Nichola Verstraelen
Operational Manager


Dennis Hadjiyiannakis
Medical Director

NIHR Lancashire Clinical Research Facility

Review Article

Kidney360

Biomarkers in ANCA-Associated Vasculitis: Potential Pitfalls and Future Prospects

Adam D. Morris ¹, Anthony W. Rowbottom,^{2,3} Francis L. Martin,⁴ Alexander Woywodt,¹ and Ajay P. Dhaygude¹

Abstract

Over the past 3 decades, significant advancements in the understanding of the pathophysiology of ANCA-associated vasculitis has led to the development of a multitude of potential candidate biomarkers. Accompanied by the advent of increasingly effective therapeutic strategies, the need for a dependable biomarker to help determine the extent of disease activity and risk of relapse is ever present. Implementation of such a biomarker would enable tailored therapy, optimizing disease control while helping to mitigate unnecessary exposure to therapy and potential treatment-related damage. Although far from perfect, ANCA serology and B-cell population are the two main staple biomarker tools widely used in practice to help supplement clinical assessment. Over recent years, the application and progress of more novel biomarker tools have arisen in both organ-limited and multisystem disease, including genomics, urinary proteins, degradation products of the alternative complement system, cytokines, metabolomics, and biospectroscopy. Validation studies and clinical translation of these tools are required, with serial assessment of disease activity and determination of therapy according to biomarker status correlated with patient outcomes.

KIDNEY360 2: 586–597, 2021. doi: <https://doi.org/10.34067/KID.0006432020>

Introduction

Pauci-immune small-vessel vasculitis characterizes a group of relapsing diseases with potential multiorgan involvement, typically with circulating ANCA. The last decade has seen the advent of less toxic therapies and the move to a more tailored approach in the ANCA-associated vasculitides (AAV). These advances have improved patient outcomes, especially in the elderly and those with significant comorbidity, although treatment toxicity remains a significant risk (1–3). Since their first description nearly 40 years ago, ANCA have been used to aid initial diagnosis, with limited utility for disease monitoring. Given the continued therapeutic advances over the same period, it is surprising that comparatively little progress has been made in the use of laboratory biomarkers. This is particularly relevant given the role of histopathology to monitor disease activity is restricted by the risks of biopsy, and the accessibility and potential low diagnostic yield contingent on any extrarenal biopsy site (4–8). The use of imaging to monitor disease activity is equally limited. Computerized tomography is commonly used in patients with respiratory tract disease, but the radiologic features described are not specific to vasculitis (4,9,10). The time to interval change and repeated exposure to ionizing radiation further limits the use of such serial imaging for disease monitoring. More modern imaging techniques, such as positron emission tomography, are only validated for large-vessel vasculitis. These limitations are even more

relevant in relapsing disease, where clinicians want to avoid both under- or over-treatment, and in distinguishing active AAV from infection. Therefore, a practical and specific biomarker that accurately correlates with systemic-disease activity remains a significant unmet need in the field. Its absence presents a significant challenge to clinicians when gauging the presence of relapsing or persistent disease. This unmet need also contrasts with the move toward less toxic and more individualized options for immunosuppressive therapy. In this primer for treating clinicians, we review currently used biomarkers in AAV and discuss their limitations. We also discuss novel biomarkers, highlight potential avenues for further research and aim to define the ideal biomarker for AAV (Figure 1). In the review that follows, PubMed and Cochrane databases were each searched using the search criteria: “ANCA” OR “anti-neutrophil cytoplasmic antibody” OR “vasculitis” OR “PR3” OR “MPO” OR “ANCA-associated” OR “renal vasculitis” AND “biomarker” OR “marker” OR “activity” OR “relapse,” with further literature searches according to the presented subsections identified. The included articles reported potential biomarker application in AAV after assessment by two authors *via* a consensus process. Case reports, editorials, letters to the editor, review articles, conference abstracts, and studies not published in English were excluded. Table 1 provides a summary of the current and prospective noninvasive biomarkers in AAV discussed.

¹Renal Medicine, Royal Preston Hospital, Preston, United Kingdom

²Department of Immunology, Royal Preston Hospital, Preston, United Kingdom

³School of Medicine, University of Central Lancashire, Preston, United Kingdom

⁴Biocel Ltd., Hull, United Kingdom

Correspondence: Dr. Adam D. Morris, Department of Nephrology, Royal Preston Hospital, Lancashire National Health Service Foundation Trust, Sharoe Green Lane, Fulwood, Preston PR2 9HT, United Kingdom. Email: adam.morris@lthtr.nhs.uk

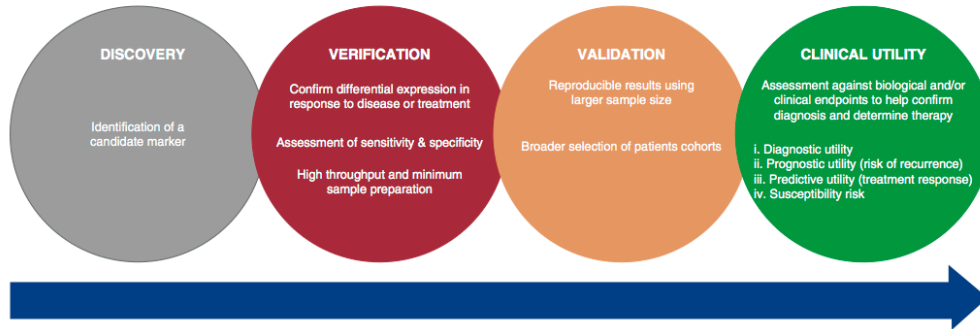


Figure 1. | The required stages of biomarker development.

ANCA

The diagnostic value of ANCA in the context of clinical symptoms is well established, yet its role in the prediction of relapsing disease remains debatable. Numerous studies have attempted to delineate the role of serial ANCA monitoring with varying results and a lack of consensus on reported outcomes. The subsequent discordance between ANCA serology and disease activity limits any support for its use as a reliable biomarker.

Early retrospective studies supported the relationship between ANCA and disease activity; however, their sensitivity and positive predictive value for relapse remained relatively low at 23%–28% (11–15). An initial systematic review in 2006 attempted to provide more insight, but was unable to undertake a meta-analysis and offer any meaningful conclusion due to the considerable method heterogeneity and suboptimal design of most studies for the assessment of test accuracy (16). A subsequent meta-analysis by Tomasson *et al.* (17) was more stringent in its study selection, identifying a modest association, at best, for persisting ANCA positivity or rising titers with the risk of relapse. Several studies with more longitudinal data, including follow-up data from large trials, have since corroborated earlier findings that persistent ANCA positivity, ANCA reappearance, and the presence of anti-proteinase 3 (anti-PR3) antibodies are risk factors for relapsing disease (18–24). Similarly, seronegativity after remission-induction therapy is associated with a longer relapse-free survival period (18,19). The positive predictive value of detectable ANCA and disease relapse increases when combined with the clinical index of suspicion for active disease (25).

Ultimately, it is the presence of seronegative disease and positivity in the absence of disease that limits the use of ANCA as a functional biomarker. Despite the compelling *in vitro* and limited *in vivo* evidence base for the pathogenicity of ANCA, the reported rate of *de novo*, seronegative, pauci-immune GN varies from 12% to 30%, with up to 54% of patients with limited extrarenal disease and a significant proportion of those with relapsing disease exhibiting undetectable circulating ANCA (26–33). This prompts reconsideration of the current putative pathogenesis and assays. One possibility is the presence of a novel autoantibody. One candidate is anti-tissue plasminogen autoantibodies, which

are thought to be integral to the fibrinolytic system and have been observed in up to 25% of patients with anti-PR3 and anti-myeloperoxidase (anti-MPO) positivity (34). These patients tended to display more severe glomerular inflammation, microthrombi, and increased thrombotic events; however, future study is required to further evaluate its role in disease. Another potential candidate is the anti-lysosomal-associated membrane protein-2 (anti-LAMP2) autoantibody. LAMP2 is a heavily glycosylated membrane protein that plays a key role in cellular homeostasis and is coexpressed on neutrophils with MPO and PR3 as a target of ANCA. Initial studies suggested a high degree of correlation with disease activity and a potential pathogenic role in ANCA-negative disease; however, these findings were not validated on subsequent study (35–37). A second consideration is that anti-PR3 and anti-MPO antibodies may be present, but either remain below the detection limit of current enzyme immunoassays or epitope masking may confound their detection (38,39). In 2013, Roth *et al.* (39) undertook a study in linear ANCA epitope mapping and disease correlation. In doing so, they identified a pathogenic anti-MPO autoantibody to a new, immunodominant, sole, linear-sequence epitope in seronegative disease—the detection of which is obscured by a fragment of ceruloplasmin in serum on conventional tests (39). It is also possible that disease is mediated by IgA ANCA (40). Current mainstream ELISAs for ANCA detect IgG. Kelley *et al.* (40) identified the presence of IgA ANCA in a significant proportion of patients who otherwise tested negative for IgG ANCA, and demonstrated the ability of IgA ANCA to mediate disease through neutrophil stimulation.

Lastly, circulating ANCA has been detected in individuals without any known history of disease. Two case-control studies confirmed positive ANCA serology from biobank samples of asymptomatic individuals up to 19 years before disease onset (41,42). In this context, it is possible that these individuals might have been lacking the “second hit” required for disease at the time of sample collection. Similarly, anti-PR3 and anti-MPO positivity have been detected in healthy individuals and with other diagnoses, including inflammatory bowel disease, liver disease, rheumatic disease, and infection, such as tuberculosis (39,43,44). The

Biomarker	Source	Organ System	Comment	Reference
ANCA	Serum	Multisystem disease	Diagnostic value in the context of clinical symptoms is well established. Persistent ANCA positivity, ANCA reappearance and the presence of anti-proteinase 3 antibodies are risk factors for relapsing disease. Discordance with serology and disease activity, with seronegative disease and positivity in the absence of disease restricting its use as a reliable biomarker.	18–24 26–33,39,41–44
Anti-LAMP2 Ab	Serum	Multisystem disease	Initial studies suggested a potential role in pathogenesis and association with disease activity, although these findings were not corroborated in subsequent study.	35–37
Anti-tissue plasminogen Ab	Serum	Multisystem disease	Associated with ANCA seropositivity and a higher degree of acute inflammatory renal lesions. Validation studies are required along with determination of its prognostic and predictive utility.	34
CD19+ B-cell population	Serum	Multisystem disease	Conflicting data on the prognostic utility of B-cell reconstitution from follow-up data of several large trials. Relapsing disease can occur despite peripheral B-cell depletion with B-cells present in tissue sites of active disease. B-cell depletion should not provide reassurance of a reduced relapse risk and repopulation may indicate susceptibility when taken into account with other clinical parameters.	22,24,46,47 48
Cytokines	Serum	Multisystem disease	CXCL-13, TIMP-1, and MMP-3 each distinguish active disease from remission with a high degree of accuracy. Further validation study is required to assess their use.	55
T-cells	Serum	Multisystem disease	Conflicting data exist on the association of BAFF with disease activity. Conflicting data exist on the association of Bregs, such as CD5+ B-cells, with disease activity and its prognostic utility.	51–54 49,50
ESR and acute-phase proteins	Serum	Multisystem disease	T-cell activity is associated with disease activity, with elevated levels of IL-2 and CD30; further validation study and assessment of its clinical utility are required.	54
N/L and P/L ratio	Plasma	Multisystem disease	ESR and acute-phase proteins—including CRP, calprotectin, hepcidin and procalcitonin—remain nonspecific for active AAV with limited clinical use. Both the N/L and P/L ratio are potential predictors of disease severity, but both require larger prospective study.	55–64 57,65,66

Biomarker	Source	Organ System	Comment	Reference
NGAL	Serum	Multisystem disease	Higher levels of NGAL are associated with relapsing disease, but this remains nonspecific and should be cautiously interpreted.	67
Endothelial cells	Plasma	Multisystem disease	Circulating necrotic endothelial cells offer a direct index of vascular damage, with a high degree of correlation in active AAV, although intensive resource requirements limit its clinical application and possibility for validation study.	68
Angiotensin 2	Plasma	Multisystem disease	Limited ability to distinguish active from quiescent disease or predict relapse.	69
Complement	Serum	Multisystem disease	Higher plasma concentrations of alternative complement-pathway degradation products in active disease. Prospective study is required with assessment in relapsing disease.	71–76
	Urine	Renal-limited disease	Higher urinary degradation products associated with active renal vasculitis, with urinary Bb inversely correlated with the percentage of normal glomeruli. These results require validation study.	70
mRNA	Plasma	Multisystem disease	Autoantigen gene expression is a risk factor for disease through histone depletion, hypomethylation and impaired transcriptional repression. Lower levels of DNMT1 mRNA and subsequent DNA hypomethylation is associated with active disease and a higher risk of relapse. CD8+ T-cell transcriptional profile is predictive of relapsing disease.	88,89 90
MCP-1	Urine	Renal-limited disease	Further prospective validation studies of gene-expression profiles are required. Prospective validation studies have demonstrated a positive association of urinary MCP-1 levels with active renal vasculitis, with a corresponding fall after remission-induction therapy. Evaluation of its clinical utility now required.	79–82
Soluble CD163	Urine	Renal-limited disease	Higher urinary levels of soluble CD163 cleaved from macrophages and monocytes conferred a high sensitivity and specificity for active renal vasculitis compared with remission. This correlates with the degree of inflammatory lesions on histopathology in both new and relapsing ANCA-associated GN. Potential elevation can occur in infection with study of its clinical utility required.	83,84

Biomarker	Source	Organ System	Comment	Reference
Metabolomics	Serum	Multisystem disease	Active vasculitis is associated with a distinctive metabolomic profile of raised N-acetyl glycoproteins, LDLs/VLDLs, choline, and glycerophosphocholine, whereas glucose and amino acids were reduced compared with control groups.	91
	Urine	Renal-limited disease	Raised urinary myo-inositol and hypocitraturia is present in active disease, and a ratio of the two closely associated with active renal vasculitis. Validation study and evaluation in relapsing disease required.	92
Biospectroscopy	Urine	Renal-limited disease	Biospectroscopy offers a novel and low-cost surrogate technique of determining a sample's metabolomic profile. One study observed the 1545 cm^{-1} spectral band increasing in intensity in line with glomerular inflammation and treatment response, whereas 1033 cm^{-1} was inversely related with the degree of fibrosis.	101

Anti-LAMP2, anti-lysosomal-associated membrane antibody; Ab, antibody; CXCL-13, chemoattractant chemokine (C-X-C motif) ligand 13; TIMP-1, tissue inhibitor of metalloproteinase inhibitor 1; MMP-3, matrix metalloproteinase 3; BAFF, B-cell activating factor; Breg, regulatory B cells; ESR, erythrocyte sedimentation rate; CRP, C-reactive protein; N/L, neutrophil/lymphocyte; P/L, platelet/lymphocyte; NGAL, neutrophil gelatinase-associated lipocalin; DNMT1, DNA methyltransferase 1; MCP-1, monocyte chemoattractant protein-1.

presence of anti-MPO ANCA in healthy individuals may represent differing epitope specificity (39).

B-Cell Population and Cytokines

Data from observational studies suggest that incomplete B-cell depletion and B-cell repopulation after rituximab treatment is associated with a significantly higher relapse rate (18,45). Supporting this, follow-up data from RITUXVAS observed that B-cell repopulation accompanied all cases of relapsing disease (46). However, the trial was not powered to draw any significant conclusion from this subgroup and follow-up data from several other larger trials did not corroborate this finding. Among the RAVE cohort, B-cell population did not predict relapse with disease occurring despite undetectable CD19+ B-cells in the vast majority of relapsing cases and the presence of B-cell detectability in quiescent disease (22). Similarly, data from both the MAINRITSAN and MAINRITSAN 2 trials found that CD19+ B-cell reconstitution was not predictive of relapse (24,47). Confirmation of the tenuous association of B-cell population with disease activity comes from a case report by Ferraro *et al.* (48) that demonstrated relapsing disease with B-cells present in tissue sites of active disease, despite peripheral depletion. As such, B-cell depletion should not provide reassurance of a reduced relapse risk and repopulation may indicate susceptibility when taken into account with other clinical parameters.

B-cell subset populations that have drawn interest include regulatory B-cells (*Bregs*), such as CD5+ cells. The CD5 protein attenuates activating signals from the B-cell receptor, downregulating B-cell activity. Measurement of *Bregs* showed initial promise with a lower CD5+ B-cell count correlating with active disease, whereas maintaining a normal count conferred a longer relapse-free survival period (49). Data from the RAVE study observed similar findings, but subsequent analysis found that serial CD5+ B-cell count was not predictive of disease relapse, severity, or treatment failure (50).

Key cytokines may offer another predictive tool. Elevated levels of B-cell activating factor (BAFF) have been found in active disease, with a corresponding fall post-treatment (51,52). However, the few studies evaluating its predictive value found no association with disease activity and a potential inverse correlation with ANCA titer, bringing into question its role in autoantibody production (53,54). Indicators of T-cell activation have also been observed, with elevated levels of soluble IL-2 receptors and CD30 in active disease, but further study is required to elicit their potential biomarker role (54). A panel of chemokines and circulating proteins have been prospectively evaluated from patients enrolled in the RAVE trial at presentation and 6 months postremission. This identified three candidate markers: the B-lymphocyte chemoattractant chemokine (C-X-C motif) ligand 13, matrix metalloproteinase 3 (MMP-3) and tissue inhibitor of metalloproteinase inhibitor 1 (TIMP-1). These distinguished active disease from remission with an area under the curve of >0.8 and likelihood ratio of 4.3–4.6, warranting future assessment (55).

Inflammatory Markers

Traditional inflammatory markers, such as erythrocyte sedimentation rate and C-reactive protein, are nonspecific

for AAV with limited clinical use (55–57). A large, cross-sectional study of the Birmingham Vasculitis Activity Score 3 (BVAS) provided confirmation of this, demonstrating a poor correlation between BVAS and C-reactive protein, with a limited role for such inflammatory markers in assessing disease activity (58). Other inflammatory markers—such as calprotectin, hepcidin, and procalcitonin—have also been evaluated, but face the same limitation (57,59–64).

The function of activated platelets in disease propagation has drawn attention to their level as a potential gauge of disease activity. Willeke *et al.* (57) observed significantly higher counts in active AAV, although there was an irregularity in their findings with relatively lower levels in more severe disease. Park *et al.* (65) evaluated the platelet/lymphocyte ratio, identifying a value >272 as an independent predictor of severe disease; however, confounding factors could not be accounted for. Similarly, Ahn *et al.* (66) observed that patients exhibiting a neutrophil/lymphocyte ratio >5.9 at diagnosis tended to present with more severe disease and have a higher frequency of future relapse. Application of the neutrophil/lymphocyte ratio is needed in larger prospective studies to determine its reliability.

Neutrophil gelatinase-associated lipocalin (NGAL) provides a marker of neutrophil degranulation, with significantly higher levels found at the time of diagnosis and in relapsing AAV (67). NGAL has also been extensively investigated as an early predictor of AKI and as with the other inflammatory markers discussed, if used it should be interpreted alongside an array of other clinical parameters to help inform an assessment of disease activity.

More direct indices of vascular damage have been investigated. Analysis of circulating necrotic endothelial cells yielded promising results, with higher levels in ANCA-associated GN compared with remission and control groups, although its intensive resource requirements may have restricted clinical application (68). Investigation of angiotensin 2 was of limited clinical utility, failing to discriminate disease activity after clinically successful treatment or to predict relapses (69).

Complement

Alternative complement-pathway activation is fundamental for the development of disease and urinary degradation products provide a potential biomarker of renal vasculitis. Gou *et al.* (70) found that urinary levels of Bb, C3a, C5a, and soluble C5b-9 were significantly higher in active disease, in addition to Bb—in effect—providing a surrogate marker of renal histopathology with inverse correlation with the percentage of normal glomeruli. The same group subsequently demonstrated that these degradation products were also significantly higher in plasma among patients with active multisystem disease (71). Several retrospective studies have since analyzed circulating levels of C3 and their relation to patient outcomes. A low level is present in up to 35% of patients at the time of initial diagnosis, with a higher likelihood of more severe disease and poorer renal function at presentation (72,73). Prognostically, this has been associated with a poorer renal and patient survival (74–76). Circulating markers of alternative complement-pathway activation holds promise, but studies assessing their use in relapsing disease are lacking and their role as a functional biomarker of disease activity requires further study.

In 2015, Chen *et al.* (77) concluded that plasma levels of complement factor H (CFH), a negative regulator of the alternative pathway, were lower in patients with active disease and were inversely correlated with renal function, renal inflammation, and BVAS. An *in vitro* study by the same group supported the hypothesis that higher CFH inhibited ANCA-induced neutrophil activation with reduced functional activity in patients with active disease (78). This raises the question of whether a subgroup of patients has a predisposition to disease due to an absolute or functional deficiency of CFH. Measurement of circulating CFH may help identify those patients who may be more susceptible to disease and subsequent future potential relapse.

Urinary Proteins and Chemokines

Elevated levels of urinary monocyte chemoattractant protein-1 (MCP-1) have been found among patients with active or persistent renal vasculitis, correlating with upregulated macrophage infiltration in severely inflamed glomeruli and a corresponding fall in urinary MCP-1 after successful treatment (79–82). CD163 is expressed on monocytes and macrophages, functioning as a scavenger receptor for the hemoglobin-haptoglobin complex. It also provides a surrogate marker of cell activity, with cleavage to soluble CD163 (sCD163) in a proinflammatory state. In a rodent model of disease, O'Reilly *et al.* (83) detected higher levels from urine in small-vessel vasculitis compared with other glomerular pathologies. Subsequent human study with an external validation cohort confirmed noticeably higher urinary levels in active disease (likelihood ratio, 20.8) (83). Evaluation of urinary sCD163 with serial renal biopsy specimen data has since demonstrated a high degree of correlation with fibrinoid necrosis and cellular crescents in those with both *de novo* and relapsing ANCA-associated GN compared with remission and healthy controls (84). This also lends support to the position that serial comparative analysis of non-invasive biomarkers and histopathology in renal vasculitis is potentially feasible and, arguably, needed as the ideal reference standard when determining their clinical utility in predicting outcomes and disease recurrence (85,86).

Moran *et al.* (87) combined urinary MCP-1 in patients positive for urinary sCD163, with a 98% specificity and positive likelihood ratio of 19.2 for relapsing disease in the presence of new-onset proteinuria, subject to pretest probability. Both urinary proteins offer a promising non-invasive candidate biomarker that could be translated into clinical practice, although their use is limited to renal vasculitis with potential elevation in the context of infection.

mRNA

Variation in autoantigen gene expression has been confirmed as a risk factor for disease through histone depletion, hypomethylation, and impaired transcriptional repression due to reduced RUNX3 at the MPO and PRTN3 gene loci. Jones *et al.* (88) confirmed this link by investigating the DNA methyltransferase 1 (DNMT1) gene expression required for DNA methylation and downregulation of autoantigen expression. In doing so, they found the degree of DNMT1 mRNA positively correlated with DNA methylation and

negatively correlated with PRTN3 and MPO gene expression (88). As such, a reduction in DNMT1 mRNA and DNA hypomethylation was associated with active disease and predicted a higher risk of relapse (hazard ratio, 4.55; 95% CI, 2.09 to 9.91), whereas patients exhibiting increased DNA methylation at the PRTN3 promoter in remission had a greater likelihood of a longer relapse-free survival period (88). Contrary to this, Kurz *et al.* (89) concluded that elevated leukocyte PR3 mRNA was not predictive of relapsing disease, although this may reflect the transrepressive effect of concurrent glucocorticoid therapy.

In 2010, McKinney *et al.* (90) quantified the gene-expression profiles from purified leukocytes among patients with active AAV to prospectively predict future relapse risk. This identified that transcriptional profiling of CD8⁺ T-cells with overexpression of mRNA encoding proteins for the IL-7 receptor pathway, T-cell receptor signaling, and expanded CD8⁺ T-cell memory population conferred a poorer prognosis (90). This finding has the potential for translation to clinical practice and requires validation in a prospective study with longitudinal data.

Metabolomics

Metabolomics enables the quantitative analysis of the substrates and products of metabolism to directly reflect the biochemical activity within a sample. Variation in the metabolomic profile will be reflective of changes in the underlying biochemical composition caused by physiologic processes or pathologic states. Studies applying metabolomics in AAV are limited. In 2016, Al-Ani *et al.* (91) analyzed the urinary metabolomic profile in a rodent model of disease using nuclear magnetic resonance spectroscopy and chemometric analysis. This identified a distinctive metabolomic profile in active disease, which resolved after successful treatment, with subsequent recurrence in relapsing disease. A large patient-cohort study by the same group yielded similar results (91). Gupta *et al.* (92) has since evaluated metabolomics in serum, identifying a profile that was specific to active AAV with good separation from control groups, including Takayasu arteritis and SLE. The role of metabolomics as a robust and relatively non-invasive biomarker of disease activity in AAV merits further study, but its associated costs may limit its potential application.

Biospectroscopy

Biospectroscopy provides a novel and low-cost surrogate technique of determining the metabolomic profile of a sample through one of two primary techniques: attenuated total reflection Fourier-transform infrared (ATR-FTIR) spectroscopy and Raman spectroscopy (93,94). Irrespective of the modality used, biochemical changes caused by disease will result in a unique spectral fingerprint that is representative of the underlying pathophysiologic state. Advancements in instrumentation and standardized chemometric analysis have enabled the successful application of biospectroscopy across numerous areas of medicine, including rheumatic disease, lymphocyte subsets, cytokine monitoring, and nephrology (95–100). Its application in vasculitis is emerging, with one previous study using ATR-FTIR to identify potential urinary biomarkers in an animal model of crescentic GN and in patients with ANCA-associated GN (101). This

identified the 1545 cm^{-1} spectral marker as a key wave-number variable, increasing in intensity in line with the degree of glomerular injury and subsiding after treatment. In parallel, the intensity of 1033 cm^{-1} was inversely related with the degree of fibrosis. These findings suggest that ATR-FTIR could be used as a fast, innovative method of monitoring disease progression and treatment response in renal vasculitis. The promising use of biospectroscopy to provide a robust biomarker of disease activity in AAV, which can be readily translated to clinical practice requires further study.

Conclusions

The remarkable progress in treatment strategies over the past 3 decades has been accompanied by a rising disease prevalence. Yet a reliable biomarker to detect relapsing or persistent disease is lacking, risking increasing morbidity and mortality from suboptimal disease control or unnecessary patient exposure to potentially harmful therapy. As such, there is a need for the development of a functional biomarker to enable risk stratification and individualization of treatment. Alongside the use of more innovative analytic tools, an improved understanding of the underlying immunopathogenesis and treatment targets has led to the identification of several promising novel candidate markers for renal-limited and multisystem disease. With favorable initial results, further validation studies with longitudinal data are required to elicit their potential role and translation into clinical practice.

Disclosures

F.L. Martin reports having ownership interest in Biocel UK Ltd. All remaining authors have nothing to disclose.

Funding

None.

Acknowledgments

The authors would like to acknowledge the support of the Renal Department at Royal Preston Hospital Lancashire National Health Service Foundation Trust, and the team at the National Institute for Health Research Lancashire Clinical Research Facility in undertaking this work.

Author Contributions

A.P. Dhaygude, F.L. Martin, A.D. Morris, A.W. Rowbottom, and A. Woywodt reviewed and edited the manuscript; A.P. Dhaygude, F.L. Martin, and A.W. Rowbottom provided supervision; and A.D. Morris conceptualized the study, was responsible for data curation, and wrote the original draft.

References

- Little MA, Nightingale P, Verburgh CA, Hauser T, De Groot K, Savage C, Jayne D, Harper L; European Vasculitis Study (EUVAS) Group: Early mortality in systemic vasculitis: Relative contribution of adverse events and active vasculitis. *Ann Rheum Dis* 69: 1036–1043, 2010 <https://doi.org/10.1136/ard.2009.109389>
- Robson J, Doll H, Suppiah R, Flossmann O, Harper L, Höglund P, Jayne D, Mahr A, Westman K, Luqmani R: Damage in the ANCA-associated vasculitides: Long-term data from the European vasculitis study group (EUVAS) therapeutic trials. *Ann Rheum Dis* 74: 177–184, 2015 <https://doi.org/10.1136/annrheumdis-2013-203927>
- Robson J, Doll H, Suppiah R, Flossmann O, Harper L, Höglund P, Jayne D, Mahr A, Westman K, Luqmani R: Glucocorticoid treatment and damage in the anti-neutrophil cytoplasm antibody-associated vasculitides: Long-term data from the European Vasculitis Study Group trials. *Rheumatology (Oxford)* 54: 471–481, 2015 <https://doi.org/10.1093/rheumatology/keu366>
- Gómez-Gómez A, Martínez-Martínez MU, Cuevas-Orta E, Bernal-Blanco JM, Cervantes-Ramírez D, Martínez-Martínez R, Abud-Mendoza C: Pulmonary manifestations of granulomatosis with polyangiitis. *Reumatol Clin* 10: 288–293, 2014 <https://doi.org/10.1016/j.reuma.2014.03.007>
- Schnabel A, Holl-Ulrich K, Dalhoff K, Reuter M, Gross WL: Efficacy of transbronchial biopsy in pulmonary vasculitides. *Eur Respir J* 10: 2738–2743, 1997 <https://doi.org/10.1183/09031936.97.10122738>
- Diamantopoulos II, Jones NS: The investigation of nasal septal perforations and ulcers. *J Laryngol Otol* 115: 541–544, 2001 <https://doi.org/10.1258/0022215011908441>
- Murray A, McGarry GW: The clinical value of septal perforation biopsy. *Clin Otolaryngol Allied Sci* 25: 107–109, 2000 <https://doi.org/10.1046/j.1365-2273.2000.00332.x>
- Bischof A, Jaeger VK, Hadden RDM, Luqmani RA, Pröbstel AK, Merkel PA, Suppiah R, Craven A, Collins MP, Daikeler T: Peripheral neuropathy in antineutrophil cytoplasmic antibody-associated vasculitides: Insights from the DCVAS study. *Neuro Immunol Neuroinflamm* 6: e615, 2019
- Seo JB, Im JG, Chung JW, Song JW, Goo JM, Park JH, Yeon KM: Pulmonary vasculitis: The spectrum of radiological findings. *Br J Radiol* 73: 1224–1231, 2000 <https://doi.org/10.1259/bjr.73.875.11144805>
- D'Anza B, Langford CA, Sindwani R: Sinonasal imaging findings in granulomatosis with polyangiitis (Wegener granulomatosis): A systematic review. *Am J Rhinol Allergy* 31: 16–21, 2017 <https://doi.org/10.2500/ajra.2017.31.4408>
- De'Oliviera J, Gaskin G, Dash A, Rees AJ, Pusey CD: Relationship between disease activity and anti-neutrophil cytoplasmic antibody concentration in long-term management of systemic vasculitis. *Am J Kidney Dis* 25: 380–389, 1995 [https://doi.org/10.1016/0272-6386\(95\)90098-5](https://doi.org/10.1016/0272-6386(95)90098-5)
- Davenport A, Lock RJ, Wallington T: Clinical significance of the serial measurement of autoantibodies to neutrophil cytoplasm using a standard indirect immunofluorescence test. *Am J Nephrol* 15: 201–207, 1995 <https://doi.org/10.1159/000168833>
- Kyndt X, Reumaux D, Bridoux F, Tribout B, Bataille P, Hachulla E, Hatron PY, Duthilleul P, Vanhille P: Serial measurements of antineutrophil cytoplasmic autoantibodies in patients with systemic vasculitis. *Am J Med* 106: 527–533, 1999 [https://doi.org/10.1016/S0002-9343\(99\)00064-9](https://doi.org/10.1016/S0002-9343(99)00064-9)
- Girard T, Mahr A, Noël LH, Cordier JF, Lesavre P, André MH, Guillevin L: Are antineutrophil cytoplasmic antibodies a marker predictive of relapse in Wegener's granulomatosis? A prospective study. *Rheumatology (Oxford)* 40: 147–151, 2001 <https://doi.org/10.1093/rheumatology/40.2.147>
- Hogan SL, Falk RJ, Chin H, Cai J, Jennette CE, Jennette JC, Nachman PH: Predictors of relapse and treatment resistance in antineutrophil cytoplasmic antibody-associated small-vessel vasculitis. *Ann Intern Med* 143: 621–631, 2005 <https://doi.org/10.7326/0003-4819-143-9-200511010-00005>
- Birck R, Schmitt WH, Kaelsch IA, van der Woude FJ: Serial ANCA determinations for monitoring disease activity in patients with ANCA-associated vasculitis: Systematic review. *Am J Kidney Dis* 47: 15–23, 2006 <https://doi.org/10.1053/j.ajkd.2005.09.022>
- Tomasson G, Grayson PC, Mahr AD, Lavalley M, Merkel PA: Value of ANCA measurements during remission to predict a relapse of ANCA-associated vasculitis—a meta-analysis. *Rheumatology (Oxford)* 51: 100–109, 2012 <https://doi.org/10.1093/rheumatology/ker280>
- van Dam LS, Dirikgil E, Bredewold EW, Ray A, Bakker JA, van Kooten C, Rabelink TJ, Teng YKO: Proteinase-3-anti-neutrophil cytoplasmic antibodies (PR3-ANCA) predict relapses in ANCA-

- associated vasculitis patients after rituximab [published online ahead of print June 30, 2020]. *Nephrol Dial Transplant* <https://doi.org/10.1093/ndt/gfaa066>
19. McClure ME, Wason J, Gopaluni S, Tieu J, Smith RM, Jayne DR, Jones RB: Evaluation of PR3-ANCA status after rituximab for ANCA-associated vasculitis. *J Clin Rheumatol* 25: 217–223, 2019 <https://doi.org/10.1097/RHU.0000000000001030>
 20. Thai LH, Charles P, Resche-Rigon M, Desseaux K, Guillevin L: Are anti-proteinase-3 ANCA a useful marker of granulomatosis with polyangiitis (Wegener's) relapses? Results of a retrospective study on 126 patients. *Autoimmun Rev* 13: 313–318, 2014 <https://doi.org/10.1016/j.autrev.2013.11.003>
 21. Fijolek J, Wiatr E, Petroniec V, Augustynowicz-Kopec E, Bednarek M, Gawryluk D, Roszkowski-Sliz K: Antineutrophil cytoplasmic antibodies and their relationship with disease activity and presence of staphylococcal superantigens in nasal swabs in patients having granulomatosis with polyangiitis: results of a study involving 115 patients from a single center. *Clin Rheumatol* 38: 3297–3305, 2019 <https://doi.org/10.1007/s10067-019-04693-0>
 22. Miloslavsky EM, Specks U, Merkel PA, Seo P, Spiera R, Langford CA, Hoffman GS, Kallenberg CG, St Clair EW, Tchao NK, Viviano L, Ding L, Sejismundo LP, Mieras K, Iklé D, Jepson B, Mueller M, Brunetta P, Allen NB, Fervenza FC, Geetha D, Keogh K, Kissin EY, Monach PA, Peikert T, Stegeman C, Ytterberg SR, Stone JH; Rituximab in ANCA-Associated Vasculitis-Immune Tolerance Network Research Group: Clinical outcomes of remission induction therapy for severe antineutrophil cytoplasmic antibody-associated vasculitis. *Arthritis Rheum* 65: 2441–2449, 2013 <https://doi.org/10.1002/art.38044>
 23. Terrier B, Pagnoux C, Perrodeau E, Karras A, Khouatra C, Aumaitre O, Cohen P, Decaux O, Desmurs-Clavel H, Maurier F, Gobert P, Quémeuneur T, Blanchard-Delaunay C, Bonnotte B, Carron PL, Daugas E, Ducret M, Godmer P, Hamidou M, Lidove O, Limal N, Puéchal X, Mouthon L, Ravaud P, Guillevin L; French Vasculitis Study Group: Long-term efficacy of remission-maintenance regimens for ANCA-associated vasculitides. *Ann Rheum Dis* 77: 1150–1156, 2018 <https://doi.org/10.1136/annrheumdis-2017-212768>
 24. Guillevin L, Pagnoux C, Karras A, Khouatra C, Aumaitre O, Cohen P, Maurier F, Decaux O, Ninet J, Gobert P, Quémeuneur T, Blanchard-Delaunay C, Godmer P, Puéchal X, Carron PL, Hatron PY, Limal N, Hamidou M, Ducret M, Daugas E, Papo T, Bonnotte B, Mahr A, Ravaud P, Mouthon L; French Vasculitis Study Group: Rituximab versus azathioprine for maintenance in ANCA-associated vasculitis. *N Engl J Med* 371: 1771–1780, 2014 <https://doi.org/10.1056/NEJMoa1404231>
 25. Verstockt B, Bossuyt X, Vanderschueren S, Blockmans D: There is no benefit in routinely monitoring ANCA titres in patients with granulomatosis with polyangiitis. *Clin Exp Rheumatol* 33[Suppl 89]: S-72–S-76, 2015
 26. Hedger N, Stevens J, Drey N, Walker S, Roderick P: Incidence and outcome of pauci-immune rapidly progressive glomerulonephritis in Wessex, UK: a 10-year retrospective study. *Nephrol Dial Transplant* 15: 1593–1599, 2000 <https://doi.org/10.1093/ndt/15.10.1593>
 27. Chen M, Yu F, Wang SX, Zou WZ, Zhao MH, Wang HY: Antineutrophil cytoplasmic autoantibody-negative Pauci-immune crescentic glomerulonephritis. *J Am Soc Nephrol* 18: 599–605, 2007 <https://doi.org/10.1681/ASN.2006091021>
 28. Kim HW, Kim JW, Im CH, Shin KC, Lee EY, Lee EB, Song YW: The clinicopathologic characteristics of granulomatosis with polyangiitis (Wegener's): A retrospective study of 45 patients in Korea. *Mod Rheumatol* 23: 864–871, 2013 <https://doi.org/10.3109/s10165-012-0754-2>
 29. Lee SW, Yu MY, Baek SH, Ahn SY, Kim S, Na KY, Chae DW, Chin HJ: Long-term prognosis of anti-neutrophil cytoplasmic antibody-negative renal vasculitis: Cohort study in Korea. *J Korean Med Sci* 31: 542–546, 2016 <https://doi.org/10.3346/jkms.2016.31.4.542>
 30. Córdova-Sánchez BM, Mejía-Vilet JM, Morales-Buenrostro LE, Loyola-Rodríguez G, Uribe-Uribe NO, Correa-Rotter R: Clinical presentation and outcome prediction of clinical, serological, and histopathological classification schemes in ANCA-associated vasculitis with renal involvement. *Clin Rheumatol* 35: 1805–1816, 2016 <https://doi.org/10.1007/s10067-016-3195-z>
 31. Holle JU, Gross WL, Holl-Ulrich K, Ambrosch P, Noelle B, Both M, Csernok E, Moosig F, Schinke S, Reinhold-Keller E: Prospective long-term follow-up of patients with localised Wegener's granulomatosis: Does it occur as persistent disease stage? *Ann Rheum Dis* 69: 1934–1939, 2010 <https://doi.org/10.1136/ard.2010.130203>
 32. Morgan MD, Szeto M, Walsh M, Jayne D, Westman K, Rasmussen N, Hiemstra TF, Flossmann O, Berden A, Höglund P, Harper L; European Vasculitis Society: Negative anti-neutrophil cytoplasm antibody at switch to maintenance therapy is associated with a reduced risk of relapse. *Arthritis Res Ther* 19: 129, 2017 <https://doi.org/10.1186/s13075-017-1321-1>
 33. Smith RM, Jones RB, Guery MJ, Laurino S, Catapano F, Chaudhry A, Smith KG, Jayne DR: Rituximab for remission maintenance in relapsing antineutrophil cytoplasmic antibody-associated vasculitis. *Arthritis Rheum* 64: 3760–3769, 2012 <https://doi.org/10.1002/art.34583>
 34. Berden AE, Nolan SL, Morris HL, Bertina RM, Erasmus DD, Hagen EC, Hayes DP, van Tilburg NH, Brujin JA, Savage CO, Bajema IM, Hewins P: Anti-plasminogen antibodies compromise fibrinolysis and associate with renal histology in ANCA-associated vasculitis. *J Am Soc Nephrol* 21: 2169–2179, 2010 <https://doi.org/10.1681/ASN.2010030274>
 35. Kain R, Tadema H, McKinney EF, Benharkou A, Brandes R, Peschel A, Hubert V, Feenstra T, Sengölge G, Stegeman C, Heeringa P, Lyons PA, Smith KG, Kallenberg C, Rees AJ: High prevalence of autoantibodies to hLAMP-2 in anti-neutrophil cytoplasmic antibody-associated vasculitis. *J Am Soc Nephrol* 23: 556–566, 2012 <https://doi.org/10.1681/ASN.2011090920>
 36. Peschel A, Basu N, Benharkou A, Brandes R, Brown M, Rees AJ, Kain R: Autoantibodies to hLAMP-2 in ANCA-negative pauci-immune focal necrotizing GN. *J Am Soc Nephrol* 25: 455–463, 2014 <https://doi.org/10.1681/ASN.2013030320>
 37. Roth AJ, Brown MC, Smith RN, Badhwar AK, Parente O, Chung H, Bunch DO, McGregor JC, Hogan SL, Hu Y, Yang JJ, Berg EA, Niles J, Jennette JC, Preston GA, Falk RJ: Anti-LAMP-2 antibodies are not prevalent in patients with antineutrophil cytoplasmic autoantibody glomerulonephritis. *J Am Soc Nephrol* 23: 545–555, 2012 <https://doi.org/10.1681/ASN.2011030273>
 38. Tateyama K, Kodama S, Kishibe K, Harabuchi Y, Suzuki M: A novel strategy with combined assays for detection of antineutrophil cytoplasmic antibody (ANCA) in clinically ANCA-negative granulomatosis with polyangiitis patients. *Auris Nasus Larynx* 44: 735–741, 2017 <https://doi.org/10.1016/j.janl.2017.03.002>
 39. Roth AJ, Ooi JD, Hess JJ, van Timmeren MM, Berg EA, Poulton CE, McGregor J, Burkart M, Hogan SL, Hu Y, Winnik W, Nachman PH, Stegeman CA, Niles J, Heeringa P, Kitching AR, Holdsworth S, Jennette JC, Preston GA, Falk RJ: Epitope specificity determines pathogenicity and detectability in ANCA-associated vasculitis. *J Clin Invest* 123: 1773–1783, 2013 <https://doi.org/10.1172/JCI65292>
 40. Kelley JM, Monach PA, Ji C, Zhou Y, Wu J, Tanaka S, Mahr AD, Johnson S, McAlear C, Cuthbertson D, Carette S, Davis JC Jr, Dellaripa PF, Hoffman GS, Khalidi N, Langford CA, Seo P, St Clair EW, Specks U, Stone JH, Spiera RF, Ytterberg SR, Merkel PA, Edberg JC, Kimberly RP: IgA and IgG antineutrophil cytoplasmic antibody engagement of Fc receptor genetic variants influences granulomatosis with polyangiitis. *Proc Natl Acad Sci U S A* 108: 20736–20741, 2011 <https://doi.org/10.1073/pnas.1109227109>
 41. Olson SW, Arbogast CB, Baker TP, Owshalimpur D, Oliver DK, Abbott KC, Yuan CM: Asymptomatic autoantibodies associate with future anti-glomerular basement membrane disease. *J Am Soc Nephrol* 22: 1946–1952, 2011 <https://doi.org/10.1681/ASN.2010090928>
 42. Olson SW, Owshalimpur D, Yuan CM, Arbogast C, Baker TP, Oliver D, Abbott KC: Relation between asymptomatic proteinase 3 antibodies and future granulomatosis with polyangiitis. *Clin J Am Soc Nephrol* 8: 1312–1318, 2013 <https://doi.org/10.2215/CJN.10411012>
 43. Houben E, Bax WA, van Dam B, Sliker WAT, Verhave G, Frerichs FCP, van Eijk IC, Boersma WG, de Kuyper GTM, Penne

- EL: Diagnosing ANCA-associated vasculitis in ANCA positive patients: A retrospective analysis on the role of clinical symptoms and the ANCA titre. *Medicine (Baltimore)* 95: e5096, 2016 <https://doi.org/10.1097/MD.0000000000005096>
44. Flores-Suárez LF, Cabiedes J, Villa AR, van der Woude FJ, Alcocer-Varela J: Prevalence of antineutrophil cytoplasmic autoantibodies in patients with tuberculosis. *Rheumatology (Oxford)* 42: 223–229, 2003 <https://doi.org/10.1093/rheumatology/keg066>
 45. Cartin-Ceba R, Golbin JM, Keogh KA, Peikert T, Sánchez-Menéndez M, Ytterberg SR, Fervenza FC, Specks U: Rituximab for remission induction and maintenance in refractory granulomatosis with polyangiitis (Wegener's): Ten-year experience at a single center. *Arthritis Rheum* 64: 3770–3778, 2012 <https://doi.org/10.1002/art.34584>
 46. Jones RB, Furuta S, Tervaert JWC, Hauser T, Luqmani R, Morgan MD, Peh CA, Savage CO, Segelmark M, Tesar V, van Paassen P, Walsh M, Westman K, Jayne DR; European Vasculitis Society (EUVAS): Rituximab versus cyclophosphamide in ANCA-associated renal vasculitis: 2-year results of a randomised trial. *Ann Rheum Dis* 74: 1178–1182, 2015 <https://doi.org/10.1136/annrheumdis-2014-206404>
 47. Charles P, Terrier B, Perronneau É, Cohen P, Faguer S, Huart A, Hamidou M, Agard C, Bonnotte B, Samson M, Karras A, Jourde-Chiche N, Lifermann F, Gobert P, Hanrotel-Saliou C, Godmer P, Martin-Silva N, Pugnet G, Matignon M, Aumaitre O, Viillard JF, Maurin F, Meaux-Ruault N, Rivière S, Sibilia J, Puéchal X, Ravaud P, Mouthon L, Guillevin L; French Vasculitis Study Group: Comparison of individually tailored versus fixed-schedule rituximab regimen to maintain ANCA-associated vasculitis remission: Results of a multicentre, randomised controlled, phase III trial (MAINRITSAN2) [published correction appears in *Ann Rheum Dis* 78: e101, 2019 10.1136/annrheumdis-2017-212878corr1]. *Ann Rheum Dis* 77: 1143–1149, 2018 <https://doi.org/10.1136/annrheumdis-2017-212878>
 48. Ferraro AJ, Smith SW, Neil D, Savage COS: Relapsed Wegener's granulomatosis after rituximab therapy—B cells are present in new pathological lesions despite persistent 'depletion' of peripheral blood. *Nephrol Dial Transplant* 23: 3030–3032, 2008 <https://doi.org/10.1093/ndt/gfn318>
 49. Bunch DOD, McGregor JG, Khandooobhai NB, Aybar LT, Burkart ME, Hu Y, Hogan SL, Poulton CJ, Berg EA, Falk RJ, Nachman PH: Decreased CD5⁺ B cells in active ANCA vasculitis and relapse after rituximab. *Clin J Am Soc Nephrol* 8: 382–391, 2013 <https://doi.org/10.2215/CJN.03950412>
 50. Unizony S, Lim N, Phippard DJ, Carey VJ, Eli M, Tchao NK, Iklé D, Asare AL, Merkel PA, Monach PA, Seo P, St Clair EW, Langford CA, Spiera R, Hoffman GS, Kallenberg CGM, Specks U, Stone JH: Peripheral CD5⁺ B cells in antineutrophil cytoplasmic antibody-associated vasculitis. *Arthritis Rheumatol* 67: 535–544, 2015 <https://doi.org/10.1002/art.38916>
 51. Krumbholz M, Specks U, Wick M, Kalled SL, Jenne D, Meinel E: BAFF is elevated in serum of patients with Wegener's granulomatosis. *J Autoimmun* 25: 298–302, 2005 <https://doi.org/10.1016/j.jaut.2005.08.004>
 52. Nagai M, Hirayama K, Ebihara I, Shimohata H, Kobayashi M, Koyama A: Serum levels of BAFF and APRIL in myeloperoxidase anti-neutrophil cytoplasmic autoantibody-associated renal vasculitis: association with disease activity. *Nephron Clin Pract* 118: c339–c345, 2011 <https://doi.org/10.1159/000323393>
 53. Bader L, Koldingsnes W, Nossent J: B-lymphocyte activating factor levels are increased in patients with Wegener's granulomatosis and inversely correlated with ANCA titer. *Clin Rheumatol* 29: 1031–1035, 2010 <https://doi.org/10.1007/s10067-010-1526-z>
 54. Sanders JSF, Huitma MC, Kallenberg CGM, Stegeman CA: Plasma levels of soluble interleukin 2 receptor, soluble CD30, interleukin 10 and B cell activator of the tumour necrosis factor family during follow-up in vasculitis associated with proteinase 3-antineutrophil cytoplasmic antibodies: Associations with disease activity and relapse. *Ann Rheum Dis* 65: 1484–1489, 2006
 55. Monach PA, Warner RL, Tomasson G, Specks U, Stone JH, Ding L, Fervenza FC, Fessler BJ, Hoffman GS, Iklé D, Kallenberg CG, Krischer J, Langford CA, Mueller M, Seo P, St Clair EW, Spiera R, Tchao N, Ytterberg SR, Johnson KJ, Merkel PA: Serum proteins reflecting inflammation, injury and repair as biomarkers of disease activity in ANCA-associated vasculitis. *Ann Rheum Dis* 72: 1342–1350, 2013 <https://doi.org/10.1136/annrheumdis-2012-201981>
 56. Liang H, Xin M, Zhao L, Wang L, Sun M, Wang J: Serum creatinine level and ESR values associated to clinical pathology types and prognosis of patients with renal injury caused by ANCA-associated vasculitis. *Exp Ther Med* 14: 6059–6063, 2017 <https://doi.org/10.3892/etm.2017.5306>
 57. Willeke P, Kümpers P, Schlüter B, Limani A, Becker H, Schotte H: Platelet counts as a biomarker in ANCA-associated vasculitis. *Scand J Rheumatol* 44: 302–308, 2015 <https://doi.org/10.3109/03009742.2015.1006247>
 58. Suppiah R, Mukhtyar C, Flossmann O, Alberici F, Baslund B, Batra R, Brown D, Holle J, Hruskova Z, Jayne DR, Judge A, Little MA, Palmisano A, Stegeman C, Tesar V, Vaglio A, Westman K, Luqmani R: A cross-sectional study of the Birmingham Vasculitis Activity Score version 3 in systemic vasculitis. *Rheumatology (Oxford)* 50: 899–905, 2011 <https://doi.org/10.1093/rheumatology/keq400>
 59. Prikryl P, Hrušková Z, Konopásek P, Hladinová Z, Tesáň V, Vokurka M: Serum hepcidin is increased in ANCA-associated vasculitis and correlates with activity markers. *Physiol Res* 67: 945–954, 2018 <https://doi.org/10.33549/physiolres.933765>
 60. Martínez Valenzuela L, Draibe J, Quero Ramos M, Fulladosa Oliveras X, Melilli E, Cruzado Garrit JM, Torres Ambrós J: Calprotectin as a smoldering activity detection tool and renal prognosis biomarker in ANCA associated vasculitis. *PLoS One* 13: e0205982, 2018 <https://doi.org/10.1371/journal.pone.0205982>
 61. Zycinska K, Wardyn KA, Zielonka TM, Tyszko P, Straburzynski M: Procalcitonin as an indicator of systemic response to infection in active pulmonary Wegener's granulomatocytosis. *J Physiol Pharmacol* 59(Suppl 6): 839–844, 2008
 62. Brunkhorst R, Eberhardt OK, Haubitz M, Brunkhorst FM: Procalcitonin for discrimination between activity of systemic autoimmune disease and systemic bacterial infection. *Intensive Care Med* 26(Suppl 2): S199–S201, 2000 <https://doi.org/10.1007/s001340051144>
 63. Herrmann K, Schinke S, Csernok E, Moosig F, Holle JU: Diagnostic value of procalcitonin in ANCA-Associated Vasculitis (AAV) to differentiate between disease activity, infection and drug hypersensitivity. *Open Rheumatol J* 9: 71–76, 2015 <https://doi.org/10.2174/1874312901409010071>
 64. Eberhardt OK, Haubitz M, Brunkhorst FM, Kliem V, Koch KM, Brunkhorst R: Usefulness of procalcitonin for differentiation between activity of systemic autoimmune disease (systemic lupus erythematosus/systemic antineutrophil cytoplasmic antibody-associated vasculitis) and invasive bacterial infection. *Arthritis Rheum* 40: 1250–1256, 1997 [https://doi.org/10.1002/1529-0131\(199707\)40:7<1250::AID-ART9>3.0.CO;2-A](https://doi.org/10.1002/1529-0131(199707)40:7<1250::AID-ART9>3.0.CO;2-A)
 65. Park HJ, Jung SM, Song JJ, Park YB, Lee SW: Platelet to lymphocyte ratio is associated with the current activity of ANCA-associated vasculitis at diagnosis: A retrospective monocentric study. *Rheumatol Int* 38: 1865–1871, 2018 <https://doi.org/10.1007/s00296-018-4125-y>
 66. Ahn SS, Jung SM, Song JJ, Park YB, Lee SW: Neutrophil to lymphocyte ratio at diagnosis can estimate vasculitis activity and poor prognosis in patients with ANCA-associated vasculitis: A retrospective study. *BMC Nephrol* 19: 187, 2018 <https://doi.org/10.1186/s12882-018-0992-4>
 67. Chen M, Wang F, Zhao MH: Circulating neutrophil gelatinase-associated lipocalin: a useful biomarker for assessing disease activity of ANCA-associated vasculitis. *Rheumatology (Oxford)* 48: 355–358, 2009 <https://doi.org/10.1093/rheumatology/ken500>
 68. Woywodt A, Streiber F, de Groot K, Regelsberger H, Haller H, Haubitz M: Circulating endothelial cells as markers for ANCA-associated small-vessel vasculitis. *Lancet* 361: 206–210, 2003 [https://doi.org/10.1016/S0140-6736\(03\)12269-6](https://doi.org/10.1016/S0140-6736(03)12269-6)
 69. Monach PA, Kümpers P, Lukasz A, Tomasson G, Specks U, Stone JH, Cuthbertson D, Krischer J, Carrette S, Ding L, Hoffman GS, Iklé D, Kallenberg CG, Khalidi NA, Langford CA, Seo P, St Clair EW, Spiera R, Tchao N, Ytterberg SR, Haubitz M, Merkel PA:

- Circulating angiopoietin-2 as a biomarker in ANCA-associated vasculitis. *PLoS One* 7: e30197, 2012 <https://doi.org/10.1371/journal.pone.0030197>
70. Gou SJ, Yuan J, Wang C, Zhao MH, Chen M: Alternative complement pathway activation products in urine and kidneys of patients with ANCA-associated GN. *Clin J Am Soc Nephrol* 8: 1884–1891, 2013 <https://doi.org/10.2215/CJN.02790313>
 71. Gou SJ, Yuan J, Chen M, Yu F, Zhao MH: Circulating complement activation in patients with anti-neutrophil cytoplasmic antibody-associated vasculitis. *Kidney Int* 83: 129–137, 2013 <https://doi.org/10.1038/ki.2012.313>
 72. Choi H, Kim Y, Jung SM, Song JJ, Park YB, Lee SW: Low serum complement 3 level is associated with severe ANCA-associated vasculitis at diagnosis. *Clin Exp Nephrol* 23: 223–230, 2019 <https://doi.org/10.1007/s10157-018-1634-7>
 73. Nanenti L, Vaglio A, Gnappi E, Maggiore U, Allegri L, Allinovi M, Urban ML, Delsante M, Galetti M, Nicastro M, Pilato FP, Buzio C: Association of serum C3 concentration and histologic signs of thrombotic microangiopathy with outcomes among patients with ANCA-associated renal vasculitis. *Clin J Am Soc Nephrol* 10: 2143–2151, 2015 <https://doi.org/10.2215/CJN.00120115>
 74. Augusto JF, Langs V, Demiselle J, Lavigne C, Brilland B, Duveau A, Poli C, Chevailler A, Croue A, Tollis F, Sayegh J, Subra JF: Low serum complement C3 levels at diagnosis of renal ANCA-associated vasculitis is associated with poor prognosis. *PLoS One* 11: e0158871, 2016 <https://doi.org/10.1371/journal.pone.0158871>
 75. Villacorta J, Diaz-Crespo F, Acevedo M, Caverro T, Guerrero C, Praga M, Fernandez-Juarez G: Circulating C3 levels predict renal and global outcome in patients with renal vasculitis. *Clin Rheumatol* 35: 2733–2740, 2016 <https://doi.org/10.1007/s10067-016-3384-9>
 76. Crnogorac M, Horvatic I, Kacinari P, Ljubanovic DG, Galesic K: Serum C3 complement levels in ANCA associated vasculitis at diagnosis is a predictor of patient and renal outcome. *J Nephrol* 31: 257–262, 2018 <https://doi.org/10.1007/s40620-017-0445-3>
 77. Chen SF, Wang FM, Li ZY, Yu F, Zhao MH, Chen M: Plasma complement factor H is associated with disease activity of patients with ANCA-associated vasculitis [published correction appears in *Arthritis Res Ther* 19: 82, 2017 10.1186/s13075-017-1298-9]. *Arthritis Res Ther* 17: 129, 2015 <https://doi.org/10.1186/s13075-015-0656-8>
 78. Chen SF, Wang FM, Li ZY, Yu F, Chen M, Zhao MH: Complement factor H inhibits anti-neutrophil cytoplasmic autoantibody-induced neutrophil activation by interacting with neutrophils. *Front Immunol* 9: 559, 2018 <https://doi.org/10.3389/fimmu.2018.00559>
 79. Tam FWK, Sanders JS, George A, Hammad T, Miller C, Dougan T, Cook HT, Kallenberg CG, Gaskin G, Levy JB, Pusey CD: Urinary monocyte chemoattractant protein-1 (MCP-1) is a marker of active renal vasculitis. *Nephrol Dial Transplant* 19: 2761–2768, 2004 <https://doi.org/10.1093/ndt/gfh487>
 80. Ohlsson S, Bakoush O, Tencer J, Torffvit O, Segelmark M: Monocyte chemoattractant protein 1 is a prognostic marker in ANCA-associated small vessel vasculitis. *Mediators Inflamm* 2009: 584916, 2009 <https://doi.org/10.1155/2009/584916>
 81. Lieberthal JG, Cuthbertson D, Carette S, Hoffman GS, Khalidi NA, Koenig CL, Langford CA, Maksimowicz-McKinnon K, Seo P, Specks U, Ytterberg SR, Merkel PA, Monach PA: Vasculitis Clinical Research Consortium: Urinary biomarkers in relapsing antineutrophil cytoplasmic antibody-associated vasculitis. *J Rheumatol* 40: 674–683, 2013 <https://doi.org/10.3899/jrheum.120879>
 82. Jönsson N, Erlandsson E, Gunnarsson L, Pettersson Å, Ohlsson S: Monocyte chemoattractant protein-1 in antineutrophil cytoplasmic autoantibody-associated vasculitis: Biomarker potential and association with polymorphisms in the MCP-1 and the CC chemokine receptor-2 gene. *Mediators Inflamm* 2018: 6861257, 2018
 83. O'Reilly VP, Wong L, Kennedy C, Elliot LA, O'Meachair S, Coughlan AM, O'Brien EC, Ryan MM, Sandoval D, Connolly E, Deekema GJ, Lau J, Abdulahad WH, Sanders JS, Heeringa P, Buckley C, O'Brien C, Finn S, Cohen CD, Lindemeyer MT, Hickey FB, O'Hara PV, Feighery C, Moran SM, Mellotte G, Clarkson MR, Dorman AJ, Murray PT, Little MA: Urinary soluble CD163 in active renal vasculitis. *J Am Soc Nephrol* 27: 2906–2916, 2016 <https://doi.org/10.1681/ASN.2015050511>
 84. Aendekerk JP, Timmermans SAMEG, Busch MH, Potjewijd J, Heeringa P, Damoiseaux JGMC, Reutelingsperger CP, van Paassen P; Limburg Renal Registry: Urinary soluble CD163 and disease activity in biopsy-proven ANCA-associated glomerulonephritis. *Clin J Am Soc Nephrol* 15: 1740–1748, 2020 <https://doi.org/10.2215/CJN.07210520>
 85. Hruskova Z, Honsova E, Berden AE, Rychlik I, Lanska V, Zabka J, Bajema IM, Tesar V: Repeat protocol renal biopsy in ANCA-associated renal vasculitis. *Nephrol Dial Transplant* 29: 1728–1732, 2014 <https://doi.org/10.1093/ndt/gfu042>
 86. Hauer HA, Bajema IM, Hagen EC, Noël LH, Ferrario F, Waldherr R, van Houwelingen HC, Lesavre P, Sinico RA, van der Woude F, Gaskin G, Verburgh CA, de Heer E, Bruijn JA: Long-term renal injury in ANCA-associated vasculitis: An analysis of 31 patients with follow-up biopsies. *Nephrol Dial Transplant* 17: 587–596, 2002 <https://doi.org/10.1093/ndt/17.4.587>
 87. Moran SM, Monach PA, Zgaga L, Cuthbertson D, Carette S, Khalidi NA, Koenig CL, Langford CA, McAlear CA, Moreland L, Pagnoux C, Seo P, Specks U, Sreih A, Wyse J, Ytterberg SR, Merkel PA, Little MA; Vasculitis Clinical Research Consortium: Urinary soluble CD163 and monocyte chemoattractant protein-1 in the identification of subtle renal flare in anti-neutrophil cytoplasmic antibody-associated vasculitis. *Nephrol Dial Transplant* 35: 283–291, 2020
 88. Jones BE, Yang J, Muthigi A, Hogan SL, Hu Y, Starmer J, Henderson CD, Poulton CJ, Brant EJ, Pendergraft WF 3rd, Jennette JC, Falk RJ, Ciavatta DJ: Gene-specific DNA methylation changes predict remission in patients with ANCA-associated vasculitis. *J Am Soc Nephrol* 28: 1175–1187, 2017 <https://doi.org/10.1681/ASN.2016050548>
 89. Kurz T, Weiner M, Skoglund C, Basnet S, Eriksson P, Segelmark M: A myelopoiesis gene signature during remission in anti-neutrophil cytoplasm antibody-associated vasculitis does not predict relapses but seems to reflect ongoing prednisolone therapy. *Clin Exp Immunol* 175: 215–226, 2014 <https://doi.org/10.1111/cei.12236>
 90. McKinney EF, Lyons PA, Carr EJ, Hollis JL, Jayne DRW, Willcocks LC, Koukoulaki M, Brazma A, Jovanovic V, Kemeny DM, Pollard AJ, Macary PA, Chaudhry AN, Smith KG: A CD8+ T cell transcription signature predicts prognosis in autoimmune disease. *Nat Med* 16: 586–591, 1p following 591, 2010 <https://doi.org/10.1038/nm.2130>
 91. Al-Ani B, Fitzpatrick M, Al-Nuaimi H, Coughlan AM, Hickey FB, Pusey CD, Savage C, Benton CM, O'Brien EC, O'Toole D, Mok KH, Young SP, Little MA: Changes in urinary metabolomic profile during relapsing renal vasculitis. *Sci Rep* 6: 38074, 2016 <https://doi.org/10.1038/srep38074>
 92. Gupta L, Jain A, Ekbote GG, Mishra R, Kumar D, Guleria A, Raj R, Kumar U: NMR based serum metabolomics revealed distinctive metabolic patterns of ANCA-associated vasculitis. *Int J Rheum Dis* 22[S3]: 40–226, 2019
 93. Trevisan J, Angelov PP, Carmichael PL, Scott AD, Martin FL: Extracting biological information with computational analysis of Fourier-transform infrared (FTIR) biospectroscopy datasets: Current practices to future perspectives. *Analyst (Lond)* 137: 3202–3215, 2012 <https://doi.org/10.1039/c2an16300d>
 94. Morais CLM, Lima KMG, Singh M, Martin FL: Tutorial: Multivariate classification for vibrational spectroscopy in biological samples. *Nat Protoc* 15: 2143–2162, 2020 <https://doi.org/10.1038/s41596-020-0322-8>
 95. Shaw RA, Kotowich S, Eysel HH, Jackson M, Thomson GTD, Mantsch HH: Arthritis diagnosis based upon the near-infrared spectrum of synovial fluid. *Rheumatol Int* 15: 159–165, 1995 <https://doi.org/10.1007/BF00301774>
 96. Chen M, McReynolds N, Campbell EC, Mazilu M, Barbosa J, Dholakia K, Powis SJ: The use of wavelength modulated Raman spectroscopy in label-free identification of T lymphocyte subsets, natural killer cells and dendritic cells. *PLoS One* 10: e0125158, 2015 <https://doi.org/10.1371/journal.pone.0125158>
 97. Kamińska A, Winkler K, Kowalska A, Witkowska E, Szymborski T, Janeczka A, Waluk J: SERS-based immunoassay in

- a microfluidic system for the multiplexed recognition of interleukins from blood plasma: towards picogram detection. *Sci Rep* 7: 10656, 2017 <https://doi.org/10.1038/s41598-017-11152-w>
98. Carvalho CS, Martin AA, Santo AME, Andrade LEC, Pinheiro MM, Cardoso MAG, et al: A rheumatoid arthritis study using Raman spectroscopy. *Theor Chem Acc* 130: 1211–1220, 2011 <https://doi.org/10.1007/s00214-011-0905-0>
99. Prentice BM, Caprioli RM, Vuiblet V: Label-free molecular imaging of the kidney. *Kidney Int* 92: 580–598, 2017 <https://doi.org/10.1016/j.kint.2017.03.052>
100. Varma VK, Kajdacsy-Balla A, Akkina SK, Setty S, Walsh MJ: A label-free approach by infrared spectroscopic imaging for interrogating the biochemistry of diabetic nephropathy progression. *Kidney Int* 89: 1153–1159, 2016 <https://doi.org/10.1016/j.kint.2015.11.027>
101. Yu MC, Rich P, Foreman L, Smith J, Yu MS, Tanna A, Dibbur V, Unwin R, Tam FWK: Label free detection of sensitive mid-infrared biomarkers of glomerulonephritis in urine using Fourier transform infrared spectroscopy. *Sci Rep* 7: 4601, 2017 <https://doi.org/10.1038/s41598-017-04774-7>

Received: October 29, 2020 Accepted: January 18, 2021



OPEN

Distinguishing active from quiescent disease in ANCA-associated vasculitis using attenuated total reflection Fourier-transform infrared spectroscopy

Adam D. Morris^{1✉}, Camilo L. M. Morais², Kássio M. G. Lima³, Daniel L. D. Freitas³, Mark E. Brady¹, Ajay P. Dhaygude¹, Anthony W. Rowbottom^{4,5} & Francis L. Martin^{6✉}

The current lack of a reliable biomarker of disease activity in anti-neutrophil cytoplasmic autoantibody (ANCA) associated vasculitis poses a significant clinical unmet need when determining relapsing or persisting disease. In this study, we demonstrate for the first time that attenuated total reflection Fourier-transform infrared (ATR-FTIR) spectroscopy offers a novel and functional candidate biomarker, distinguishing active from quiescent disease with a high degree of accuracy. Paired blood and urine samples were collected within a single UK centre from patients with active disease, disease remission, disease controls and healthy controls. Three key biofluids were evaluated; plasma, serum and urine, with subsequent chemometric analysis and blind predictive model validation. Spectrochemical interrogation proved plasma to be the most conducive biofluid, with excellent separation between the two categories on PC2 direction (AUC 0.901) and 100% sensitivity (F-score 92.3%) for disease remission and 85.7% specificity (F-score 92.3%) for active disease on blind predictive modelling. This was independent of organ system involvement and current ANCA status, with similar findings observed on comparative analysis following successful remission-induction therapy (AUC > 0.9, 100% sensitivity for disease remission, F-score 75%). This promising technique is clinically translatable and warrants future larger study with longitudinal data, potentially aiding earlier intervention and individualisation of treatment.

Anti-neutrophil cytoplasmic autoantibody (ANCA)-associated vasculitis (AAV) characterises an autoimmune disorder that results in inflammation and necrosis of small- and medium-sized blood vessels, causing potential multi-organ and life threatening disease. Central to its pathogenesis is the activation of primed neutrophils through the interaction of ANCA with myeloperoxidase (MPO) and proteinase-3 (PR3) target antigens expressed on their cell surface, resulting in neutrophil degranulation, endothelial damage and amplification loop that ensues¹⁻³. Current immunosuppressive treatment strategies are effective with improved patient survival, but carry a significant risk of treatment-related toxicity and long-term patient morbidity that often results from the sequelae of relapsing disease and required re-exposure to therapy⁴⁻⁶. The lack of a reliable biomarker of disease activity to aid the early detection of relapsing disease represents a significant clinical challenge, risking potentially undertreated disease or over exposure to therapy.

¹Department of Renal Medicine, Royal Preston Hospital, Lancashire NHS Foundation Trust, Preston, UK. ²School of Pharmacy and Biomedical Sciences, University of Central Lancashire, Preston, UK. ³Institute of Chemistry, Biological Chemistry and Chemometrics, Federal University of Rio Grande Do Norte, Natal, Brazil. ⁴Department of Immunology, Royal Preston Hospital, Lancashire NHS Foundation Trust, Preston, UK. ⁵School of Medicine, University of Central Lancashire, Preston, UK. ⁶Biocel UK Ltd, Hull, UK. ✉email: Adam.Morris@lthtr.nhs.uk; flm13@biocel.uk

Attenuated total reflection Fourier-transform infrared (ATR-FTIR) biospectroscopy offers a highly versatile, non-destructive and cost-effective means of analysing a given biological sample to determine its chemical composition; in effect providing a surrogate of its metabolomic profile. Within any sample, the chemical bonds that make up its constituent molecules will exhibit a periodic vibrational pattern. Those with a dipole moment are active within the infrared (IR) spectral range. ATR-FTIR exploits this by exposing a biological sample to mid-IR radiation to provide a spectral pattern based on the degree of IR absorption. As such, it can be used to quantitatively detect biochemical changes caused by pathology and provide a unique spectral fingerprint for disease states. Advancements in instrumentation and computational chemometric analysis have enabled ATR-FTIR to be applied to a wide range of biofluids and tissue samples, across numerous medical disciplines. Studies have employed it to detect disease with a high degree of sensitivity and specificity, including inflammatory arthropathy, neurodegenerative disease and malignancy^{9–10}. Its use in the field of nephrology is emerging with tissue analysis of both native and transplanted kidneys to aid current histological assessment and prognostication^{11–14}, detection of cast nephropathy¹⁵, renal stone analysis^{16,17} and more recently analysis of peritoneal and haemodialysis effluent^{18,19}.

One previous study has applied ATR-FTIR spectroscopy in vasculitis, demonstrating promising results, with several characteristic spectral markers identified from urine in a rodent model of crescentic glomerulonephritis and patients with renal limited disease²⁰. This phase one proof-of-concept study aims to determine the potential use of ATR-FTIR spectroscopy in AAV as novel biomarker of disease activity, through analysis of a range of biofluids and correlation with clinical parameters from patients with multisystem disease.

Results

Study population. One hundred and eight participants are included in the present study; 25 with active disease (AD), 38 in disease remission (DR), 10 with membranous nephropathy (MM), five with minimal change disease (MCD), 10 with immunoglobulin A nephropathy (IgA), 10 with pre-renal acute kidney injury (AKI) in the context of infection and 10 healthy controls (HC). Descriptive baseline characteristics for the active and remission disease cohorts are shown in Table 1. AAV participant flow through the study is shown in Supplementary Information (SI) Fig. S1. Amongst these two groups, overall mean age was 66 ± 11.9 years with no significant gender predominance. The majority were Caucasian, with only one South-Asian participant in the remission cohort. Baseline characteristics for the disease control groups are outlined in SI Table S1.

Of those with active disease, 16% ($n = 4$) had undetectable circulating ANCA, 68% ($n = 17$) had multisystem disease and of the remaining 32% ($n = 8$) with single organ disease, 4 were renal limited, 3 were limited to ear nose and throat disease and one had ophthalmic disease. Amongst the remission cohort 52% ($n = 20$) had persisting positive ANCA serology despite clinically quiescent disease. Overall two patients died, both in the AD cohort and both due to infection. No patients were lost to follow up. Paired remission samples were attained from 14 patients in the AD cohort for comparative analysis following successful remission induction therapy. Amongst this group the majority ($n = 13$) were ANCA positive at initial diagnosis, of which six remained ANCA positive at the time of paired remission sample collection.

ATR-FTIR: spectral data and classification models. ATR-FTIR spectrochemical interrogation of plasma samples yielded the highest degree of accuracy for discrimination between AD and DR, followed by serum and urine sample analysis respectively. Plasma sample data is presented below, with serum and urine datasets provided in the SI.

Figures 1a and 1b show the raw and pre-processed IR absorption spectra attained from plasma samples between the $900\text{--}1800\text{ cm}^{-1}$ spectral range for participants with AD and DR. Spectra initially appear to overlap. Given that a vast majority of constituent biomolecules present in plasma will be common to most individuals, this would be expected. Following second order differentiation to resolve overlapping peaks, multivariate analysis using principal component analysis (PCA) exhibits good separation between AD and DR on PC2 direction (Fig. 1c). A subsequent supervised classification model using partial least squares discriminant analysis (PLS-DA) was undertaken (Fig. 1d). In this process 60% of samples with known categories of either AD or DR were used as a training set to generate the classification model, with cross validation to prevent overfitting and blind assessment of the remaining 40% of samples to test the models predictive performance. The receiver operating characteristic (ROC) curve (Fig. 1e) demonstrates excellent ability of ATR-FTIR spectroscopy to distinguish between AD and DR using this classification system with an area under the curve of 0.901. This predictive classification model is shown in Table 2, with 100% sensitivity (F-score 92.3%) for DR and 85.7% specificity (F-score 92.3%) for correctly identifying AD.

Following successful remission induction therapy, analysis of paired remission samples revealed similar findings with good ability to discriminate AD and DR; PLS-DA AUC > 0.9 (Fig. 2) and 100% sensitivity (F-score 75%) for DR on predictive modelling (Table 3). There is a high level of accuracy in distinguishing AD from healthy controls (see SI, Fig. S2b,c and Table S2). On PCA scores of HC and DR, there was no clear segregation pattern between the two groups on PC2 direction following removal three outlier spectra from the HC cohort (see SI, Fig. S2e). Subsequent analysis of all participants in disease remission ($n = 52$), inclusive of those in remission at the time of study enrolment ($n = 38$) and paired remission samples ($n = 14$), confirmed excellent separation of spectral data from all control groups (see SI, Fig. S3e,f and Table S3). There was equally good separation of AD from all control groups (see SI, Fig. S3b,c and Table S3).

Correlation with clinical parameters. The correlation between ATR-FTIR spectral data for plasma and relevant clinical variables amongst those with AD is shown in Table 4. Based on the determination coefficient (R^2), other than serum albumin and total protein, there is no demonstrable significant correlation shown and

	Active Disease (n=25)	Disease Remission (n=38)
Mean Age (SD)	64 ± 11.9	67 ± 11.9
Sex		
Male	12/25 (48%)	20/38 (53%)
Female	13/25 (52%)	18/38 (47%)
Median serum creatinine (µmol/L)	216 (347–132)	122 (174–94)
Mean eGFR (mls/min/1.73m²)	22 (48–8)	47 (65–29)
Newly diagnosed disease	20/25 (80%)	–
Relapsing disease	5/25 (20%)	–
ANCA serotype		
MPO	9/25 (36%)	6/38 (16%)
PR3	12/25 (48%)	14/38 (37%)
Negative	4/25 (16%)	18/38 (47%)
BVAS	16 ± 9.6	0
Organ involvement		
Constitutional signs or symptoms	15/25 (60%)	–
Mucous membranes/Ophthalmic	6/25 (24%)	–
Cutaneous	1/25 (4%)	–
ENT	12/25 (48%)	–
Respiratory	6/25 (24%)	–
Cardiovascular	1/25 (4%)	–
Gastrointestinal	0	–
Renal	18/25 (72%)	–
Neurological	5/25 (20%)	–
Multisystem disease	17/25 (68%)	–
Renal limited	4/25 (16%)	–
Other laboratory salient laboratory results:		
Mean Haemoglobin (g/L)	100 ± 28.3	130 ± 13.4
Mean White cell count (10 ⁹ /L)	9 ± 3.7	7.2 ± 2.2
Mean Lymphocyte count (10 ⁹ /L)	1.2 ± 0.7	1.3 ± 0.6
Mean Neutrophil count (10 ⁹ /L)	7 ± 3.6	5.1 ± 2.2
Mean Platelet count (10 ⁹ /L)	309 ± 143.5	270 ± 80.6
Median CRP (mg/L)	42 (64.8–4.8)	2.6 (5.3–1.2)
Median ESR (mm/hr)	42 (80.5–9)	12 (19.8–5)
Median ESR (mm/hr)	42 (80.5–9)	12 (19.8–5)
Mean serum albumin (g/L)	34.7 ± 7.3	44.4 ± 2.9
Mean serum total protein (g/L)	62 ± 9.8	67.1 ± 4.7
Co-morbidities		
Ischaemic heart disease	1 (4%)	4 (11%)
Congestive cardiac failure	0	1 (3%)
Cerebrovascular disease	1 (4%)	2 (5%)
Hypertension	5 (20%)	18 (47%)
Peripheral vascular disease	0	1(3%)
Diabetes Mellitus	2 (8%)	3 (8%)
Chronic pulmonary disease	6 (24%)	5 (13%)
Chronic liver disease	0	0
Connective tissue disease	1 (4%)*	0
Malignancy	2 (8%)**	1 (3%)***
Immunosuppression		
None	8 (26%)	7 (18%)
Prednisolone****	14 (56%)	15 (39%)
Methylprednisolone	7 (28%)	0
Rituximab within the preceding 6 months	1 (4%)	13 (34%)
Cyclophosphamide	2 (8%)	2 (5%)
Azathioprine	0	6 (16%)
Mycophenolate	0	4 (11%)
Methotrexate	0	1 (3%)

Table 1. Characteristics of study population at the time of enrolment. *eGFR* estimated glomerular filtration rate, *ANCA* anti-neutrophil cytoplasmic autoantibody, *MPO* myeloperoxidase, *PR3* proteinase-3, *ESR* erythrocyte sedimentary rate, *CRP* C-reactive protein. *One case of rheumatoid arthritis in remission, **One case of non-metastatic prostate cancer in remission & one case of colonic tubular adenoma, ***One case of non-melanoma skin cancer, **** Amongst the remission cohort a daily dose of prednisolone ≥ 5 mg was considered significant.

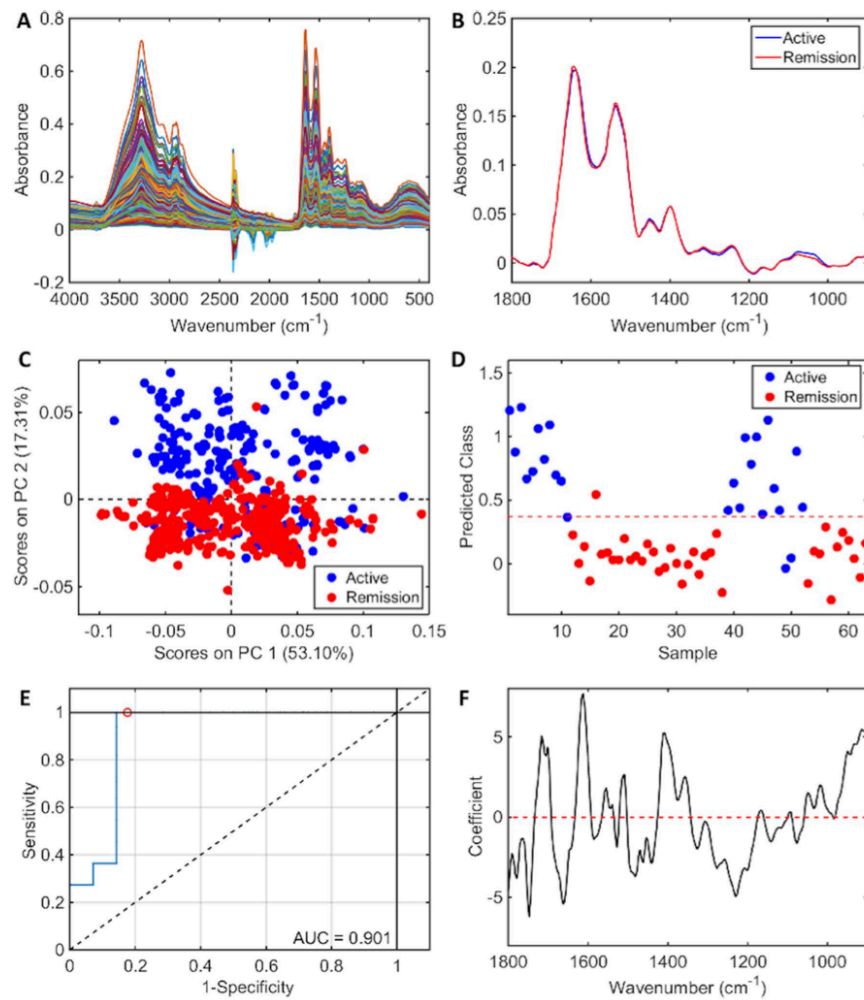


Figure 1. ATR-FTIR spectral classification of active disease vs. disease remission for plasma samples—(A) Raw spectral data, (B) Pre-processed spectra, (C) PCA scores plot, (D) PLS-DA discriminant function graph, (E) ROC curve for PLS-DA, (F) PLS-DA coefficients for identification of spectral biomarkers.

AD vs. DR	Accuracy (%)	Sensitivity (%)	Specificity (%)	F-Score (%)
Training (5 LVs)	93.6	96.3	90.9	93.5
Cross-validation	91.7	92.6	90.9	91.7
Test	92.8	100	85.7	92.3

Table 2. Classification parameters for plasma samples in active disease (AD) vs. disease remission (DR).

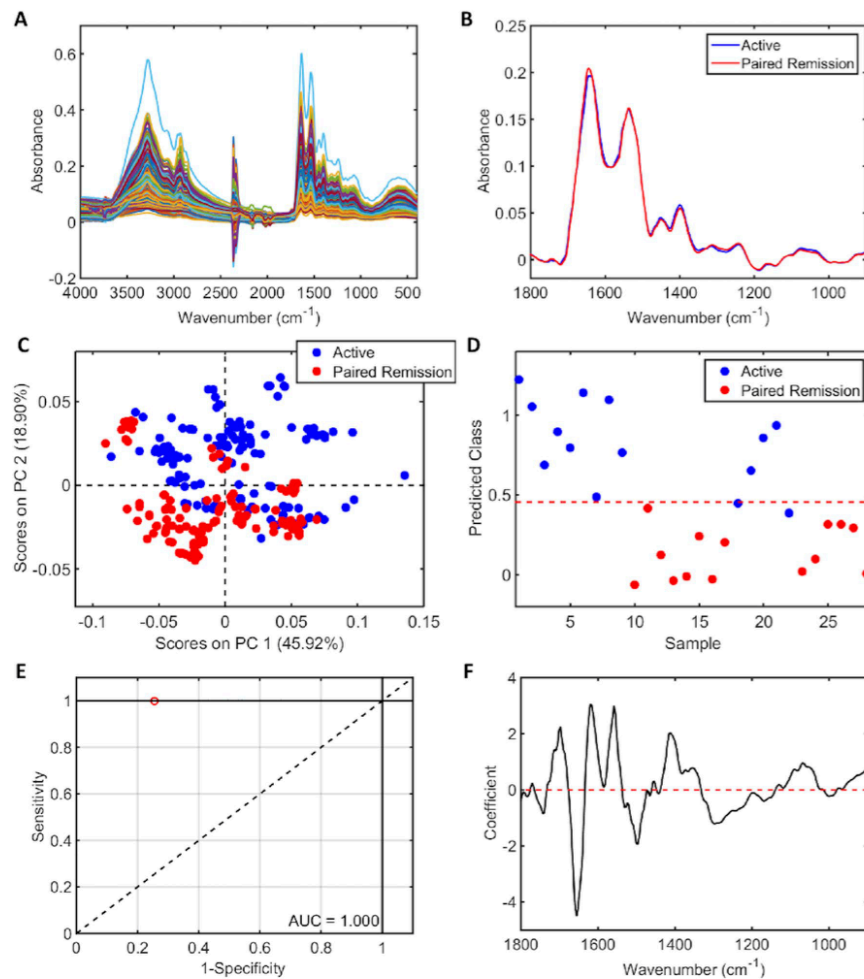


Figure 2. ATR-FTIR spectral classification of active disease vs. paired remission for plasma samples following successful remission induction therapy—(A) Raw spectral data, (B) Pre-processed spectra, (C) PCA scores plot, (D) PLS-DA discriminant function graph, (E) ROC curve for PLS-DA, (F) PLS-DA coefficients for identification of spectral biomarkers.

AD vs. PR	Accuracy (%)	Sensitivity (%)	Specificity (%)	F-Score (%)
Training (2 LVs)	100	100	100	100
Cross-validation	82.6	87.5	77.8	82.4
Test	80.0	100	60.0	75.0

Table 3. Classification parameters for plasma samples in active disease (AD) vs. paired remission (PR).

Active disease	Sensitivity of clinical variable	Specificity of clinical variable	Coefficients of determination (R ²)
Age	–	–	0.01
Gender	0.75	0.77	0.29
BVAS	–	–	0.19
Organ involvement:			
Constitutional signs or symptoms	0.60	0.60	0.00
Mucous Membrane/Ophthalmic	0.58	0.50	0.12
Cutaneous	0.83	1.00	0.02
ENT	0.39	0.67	0.14
Respiratory	0.58	0.50	0.02
Cardiovascular	1.00	1.00	0.00
Renal	1.00	0.94	0.52
Neurological	0.50	0.20	0.04
ANCA Positivity	0.67	0.75	0.06
ANCA Serotype			
MPO	0.44	0.50	0.00
PR3	0.67	0.38	0.01
Negative	0.75	0.71	0.02
ANCA titre	–	–	0.12
Serum creatinine (µmol/L)	–	–	0.27
eGFR(mls/min/1.73m ²)	–	–	0.45
Haemoglobin	–	–	0.51
White cell count	–	–	0.51
Lymphocyte count	–	–	0.24
Neutrophil count	–	–	0.52
Platelet count	–	–	0.08
CRP	–	–	0.18
ESR	–	–	0.29
Serum albumin	–	–	0.86
Total protein	–	–	0.65

Table 4. Comparative analysis between clinical variables and ATR-FTIR spectral data from plasma samples. ENT ear nose and throat, ANCA anti-neutrophil cytoplasmic autoantibody, MPO myeloperoxidase, PR3 proteinase-3, BVAS Birmingham vasculitis activity score, eGFR estimated glomerular filtration rate, ESR erythrocyte sedimentary rate, CRP C-reactive protein.

the ability of ATR-FTIR spectroscopy to accurately discriminate between AD and DR was independent of organ system involvement, detectable circulating ANCA, ANCA titre in cases of seropositive disease, renal function, commonly used markers of inflammation and other salient laboratory results. There was no significant correlation between spectral data and BVAS, a validated and widely applied clinical assessment tool of disease severity. Correlation between ATR-FTIR spectral data for plasma and relevant clinical variables amongst those with DR is shown in SI Table S4. This confirmed no significant findings. The sensitivities and specificities provided in both tables only relates to the ability to separate the two groups. It was not possible to calculate these respective values for age, BVAS ANCA titre and other routine salient laboratory results, as these are variables with defined numerical values for which discriminatory algorithms could not be executed.

Treatment data at the time of sample collection is outlined in Table 1. The varied distribution of therapy provided the opportunity to tentatively determine the impact of immunosuppression on spectral analysis independently of the effects of disease activity. Of the 56% (n = 14) of patients in the AD cohort and 39% (n = 15) in the DR cohort on prednisolone, the median daily dose was 40 mg (IQR 60–20) and 5 mg (IQR 10–5) respectively. Neither dosing regimens accounted for any difference in data variance (see SI, Figs. S4 and S5). Similarly, rituximab exposure up to six months prior to sample collection did not influence spectral analysis in the DR cohort (see

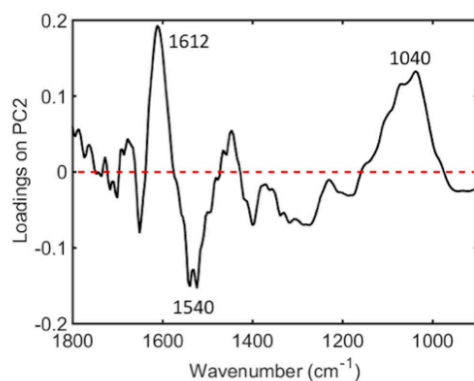


Figure 3. Main band differences for healthy controls (HC) vs. active disease (AD) using PCA loadings on PC2 from plasma samples—1612 cm^{-1} (higher in AD, adenine vibration in DNA), 1540 cm^{-1} (higher in HC, protein Amide II β -sheet), 1040 cm^{-1} (higher in AD, symmetric PO_2^- stretching in RNA/DNA).

Wavenumber (cm^{-1})	Tentative assignment	Influence on AD
1778	$\nu(\text{C}=\text{C})$ lipids	↓
1748	$\nu(\text{C}=\text{C})$ lipids	↓
1716	$\nu(\text{C}=\text{O})$ DNA/RNA	↑
1701	$\nu(\text{C}=\text{O})$ thymine	↑
1662	Amide I	↓
1509	In-plane $\delta(\text{CH})$ phenyl ring	↑
1481	Amide II	↓
1408	$\delta(\text{CH}_3)$	↑
1358	$\nu(\text{C}-\text{O})$, $\delta(\text{CH})$, $\delta(\text{NH})$	↑
1230	$\nu_{\text{as}}(\text{PO}_2^-)$	↓
948	Phosphodiester region (collagen and glycogen)	↑
914	Phosphodiester region (collagen and glycogen)	↑
1698	$\text{C}_2=\text{O}$ guanine	↑
1654	$\text{C}=\text{O}$, $\text{C}=\text{N}$, $\text{N}-\text{H}$ of adenine, thymine, guanine, cytosine	↓
1620	Base carbonyl stretching and ring breathing mode of nucleic acids	↑
1558	Ring base mode	↑
1415	CH deformation	↑

Table 5. Potential spectral biomarkers for distinguishing active disease and disease remission using plasma samples based on the PLS-DA coefficients (ν =stretching; δ =bending).

SI, Fig. S6). Meaningful subgroup analysis evaluating the impact of methylprednisolone, cyclophosphamide, azathioprine, methotrexate and mycophenolate were not feasible owing to the limited sample size of each subgroup.

Key spectral biomarkers. Key distinguishing peaks can be identified amongst the spectral data in each model based on PLS-DA coefficients. The wavenumber-variables responsible for largest between group differences provide biomarker extraction through the chemical bond they represent, which in turn can be associated with a particular cellular activity. Amongst AD and HC cohorts, wavenumber-variables 1612 cm^{-1} (adenine vibration in DNA) and 1040 cm^{-1} (symmetric PO_2^- stretching in RNA/DNA) were both higher in AD, whereas 1540 cm^{-1} (protein Amide II β -sheet) was higher in HC (Fig. 3).

Notable wave-number variables characterising AD from DR and their potential corresponding chemical bonds are outlined in Table 5. Noteworthy peaks for AD were in the 1620 – 1716 cm^{-1} range, representing nucleobase functional group expression as the main contributors; 1620 cm^{-1} (base carbonyl stretching and ring breathing mode of nucleic acids), 1698 cm^{-1} ($\text{C}_2=\text{O}$ guanine), 1701 cm^{-1} ($\nu(\text{C}=\text{O})$ thymine) and 1716 cm^{-1} ($\nu(\text{C}=\text{O})$ DNA/RNA). Lipid (1748 cm^{-1} , 1778 cm^{-1}) and protein functional groups at the Amide I (1662 cm^{-1}) and Amide II (1481 cm^{-1}) bands were associated with disease remission.

Discussion

The present study provides the first evidence that ATR-FTIR spectroscopy has the potential to provide an accurate biomarker of active disease and treatment response in multisystem AAV. To our knowledge this is the first study of its kind, in which we demonstrate its use as a quantitative method to distinguish active from quiescent disease with a high degree of sensitivity and specificity from plasma. This was applicable both in renal and extra-renal disease irrespective of current ANCA serology.

Given the inherent procedural risks, serial renal biopsies for histological confirmation of active disease is not practical and in the context of extra-renal disease, a tissue biopsy is often not feasible and typically has a low diagnostic yield²¹. Current approaches in clinical practice use two main biomarkers to help predict potential relapse; ANCA and B-cell population, however their clinical utility remains limited. Persisting ANCA positivity, ANCA reappearance and anti-PR3 associated disease have been associated with a higher rate of relapse^{22–25}, but despite this a significant proportion of de-novo and relapsing disease occurs in the absence of detectable circulating ANCA^{26–30}, particularly amongst patients with extra-renal disease³¹. The significance of rising titres also remains debateable^{32,33}. Moreover, ANCA positivity has been shown to occur in healthy individuals^{34–36} as well as other systemic illnesses³⁷, further restricting its use. Similarly, while B-cell repopulation following targeted therapy with rituximab has been associated with relapsing disease^{22,38,39}, follow up data from other large trials has not corroborated this finding^{33,40} and active disease has been shown to occur with B-cell activity in tissue despite depletion in serum⁴¹. Amongst other potential biomarker tools, urinary soluble CD163 (sCD163) and urinary monocyte chemoattractant protein-1 (MCP-1) have both demonstrated significant promise, with higher levels of both associated with active ANCA-associated glomerulonephritis^{42–47}. Furthermore, combination of the two has yielded a high specificity and positive likelihood ratio for relapsing disease⁴⁸. However, any potential role of urinary sCD163 and MCP-1 remains limited to renal vasculitis, with a robust non-invasive biomarker of multisystem disease still lacking. Other potential biomarkers including novel autoantibodies, autoantigen gene expression, serum cytokines and degradation products of the alternative complement pathway have either failed to be validated or require further investigation⁴⁹.

Biospectroscopy is an innovative candidate for the development of a functional biomarker of disease activity. Yu et al. used ATR-FTIR spectroscopy to analyse urine samples from rodent models of inflammatory glomerulonephritis, as well as a limited number of patients with ANCA positive pauci-immune glomerulonephritis to determine renal inflammation and injury²⁰. Several key characteristic spectral markers were identified that correlated with the progression and severity of disease. In particular, both the 1545 cm^{-1} and 1033 cm^{-1} wavenumber intensity correlated with disease severity in the rodent model, with normalisation to baseline following treatment with dexamethasone. However, the 1545 cm^{-1} band intensity increased with declining renal function amongst both patients with active disease and those in remission, failing to discriminate between the two groups. The 1545 cm^{-1} band was also present in the murine model of lupus nephritis, suggesting that it may not be specific to vasculitis, instead reflecting glomerular inflammation and damage. Nonetheless, these original findings demonstrated the potential application of ATR-FTIR spectra from urine as marker of disease activity in patients with ANCA positive renal limited disease.

In order to detect differences between patients with active disease and those in clinical remission, we employed ATR-FTIR to extract spectral data from three key biofluids; plasma, serum and urine. Using unsupervised learning where spectra are classified without any prior sample knowledge, overall category separation using PCA was good in both plasma and serum samples. On subsequent blind predictive modelling of known and unknown spectral profiles with PLS-DA, our findings demonstrated that plasma was the most accurate biofluid for discriminating between the two categories, correctly identifying active disease in 85.7% of cases and 100% of those in remission. This finding was independent of ANCA serology with 16% of patients in the AD cohort having undetectable circulating ANCA and 53% of patients having persistent ANCA positivity despite disease remission. Parallel findings were also seen in the AD cohort where paired remission samples were attained; demonstrating that not only can ATR-FTIR spectroscopy be used as a biomarker of active disease, but it could also be applied help determine treatment response. Our results were also applicable to both renal and non-renal disease with the majority of patients in the AD cohort having multisystem disease and no demonstrable correlation of discriminating spectral data with organ system involvement. The lack of any significant correlation between the spectral data and currently used clinical markers including ANCA, CRP and ESR is unsurprising as the latter are all known to have a limited association with disease activity. Similarly, the absence of any significant correlation with BVAS suggests that the application of ATR-FTIR spectroscopy may only be used to identify active disease and not disease severity. Group separation on PCA plot of spectral data attained from urine may have been restricted as not all included patients had renal involvement and of those who did, a urine sample could not be attained from three patients.

Several key wavenumber-variables associated with active disease from plasma samples were of particular interest, namely 1620 cm^{-1} , 1698 cm^{-1} , 1701 cm^{-1} and 1716 cm^{-1} which are all associated increased nucleic acid expression. This may reflect the known genetic contribution to disease susceptibility and epigenetic factors of disease activity, with reduced DNA methylation of MPO and PRN3 resulting in increased autoantigen expression and disease activity^{50–52}. Alternatively, recognising the role of nuclear extracellular traps (NETs) in disease pathogenesis, this finding may simply reflect increased free cell DNA as a result of NET remnants and apoptotic cells^{53–56}. Protein groups at the Amide I (1662 cm^{-1}) and Amide II (1481 cm^{-1}) bands were associated with disease remission. This may be a reflection of plasma protein abundance in the acute phase of illness with slightly lower trend in serum albumin observed in active disease (34.7 \pm 7.3 g/L) compared to disease remission (44.4 \pm 2.9 g/L). However, the determination coefficient (R^2) for both serum albumin and total protein did not confirm a positive correlation with spectral data amongst the disease remission cohort, but trended towards significance in active disease leaving the relevance of this result unclear. Mean serum total protein was largely

similar between the two groups; 62 ± 9.8 g/L vs. 67.1 ± 4.7 g/L. Mass spectrometric analysis could be applied in future study to help correlate the ATR-FTIR spectral pattern with potential key compositional properties.

The translation of ATR-FTIR spectroscopy into clinical practice is feasible. Portable handheld devices are currently in use in non-medical fields³⁷. Coupled with the integration of chemometric algorithms, minimal sample requirements and label free preparation means that ATR-FTIR spectroscopy offers a potential low cost, fast, automated near-patient test to complement current clinical practice and help identify patients with active disease. Although our results are encouraging they should be considered within the context of its primary limitation; despite taking measures to avoid the risk of overfitting, the risk of bias from insufficient training data remains a potential factor in this phase one study for biomarker discovery. A larger future phase two validation study is required to provide sufficient longitudinal training data and prevent bias from small sample size. Based on known outcomes, machine-learning using forward feature extraction algorithms could then be used to construct prediction models based on extracted spectral features. Such features would also lend novel insight into evolving mechanisms of action. We calculate that the optimal sample size for validation would be 199 samples (79 active and 120 remission cases) for a power of 80%. For the optimal sample size we used a Fisher's exact test considering the spectral proportion of active and remission cases, which is roughly 0.4:0.6 (see SI, Figure S15). Given the rare nature of disease, such a timely study would be feasible using existing biobanks from previous large randomised control trials in the field, with samples from various disease time points alongside current standard diagnostic methods. A second limitation to consider is the control groups used in the present study. Although good separation of active disease from all control groups was seen, other than AKI with systemic infection, disease control groups were otherwise restricted to renal limited pathology. Any future study of ATR-FTIR as a biomarker of multisystem AAV would benefit from inclusion of controls with other systemic inflammatory conditions, such as systemic lupus erythematosus or rheumatoid arthritis to help evaluate its clinical utility further.

The absence of a functional biomarker that accurately correlates with disease activity in AAV represents a significant clinical need. Our findings demonstrate that ATR-FTIR spectroscopy offers a novel means of distinguishing between active disease and remission in multisystem disease, independent of ANCA status. As well as aiding diagnosis, this may facilitate early intervention and tailored maintenance therapy to help improve patient outcomes, particularly in seronegative disease. These findings require validation in a larger study with longitudinal data and comparison against a wider range of glomerular and autoimmune conditions.

Materials and methods

Patients and ethics. Over a fourteen-month period from February 2019 to March 2020, paired blood and urine samples were collected from consecutive patients with active AAV and those in disease remission. The active disease cohort consisted of patients with new presentation or relapsing disease. The definition of AAV as outlined by the 2012 Chapel Hill Consensus Conference was used. As the histological confirmation of disease is often not a viable diagnostic tool in the context of extra-renal disease and a reference standard test with a sufficient degree of sensitivity and specificity is lacking in such cases, the index test of ATR-FTIR spectroscopy was evaluated in the context of this widely used criterion as reference standard for clinical diagnosis. Patients who did not meet this criterion, who were aged < 18 years, unable to provide consent or exhibited dual positivity with anti-glomerular basement membrane disease were excluded. Disease remission was defined as a Birmingham Vasculitis Activity Score (BVAS) of 0. A significant difference in the spectral data amongst patients with and without active AAV was the primary outcome of interest. As this study is applying a novel and previously untested technology to this patient group a sample size could not be calculated. All participants were registered with the Department of Renal Medicine regional vasculitis service at Lancashire Hospitals NHS Foundation Trust, UK. Informed written consent was obtained prior to enrolment in accordance with study approval from the Health Research Authority, Cambridge South Research Ethics Committee (REC reference 18/EE/0194) and the Research and Development team in the Centre for Health Research and Innovation at Lancashire Teaching Hospitals NHS Foundation Trust. All experiments were carried out in accordance with the relevant guidelines and regulations.

The following clinical data was collected at baseline assessment; demographics, clinical presentation, BVAS and salient laboratory results including current ANCA serotype were applicable, serum creatinine, haemoglobin, white cell count, lymphocyte count, neutrophil count, platelet count, C-reactive protein erythrocyte sedimentary rate and urine protein creatinine ratio. Urine samples were sent for microscopy and culture to determine the presence of bacteriuria and its potential impact as a confounding factor on ATR-FTIR sample analysis. For patients with active disease, further samples were collected following successful remission induction therapy where possible for comparative analysis. Control groups including membranous nephropathy, minimal change disease, immunoglobulin A nephropathy, acute kidney injury in the context of infection and healthy individuals were included for analysis. Participants in the healthy control group were not known to have renal impairment and had a normal dipstick urinalysis.

Sample collection and preparation. Samples from participants with active disease were taken in both the outpatient clinic and acute in-patient setting. All remission and disease control samples were taken in the outpatient clinic. Healthy control samples were attained from individuals working in the hospital outside of the laboratory setting. Whole blood samples were collected in EDTA and serum separator tubes. All blood and urine samples were centrifuged at 3000 rpm, 4 °C for 10 min. The resulting plasma, serum and supernatant urine were collected in 0.5 ml Eppendorf tubes and stored on site at - 80 °C. When required for experimentation samples were thawed at room temperature, after which 30 μ l aliquots were placed on IR-reflective aluminium coated FisherBrand slides and left to air dry for a minimum of 2 h prior to spectroscopic analysis.

ATR-FTIR spectral acquisition. ATR-FTIR spectra were attained using a Bruker Tensor 27 FTIR spectrometer with Helios ATR attachment (Bruker Optics Ltd, Coventry UK), operated by OPUS 6.5 software. The sample area was defined by the diamond crystal internal reflective element, approximately 250 μm by 250 μm . Spectra were acquired from 10 locations on each sample; five central and five peripheral to help minimise any potential bias. Parameters for spectral acquisition consisted of 32 scans per location, 8 cm^{-1} spectral resolution with 2 \times zero-filling and 6 mm aperture setting, yielding a data spacing of 4 cm^{-1} over 4000–400 cm^{-1} spectral range. The diamond crystal was cleaned with distilled water, dried with Kimwipes and a background absorption spectra was taken at the start of each new sample analysis to account for atmospheric conditions.

Spectral pre-processing. The spectral data were imported into MATLAB R2014b environment (MathWorks Inc., USA) for pre-processing and subsequent multivariate analysis. Pre-processing consists of mathematical techniques employed to the raw spectral data to remove or reduce contributions of signals that are not related to the analyte target property or to the sample discrimination, hence, reducing chemically irrelevant variations in order to improve the accuracy and precision of qualitative and quantitative analyses⁵⁸. Herein, the raw spectral data were pre-processed by automatic weighted least squares (AWLS) baseline correction and vector normalisation⁵⁹. Finally, prior to model construction by partial least squares discriminant analysis (PLS-DA), the pre-processed data are mean-centred.

Multivariate analysis. Multivariate classification by means of PLS-DA was employed to discriminate the spectral data based on the experimental classes. Firstly, the pre-processed data were split into training and test (external validation) sets using the MLM algorithm⁶⁰. The training set, composed of 60% of the samples, was used for model construction, whose optimisation step (defining the number of latent variables (LVs) for PLS-DA) was performed via venetian blinds cross-validation. The remaining samples (40% of the dataset) assigned to the test set were used to evaluate the model classification performance. The spectral replicas per sample were averaged prior to model construction so the model was constructed on a sample-basis, hence, with no overlap of samples between the training and test sets.

PLS-DA is a well-known chemometric technique of supervised classification. It is based on a linear classification model for which the classification criterion is obtained by partial least squares (PLS)⁶¹. In PLS-DA, PLS is applied to the pre-processed data, reducing them to a few number of LVs, in which the category variables for each class in the training set is used to optimise the model. Then, a straight line that divides the classes' spaces is delineated⁶². In addition to PLS-DA, prior to supervised classification, the pre-processed data also underwent an exploratory analysis by principal component analysis (PCA) in order to identify possible natural clustering patterns or trends in the data through the analysis of the 2D PCA scores plots on principal components (PCs) 1 and 2⁶³.

Model validation. Model validation was performed by the calculation of accuracy, sensitivity, specificity and F-scores for the test set. The accuracy represents the total number of samples correctly classified, considering true and false negatives. The sensitivity represents the proportion of positive samples correctly classified, the specificity represents the proportion of negative samples correctly classified and the F-score measures the model performance considering imbalanced data⁶⁴.

Correlation with clinical variables. Correlation between the pre-processed spectra and individual clinical variables was evaluated by PLS regression (for continuous variables) and PLS-DA (for categorical variables). PLS and PLS-DA models were built using cross-validation. The association between spectra and a clinical variable was evaluated by assessing the determination coefficient (R^2) and root mean square error of cross-validation (RMSECV). Clinical parameters for which the R^2 was low, or RMSECV elevated, were considered to have poor correlation with the spectral data.

Data availability

The authors declare that the data supporting the findings of this study are available within the paper and its supplementary information. The MATLAB code and instructions on how to process the data are presented in previous publications^{49–51}.

Received: 28 December 2020; Accepted: 22 April 2021

Published online: 11 May 2021

References

- Falk, R. J., Terrell, R. S., Charles, L. A. & Jennette, J. C. Anti-neutrophil cytoplasmic autoantibodies induce neutrophils to degranulate and produce oxygen radicals in vitro. *Proc. Natl. Acad. Sci. USA* **87**(11), 4115–4119 (1990).
- Xiao, H. *et al.* Antineutrophil cytoplasmic autoantibodies specific for myeloperoxidase cause glomerulonephritis and vasculitis in mice. *J. Clin. Invest.* **110**(7), 955–963 (2002).
- Jennette, J. C. & Falk, R. J. Pathogenesis of antineutrophil cytoplasmic autoantibody-mediated disease. *Nat. Rev. Rheumatol.* **10**(8), 463–473 (2014).
- Little, M. A. *et al.* Early mortality in systemic vasculitis: Relative contribution of adverse events and active vasculitis. *Ann. Rheum. Dis.* **69**(6), 1036–1043 (2010).
- Robson, J. *et al.* Damage in the ANCA-associated vasculitides: Long-term data from the European Vasculitis Study Group (EUVAS) therapeutic trials. *Ann. Rheum. Dis.* **74**(1), 177–184 (2013).
- Robson, J. *et al.* Glucocorticoid treatment and damage in the anti-neutrophil cytoplasm antibody-associated vasculitides: Long-term data from the European Vasculitis Study Group trials. *Rheumatol (United Kingdom)*. **54**(3), 471–481 (2014).

7. Trevisan, J., Angelov, P. P., Carmichael, P. L., Scott, A. D. & Martin, F. L. Extracting biological information with computational analysis of Fourier-transform infrared (FTIR) biospectroscopy datasets: Current practices to future perspectives. *Analyst* **137**(14), 3202–3215 (2012).
8. Shaw, R. A. *et al.* Arthritis diagnosis based upon the near-infrared spectrum of synovial fluid. *Rheumatol. Int.* **15**(4), 159–165 (1995).
9. Paraskevaidi, M. *et al.* Differential diagnosis of Alzheimer's disease using spectrochemical analysis of blood. *Proc. Natl. Acad. Sci. USA* **114**(38), 7929–7938 (2017).
10. Purandare, N. C. *et al.* Exploiting biospectroscopy as a novel screening tool for cervical cancer: Towards a framework to validate its accuracy in a routine clinical setting. *Bioanalysis* **5**(21), 2697–2711 (2013).
11. De Bruyne, S. *et al.* Detection and characterization of a biochemical signature associated with diabetic nephropathy using near-infrared spectroscopy on tissue sections. *J. Clin. Med.* **8**(7), 1022 (2019).
12. Varma, V. K., Kajdacsy-Balla, A., Akkina, S. K., Setty, S. & Walsh, M. J. A label-free approach by infrared spectroscopic imaging for interrogating the biochemistry of diabetic nephropathy progression. *Kidney Int.* **89**(5), 1153–1159 (2016).
13. Severcan, F., Bozkurt, O., Gurbanov, R. & Gorgulu, G. FT-IR spectroscopy in diagnosis of diabetes in rat animal model. *J. Biophotonics* **3**(8–9), 621–631 (2010).
14. Vuiblet, V. *et al.* Renal graft fibrosis and inflammation quantification by an automated fourier-transform infrared imaging technique. *J. Am. Soc. Nephrol.* **27**(8), 2382–2391 (2016).
15. Esteve, E. *et al.* Nanometric chemical speciation of abnormal deposits in kidney biopsy: Infrared-nanospectroscopy reveals heterogeneities within vancomycin casts. *Anal. Chem.* **92**(11), 7388–7392 (2020).
16. Khan, A. H., Imran, S., Talati, J. & Jafri, L. Fourier transform infrared spectroscopy for analysis of kidney stones. *Investig. Clin. Urol.* **59**(1), 32–37 (2018).
17. Oliver, K. V. *et al.* Infrared vibrational spectroscopy: A rapid and novel diagnostic and monitoring tool for cystinuria. *Sci. Rep.* **6**, 1–7 (2016).
18. Grunert, T. *et al.* Vibrational spectroscopy of peritoneal dialysis effluent for rapid assessment of patient characteristics. *Biomolecules* **10**(6), 1–13 (2020).
19. Roth, A. *et al.* Infrared spectroscopy in hemodialysis: Reagent-free monitoring of patient detoxification by infrared spectroscopy. *Anal. Bioanal. Chem.* **403**(2), 391–399 (2012).
20. Yu, M. C. *et al.* Label free detection of sensitive mid-infrared biomarkers of glomerulonephritis in urine using Fourier transform infrared spectroscopy. *Sci. Rep.* **7**(1), 1–12 (2017).
21. Maguchi, S., Fukuda, S. & Takizawa, M. Histological findings in biopsies from patients with cytoplasmic-antineutrophil cytoplasmic antibody (cANCA)-positive Wegener's granulomatosis. *Auris Nasus Larynx* **28**(SUPPL), 53–58 (2001).
22. van Dam, L. S. *et al.* Proteinase-3-anti-neutrophil cytoplasmic antibodies (PR3-ANCAs) predict relapses in ANCA-associated vasculitis patients after rituximab. *Nephrol. Dial. Transpl.* **2020**, 1–10 (2020).
23. McClure, M. E. *et al.* Evaluation of PR3-ANCA status after rituximab for ANCA-associated vasculitis. *J. Clin. Rheumatol.* **25**(5), 217–223 (2019).
24. DeOliviera, J., Gaskin, G., Dash, A., Rees, A. J. & Pusey, C. D. Relationship between disease activity and anti-neutrophil cytoplasmic antibody concentration in long-term management of systemic vasculitis. *Am. J. Kidney Dis.* **25**(3), 380–389 (1995).
25. Hogan, S. L. *et al.* Predictors of relapse and treatment resistance in antineutrophil. *Ann. Intern. Med.* **2005**, 621–632 (2005).
26. Hedger, N., Stevens, J., Drey, N., Walker, S. & Roderick, P. Incidence and outcome of pauci-immune rapidly progressive glomerulonephritis in Wessex, UK: A 10-year retrospective study. *Nephrol. Dial. Transpl.* **15**(10), 1593–1599 (2000).
27. Hung, P. H. *et al.* Poor renal outcome of antineutrophil cytoplasmic antibody negative pauci-immune glomerulonephritis in Taiwanese. *J. Formos. Med. Assoc.* **105**(10), 804–812 (2006).
28. Chen, M. *et al.* Antineutrophil cytoplasmic autoantibody-negative pauci-immune crescentic glomerulonephritis. *J. Am. Soc. Nephrol.* **18**(2), 599–605 (2007).
29. Morgan, M. D. *et al.* Negative anti-neutrophil cytoplasm antibody at switch to maintenance therapy is associated with a reduced risk of relapse. *Arthritis. Res. Ther.* **19**(1), 1–7 (2017).
30. Smith, R. M. *et al.* Rituximab for remission maintenance in relapsing antineutrophil cytoplasmic antibody-associated vasculitis. *Arthritis. Rheum.* **64**(11), 3760–3769 (2012).
31. Holle, J. U. *et al.* Prospective long-term follow-up of patients with localised Wegener's granulomatosis: Does it occur as persistent disease stage? *Ann. Rheum. Dis.* **69**(11), 1934–1939 (2010).
32. Tomasson, G., Grayson, P. C., Mahr, A. D., LaValley, M. & Merkel, P. A. Value of ANCA measurements during remission to predict a relapse of ANCA-associated vasculitis—a meta-analysis. *Rheumatology* **51**(1), 100–109 (2012).
33. Miloslavsky, E. M. *et al.* Clinical outcomes of remission induction therapy for severe antineutrophil cytoplasmic antibody-associated vasculitis. *Arthritis Rheum.* **65**(9), 2441–2449 (2013).
34. Roth, A. J. *et al.* Epitope specificity determines pathogenicity and detectability in anca-associated vasculitis. *J. Clin. Invest.* **123**(4), 1773–1783 (2013).
35. Cui, Z., Zhao, M. H., Segelmark, M. & Hellmark, T. Natural autoantibodies to myeloperoxidase, proteinase 3, and the glomerular basement membrane are present in normal individuals. *Kidney Int.* **78**(6), 590–597 (2010).
36. Olson, S. W. *et al.* Asymptomatic autoantibodies associate with future anti-glomerular basement membrane disease. *J. Am. Soc. Nephrol.* **22**(10), 1946–1952 (2011).
37. Houben, E. *et al.* Diagnosing ANCA-associated vasculitis in ANCA positive patients. *Medicine (Baltimore)* **95**(40), e5096 (2016).
38. Jones, R. B. *et al.* Rituximab versus cyclophosphamide in ANCA-associated renal vasculitis: 2-year results of a randomised trial. *Ann. Rheum. Dis.* **74**(6), 1178–1182 (2015).
39. Guillevin, L. *et al.* Rituximab versus azathioprine for maintenance in ANCA-associated vasculitis. *N. Engl. J. Med.* **371**(19), 1771–1780 (2014).
40. Charles, P. *et al.* Comparison of individually tailored versus fixed-schedule rituximab regimen to maintain ANCA-associated vasculitis remission: Results of a multicentre, randomised controlled, phase III trial (MAINRITSAN2). *Ann. Rheum. Dis.* **77**(8), 1144–1150 (2018).
41. Ferraro, A. J., Smith, S. W., Neil, D. & Savage, C. O. S. Relapsed Wegener's granulomatosis after rituximab therapy: B cells are present in new pathological lesions despite persistent "depletion" of peripheral blood. *Nephrol. Dial. Transpl.* **23**(9), 3030–3032 (2008).
42. Tam, F. W. K. *et al.* Urinary monocyte chemoattractant protein-1 (MCP-1) is a marker of active renal vasculitis. *Nephrol. Dial. Transpl.* **19**(11), 2761–2768 (2004).
43. Ohlsson, S., Bakoush, O., Tencer, J., Torffvit, O. & Segelmark, M. Monocyte chemoattractant protein 1 is a prognostic marker in ANCA-associated small vessel vasculitis. *Mediators Inflamm.* **2009**, 584916 (2009).
44. Lieberthal, J. G. *et al.* Urinary biomarkers in relapsing antineutrophil cytoplasmic antibody-associated vasculitis. *J. Rheumatol.* **40**(5), 674–683 (2013).
45. Jönsson, N., Erlandsson, E., Gunnarsson, L., Pettersson, Å. & Ohlsson, S. Monocyte chemoattractant protein-1 in antineutrophil cytoplasmic autoantibody-associated vasculitis: Biomarker potential and association with polymorphisms in the MCP-1 and the CC chemokine receptor-2 gene. *Mediators Inflamm.* **2018**, 2018 (2018).
46. O'Reilly, V. P. *et al.* Urinary soluble CD163 in active renal vasculitis. *J. Am. Soc. Nephrol.* **27**(9), 2906–2916 (2016).

47. Aendekerck, J. P. *et al.* Urinary soluble CD163 and disease activity in biopsy-proven ANCA-associated glomerulonephritis. *Clin. J. Am. Soc. Nephrol.* **15**, 07210520 (2020).
48. Moran, S. M. *et al.* Urinary soluble CD163 and monocyte chemoattractant protein-1 in the identification of subtle renal flare in anti-neutrophil cytoplasmic antibody-associated vasculitis. *Nephrol. Dial. Transpl.* **35**(2), 283–291 (2018).
49. Morris, A. D., Rowbottom, A. W., Martin, F. L., Woywodt, A. & Dhaygude, A. P. Biomarkers in ANCA-associated vasculitis: Potential pitfalls and future prospects. *Kidney* <https://doi.org/10.34067/KID.0006432020> (2021).
50. Lyons, P. A. *et al.* Genetically distinct subsets within ANCA-associated vasculitis. *N. Engl. J. Med.* **367**(3), 214–223 (2012).
51. Ciavatta, D. J. *et al.* Epigenetic basis for aberrant upregulation of autoantigen genes in humans with ANCA vasculitis. *J. Clin. Invest.* **120**(9), 3209–3219 (2010).
52. Jones, B. E. *et al.* Gene-specific DNA methylation changes predict remission in patients with ANCA-associated vasculitis. *J. Am. Soc. Nephrol.* **28**(4), 1175–1187 (2016).
53. Kessenbrock, K. *et al.* Netting neutrophils in autoimmune small-vessel vasculitis. *Nat. Med.* **15**(6), 623–625 (2010).
54. Abreu-Velez, A. M., Smith, J. G. & Howard, M. S. Presence of neutrophil extracellular traps and antineutrophil cytoplasmic antibodies associated with vasculitides. *N. Am. J. Med. Sci.* **1**(6), 309–313 (2009).
55. Björnsdóttir, H. *et al.* Neutrophil NET formation is regulated from the inside by myeloperoxidase-processed reactive oxygen species. *Free Radic. Biol. Med.* **89**, 1024–1035 (2015).
56. Antonelou, M. *et al.* Therapeutic myeloperoxidase inhibition attenuates neutrophil activation, anca-mediated endothelial damage, and crescentic GN. *J. Am. Soc. Nephrol.* **31**(2), 350–364 (2020).
57. De Bruyne, S., Speeckaert, M. M. & Delanghe, J. R. Applications of mid-infrared spectroscopy in the clinical laboratory setting. *Crit. Rev. Clin. Lab. Sci.* **55**(1), 1–20 (2018).
58. Morais, C. L. M., Lima, K. M. G., Singh, M. & Martin, F. L. Tutorial: multivariate classification for vibrational spectroscopy in biological samples. *Nat. Protoc.* **15**(7), 2143–2162 (2020).
59. Morais, C. L. M. *et al.* Standardization of complex biologically derived spectrochemical datasets. *Nat. Protoc.* **14**, 1546–1577 (2019).
60. Morais, C. L. M., Santos, M. C. D., Lima, K. M. G. & Martin, F. L. Improving data splitting for classification applications in spectrochemical analyses employing a random-mutation Kennard-Stone algorithm approach. *Bioinformatics* **35**(24), 5257–5263 (2019).
61. Hibbert, D. B. Vocabulary of concepts and terms in chemometrics (IUPAC Recommendations 2016). *Pure Appl. Chem.* **88**(4), 407–443 (2016).
62. Breerton, R. G. & Lloyd, G. R. Partial least squares discriminant analysis: Taking the magic away. *J. Chemom.* **28**(4), 213–225 (2014).
63. Bro, R. & Smilde, A. K. Principal component analysis. *Anal. Methods* **6**(9), 2812–2831 (2014).
64. Morais, C. L. M. & Lima, K. Comparing unfolded and two-dimensional discriminant analysis and support vector machines for classification of EEM data. *Chemom. Intell. Lab. Syst.* **162**, 123–129 (2017).

Acknowledgements

The authors would like to acknowledge the support of the Renal Department at Royal Preston Hospital Lancashire NHS Foundation Trust and the team at the NIHR Lancashire Clinical Research Facility in undertaking this study. We are also grateful for the participation and support of all of the patients in this study.

Author contributions

A.D.M., A.W.R., A.P.D. & F.L.M. were responsible for conception, design and oversight of the study. Participant recruitment, sample collection, sample processing and ATR-FTIR spectroscopy was undertaken by A.D.M. F.L.M. was lead research supervisor, facilitating and directing the project. Chemometric data analysis and interpretation was performed by C.L.M., K.M.G.L. & D.L.D.F. A.D.M. prepared the manuscript with critical review & contributions from all authors.

Competing interests

F.L.M. has a senior management role in Biocel UK Ltd, a company with a subsidiary interested in developing similar algorithms as used in this manuscript for commercial gain. He is also a significant shareholder in this company. No other conflicts of interest are declared. All authors have no conflict of interest to declare. The results presented in this paper have not been published previously in whole or part.

Additional information

Supplementary Information The online version contains supplementary material available at <https://doi.org/10.1038/s41598-021-89344-8>.

Correspondence and requests for materials should be addressed to A.D.M. or F.L.M.

Reprints and permissions information is available at www.nature.com/reprints.

Publisher's note Springer Nature remains neutral with regard to jurisdictional claims in published maps and institutional affiliations.



Open Access This article is licensed under a Creative Commons Attribution 4.0 International License, which permits use, sharing, adaptation, distribution and reproduction in any medium or format, as long as you give appropriate credit to the original author(s) and the source, provide a link to the Creative Commons licence, and indicate if changes were made. The images or other third party material in this article are included in the article's Creative Commons licence, unless indicated otherwise in a credit line to the material. If material is not included in the article's Creative Commons licence and your intended use is not permitted by statutory regulation or exceeds the permitted use, you will need to obtain permission directly from the copyright holder. To view a copy of this licence, visit <http://creativecommons.org/licenses/by/4.0/>.

© The Author(s) 2021

FULL ARTICLE

A comparative analysis of different biofluids using Raman spectroscopy to determine disease activity in ANCA-associated vasculitis

Adam D. Morris^{1*} | Camilo L. M. Morais² | Kássio M. G. Lima³ |
Daniel L. D. Freitas³ | Mark E. Brady¹ | Ajay P. Dhaygude¹ |
Anthony W. Rowbottom^{4,5} | Francis L. Martin^{6*}

¹Renal Medicine, Royal Preston Hospital, Preston, UK

²School of Pharmacy and Biomedical Sciences, University of Central Lancashire, Preston, UK

³Institute of Chemistry, Biological Chemistry and Chemometrics, Federal University of Rio Grande do Norte, Natal, Brazil

⁴Department of Immunology, Royal Preston Hospital, Preston, UK

⁵School of Medicine, University of Central Lancashire, Preston, UK

⁶Biocel Ltd, Hull, UK

*Correspondence

Dr Adam D. Morris, Department of Nephrology, Renal Medicine, Royal Preston Hospital, Lancashire NHS Foundation Trust, Sharoe Green Lane, Fulwood, Preston PR2 9HT, UK.
Email: adam.morris@lthtr.nhs.uk

Prof Francis L. Martin, Biocel Ltd, Hull HU10 7TS, UK.
Email: flm13@biocel.uk

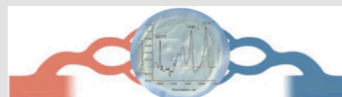
Abstract

Identifying persistent or relapsing disease in anti-neutrophil cytoplasmic autoantibody-associated

vasculitis (AAV) remains a clinical challenge with an unmet need for a reliable biomarker of multisystem disease. In this study, we confirm for the first time that Raman spectroscopy offers a novel cost-effective candidate biomarker to discriminate active disease from remission in AAV with excellent accuracy. Spectrochemical interrogation of plasma and serum samples demonstrated equal ability to discriminate disease activity with good group separation on PC1 direction and a high degree of accuracy on validation testing using blind predictive modelling: F-score 80% for plasma (specificity 93.3%, sensitivity 70%, AUC 0.95) and 80% for serum (specificity 80%, sensitivity 80%, AUC 0.92). Similar findings were seen on analysis of paired remission samples following successful remission-induction therapy. A larger study with longitudinal data is required to validate these findings with the potential to aid patient care.

KEYWORDS

ANCA-associated vasculitis, biomarker, disease activity, Raman spectroscopy



1 | INTRODUCTION

Anti-neutrophil cytoplasmic autoantibody (ANCA)-associated vasculitis is a term used to describe a group of multisystem small vessel vasculitides that are characterised by a pauci-immune appearance on histopathology and often accompanied by detectable circulating autoantibody. Since its initial description in the early 1980s the prevalence rate of disease has steadily increased with most recent estimates of 46 to 184/million, reflecting

improved patient survival in line with improved treatment strategies [1]. Current standard remission-induction therapy for organ or life threatening ANCA-associated vasculitis (AAV) centres around the use of glucocorticoids in conjunction with either cytotoxic or B-cell depleting therapy, with a greater patient burden now arising from potential adverse effects of therapy [2–4]. In particular, recurrent glucocorticoid exposure is associated with significant morbidity and mortality, with long term follow up data from several key landmark trials

evaluating remission-induction therapy confirming high levels of treatment related damage [3,4]. Any such effect is compounded by the natural course of AAV as one of relapsing disease and subsequent reexposure to therapy. Complicating this is the lack of an effective biomarker of disease activity, generating potential uncertainty when assessing relapsing or persistent disease and determining re-exposure to intensified immunosuppression.

Biospectroscopy is a non-invasive and efficient analytical tool capable of determining differences in the chemical and molecular composition of sample. Methods include Raman spectroscopy, which centres on the interaction of light with the underlying chemical bonds present in any given sample. The resulting effect of Raman scattering is based on molecular polarizability changes. When certain chemical bonds, both polar and non-polar, are exposed to a monochromatic laser light source, a small portion of absorbed photons (less than 1%) suffers a frequency deviation. This frequency shift is known as inelastic scattering and is divided into Stokes and anti-Stokes, whereby the emitted photons after energy transition have a lower or higher energy frequency than the initial absorbed radiation, respectively. These energy shifts occur between vibrational energy levels, thus its wave frequency is at the same range of the infrared radiation. Only a small proportion of incident photons undergo this effect with the remainder being scattered without any interaction [5]. The scattered spectra obtained will therefore be representative of the samples chemical composition, with the intensity and position of each spectral peak corresponding to a specific molecular bond. As a result, biochemical changes caused by pathology will generate a distinct spectrochemical fingerprint that can be used to differentiate it from other pathological and physiological states.

In effect this label-free technique provides a fast and cost effective surrogate index of a biosamples metabolomic profile and has been successfully used across a wide range of medical applications including immune cell identity [6], cytokine detection [7], malignancy [8,9] and nephrology [10–13]. The complimentary technique of attenuated total reflection Fourier-transform infrared (ATR-FTIR) has been assessed in ANCA-associated vasculitis with promising results demonstrated [14]; however, the application Raman spectroscopy in vasculitis has not previously been reported. Raman spectroscopy offers the additional advantage of a potentially automated near patient test with a high throughput. In this study, we aim to evaluate the use of Raman spectroscopy as a novel biomarker of disease activity in AAV across a range of biofluids.

2 | METHOD

2.1 | Patients and ethics

Alongside a healthy control group, paired blood and urine samples were collected from consecutive patients with active AAV and disease remission between February 2019 and March 2020. Exclusion criteria consisted of failure to meet the 2012 Chapel Hill Consensus Conference definition of disease [15], dual positivity with anti-glomerular basement membrane autoantibody, patient age <18 years or inability to provide consent. Participants in the healthy control group had a normal dipstick urinalysis at the time of recruitment with no known history of renal impairment. The primary outcome was the ability of Raman spectroscopy to accurately differentiate active and inactive disease. All AAV participants were registered with the Department of Renal Medicine regional vasculitis service at Lancashire Hospitals NHS Foundation Trust, UK. This study received ethical approval from the Health Research Authority, Cambridge South Research Ethics Committee (REC reference 18/EE/0194) and the Research and Development team in the Centre for Health Research and Innovation at Lancashire Teaching Hospitals NHS Foundation Trust. A sample size could not be calculated as this study applied a novel and previously untested technology to this patient group.

Baseline clinical assessment included participant demographics, clinical presentation, Birmingham Vasculitis Activity Score (BVAS), ANCA serotype and other salient laboratory results. To account for the presence of bacteriuria as a potentially confounding factor all urine samples were sent for microscopy and culture. Following successful remission induction therapy in cases of active disease, paired remission samples were collected where possible for comparative analysis.

2.2 | Sample collection and preparation

EDTA and serum separator tubes were used to collect whole blood samples. Prior to storage at -80°C , blood and urine samples were centrifuged at 3000 rpm, 4°C for 10 minutes with collection of resulting plasma, serum and supernatant urine in 0.5mLs Eppendorf tubes. When required for spectroscopic analysis, after thawing at room temperature, 30 μL aliquots were placed on IR-reflective aluminium coated FisherBrand slides and left to air dry for a minimum of 2 hours samples prior to experimentation.

2.3 | Spectral acquisition

Spectral data were attained using a Renishaw InVia Raman spectrometer in conjunction with a charge-coupled device and Leica confocal microscope (Renishaw pls UK). This system utilised a 200 mW laser diode at a wavelength of 785 nm with a grating of 1200 lines/mm. Renishaw WiRE was used to control data acquisition. The spectral range was set between 400 and 2000 cm^{-1} with a 1 cm^{-1} spectral resolution and extended grading scale. Ten individual spectral points were taken per sample over a randomly selected acquisition area of $250 \times 125 \mu\text{m}$ using $\times 20$ magnification, with 10% laser power and an exposure time of 10 seconds. Within each acquisition area, four spectral points were taken along the superior horizontal plane, four along the inferior horizontal plane and two in the middle. Before measuring each sample batch, a Renishaw silicon reference was measured to ensure signal consistence, where the resulting silicon peak signal centred at 520 cm^{-1} was consistently observed, thus indicating no spectral shift over time.

2.4 | Spectral pre-processing

Initially raw spectral data were evaluated for anomalous spectra or biased patterns through a Hotelling's T^2 vs Q residuals chart [5]. No outlier was identified; hence, no spectra were excluded from the analysis. Pre-processing was then undertaken, applying mathematical techniques to remove or reduce chemical signals that are not relevant to the analyte target property or sample discrimination in order to improve the precision of any qualitative and quantitative analysis [5]. To facilitate this and subsequent multivariate analysis all spectral data were imported into MATLAB R2014b environment (MathWorks Inc., USA). Raw spectral data were cut between 900 and 1800 cm^{-1} spectral range with application of Savitzky-Golay smoothing to correct for random noise, followed by automatic weighted least squares (AWLS) baseline correction and vector normalisation to correct for baseline distortions and physical difference between samples [16]. All pre-processed data were then mean-centred prior to model construction by partial least squares discriminant analysis (PLS-DA).

2.5 | Multivariate analysis and model validation

In order to identify any natural clustering patterns or trends in the data, principal component analysis (PCA)

was used for initial exploratory analysis through 2D PCA plot scores on principal components (PCs) 1 and 2 [17]. PCA is a multivariate technique of exploratory analysis and data reduction, in which the original variables such as spectral wavenumbers are reduced to a few numbers of PCs responsible for the majority of the original data variance. Each PC is composed of scores and loadings. The scores represent the variance on sample direction, thus being used to identify similarity/dissimilarity patterns between the samples. Whereas the loadings represent the variance on the variable direction, thus being used to identify possible spectral markers responsible for the patterns observed on the scores plot. PLS-DA was then employed for supervised classification, differentiating the spectral data according to the experimental classes of active disease (AD), disease remission (DR) and healthy control (HC). PLS-DA is an established chemometric technique based on a partial least squares (PLS) decomposition of the dataset [18]. In PLS, the dataset is decomposed into a few latent variables (LVs) responsible for maximising the covariance between the spectral data and the response information, which in this case is the disease category. Then, a straight line that divides the projected classes' spaces is delineated maximising the classes separation [19].

For this process, the data were split into training and test sets at the patient level using the Morais-Lima-Martin algorithm [20]. The training set consisted of 60% of the samples for model construction, with the optimisation step of defining the number of LVs for PLS-DA via venetian blind cross-validation to prevent overfitting. The remaining 40% of samples were used as the test set for blind predictive modelling to evaluate the classification systems performance.

Calculation of accuracy (AC), sensitivity (SENS), specificity (SPEC), G-scores and F-scores for the test set was used for model validation. Accuracy represents the total number of samples correctly classified, considering true and false negatives. The proportion of DR and AD samples correctly classified represents the sensitivity and specificity, respectively. The G-score is a metric that is used to evaluate the models performance without considering class size, whereas the F-score measures a models performance considering imbalanced data [21].

$$AC (\%) = \left(\frac{TP + TN}{TP + FP + TN + FN} \right) \times 100,$$

$$SENS (\%) = \left(\frac{TP}{TP + FN} \right) \times 100,$$

$$SPEC (\%) = \left(\frac{TN}{TN + FP} \right) \times 100,$$

$$F\text{-score} = \frac{2 \times \text{SENS} \times \text{SPEC}}{\text{SENS} + \text{SPEC}},$$

$$G\text{-score} = \sqrt{\text{SENS} \times \text{SPEC}}.$$

3 | RESULTS

3.1 | Study population

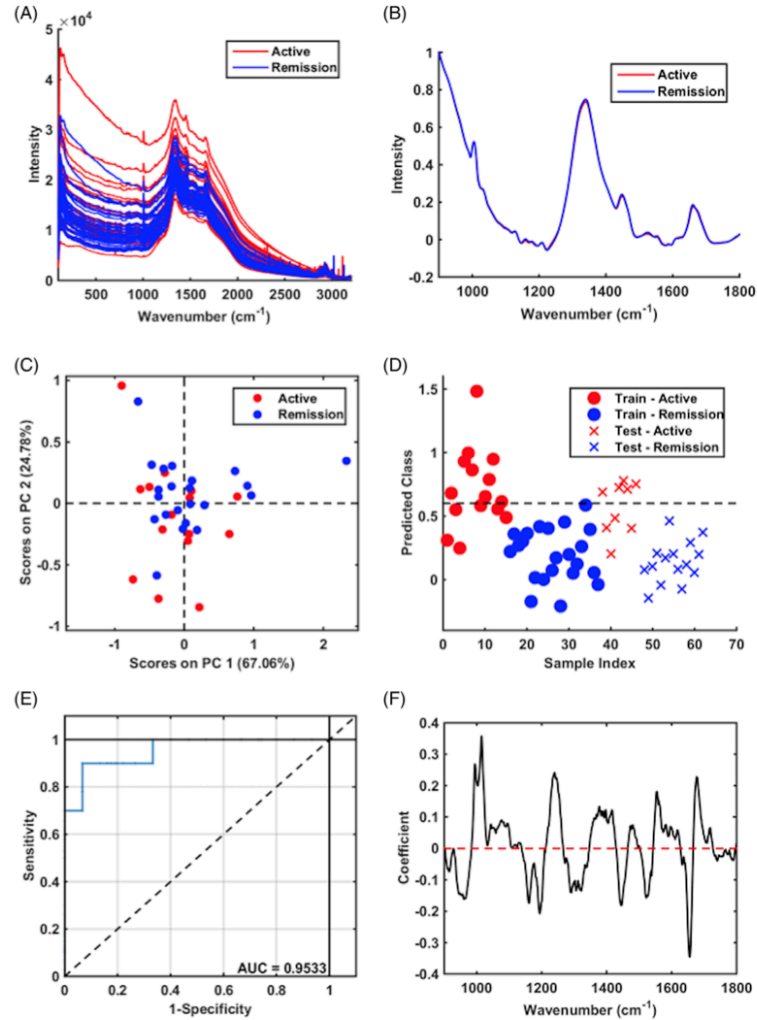
Within the 14 month study period, 73 participants were recruited; 25 with AD, 38 in DR and 10 HC. Table 1 out-

TABLE 1 Characteristics of study population at the time of enrolment

	Active disease (n = 25)	Disease remission (n = 38)
Mean age (SD)	64 + 11.9	67 + 11.9
Sex		
Male	12/25 (48%)	20/38 (53%)
Female	13/25 (52%)	18/38 (47%)
Median serum creatinine (µmol/L)	216 (347-132)	122 (174-94)
Mean eGFR (mLs/min/1.73m ²)	48 (48-8)	47 (65-29)
Newly diagnosed disease	20/25 (80%)	—
Relapsing disease	5/25 (20%)	—
ANCA serotype		
MPO	9/25 (36%)	6/38 (16%)
PR3	12/25 (48%)	14/38 (37%)
Negative	4/25 (16%)	18/38 (47%)
BVAS	16 + 9.6	—
Organ involvement		
Constitutional signs or symptoms	15/25 (60%)	—
Mucous membranes/ophthalmic	6/25 (24%)	—
Cutaneous	1/25 (4%)	—
ENT	12/25 (48%)	—
Respiratory	6/25 (24%)	—
Cardiovascular	1/25 (4%)	—
Gastrointestinal	0	—
Renal	18/25 (72%)	—
Neurological	5/25 (20%)	—
Multisystem disease	17/25 (68%)	—
Renal limited	4/25 (16%)	—
Other laboratory salient laboratory results:		
Mean haemoglobin (g/L)	100 + 28.3	—
Mean white cell count (10 ⁹ /L)	9 + 3.7	—
Mean lymphocyte count (10 ⁹ /L)	1.21 + 0.7	—
Mean neutrophil count (10 ⁹ /L)	7 + 3.6	—
Mean platelet count (10 ⁹ /L)	309 + 143.5	—
Median CRP (mg/L)	42 (64.8-4.8)	—
Median ESR (mm/hr)	42 (80.5-9)	—

Abbreviations: ANCA, anti-neutrophil cytoplasmic autoantibody; BVAS, Birmingham vasculitis activity score; CRP, C-reactive protein; eGFR, estimated glomerular filtration rate; ENT, ear nose and throat; ESR, erythrocyte sedimentary rate; MPO, myeloperoxidase; PR3, proteinase-3.

FIGURE 1 Raman spectral data for classification of active disease vs disease remission for plasma samples. A, Raw spectral data; B, Average pre-processed spectra; C, PCA scores plot; D, PLS-DA discriminant function graph; E, ROC curve for PLS-DA; F, PLS-DA coefficients for identification of spectral biomarkers



lines the baseline characteristics for the AD and DR study populations. Mean age was 66 ± 11.9 years with a predominant Caucasian ethnicity and near equal gender distribution. The AD cohort was comprised of 80% ($n = 20$) newly diagnosed cases and five ($n = 20\%$) patients with relapsing disease. Among this group, 16% ($n = 4$) had negative ANCA serology and 68% ($n = 17$) had multi-system disease with renal and sinonasal disease as the most frequently affected organ systems. Of the 32% ($n = 8$) with single organ disease, four were renal limited, three were limited to sinonasal disease and one patient had ophthalmic disease. Following successful remission-induction therapy, paired remission samples were collected

from 14 patients for comparative analysis. Inclusive of these patients, of the total number of number of remission samples included in this study 50% ($n = 26$) had detectable circulating ANCA despite clinically quiescent disease. Overall, no patients were lost to follow up and two patients in the AD cohort died, both secondary to infection.

3.2 | Spectral data and classification models

Spectral data from plasma and serum samples demonstrated equal efficacy in distinguishing active disease

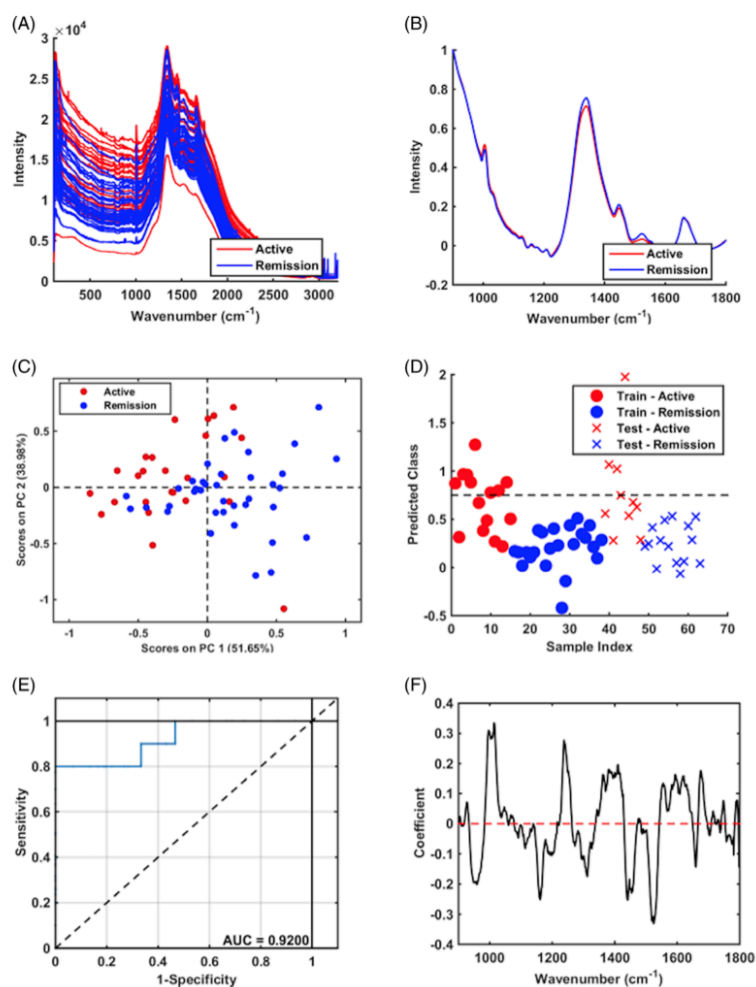


FIGURE 2 Raman spectral data for classification of active disease vs disease remission for serum samples. A, Raw spectral data; B, Average pre-processed spectra; C, PCA scores plot; D, PLS-DA discriminant function graph; E, ROC curve for PLS-DA; F, PLS-DA coefficients for identification of spectral biomarkers

from remission. Figures 1A,B and 2A,B show the raw and average pre-processed data within the 900 to 1800 cm^{-1} spectral range from plasma and serum samples, respectively. Savitzky-Golay smoothing, baseline correction and vector normalisation was performed to reduce spectral interferences, such as noise and baseline distortions, hence highlighting the analytical information used to identify key discriminatory spectrochemical signatures. Following this, initial data exploration without prior sample knowledge showed reasonable separation between AD and DR amongst both biofluids (Figures 1C and 2C). Application of discriminant analysis through partial least PLS-DA algorithm and subsequent blind predictive modelling of the remaining pre-processed data

demonstrated excellent cluster separation and outstanding ability to distinguish between to AD and DR (Figures 1D and 2D). The diagnostic ability of this classification model is evident with an F-score of 80% for plasma (specificity 93.3%, sensitivity 70%, AUC 0.95) and 80% for serum (specificity 80%, sensitivity 80%, AUC 0.92) (Tables 2 and 3). Similar findings were observed following successful remission induction therapy and comparative analysis of paired remission samples (Figures 3 and 4, Tables 4 and 5). Discriminatory analysis showed excellent ability to distinguish healthy controls from both AD and DR cohorts (AUC 1) (see Electronic Supplementary Information (ESI); Figures S1 and S3, Tables S1 and S2).

TABLE 2 Classification parameters for plasma samples in AD vs DR

AD vs DR	Accuracy (%)	Sensitivity (%)	Specificity (%)	G-Score (%)	F-Score (%)
Training (3 LVs)	88.8	86.7	90.9	88.8	88.8
Cross-validation	78.7	80	77.3	78.6	78.6
Test	81.7	70	93.3	80.8	80

Abbreviations: AD, active disease; DR, disease remission.

TABLE 3 Classification parameters for serum samples in AD vs DR

AD vs DR	Accuracy (%)	Sensitivity (%)	Specificity (%)	G-Score (%)	F-Score (%)
Training (3 LVs)	84.5	73.3	95.7	83.8	83
Cross-validation	71.3	60	82.6	70.4	69.5
Test	80	80	80	80	80

Abbreviations: AD, active disease; DR, disease remission.

Spectral data attained from urine samples are shown in the ESI with overall poor ability to differentiate between active and quiescent disease, as well as healthy controls. This may have been contributed to in part by the presence of renal vasculitis in only 75% ($n = 18$) of participants with active disease, of which only 60% ($n = 15$) were able to provide a urine sample for analysis.

3.3 | Key discriminating spectral bands

Key wavenumber variables responsible for AD and DR class separation for both plasma and serum are shown in Figures 5 and 6, respectively. This was attained following a combination of the difference-between-mean spectrum of AWLS baseline corrected pre-processed data with the PCA loadings on PC1 among the two groups. For plasma samples the key distinguishing peaks responsible for the largest between group differences were 1015 cm^{-1} (carbohydrates peak for solids), 1678 cm^{-1} (bound and free nicotinamide adenine dinucleotide) and 1446 cm^{-1} (CH_2 bending mode for proteins and lipids, CH_2 deformation). The former two were higher amongst those with AD, whereas 1146 cm^{-1} was associated with DR. Notable wavenumber variables for DR in serum were 1311 cm^{-1} (CH_3/CH_2 twisting or bending mode of lipid/collagen), 1441 cm^{-1} (CH_2 scissoring and CH_3 bending in lipids), 1524 cm^{-1} (carotenoid). The only characterising spectral peak for AD in serum was 1659 cm^{-1} (amide I vibration collagen-like proteins, amide $\text{C}=\text{O}$ stretching absorption for the α -folded polypeptide films).

4 | DISCUSSION

Currently a reliable biomarker of disease activity in AAV is lacking. This can leave treating clinicians in a

precarious position, unsure of the presence of relapsing or persistent disease when considering the need to reintroduce or escalate immunosuppression. This risks treatment related harm or unimpeded disease activity and associated ensuing organ damage in the absence of therapy. This is the first study to utilise Raman spectroscopy in vasculitis. In doing so, we confirm its potential application as a novel and highly accurate biomarker of disease activity and treatment response in multisystem AAV.

The use of Raman spectroscopy provides the ability to optically characterise the biomolecular changes associated with disease. The unique spectrochemical fingerprint generated can be considered akin to the samples metabolomic profile. A limited number of studies have successfully applied metabolomics as a potential candidate biomarker for disease activity in vasculitis. Its use in Takayasu's arteritis (TA) has been evaluated, demonstrating good ability to distinguish active from quiescent disease, with acute phase protein associated N-acetyl glycoprotein (NAG) as the key discriminating metabolite [22,23]. Al-Ani et al analysed the urinary metabolomic profile in cases of renal limited AAV, demonstrating good discriminatory capacity with hypocitraturia and raised levels of myo-inositol associating with active disease [24]. Nuclear magnetic resonance-based metabolomics has since been applied to AAV in serum with similar diagnostic potential and in line with those studies undertaken in TA, one of the metabolites characterising active disease was NAG [25]. However, despite these promising results, further research into the use and clinical application of metabolomics is often hindered by the associated costs.

Advancements in chemometric analysis positions Raman spectroscopy as a fast, cost effective and reagent-free analytical tool with minimal sample requirements

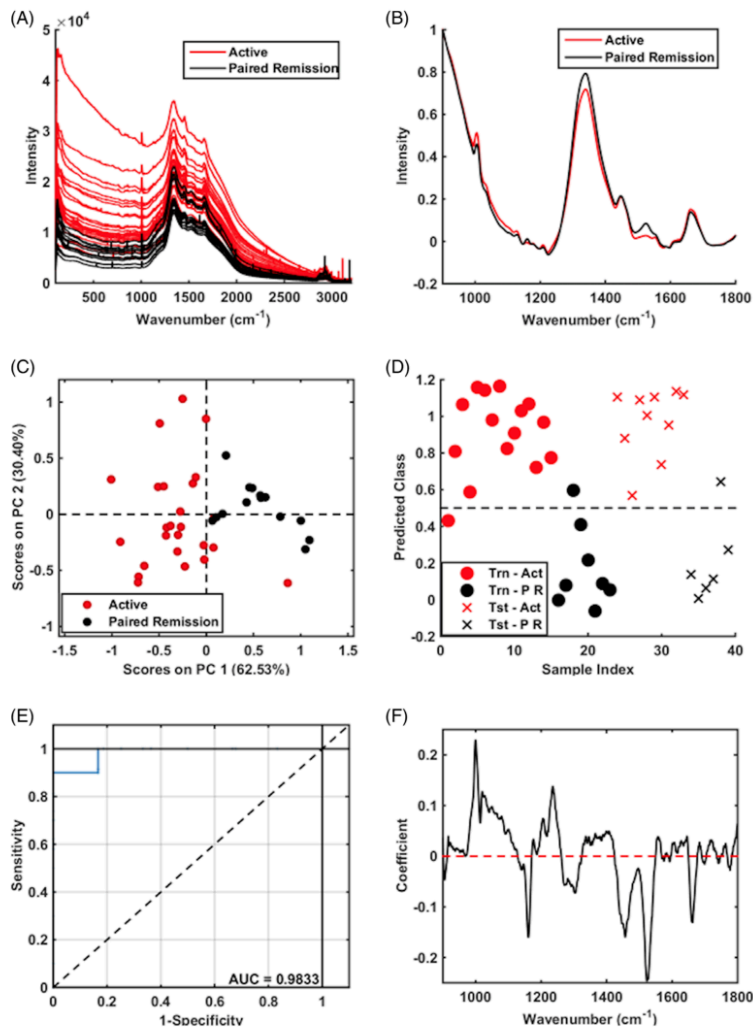


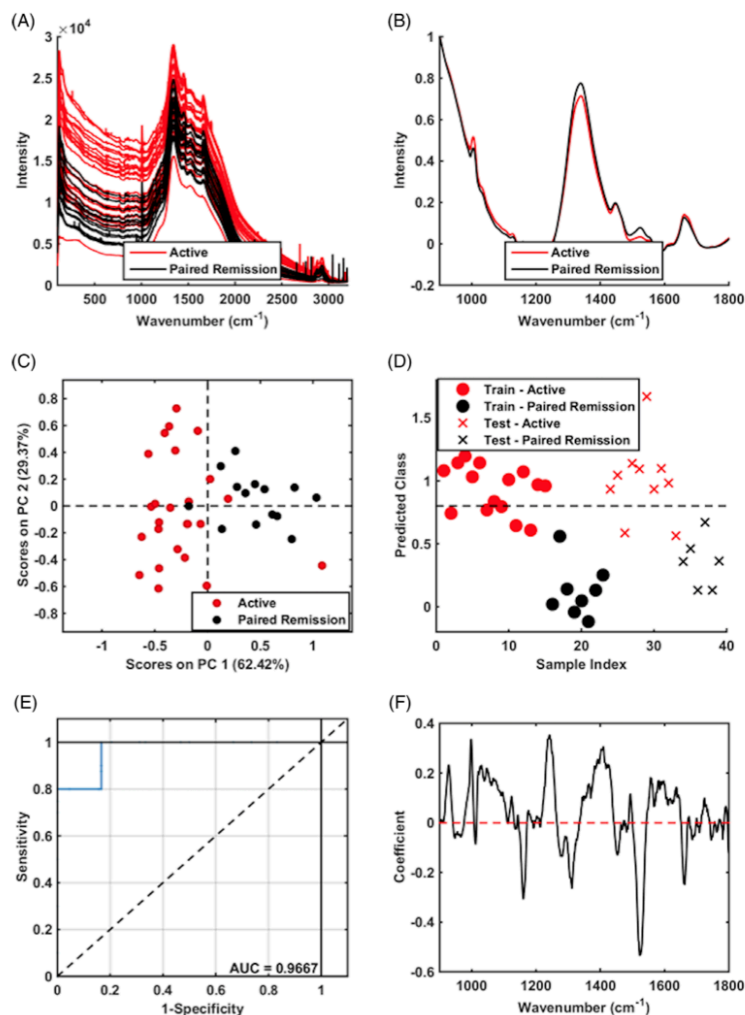
FIGURE 3 Raman spectral data for classification of active disease vs paired remission for plasma samples following successful remission induction therapy. A, Raw spectral data; B, Pre-processed spectra; C, PCA scores plot; D, PLS-DA discriminant function graph; E, ROC curve for PLS-DA; F, PLS-DA coefficients for identification of spectral biomarkers

and the potential for automated clinical laboratory use. Its use as a candidate biomarker of disease activity has been tested in other autoimmune diseases. In 2011, Caralho et al determined the spectrochemical fingerprint of rheumatoid arthritis compared to healthy controls, identifying superior diagnostic ability of Raman spectroscopy when compared to rheumatoid factor and C-reactive protein with 92% accuracy (sensitivity 88%, specificity 96%) [26].

In our study, good separation between active AAV and quiescent disease was observed on applying unsupervised learning with PCA to serum and plasma

sample spectral data. Further investigation with validation testing using PLS-DA blind predictive modelling of the remaining 40% of samples yielded excellent results, with robust models and statistically significant discrimination of the two groups. In this model the diagnostic accuracy for active disease was 81.7% for plasma samples, with 70% sensitivity for disease remission and 93.3% specificity for active disease (F-score 80%, AUC 0.95). Similar results were attained from serum samples. With only 32% of patients exhibiting single organ disease and an overall mean BVAS of 16 ± 9.6 , this suggests that our findings are independent of the organ system affected and that

FIGURE 4 Raman spectral data for classification of active disease vs paired remission for serum samples following successful remission induction therapy. A, Raw spectral data; B, Pre-processed spectra; C, PCA scores plot; D, PLS-DA discriminant function graph; E, ROC curve for PLS-DA; F, PLS-DA coefficients for identification of spectral biomarkers



this classification model is applicable to multisystem disease of varying clinical severity. Furthermore, given the absence of detectable circulating ANCA in 16% of patients with active disease and persisting seropositivity in 50% of overall remission samples, this indicates that the spectral data attained is independent of ANCA status with potential application in ANCA negative disease. The shift in the spectral profile following successful remission induction therapy, with accurate characterisation of disease remission indicates that the spectrochemical fingerprint attained can also be used to help determine treatment response.

Notable discriminating wavenumber variables for AD were 1015 and 1678 cm^{-1} from plasma and 1659 cm^{-1} from serum. The key chemical bonds and biomolecular changes represented by these included increased collagen synthesis, carbohydrate activity and nicotinamide adenine dinucleotide (NADH), which plays an essential role in cellular metabolism. These are reflective of the increased metabolic activity that would be expected in a proinflammatory state of active disease and subsequent organ damage. This is not dissimilar to the metabolomic profile characterising active AAV in the previous metabolomic study by Gupta et al with elevated levels of

TABLE 4 Classification parameters for plasma samples in AD vs PR

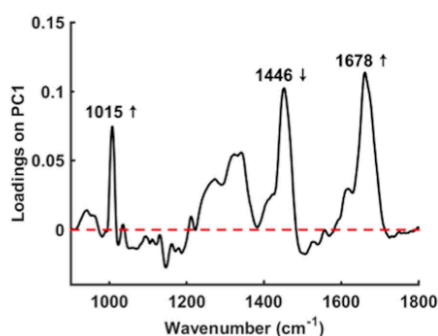
AD vs PR	Accuracy (%)	Sensitivity (%)	Specificity (%)	G-Score (%)	F-Score (%)
Training (3 LVs)	90.4	93.3	87.5	90.4	90.3
Cross-validation	87.1	86.7	87.5	87.1	87.1
Test	91.7	100	83.3	91.3	90.9

Abbreviations: AD, active disease; PR, paired remission.

TABLE 5 Classification parameters for serum samples in AD vs PR

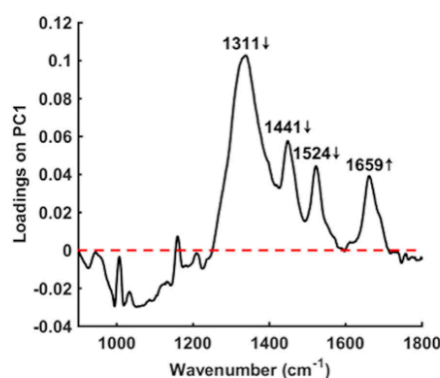
AD vs PR	Accuracy (%)	Sensitivity (%)	Specificity (%)	G-Score (%)	F-Score (%)
Training (3 LVs)	93.8	100	87.5	93.5	93.3
Cross-validation	87.1	86.7	87.5	87.1	87.1
Test	91.7	100	83.3	91.3	90.9

Abbreviations: AD, active disease; PR, paired remission.

**FIGURE 5** Main band differences for active disease (AD) vs disease remission (DR) using PCA loadings on PC1 from plasma samples: 1015 cm^{-1} (higher in AD, carbohydrates peak for solids), 1446 cm^{-1} (higher in DR, CH_2 bending mode for proteins and lipids, CH_2 deformation), 1678 cm^{-1} (higher in AD, bound and free NADH)

NAG [25]. Identification of the spectral changes directly associated with levels NADH and NAG is difficult to ascertain in the milieu of a biological sample with Raman spectroscopy alone and is beyond the scope of this current study. An approach of immunolabelling pioneered by Hodges et al using surface-enhanced Raman spectroscopy coupled with cationic gold-conjugated antibodies could be undertaken in future work to directly target these tentative biomarkers [27].

ATR-FTIR spectroscopy is a complimentary bioanalytical tool to Raman spectroscopy. When considering the two analytical modalities, both have the potential for translation into clinical practice, although Raman may have two key advantages; it is not constrained by the need for sample uniformity or potential need for

**FIGURE 6** Main band differences for active disease (AD) vs disease remission (DR) using PCA loadings on PC1 from serum samples: 1311 cm^{-1} (higher in DR, CH_3/CH_2 twisting or bending mode of lipid/collagen), 1441 cm^{-1} (higher in DR, CH_2 scissoring and CH_3 bending in lipids), 1524 cm^{-1} (higher in DR, carotenoid), 1659 cm^{-1} (higher in AD, amide I vibration collagen like proteins, amide $\text{C}=\text{O}$ stretching absorption for the α -folded polypeptide films)

dilution to avoid saturation and there is no potential risk of interference from water. Yet, fluorescence can cause interference with attainment of spectrochemical data when using Raman spectroscopy, which would not be a factor when using ATR-FTIR spectroscopy.

The findings of our study should be considered in context of its primary limitation. Although measures were taken to avoid overfitting, the risk for bias from insufficient training data remains a potential factor. Nevertheless, this should be weighed against the rigorous analytical approach taken and the previously untested

application of Raman spectroscopy as an innovative means of addressing a significant unmet clinical need amongst a rare disease cohort. Larger future study is required to ensure adequate training data.

Determining the presence of persistent or relapsing AAV remains a diagnostic challenge in the absence of a reliable functional biomarker. We have confirmed that Raman spectroscopy can be used as an accurate quantitative analytical tool to distinguish active multisystem AAV from quiescent disease using plasma and serum samples. These findings require further longitudinal study among a larger cohort with the potential for clinical application to aid patient assessment and tailored therapy.

ACKNOWLEDGMENTS

The authors would like to acknowledge the support of the Renal Department at Royal Preston Hospital Lancashire NHS Foundation Trust and the team at the NIHR Lancashire Clinical Research Facility in undertaking this study. We are also grateful for the participation and support of all of the patients in this study.

CONFLICT OF INTEREST

Francis L. Martin has a senior management role in Biocel UK Ltd, a company with a subsidiary interested in developing similar algorithms as used in this manuscript for commercial gain. He is also a significant shareholder in this company. No other conflicts of interest are declared. All authors have no conflict of interest to declare. The results presented in this paper have not been published previously in whole or part.

AUTHOR CONTRIBUTIONS

Adam D. Morris, Anthony W. Rowbottom, Ajay P. Dhaygude and Francis L. Martin were responsible for conception, design and oversight of the study. Participant recruitment, sample collection, sample processing and spectroscopic analysis were undertaken by Adam D. Morris. Francis L. Martin was lead research supervisor, facilitating and directing the project. Chemometric data analysis and interpretation were performed by Camilo L. M. Morais, Kássio M. G. Lima and Daniel L. D. Freitas. Adam D. Morris prepared the manuscript with critical review and contributions from all authors.

DATA AVAILABILITY STATEMENT

The authors declare that the data supporting the findings of this study are available within the paper and its supplementary information. The MATLAB code and instructions on how to process the data are presented in previous publications (References 5, 16, 20).

ORCID

Adam D. Morris  <https://orcid.org/0000-0001-8304-8349>

REFERENCES

- [1] R. A. Watts, A. Mahr, A. J. Mohammad, P. Gatenby, N. Basu, L. F. Flores-Suárez, *Nephrol. Dial. Transplant.* **2015**, *30*, i14.
- [2] M. A. Little, P. Nightingale, C. A. Verburgh, T. Hauser, K. De Groot, C. Savage, D. Jayne, L. Harper; on behalf of the European Vasculitis Study (EUVAS) Group., *Ann. Rheum. Dis.* **2010**, *69*(6), 1036.
- [3] J. Robson, H. Doll, R. Suppiah, O. Flossmann, L. Harper, P. Höglund, D. Jayne, A. Mahr, K. Westman, R. Luqmani, *Ann. Rheum. Dis.* **2013**, *74*(1), 177.
- [4] J. Robson, H. Doll, R. Suppiah, O. Flossmann, L. Harper, P. Höglund, D. Jayne, A. Mahr, K. Westman, R. Luqmani, *Rheumatology (United Kingdom)*. **2014**, *54*(3), 471.
- [5] C. L. M. Morais, K. M. G. Lima, M. Singh, F. L. Martin, *Nat. Protoc.* **2020**, *15*(7), 2143.
- [6] M. Chen, N. McReynolds, E. C. Campbell, M. Mazilu, J. Barbosa, K. Dholakia, S. J. Powis, *PLoS One* **2015**, *10*(5), 1.
- [7] A. Kamińska, K. Winkler, A. Kowalska, E. Witkowska, T. Szymborski, A. Janeczek, J. Waluk, *Sci. Rep.* **2017**, *7*(1), 1.
- [8] M. Häfler, I. Pence, Y. Sun, A. Kutikov, R. G. Uzzo, A. Mahadevan-Jansen, C. A. Patil, *J. Biophotonics* **2017**, *2018*, 1.
- [9] G. W. Auner, S. K. Koya, C. Huang, B. Broadbent, M. Trexler, Z. Auner, A. Elias, K. C. Mehne, M. A. Brusatori, *Cancer Metastasis Rev.* **2018**, *37*(4), 691.
- [10] J. L. Flores-Guerrero, A. Muñoz-Morales, F. Narea-Jimenez, R. Perez-Fuentes, E. Torres-Rasgado, G. Ruiz-Vivanco, N. Gonzalez-Viveros, J. Castro-Ramos, *Diagnostics* **2020**, *10*(3), 1.
- [11] X. I. C. Ci, Z. E. Z. Hao, G. E. Z. Hang, S. H. U. O. C. Hen, Y. U. E. Z. Hao, *Biomed. Opt. Express* **2018**, *9*(9), 4175.
- [12] S. Feng, L. Zhou, D. Lin, J. Zhao, Q. Guan, B. Zheng, K. Wang, H. Li, R. Chen, H. Zeng, C. Du, *Clin. Exp. Nephrol.* **2019**, *22*, 880.
- [13] J. Chi, Y. Ma, F. L. Weng, H. Thiessen-philbrook, R. Parikh, H. Du, *J. Biophotonics* **2017**, *13*, 1.
- [14] M. C. Yu, P. Rich, L. Foreman, J. Smith, M. S. Yu, A. Tanna, V. Dibbur, R. Unwin, F. W. K. Tam, *Sci. Rep.* **2017**, *7*(1), 1.
- [15] J. C. Jennette, R. J. Falk, P. A. Bacon, N. B. M. C. Cid, L. Ferrario, L. F. Flores-Suarez, W. L. Gross, L. Guillevin, E. C. Hagen, G. S. Hoffman, D. R. Jayne, C. G. M. Kallenberg, P. Lamprecht, C. A. Langford, R. A. Luqmani, A. D. Mahr, E. L. Matteson, P. A. Merkel, S. Ozen, C. D. Pusey, N. Rasmussen, A. J. Rees, D. G. I. Scott, U. Specks, J. H. Stone, K. Takahashi, R. A. Watts, *Arthritis Rheum.* **2012**, *65*(1), 1.
- [16] C. L. M. Morais, M. Paraskevaidi, L. Cui, N. J. Fullwood, M. Isabelle, K. M. G. Lima, P. L. Martin-Hirsch, H. Sreedhar, J. Trevisan, M. J. Walsh, D. Zhang, Y. G. Zhu, F. L. Martin, *Nat. Protoc.* **2019**, *14*, 1546.
- [17] R. Bro, A. K. Smilde, *Anal. Methods* **2014**, *6*(9), 2812.
- [18] D. B. Hibbert, *Pure Appl. Chem.* **2016**, *88*(4), 407.
- [19] R. G. Brereton, G. R. Lloyd, *J. Chemometr.* **2014**, *28*(4), 213.
- [20] C. L. M. Morais, M. C. D. Santos, K. M. G. Lima, F. L. Martin, *Bioinformatics* **2019**, *35*(24), 5257.
- [21] C. L. M. Morais, K. Lima, *Chemom. Intel. Lab. Syst.* **2017**, *162*, 123.
- [22] A. Guleria, D. P. Misra, A. Rawat, D. Dubey, C. L. Khetrapal, P. Bacon, R. Misra, D. Kumar, *J. Proteome Res.* **2015**, *14*(8), 3372.

- [23] A. Jain, D. Kumar, A. Guleria, D. P. Misra, A. Zanwar, S. Chaurasia, S. Kumar, U. Kumar, S. K. Mishra, R. Goel, D. Danda, R. Misra, *J. Proteome Res.* **2018**, *17*(9), 3317.
- [24] B. Al-Ani, M. Fitzpatrick, H. Al-Nuaimi, A. M. Coughlan, F. B. Hickey, C. D. Pusey, C. Savage, C. M. Benton, E. C. O'Brien, D. O'Toole, K. H. Mok, S. P. Young, M. A. Little, *Sci. Rep.* **2016**, *6*, 1.
- [25] L. Gupta, A. Jain, G. G. Ekbote, R. Mishra, *Int. J. Rheum. Dis.* **2019**, *22*(S3), 40.
- [26] C. S. Carvalho, A. A. Martin, A. M. E. Santo, L. E. C. Andrade, M. M. Pinheiro, M. A. G. Cardoso, L. Raniero, *Theor. Chem. Acc.* **2011**, *130*(4–6), 1211.
- [27] M. D. Hodges, J. G. Kelly, A. J. Bentley, S. Fogarty, I. I. Patel, F. L. Martin, N. J. Fullwood, *ACS Nano* **2011**, *5*(12), 9535.

SUPPORTING INFORMATION

Additional supporting information may be found online in the Supporting Information section at the end of this article.

How to cite this article: Morris AD, Morais CLM, Lima KMG, et al. A comparative analysis of different biofluids using Raman spectroscopy to determine disease activity in ANCA-associated vasculitis. *J. Biophotonics*. 2021; e202000426. <https://doi.org/10.1002/jbio.202000426>

Article

Automated Computational Detection of Disease Activity in ANCA-Associated Glomerulonephritis Using Raman Spectroscopy: A Pilot Study

 Adam D. Morris ^{1,*}, Daniel L. D. Freitas ², Kássio M. G. Lima ², Lauren Floyd ¹, Mark E. Brady ¹, Ajay P. Dhaygude ¹, Anthony W. Rowbottom ^{3,4} and Francis L. Martin ^{5,*}

- ¹ Renal Medicine, Royal Preston Hospital, Preston PR2 9HT, UK; lauren.floyd@lthtr.nhs.uk (L.F.); mark.brady@lthtr.nhs.uk (M.E.B.); ajay.dhaygude@lthtr.nhs.uk (A.P.D.)
- ² Institute of Chemistry, Biological Chemistry and Chemometrics, Federal University of Rio Grande do Norte, Natal 59072-970, Brazil; daniellucas77@hotmail.com (D.L.D.F.); kassiolima@gmail.com (K.M.G.L.)
- ³ Department of Immunology, Royal Preston Hospital, Preston PR2 9HT, UK; anthony.rowbottom@lthtr.nhs.uk
- ⁴ School of Medicine, University of Central Lancashire, Preston PR1 2HE, UK
- ⁵ Biocel Ltd., Hull HU10 7TS, UK
- * Correspondence: adam.morris@lthtr.nhs.uk (A.D.M.); flm13@biocel.uk (F.L.M.); Tel.: +44-01772-52-3748 (A.D.M.)



Citation: Morris, A.D.; Freitas, D.L.D.; Lima, K.M.G.; Floyd, L.; Brady, M.E.; Dhaygude, A.P.; Rowbottom, A.W.; Martin, F.L. Automated Computational Detection of Disease Activity in ANCA-Associated Glomerulonephritis Using Raman Spectroscopy: A Pilot Study. *Molecules* **2022**, *27*, 2312. <https://doi.org/10.3390/molecules27072312>

Academic Editors: Ivo Piantanida and Thomas Mavroumoustakos

Received: 14 February 2022

Accepted: 29 March 2022

Published: 2 April 2022

Publisher's Note: MDPI stays neutral with regard to jurisdictional claims in published maps and institutional affiliations.



Copyright: © 2022 by the authors. Licensee MDPI, Basel, Switzerland. This article is an open access article distributed under the terms and conditions of the Creative Commons Attribution (CC BY) license (<https://creativecommons.org/licenses/by/4.0/>).

Abstract: Biospectroscopy offers the ability to simultaneously identify key biochemical changes in tissue associated with a given pathological state to facilitate biomarker extraction and automated detection of key lesions. Herein, we evaluated the application of machine learning in conjunction with Raman spectroscopy as an innovative low-cost technique for the automated computational detection of disease activity in anti-neutrophil cytoplasmic autoantibody (ANCA)-associated glomerulonephritis (AAGN). Consecutive patients with active AAGN and those in disease remission were recruited from a single UK centre. In those with active disease, renal biopsy samples were collected together with a paired urine sample. Urine samples were collected immediately prior to biopsy. Amongst those in remission at the time of recruitment, archived renal tissue samples representative of biopsies taken during an active disease period were obtained. In total, twenty-eight tissue samples were included in the analysis. Following supervised classification according to recorded histological data, spectral data from unstained tissue samples were able to discriminate disease activity with a high degree of accuracy on blind predictive modelling: F-score 95% for >25% interstitial fibrosis and tubular atrophy (sensitivity 100%, specificity 90%, area under ROC 0.98), 100% for necrotising glomerular lesions (sensitivity 100%, specificity 100%, area under ROC 1) and 100% for interstitial infiltrate (sensitivity 100%, specificity 100%, area under ROC 0.97). Corresponding spectrochemical changes in paired urine samples were limited. Future larger study is required, inclusive of assigned variables according to novel non-invasive biomarkers as well as the application of forward feature extraction algorithms to predict clinical outcomes based on spectral features.

Keywords: ANCA; ANCA-associated; vasculitis; glomerulonephritis; Raman spectroscopy

1. Introduction

Anti-neutrophil cytoplasmic autoantibody (ANCA)-associated vasculitis (AAV) is a complex auto-immune disease that typically causes multi-organ and life-threatening disease. It results from the necrotising inflammation of small- and medium-sized blood vessels which characteristically lack any significant immune complex deposits on histopathology. Renal involvement with ANCA-associated glomerulonephritis (AAGN) tends to present with rapidly progressive disease and often denotes a higher mortality risk compared to patients without renal disease, particularly amongst those with dialysis dependence [1–3]. Since its initial description in the early 1980s, patient outcomes have improved in parallel

with advancing treatment strategies, with a substantial proportion of patients receiving remission-induction therapy and achieving dialysis independence by four months [4,5]. However, AAV is often characterised by a relapsing disease course and determining if changes in renal function or urinalysis are attributable to active disease without a repeat biopsy or a reliable peripheral biomarker presents a diagnostic challenge, particularly in renal limited disease with no other clinical cues.

Renal biopsy remains the gold standard for the diagnosis of AAGN, but its serial use for disease monitoring is restricted by the inherent procedural risks and resource requirements. The Berden classification system categorises histopathological findings in AAGN into four key subgroups: focal disease ($\geq 50\%$ normal glomeruli), crescentic disease ($\geq 50\%$ cellular crescents), sclerotic disease ($\geq 50\%$ globally sclerotic glomeruli) and mixed disease with no predominant lesion [6]. Since its initial description in 2010, it has been validated by numerous studies and has been shown to be of predictive clinical value, with poorer renal function amongst those with a higher degree of sclerosis and more favourable outcomes in those with a focal class of disease [6–11]. Although previously reported outcomes varied amongst crescentic and mixed class disease, a recent meta-analysis found no significant difference in end stage kidney disease between the two groups [11]. Emerging from these studies was the importance of the percentage of normal glomeruli as a significant predictor of renal survival, as well as the degree of tubulointerstitial disease [7–10]. T-cell mediated tubulitis and, as expected, a higher degree of interstitial fibrosis and tubular atrophy (IFTA) are associated with poorer renal outcomes, with the degree of IFTA increasing in parallel with the degree of glomerular scarring [8–10]. These features have since been incorporated into two predictive models: the Mayo chronicity score and the ANCA renal risk score [3,12]. The former accounts for glomerulosclerosis, IFTA, and atherosclerosis with a lower likelihood of renal recovery associated with a higher score [3]. The ANCA renal risk score accurately predicts the risk of end stage renal disease by using a graded score for renal function at presentation, the degree of IFTA and the proportion of normal glomeruli [11,12].

The ability to non-invasively determine the prevailing histopathological lesion in real time would prove to be an invaluable tool to aid disease monitoring in renal limited AAV. Furthermore, it could facilitate individualised therapy, helping to identify those least likely to benefit from continued or intensified therapy in order to mitigate any potential treatment related harm. This study aims to differentiate spectral data obtained from renal tissue according to key histological lesions in cases of AAGN to evaluate the role of Raman spectroscopy as a method for automated computational detection of disease activity. Additionally, subsequent comparative analysis of the spectral data from paired urine samples at the time of renal biopsy will explore the role of biospectroscopy as a non-invasive surrogate marker of histological activity in renal vasculitis, in effect providing a liquid biopsy.

2. Materials and Methods

2.1. Patients & Ethics

From February to August 2019, consecutive patients with active AAGN and those in disease remission were recruited. For those in disease remission at the time of recruitment, where available, archived renal tissue samples taken at the time of initial diagnosis and held by the tissue bank at Royal Preston Hospital were obtained. For those patients with active disease at the time of recruitment, renal tissue samples along with paired urine samples taken immediately prior to renal biopsy were collected. The definition of AAV as outlined by the 2012 Chapel Hill Consensus Conference was used. Patients who did not meet this criterion, who were aged < 18 years, unable to provide consent, or exhibited dual positivity with anti-glomerular basement membrane disease were excluded. All participants were registered with the Department of Renal Medicine regional vasculitis service at Lancashire Hospitals NHS Foundation Trust, Preston, UK. Informed written consent was obtained prior to enrollment in accordance with study approval from the Health Research Authority, Cambridge South Research Ethics Committee (REC reference

18/EE/0194) and the Research and Development team in the Centre for Health Research and Innovation at Lancashire Teaching Hospitals NHS Foundation Trust.

Baseline clinical assessment comprised of participant demographics, histological evaluation of renal biopsies by a renal pathologist, and salient laboratory results at the time of biopsy including ANCA serotype, serum creatinine and urine protein creatinine ratio. Recorded histological data included the assigned Berden classification (focal: $\geq 50\%$ normal glomeruli, crescentic: $\geq 50\%$ cellular crescents, sclerotic: $\geq 50\%$ globally sclerotic glomeruli, and mixed: no predominant lesion) [6], the percentage of normal glomeruli (N0 > 25%, N1 10–25%, N2 < 10%), the severity of interstitial fibrosis and tubular atrophy (IFTA) (T1 > 25%, T0 \leq 25%), and the presence of interstitial infiltrate, necrotising glomerular lesions, extra-glomeruli arteritis, and vessel wall necrosis. The percentage of normal glomeruli and degree of IFTA was assessed according to the grading scale applied by Brix et al., in the ANCA renal risk score [12]. Urine samples were sent for microscopy and culture to determine the presence of bacteriuria and its potential impact as a confounding factor on spectroscopic analysis.

2.2. Sample Collection & Preparation

Following their initial acquisition and departmental assessment, formalin-fixed paraffin-embedded tissue blocks were retrieved from the tissue bank at Royal Preston Hospital. To ensure close correlation between histopathology reports and spectroscopic measurements, contiguous sections of 10 μm thickness were used from each tissue block. After sections had been cut and placed on IR-reflective aluminium coated FisherBrand™ (Loughborough, UK) slides, all samples were deparaffinised according to local protocols using xylene and ethanol in order to avoid any potential impact on the spectral data obtained.

Urine samples were collected in reagent-free, sterile containers and centrifuged at 3000 rpm, 4 °C for 10 min. The resulting supernatant urine was collected in 0.5 mL Eppendorf tubes and stored at -80 °C. When required for experimentation, samples were thawed at room temperature, after which 30 μL aliquots were placed on IR-reflective aluminium-coated FisherBrand™ slides and left to air dry for a minimum of 2 h prior to spectroscopic analysis.

2.3. Spectral Acquisition

Spectral data was obtained using a Renishaw InVia Raman spectrometer in conjunction with a charge-coupled device and Leica confocal microscope (Renishaw pls UK). This system utilised a 200 mW laser diode at a wavelength of 785 nm with a grating of 1200 lines/mm. Renishaw WiRE™ was used to control data acquisition. The spectral range was set between 400–2000 cm^{-1} with a 1 cm^{-1} spectral resolution. For tissue mapping, spectral data was obtained over the entirety of a 1000 \times 500 μm^2 acquisition area, using 5 \times magnification, 100% laser power, exposure time of 0.1 s with 5 \times 5 steps in high confocality and spectral centre of 1300 cm^{-1} . Three select regions of interest where the highest number of glomeruli were visible within the acquisition area were analysed from each sample. For urine samples, ten individual spectral points were taken per sample over an acquisition area of 250 \times 125 μm^2 using 20 \times magnification, 10% laser power, and an exposure time of 10 s, with an extended grading scale. Within each acquisition area, four spectral points were taken along the superior horizontal plane, four along the inferior horizontal plane, and two in the middle. For both tissue and urine samples, one representative mean spectrum was subsequently generated per sample for later use in the analysis.

2.4. Spectral Pre-Processing

Three-dimensional (3D) Raman mapping images were uploaded into MATLAB R2014b environment (MathWorks Inc., Natick, MA, USA) and unfolded into two-dimensional (2D) structures containing n rows (number of spectra) and m columns (number of wavenumbers). Initially raw spectral data obtained from both tissue and urine samples were evaluated

for anomalous spectra or biased patterns. Pre-processing was then undertaken, applying mathematical techniques to remove or reduce chemical signals that are not relevant to the analyte target property or sample discrimination in order to improve the precision of any qualitative and quantitative analysis [13]. The raw data obtained for both tissue and urine samples were then submitted to the same procedures; spectral data was cut in the region of 800–1800 cm^{-1} with application of Savitzky–Golay (SG) 2nd order derivative (51 window points, 2nd order polynomial) and vector normalization to correct for random noise, baseline distortions and physical difference between samples [14]. All resulting pre-processed data was mean-centred prior to model construction for discriminant analysis. All models were trained and tested with pre-processed data only.

2.5. Multivariate Analysis

In order to identify any natural clustering patterns or trends in the pre-processed data, principal component analysis (PCA) is a multivariate technique that was used for initial exploratory analysis and data reduction. In this process, the initial spectral wavenumber variables are reduced to a few principal components (PC) responsible for the majority of the original data variance. Each PC is composed of scores and loadings. The scores represent the variance on sample direction, therefore being used to identify similarity/dissimilarity patterns between the samples, whereas the loadings represent the variance on the variable direction, therefore being used to identify possible spectral markers responsible for the patterns observed and any potential class separation on the scores plot.

In each model, the spectral data from both tissue and urine samples was segregated according to the presence of recorded histological data to generate the experimental classes of the assigned Berden classification (focal, crescentic, sclerotic, and mixed) [6], the percentage of normal glomeruli (N0 > 25%, N1 10–25%, N2 < 10%), the severity of IFTA (T1 > 25%, T0 ≤ 25%) and the presence of interstitial infiltrate, necrotising glomerular lesions, extra-glomeruli arteritis, and vessel wall necrosis. A lower proportion of normal glomeruli indicates greater disease burden with their composition guiding the degree of acute disease vs. chronicity. A higher burden of IFTA and sclerosed glomeruli represent chronic damage, whereas the remaining lesions described are indicative of active disease. An experimental class according to ANCA seropositivity and, in positive cases, ANCA serotype were also generated. For each, the total data obtained were used to build the models, without dividing samples by selection methods due to the limited sample availability in certain classes. The models were evaluated using the Venetian blinds cross-validation method. Analysis of the spectral mean was used as the test set for blind predictive modelling. These test samples are independent from training data as they are not used in the model training process and are considered new data to the model. The overall performance of each discriminant analysis algorithm was then compared.

2.6. Chemometric Models

The discriminant analysis algorithms of principal component analysis linear discriminant analysis (PCA-LDA), partial least squares discriminant analysis (PLS-DA), support vector machines (SVM), and genetic algorithm linear discriminant analysis (GA-LDA) were subsequently applied to the pre-processed data for supervised classification. Models were constructed using the PLS Toolbox and Classification Toolbox graphical user interface of the Milano Chemometrics group [15].

PLS-DA is a well-established chemometric technique for supervised classification. For this process, the dataset was broken down into a few latent variables (LVs) responsible for maximizing the covariance between the spectral data and the response information, which in this case is the histological or serological category. The number of latent variables was determined by the leave-one-out type cross-validation to prevent overfitting. The key distinguishing spectral peaks were then identified using the PLS-DA coefficient.

While PCA and PLS perform a reduction in the number of original variables generating another set of variables, the genetic algorithm (GA) selects the most important variables

based on a selection, recombination, and mutation of a set of the original variables. Thus, its main objective is to reduce the number of variables, taking advantage of not changing the type of variable and original information according to an adjustment function. The GA routine was carried out during 100 generations with 200 chromosomes each. Mutation and crossover probabilities were adjusted to 10% and 60% respectively. The best solution set for this algorithm is based on the fitness value. The adjustment function is calculated as the inverse of the cost function G , which can be defined as follows:

$$G = \frac{1}{N_V} \sum_{n=1}^{N_V} g_n \quad (1)$$

where N_V is the number of validation samples and g_n is defined as follows:

$$g_n = \frac{r^2(x_{nI(n)}, m_{I(n)})}{\min_{I(m) \neq I(n)} r^2(x_{nI(m)}, m_{I(m)})} \quad (2)$$

where the numerator is the squared Mahalanobis distance between object x_n of class index $I(n)$ and the sample mean $m_{I(n)}$ of its true class; and the denominator is the squared Mahalanobis distance between object $x(n)$ and the centre of the closest wrong class.

The classifiers used here were LDA and SVM. LDA is based on the Mahalanobis distance between samples and considers that all classes have a similar variance structure, building a model based on pooled covariance matrix. The input data used for LDA are scores obtained via PCA. The LDA classifier, non-Bayesian form, can be obtained by the following equation for a sample i in a given class k :

$$L_{ik} = (x_i - \bar{x}_k)^T C_{\text{pooled}}^{-1} (x_i - \bar{x}_k) \quad (3)$$

where x_i is a vector with variables for sample i ; \bar{x}_k is the mean of class k ; and C_{pooled} is the pooled covariance matrix between the classes.

SVM is a machine learning technique that uses the kernel transformation [16]. This projects data in a non-linear fashion into a feature dimension to provide the radial basis function (RBF) and classify samples according to a linear threshold. This has the advantage of being able to adjust for different data distributions to provide a more powerful discriminant analysis but may carry a higher risk of overfitting. The RBF is calculated as follows:

$$k(x_i, z_j) = \exp(-\gamma \|x_i - z_j\|^2) \quad (4)$$

where x_i and z_j are sample measurements vectors and γ is a tuning parameter that controls the RBF width. In the RBF function, the γ parameter was set to 1. The SVM classification is obtained by the following equation:

$$f(x) = \text{sign} \left(\sum_{i=1}^{N_{SV}} \alpha_i y_i k(x_i, z_j) + b \right) \quad (5)$$

where N_{SV} is the number of support vectors; α_i is the Lagrange multiplier; y_i is the class membership, ranging from -1 to $+1$; $k(x_i, z_j)$ is the kernel function and b is the bias parameter. The parameters used were obtained through an internal validation dataset.

2.7. Model Validation

The calculation of accuracy, sensitivity, specificity, F-scores, and G-scores were calculated for the test set for model validation. Accuracy represents the total number of samples correctly classified, considering true and false negatives. The sensitivity represents the proportion of positive samples correctly classified and the specificity represents the proportion of negative samples correctly classified. The F-score measures the models performance

considering imbalanced data, whereas the G-score is a metric that is used to evaluate the models performance independent of class size [17]. The statistical parameters presented can be calculated as follows:

$$\text{Accuracy (AC)} = \left(\frac{\text{TP} + \text{TN}}{\text{TP} + \text{FP} + \text{TN} + \text{FN}} \right) \times 100 \quad (6)$$

$$\text{Sensitivity (SENS)} = \left(\frac{\text{TP}}{\text{TP} + \text{FN}} \right) \times 100 \quad (7)$$

$$\text{Specificity (SPEC)} = \left(\frac{\text{TN}}{\text{TN} + \text{FP}} \right) \times 100 \quad (8)$$

$$\text{F-Score (Fs)} = \left(\frac{2 \times \text{SENS} \times \text{SPEC}}{\text{SENS} + \text{SPEC}} \right) \times 100 \quad (9)$$

$$\text{G-Score (Gs)} = \left(\sqrt{\text{SENS} \times \text{SPEC}} \right) \times 100 \quad (10)$$

where FN stands for false negative, FP for false positive, TP for true positive, TN for true negative, AC for accuracy, SENS for sensitivity, SPEC for specificity, Fs for F-score, and Gs for G-Score. Herein, although both were derived from the same experiment, the test samples are independent from the training samples. The validation performance depicted here are ideal for small datasets in order to have a good approximation of the real blind performance [13]. For further model validation, it would be necessary to realise a second experiment with completely new samples in order to assess the blind model performance.

3. Results

3.1. Study Population

Over the 6-month study period 28 patients were recruited for the present study; 11 with new presentation AAGN and 17 currently in disease remission. One patient was excluded due to the development of dual positivity with anti-glomerular basement autoantibodies. Table 1 outlines the characteristics of the overall study population. Recently processed and archived renal tissue samples taken at the time of active disease were obtained for all remaining 27 participants, with paired urine samples prior to biopsy in all ten cases of newly presenting AAGN.

Amongst those participants with a paired urine sample at the time of renal biopsy ($n = 10$), mean age was 63 ± 7.6 with 80% ($n = 8$) female predominance, median serum creatinine of $282 \mu\text{mol/L}$ (IQR 447–201) and 90% ($n = 9$) seropositivity; four with anti-MPO and five with anti-PR3 associated disease. The mean number of glomeruli per biopsy sample was 19 ± 9 , with a distribution of disease of 50% ($n = 5$) focal, 40% ($n = 4$) mixed and 10% ($n = 1$) crescentic according to the Berden classification system [6]. The proportion of samples with >25% normal glomeruli (grade N0) was 70% ($n = 7$) and 30% ($n = 3$) exhibited <10% (grade N2) normal glomeruli. A similar distribution for IFTA was seen; 70% ($n = 7$) $\leq 25\%$ (grade T0) and 30% ($n = 3$) >25% (grade T1). The observed frequency of necrotising glomerular lesions and interstitial infiltrate were 30% ($n = 3$). For extra-glomerular arteritis and vessel wall necrosis 20% ($n = 2$) were affected. The median uPCR and urine white cell count was 89 mg/mmol (IQR 258–63) and $31 \times 10^9/\text{L}$ (IQR 34–27) respectively. None of the collected urine samples displayed any bacterial growth.

Table 1. Characteristics of study population.

	AAGN (n = 27)
Mean Age (SD)	63 ± 10
Sex	
Male	15/27 (55.6%)
Female	12/27 (44.4%)
Median serum creatinine at biopsy (µmol/L)	215 (338–164)
Median eGFR at biopsy (mls/min/1.73 m²)	22 (33–12)
ANCA serotype at biopsy	
MPO	12/27 (44.4%)
PR3	12/27 (44.4%)
Negative	3/27 (11.1%)
Mean number of glomeruli per biopsy sample	
Berden classification	20 ± 9
Focal	15/27 (55.6%)
Crescentic	3/27 (11.1%)
Sclerosed	0
Mixed	9/27 (33.3%)
Normal glomeruli	
N0 (>25%)	21/27 (77.8%)
N1 (10–25%)	2/27 (7.4%)
N2 (<10%)	4/27 (14.8%)
IFTA	
T0 (≤25%)	20/27 (74.1%)
T1 (>25%)	7/27 (25.9%)
Necrotising glomerular lesions	16/27 (59.3%)
Interstitial infiltrate	10/27 (37%)
Extra-glomerular arteritis	5/27 (18.5%)
Vessel wall necrosis	4/27 (14.8%)

ANCA, anti-neutrophil cytoplasmic autoantibody; MPO, myeloperoxidase; PR3, proteinase-3; IFTA, interstitial fibrosis & tubular atrophy.

3.2. Spectral Data & Classification Models: All Renal Tissue Samples

For the three spectra obtained from each sample image, one representative mean spectrum was generated per sample. As such, there are a total of 81 spectra for the 27-sample cohort and consequently 27 representative mean spectra. The total raw spectra, total pre-processed spectra and average pre-processed spectral data for the overall study population are shown in Figure 1A, B and C, respectively. For the construction of supervised classification models, both the total raw spectra and pre-processed spectra were used as training data with known categories according to each experimental class. Following cross-validation using the leave-one-out approach, the mean spectral data was applied as the test set for blind predictive modelling to validate the classification systems performance. In this construct, the cross-validation data is the most significant result that should be considered, representing the model's ability to correctly predict new data based on the existing knowledge obtained from any training data. This process helps to mitigate any potential overfitting. Due to the unbalanced sample size distribution amongst all four Berden classes, comparative analysis was only feasible between focal (n = 15) and mixed (n = 9) disease. Similarly, evaluation of normal glomeruli was undertaken as a sample distribution of those with >25% normal glomeruli (group N0) (n = 21) vs. those exhibiting <25% normal glomeruli (groups N1 & N2) (n = 6).

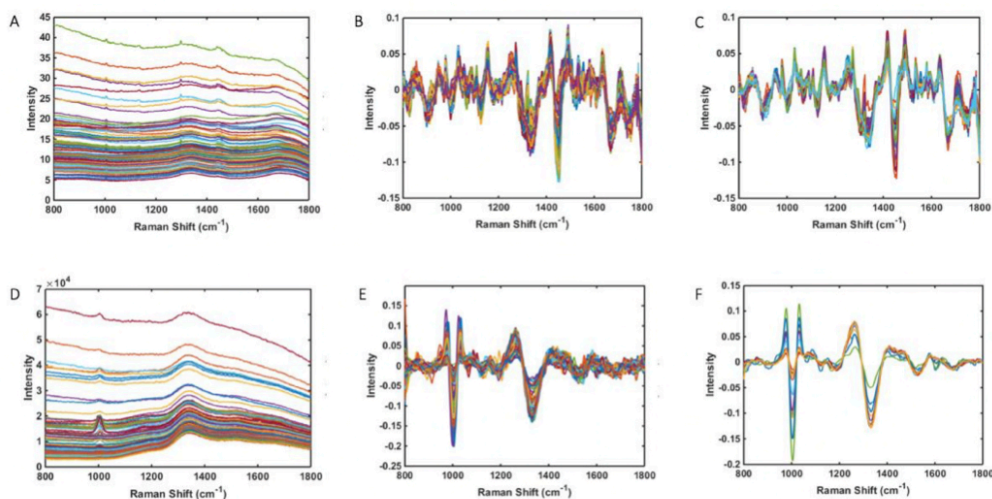


Figure 1. Raman spectral data—(A) Total raw spectra for all tissue samples (n = 81) (B) Total pre-processed spectra for all tissue samples (n = 81) (C) Average pre-processed spectra for all tissue samples (n = 27) (D) Total raw spectra for paired urine samples (n = 100) (E) Pre-processed spectra for paired urine samples (n = 100) (F) Average pre-processed spectra paired urine tissue samples (n = 10).

PLS-DA discriminant function graphs and the classification model performance according to histological data for all renal biopsy samples are shown in Figure 2 and Table 2, respectively. The mean Raman spectral data for each histological group is shown in Figure 3. The spectral profiles for necrotising glomerular lesions, interstitial infiltrate, and IFTA yielded the most accurate results. This is evident with an F-score 95% for >25% interstitial fibrosis and tubular atrophy (sensitivity 100%, specificity 90%, area under ROC 0.98), 100% for necrotising glomerular lesions (sensitivity 100%, specificity 100%, area under ROC 1), and 100% for interstitial infiltrate (sensitivity 100%, specificity 100%, area under ROC 0.97). The predictive performance in distinguishing focal from mixed disease, >25% normal glomeruli, and the presence of vessel wall necrosis was limited with a sensitivity of <60% in each model. Similarly, the discriminant model for ANCA was not significant with a sensitivity of only 56% in seropositive cases.

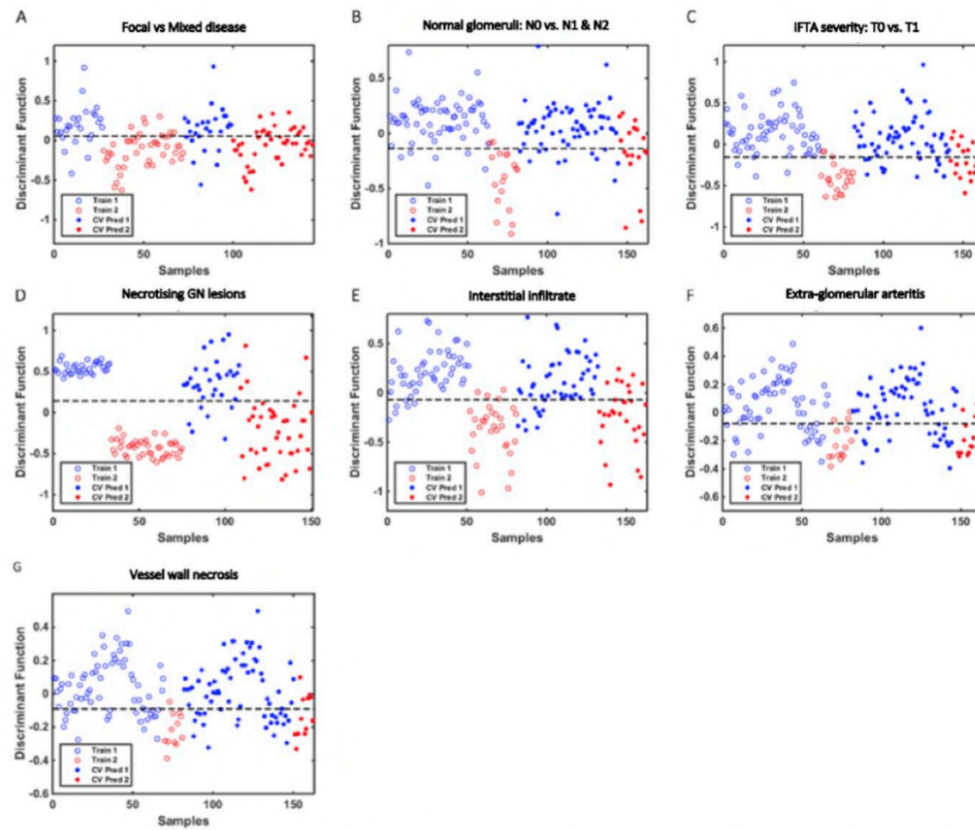


Figure 2. PLS-DA discriminant function graphs for the classification of histological data using spectral data from all tissue samples with corresponding receiver operating characteristic curve data. Train 1 and Train 2 represent training sample data for each histological group. CV Pred 1 and CV Pred 2 represent test sample data for each histological group analysed by the cross-validation (CV) prediction process: (A) Mixed vs. focal disease (train 1 & CV Pred 1 vs. train 2 & CV Pred 2) area under ROC 0.85 (B) Normal glomeruli N0 vs. N1 & N2 (train 1 & CV Pred 1 vs. train 2 & CV Pred 2) area under ROC 0.96 (C) Interstitial fibrosis and tubular atrophy (IFTA) severity T0 vs. T1 (train 1 & CV Pred 1 vs. train 2 & CV Pred 2) area under ROC 0.98 (D) Necrotising glomerular (GN) lesions absent vs. present (train 1 & CV Pred 1 vs. train 2 & CV Pred 2) area under ROC 1 (E) Interstitial infiltrate absent vs. present (train 1 & CV Pred 1 vs. train 2 & CV Pred 2) area under ROC 0.97 (F) Extraglomerular arteritis absent vs. present (train 1 & CV Pred 1 vs. train 2 & CV Pred 2) area under ROC 0.89 (G) Vessel wall necrosis absent vs. present (train 1 & CV Pred 1 vs. train 2 & CV Pred 2) area under ROC 0.92.

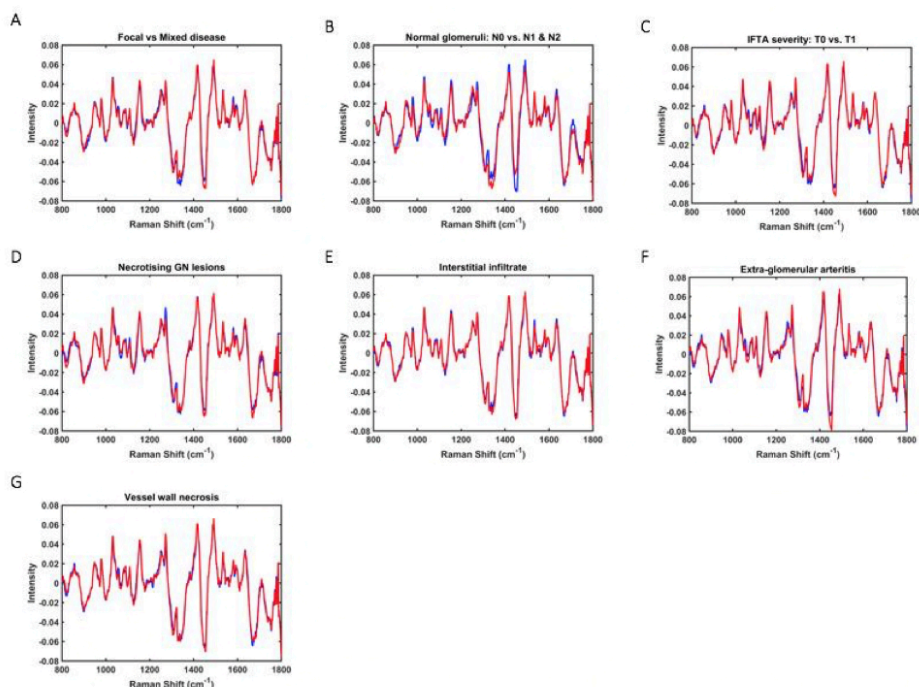


Figure 3. Mean Raman spectral data for each histological group—(A) focal vs. mixed disease, (B) proportional of normal glomeruli, (C) severity of interstitial fibrosis and tubular atrophy (IFTA), (D) presence of necrotising glomerular (GN) lesions, (E) presence of interstitial infiltrate, (F) presence of extra-glomerular arteritis, (G) presence of vessel wall necrosis.

3.3. Spectral Data and Classification Models: Comparative Results for Tissue & Paired Urine Samples

Based on the findings observed in the overall cohort, a comparative subgroup analysis was undertaken amongst those with a paired urine sample at the time of renal biopsy ($n = 10$). This sought to determine if equally good discrimination for necrotising glomerular lesions, interstitial infiltrate, and $>25\%$ IFTA could be demonstrated in both biosamples. For the three spectra obtained from each tissue sample, one representative mean spectrum was generated per sample, resulting in a total of 30 spectra and 10 representative mean spectra for the subgroup. Ten individual spectral points were obtained from each urine sample, generating a total of 100 spectra and 10 representative average spectra. Findings are shown in Table 3 and exhibit limited accuracy in distinguishing the presence of each category in urine on blind predictive modelling with a sensitivity $< 60\%$ and F-score $< 65\%$ for each. Subgroup model data for normal glomeruli, Berden classification, vessel wall necrosis, and extra-glomerular arteritis are not presented in view of their suboptimal performance in tissue analysis amongst the overall cohort.

Table 2. Classification model performance according to histological data for renal biopsy samples (n = 27).

Presence of Histological Features as an Experimental Class	Best Discriminate Model	Spectral Data	Accuracy (%)	Sensitivity (%)	Specificity (%)	F-Score (%)	G-Score (%)
Berden classification: Focal vs. Mixed	PLS-DA (3 LVs))	Training: TPS	81	82	78	80	80
		CV: TPS	75	80	67	73	73
		Test: MPS	69	69	70	69	69
Normal Glomeruli: N0 vs. N1&N2	PLS-DA (3 LVs))	Training: TPS	90	89	90	89	89
		CV: TPS	77	56	83	67	68
		Test: MPS	93	83	95	89	89
IFTA: T0 vs. T1	PLS-DA (3 LVs))	Training: TPS	91	86	93	89	89
		CV: TPS	78	67	82	74	74
		Test: MPS	93	100	90	95	95
Necrotising glomerular lesions	PLS-DA (8 LVs))	Training: TPS	100	100	100	100	100
		CV: TPS	87	88	85	86	86
		Test: MPS	100	100	100	100	100
Interstitial Infiltrate	PLS-DA (3 LVs))	Training: TPS	88	87	88	87	87
		CV: TPS	80	73	84	78	78
		Test: MPS	100	100	100	100	100
Extra-glomerular arteritis	PLS-DA (2 LVs))	Training: TPS	74	80	73	76	76
		CV: TPS	72	67	73	70	70
		Test: MPS	78	100	73	84	85
Vessel Wall Necrosis	PLS-DA (2 LVs))	Training: TPS	74	92	71	80	81
		CV: TPS	69	58	71	64	64
		Test: MPS	81	100	78	88	88

Berden classification, Focal: $\geq 50\%$ normal glomeruli, Mixed: no predominant lesion; Normal glomeruli, N0 > 25%, N1 10–25%, N2 < 10%; IFTA, interstitial fibrosis & tubular atrophy, T1 > 25%, T0 $\leq 25\%$; PLS-DA, partial least squares discriminant analysis; LVs, latent variables; TPS, total processed spectra; MPS, mean processed spectra, CV; cross-validation.

Table 3. Classification model performance according to histological data: comparative results for paired tissue & urine samples (n = 10).

Presence of Histological Features as an Experimental Class	Sample	Best Discriminate Model	Spectral Data	Accuracy (%)	Sensitivity (%)	Specificity (%)	F-Score (%)	G-Score (%)
Presence of IFTA: T0 vs. T1	Tissue	PLS-DA (6 LVs))	Training: TPS	100	100	100	100	100
			CV: TPS	83	67	90	77	78
			Test: MPS	100	100	100	100	100
	Urine	PLS-DA (10 LVs))	Training: TPS	100	100	100	100	100
			CV: TPS	66	57	70	63	63
			Test: MPS	100	100	100	100	100
Presence of Necrotising glomerular lesions	Tissue	PLS-DA (3 LVs))	Training: TPS	100	100	100	100	100
			CV: TPS	87	78	90	84	84
			Test: MPS	100	100	100	100	100
	Urine	PLS-DA (4 LVs))	Training: TPS	93	93	93	93	93
			CV: TPS	67	53	73	61	62
			Test: MPS	100	100	100	100	100
Presence of Interstitial Infiltrate	Tissue	PLS-DA (6 LVs))	Training: TPS	100	100	100	100	100
			CV: TPS	90	89	90	89	89
			Test: MPS	100	100	100	100	100
	Urine	PLS-DA (10 LVs))	Training: TPS	99	97	100	98	98
			CV: TPS	72	53	80	64	65
			Test: MPS	100	100	100	100	100

IFTA, interstitial fibrosis & tubular atrophy, T1 > 25%, T0 $\leq 25\%$; PLS-DA, partial least squares discriminant analysis; LVs, latent variables; TPS, total processed spectra; MPS, mean processed spectra, CV; cross-validation.

3.4. Key Discriminating Spectral Biomarkers: Tissue & Paired Urine Samples

Based on PLS-DA coefficients, the key distinguishing spectral peaks and wavenumber assignments identified for necrotising glomerular lesions, interstitial infiltrate, and IFTA in the subgroup of paired tissue and urine samples are shown in Figure 4. Peaks associated with necrotising glomerular lesions in tissue were 1680 cm^{-1} (C=O, stretching vibrations of cortisone), 1443 cm^{-1} (CH₂ bending mode of proteins & lipids CH₂ deformation), 1539 cm^{-1} (amide carbonyl group vibrations & aromatic hydrogens) [18]. The only corresponding peak seen in urine was reflective of cortisone (1716 cm^{-1} , C=O of cortisone), which is not specific to this type of lesion [18]. Although peaks representative of increased collagen deposition were seen in urine for IFTA, which would be anticipated (1247 cm^{-1} , amide III collagen assignment), this was not observed in tissue [18]. Similarly, parallel biochemical activity for interstitial infiltrate was not seen between the two biosamples. Figure 5 demonstrates the key wavenumber variables for these same experimental classes amongst the overall cohort of 27 tissue samples.

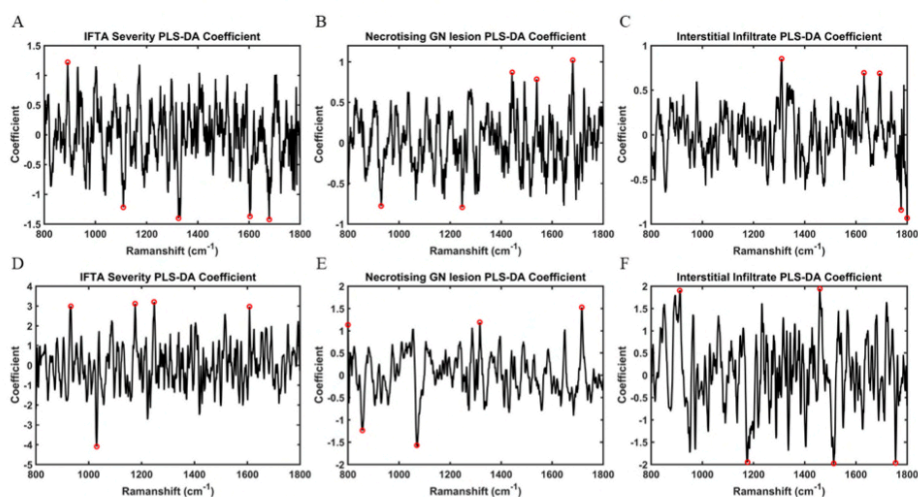


Figure 4. PLS-DA coefficients for identification of spectral biomarkers in tissue and corresponding paired urine samples ($n = 10$)—(A) Wavenumber variables associated with interstitial fibrosis & tubular atrophy (IFTA) in tissue samples— 891.92 cm^{-1} (saccharide band) (B) Wavenumber variables associated with necrotising glomerular (GN) lesions in tissue samples— 1680 cm^{-1} (C=O, stretching vibrations of cortisone), 1443 cm^{-1} (CH₂ bending mode of proteins & lipids CH₂ deformation), 1539 cm^{-1} (amide carbonyl group vibrations & aromatic hydrogens) (C) Wavenumber variables associated with interstitial infiltrate in tissue samples— 1309 cm^{-1} (CH₃/CH₂ twisting or bending mode of lipid & collagen), 1631 cm^{-1} (amide I), 1692 cm^{-1} (amide) (D) Wavenumber variables associated with interstitial fibrosis & tubular atrophy (IFTA) in paired urine samples— 1247 cm^{-1} (amide III collagen assignment), 1175 cm^{-1} (cytosine, guanine), 932 cm^{-1} (proline, hydroxyproline), 1607 cm^{-1} (C=C phenylalanine, tyrosine) (E) Wavenumber variables associated with necrotising glomerular (GN) lesions in paired urine samples— 1716 cm^{-1} (C=O of cortisone), 1316 cm^{-1} (guanine), 800 cm^{-1} (phosphate ion interactions) (F) Wavenumber variables associated with interstitial infiltrate in paired urine samples— 1458 cm^{-1} (nucleic acid), 911 cm^{-1} (glucose).

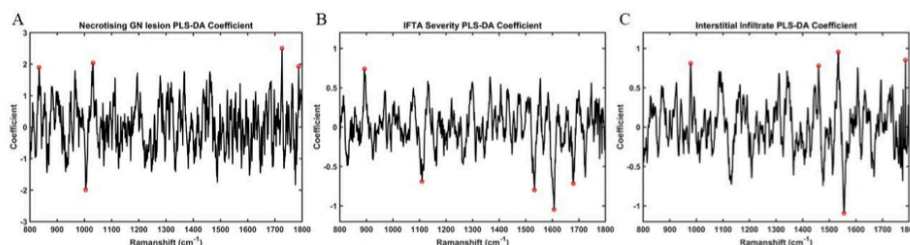


Figure 5. PLS-DA coefficients for identification of spectral biomarkers from tissue samples ($n = 27$)—(A) Wavenumber variables associated with necrotising glomerular (GN) lesions: 1726 cm^{-1} (C=O stretching vibrations of cortisone), 1031 cm^{-1} (C-H in-plane bending mode of phenylalanine), 833 cm^{-1} (asymmetric O-P-O stretching of tyrosine), 1787 cm^{-1} (C=O stretching vibrations of cortisone) (B) Wavenumber variables associated with interstitial fibrosis & tubular atrophy (IFTA): 893 cm^{-1} (phosphodiester deoxyribose) (C) Wavenumber variables associated with interstitial infiltrate: 1533 cm^{-1} (amide carbonyl group vibrations and aromatic hydrogens), 1787 cm^{-1} (C=O stretching vibrations of cortisone), 978 cm^{-1} (C-C stretching in β -sheet proteins), 1459 cm^{-1} (deoxyribose).

4. Discussion

In this exploratory work, we demonstrate for the first time that biospectroscopy offers a potential novel method of machine learning with automated computational detection of AAGN disease activity in renal biopsy specimens. This was demonstrated with the ability of spectral data to distinguish the presence of histological lesions indicative of chronic damage and active disease with a high degree of accuracy, inclusive of IFTA, interstitial infiltrate, and necrotising glomerulonephritis.

Histological evaluation of renal biopsy samples remains the optimum method for diagnosing disease, but certain challenges remain. Key histological findings such as IFTA and interstitial infiltrate are potentially subject to inter-observer variability, with important prognostic implications of the former. As such, there remains scope for adjuvant techniques to complement and aid current tissue analysis. One evolving area of interest is machine learning. In a recent study, based on tissue staining with Masson trichrome and periodic acid-Schiff, Ginley et al. applied machine learning algorithms to digital images in order to reliably identify IFTA and glomerulosclerosis in cases of diabetic nephropathy and renal transplant specimens [19].

Biospectroscopy offers a means of extracting biochemical information that would not otherwise be accessible with current standard methods. By exploiting the interaction of light with the constituent molecules present within any given biosample, biospectroscopy has the capacity to generate a unique spectral fingerprint that is representative of the chemical bonds present. In doing so, the cellular activity unique to any given pathological state can be characterised. Two key analytical techniques are available, infrared spectroscopy and Raman spectroscopy. Both benefit from being low cost and label-free with minimal sample preparation required. Additionally, technological improvements and advancements in chemometric analysis over the past decade have enabled a high throughput of large datasets with increasing investigation of its potential application in renal medicine. In recent years, infrared spectroscopy has been successfully used to detect early biochemical variations that may precede histological changes seen in diabetic nephropathy amongst both native and transplant renal biopsy samples [20–22]. The same modality has also been applied in a large study by Vuiblet et al., to correctly quantify interstitial fibrosis and inflammation in renal transplant biopsies with >90% accuracy and good correlation with clinical outcomes [23]. Whereas the complementary method of Raman microspectroscopy has been investigated and validated as a viable technique to distinguish malignant renal tissue from both healthy parenchyma and benign disease [24,25], as well as successful tumour staging using spectra from surface-enhanced Raman scattering [26].

We applied Raman spectroscopy to unstained renal tissue samples from patients with histopathology reports consistent with AAGN. The resulting spectral data was able to correctly identify the presence of necrotising glomerular lesions, interstitial infiltrate and IFTA with a high degree of diagnostic accuracy on blind predictive modelling. The wavenumber-variables responsible for largest between group differences for the former two were associated with increased amino acid and cortisone activity, whereas IFTA tended to be associated with increased nucleic acid expression. The poor performance of the classification models according to the Berden classification system, presence of vessel wall necrosis, and the proportion of normal glomeruli likely reflects the limited sample distribution amongst these groups.

The aim of the subgroup analysis was to determine if the spectral data from urine could potentially be used as a surrogate for renal biopsy, the premise being that the biomolecular signature obtained from urine could characterise and reflect histological findings at a given time point. To address this question, the histological categories associated with good discriminatory function in the initial spectral analysis of the entire study cohort were evaluated in those tissue samples with a corresponding paired urine sample at the time of biopsy. These categories included necrotising GN lesions, interstitial infiltrate, and IFTA. Using the same chemometric methodology, there was limited performance in the model's ability to reliably discriminate the presence of these categories in urine with a poor sensitivity in each group. This may have resulted from the limited sample size in each category amongst the subgroup and the possibility of insufficient training data. Taking this into account, it should not dissuade further research in this area. Excellent results have previously been obtained from the spectrochemical interrogation of other biofluids including plasma and serum, demonstrating both infrared and Raman spectroscopy as viable non-invasive candidate biomarker tools of disease activity in AAV [27,28]. Additionally, in the present study, it is worth noting that there was some similarity in the key distinguishing spectral peaks between the two biological samples, with increased protein and cortisone expression observed in both tissue and urine for necrotising glomerular lesions. As would be expected, notable biomolecular changes in urine for IFTA were representative of increased collagen synthesis, although this was not observed in tissue samples. One consideration is that the difference in the spectral acquisition method used for tissue and urine samples may account for the lack of consistency between spectral profiles obtained and the metabolic activities they represent. However, this would require a larger-sized and longitudinal temporal study to elucidate. It is also very possible that different profiles of spectral biomarkers present themselves depending on sample type.

Aside from sample size, one potential limiting factor is the absence of control groups. However, this is not essential herein with a factorial-based design determining the presence or absence of a feature in a cohort displaying a range of histological variation that is common amongst patients with AAGN. A further limitation is the lack of assigned variables to novel biomolecules reported in the literature. In our study, all experimental categories from tissue samples were based on known key histological variables. Promising non-invasive biomarkers of disease activity in AAGN include urinary monocyte chemoattractant protein-1 (uMCP-1), urinary soluble CD163 (sCD163), and degradation products of the complement cascade [29–36]. Each has been shown to correlate well with disease activity, in addition to an associated upregulation of macrophage infiltration in inflamed glomeruli with higher levels of uMCP-1 and the presence of fibrinoid necrosis and cellular crescents with sCD163 [29,37]. Tissue depositions of alternative pathway cleavage products including C3d, C3c, and Bb have been associated with a higher degree of cellular crescents and IFTA. This was mirrored in urine with higher levels of C3a, C5a, and soluble C5b-9 present in active disease, as well as higher urinary levels of Bb correlating with a lower proportion of normal glomeruli [36]. Any future study evaluating the role of biospectroscopy in AAGN would benefit from assay and analysis of these potential biomarkers with spectral data. In addition to offering a potentially cheaper and faster surrogate technique for their detection, their analysis may also help resolve the current lack of concordance in the spectral profiles

between the two biosamples. Other potential areas of research include the application of forward feature extraction algorithms to construct prediction outcome models based extracted spectral features, as well as correlation of spectral data with imaging mass spectrometry to aid in the delineation of any potential biomarkers.

Vibrational spectroscopy has the potential to offer a robust tool for machine learning and standardised automated detection of disease activity in AAGN. Its application enables the simultaneous analysis of a broad spectrum of biomolecules, providing an adjuvant technique for biomarker extraction and additional potential insight into the molecular mechanism of disease. This study highlights the potential for spectral profiles to be used as a non-invasive surrogate marker of histological changes in order to aid disease monitoring and guide patient care. The role of biospectroscopy in tissue warrants further research in a larger study of varied renal pathology, with comparison alongside biofluids to determine its plausible use as a liquid biopsy.

Author Contributions: Conceptualization, A.D.M., A.P.D., A.W.R. and F.L.M.; Data curation, A.D.M.; Formal analysis, A.D.M., D.L.D.F. and K.M.G.L.; Investigation, A.D.M.; Methodology, A.D.M. and F.L.M.; Project administration, A.D.M.; Supervision, A.P.D., A.W.R. and F.L.M.; Writing—original draft, A.D.M.; Writing—review & editing, A.D.M., D.L.D.F., K.M.G.L., L.F., M.E.B., A.P.D., A.W.R. and F.L.M. All authors have read and agreed to the published version of the manuscript.

Funding: D.L.D. has received a research grant from the Coordenação de Aperfeiçoamento de Pessoal de Nível Superior (CAPES), Brazil. No other external financial support was contributed to this study.

Institutional Review Board Statement: Study approval was received from the Health Research Authority, Cambridge South Research Ethics Committee (REC reference 18/EE/0194) and the Research and Development team in the Centre for Health Research and Innovation at Lancashire Teaching Hospitals NHS Foundation Trust. The study was conducted in accordance with the declaration of Helsinki.

Informed Consent Statement: Informed written consent was obtained from all participants prior to enrollment in the study.

Data Availability Statement: The authors declare that the data supporting the findings of this study are available within the paper and its supplementary information. The MATLAB code and instructions on how to process the data are presented in previous publications (13, 14, 17).

Acknowledgments: The authors would like to acknowledge the support of the Renal Department at Royal Preston Hospital Lancashire NHS Foundation Trust and the team at the NIHR Lancashire Clinical Research Facility in undertaking this study. We are also grateful for the support of Katherine Ashton in assisting tissue sample preparation. Thank you for the participation and support of all the patients in this study. D.L.D.F. would like to thank the Coordenação de Aperfeiçoamento de Pessoal de Nível Superior (CAPES), Brazil, for his research grant.

Conflicts of Interest: The authors declare no conflict of interest.

References

1. Flossmann, O.; Berden, A.; De Groot, K.; Hagen, C.; Harper, L.; Heijl, C.; Höglund, P.; Jayne, D.; Luqmani, R.; Mahr, A.; et al. Long-term patient survival in ANCA-associated vasculitis. *Ann. Rheum. Dis.* **2011**, *70*, 488–494. [[CrossRef](#)]
2. de Joode, A.A.E.; Sanders, J.S.F.; Stegeman, C.A. Renal survival in Proteinase 3 and Myeloperoxidase ANCA-associated systemic Vasculitis. *Clin. J. Am. Soc. Nephrol.* **2013**, *8*, 1709–1717. [[CrossRef](#)] [[PubMed](#)]
3. Berti, A.; Cornec-Le Gall, E.; Cornec, D.; Casal Moura, M.; Matteson, E.L.; Crowson, C.S.; Ravindran, A.; Sethi, S.; Fervenza, F.C.; Specks, U. Incidence, prevalence, mortality and chronic renal damage of anti-neutrophil cytoplasmic antibody-associated glomerulonephritis in a 20-year population-based cohort. *Nephrol. Dial. Transplant.* **2018**, *34*, 1508–1517. [[CrossRef](#)] [[PubMed](#)]
4. Lee, T.; Gasim, A.; Derebail, V.K.; Chung, Y.; McGregor, J.G.; Lionaki, S.; Poulton, C.; Hogan, S.L.; Jennette, J.C.; Falk, R.J.; et al. Predictors of treatment outcomes in ANCA-associated vasculitis with severe kidney failure. *Clin. J. Am. Soc. Nephrol.* **2014**, *9*, 905–913. [[CrossRef](#)] [[PubMed](#)]
5. Manno, R.L.; Seo, P.; Geetha, D. Older patients with ANCA-associated vasculitis and dialysis dependent renal failure: A retrospective study. *BMC Nephrol.* **2015**, *16*, 88. [[CrossRef](#)] [[PubMed](#)]
6. Berden, A.E.; Ferrario, F.; Hagen, E.C.; Jayne, D.R.; Jennette, J.C.; Joh, K.; Neumann, I.; Noël, L.H.; Pusey, C.D.; Waldherr, R.; et al. Histopathologic classification of ANCA-associated glomerulonephritis. *J. Am. Soc. Nephrol.* **2010**, *21*, 1628–1636. [[CrossRef](#)]

7. Hilhorst, M.; Wilde, B.; Van Breda Vriesman, P.; Van Paassen, P.; Tervaert, J.W.C. Estimating renal survival using the ANCA-associated GN classification. *J. Am. Soc. Nephrol.* **2013**, *24*, 1371–1375. [[CrossRef](#)]
8. Berden, A.E.; Jones, R.B.; Erasmus, D.D.; Walsh, M.; Noël, L.H.; Ferrario, F.; Waldherr, R.; Bruijn, J.A.; Jayne, D.R.; Bajema, I.M. Tubular lesions predict renal outcome in antineutrophil cytoplasmic antibody-associated glomerulonephritis after rituximab therapy. *J. Am. Soc. Nephrol.* **2012**, *23*, 313–321. [[CrossRef](#)]
9. Quintana, L.F.; Pérez, N.S.; De Sousa, E.; Rodas, L.M.; Griffiths, M.H.; Solé, M.; Jayne, D. ANCA serotype and histopathological classification for the prediction of renal outcome in ANCA-associated glomerulonephritis. *Nephrol. Dial. Transplant.* **2014**, *29*, 1764–1769. [[CrossRef](#)]
10. Chen, Y.X.; Xu, J.; Pan, X.X.; Shen, P.Y.; Li, X.; Ren, H.; Chen, X.N.; Ni, L.Y.; Zhang, W.; Chen, N. Histopathological classification and renal outcome in patients with antineutrophil cytoplasmic antibodies-associated renal vasculitis: A study of 186 patients and meta analysis. *J. Rheumatol.* **2017**, *44*, 304–313. [[CrossRef](#)]
11. van Daalen, E.E.; Wester Trejo, M.A.C.; Göçeroglu, A.; Ferrario, F.; Joh, K.; Noël, L.H.; Ogawa, Y.; Wilhelmus, S.; Ball, M.J.; Honsova, E.; et al. Developments in the histopathological classification of ANCA-associated glomerulonephritis. *Clin. J. Am. Soc. Nephrol.* **2020**, *15*, 1103–1111. [[CrossRef](#)] [[PubMed](#)]
12. Brix, S.R.; Noriega, M.; Tennstedt, P.; Vettorazzi, E.; Busch, M.; Nitschke, M.; Jabs, W.J.; Özcan, F.; Wendt, R.; Hausberg, M.; et al. Development and validation of a renal risk score in ANCA-associated glomerulonephritis. *Kidney Int.* **2018**, *94*, 1177–1188. [[CrossRef](#)] [[PubMed](#)]
13. Morais, C.L.M.; Lima, K.M.G.; Singh, M.; Martin, F.L. Tutorial: Multivariate classification for vibrational spectroscopy in biological samples. *Nat. Protoc.* **2020**, *15*, 2143–2162. [[CrossRef](#)] [[PubMed](#)]
14. Morais, C.L.M.; Paraskevaïdi, M.; Cui, L.; Fullwood, N.J.; Isabelle, M.; Lima, K.M.G.; Martin-Hirsch, P.L.; Sreedhar, H.; Trevisan, J.; Walsh, M.J.; et al. Standardization of complex biologically derived spectrochemical datasets. *Nat. Protoc.* **2019**, *14*, 1546–1577. [[CrossRef](#)] [[PubMed](#)]
15. Ballabio, D.; Consonni, V. Classification tools in chemistry. Part 1: Linear models. PLS-DA. *Anal. Methods* **2013**, *5*, 3790–3798. [[CrossRef](#)]
16. Cortes, C.; Vapnik, V. Support-Vector Networks. *Mach. Learn.* **1995**, *297*, 273–297. [[CrossRef](#)]
17. Morais, C.L.M.; Lima, K. Comparing unfolded and two-dimensional discriminant analysis and support vector machines for classification of EEM data. *Chemom. Intell. Lab. Syst.* **2017**, *162*, 123–129. [[CrossRef](#)]
18. Movasaghi, Z.; Rehman, S.; Rehman, I.U. Raman spectroscopy of biological tissues. *Appl. Spectrosc. Rev.* **2007**, *42*, 493–541. [[CrossRef](#)]
19. Ginley, B.; Jen, K.-Y.; Han, S.S.; Rodrigues, L.; Jain, S.; Fogo, A.B.; Zuckerman, J.; Walavalkar, V.; Miecznikowski, J.C.; Wen, Y.; et al. Automated Computational Detection of Interstitial Fibrosis, Tubular Atrophy, and Glomerulosclerosis. *J. Am. Soc. Nephrol.* **2021**, *32*, 837–850. [[CrossRef](#)]
20. De Bruyne, S.; Van Dorpe, J.; Himpe, J.; Van Biesen, W.; Delanghe, S.; Speeckaert, M.M.; Delanghe, J.R. Detection and Characterization of a Biochemical Signature Associated with Diabetic Nephropathy Using Near-infrared Spectroscopy on Tissue Sections. *J. Clin. Med.* **2019**, *8*, 1022. [[CrossRef](#)]
21. Varma, V.K.; Kajdacsy-Balla, A.; Akkina, S.K.; Setty, S.; Walsh, M.J. A label-free approach by infrared spectroscopic imaging for interrogating the biochemistry of diabetic nephropathy progression. *Kidney Int.* **2016**, *89*, 1153–1159. [[CrossRef](#)] [[PubMed](#)]
22. Severcan, F.; Bozkurt, O.; Gurbanov, R.; Gorgulu, G. FT-IR spectroscopy in diagnosis of diabetes in rat animal model. *J. Biophotonics* **2010**, *3*, 621–631. [[CrossRef](#)] [[PubMed](#)]
23. Vuiblet, V.; Fere, M.; Gobinet, C.; Birembaut, P.; Piot, O.; Rieu, P. Renal graft fibrosis and inflammation quantification by an automated fourier-transform infrared imaging technique. *J. Am. Soc. Nephrol.* **2016**, *27*, 2382–2391. [[CrossRef](#)]
24. Karim, B.; Fleureau, J.; Rolland, D.; Lavastre, O.; Rioux-Leclercq, N.; Guille, F.; Patard, J.-J.; Senhadji, L.; de Crevoisier, R. Raman Spectroscopy: A novel experimental approach to evaluating renal tumours. *Eur. Urol.* **2010**, *58*, 602–608.
25. Couapel, J.-P.; Senhadji, L.; Rioux-Leclercq, N.; Verhoest, G.; Lavastre, O.; de Crevoisier, R.; Al, E. Optical spectroscopy techniques can accurately distinguish benign and malignant renal tumours. *BJU Int.* **2013**, *111*, 865–871. [[CrossRef](#)]
26. Mert, S.; Özbek, E.; Ötünçtemur, A.; Çulha, M. Kidney tumor staging using surface-enhanced Raman scattering. *J. Biomed. Opt.* **2015**, *20*, 047002. [[CrossRef](#)]
27. Morris, A.D.; Morais, C.L.M.; Lima, K.M.G.; Freitas, D.L.D.; Brady, M.E.; Dhaygude, A.P.; Rowbottom, A.W.; Martin, F.L. Distinguishing active from quiescent disease in ANCA-associated vasculitis using attenuated total reflection Fourier-transform infrared spectroscopy. *Sci. Rep.* **2021**, *11*, 9981. [[CrossRef](#)] [[PubMed](#)]
28. Morris, A.D.; Morais, C.L.M.; Lima, K.M.G.; Freitas, D.L.D.; Brady, M.E.; Dhaygude, A.P.; Rowbottom, A.W.; Martin, F.L. A comparative analysis of different biofluids using Raman spectroscopy to determine disease activity in ANCA-associated vasculitis. *J. Biophotonics* **2021**, *14*, e202000426. [[CrossRef](#)]
29. Tam, F.W.K.; Sanders, J.S.; George, A.; Hamad, T.; Miller, C.; Dougan, T.; Cook, H.T.; Kallenberg, C.G.M.; Gaskin, G.; Levy, J.B.; et al. Urinary monocyte chemoattractant protein-1 (MCP-1) is a marker of active renal vasculitis. *Nephrol. Dial. Transplant.* **2004**, *19*, 2761–2768. [[CrossRef](#)]
30. Ohlsson, S.; Bakoush, O.; Tencer, J.; Torffvit, O.; Segelmark, M. Monocyte chemoattractant protein 1 is a prognostic marker in ANCA-associated small vessel vasculitis. *Mediat. Inflamm.* **2009**, *2009*, 584916. [[CrossRef](#)]

31. Lieberthal, J.G.; Cuthbertson, D.; Carette, S.; Hoffman, G.S.; Khalidi, N.A.; Koenig, C.L.; Langford, C.A.; Maksimowicz-McKinnon, K.; Seo, P.; Specks, U.; et al. Urinary biomarkers in relapsing antineutrophil cytoplasmic antibody-associated vasculitis. *J. Rheumatol.* **2013**, *40*, 674–683. [[CrossRef](#)] [[PubMed](#)]
32. Jönsson, N.; Erlandsson, E.; Gunnarsson, L.; Pettersson, Å.; Ohlsson, S. Monocyte chemoattractant protein-1 in antineutrophil cytoplasmic autoantibody-associated vasculitis: Biomarker potential and association with polymorphisms in the MCP-1 and the CC chemokine receptor-2 gene. *Mediat. Inflamm.* **2018**, *2018*, 6861257. [[CrossRef](#)] [[PubMed](#)]
33. O'Reilly, V.P.; Wong, L.; Kennedy, C.; Elliot, L.A.; O'Meachair, S.; Coughlan, A.M.; O'Brien, E.C.; Ryan, M.M.; Sandoval, D.; Connolly, E.; et al. Urinary soluble CD163 in active renal vasculitis. *J. Am. Soc. Nephrol.* **2016**, *27*, 2906–2916. [[CrossRef](#)] [[PubMed](#)]
34. Xing, G.Q.; Chen, M.; Liu, G.; Heeringa, P.; Zhang, J.J.; Zheng, X.; Jie, E.; Kallenberg, C.G.M.; Zhao, M.H. Complement activation is involved in renal damage in human antineutrophil cytoplasmic autoantibody associated pauci-immune vasculitis. *J. Clin. Immunol.* **2009**, *29*, 282–291. [[CrossRef](#)]
35. Hilhorst, M.; Van Paassen, P.; Van Rie, H.; Bijnens, N.; Heerings-Rewinkel, P.; Van Breda Vriesman, P.; Cohen Tervaert, J.W. Complement in ANCA-associated glomerulonephritis. *Nephrol. Dial. Transplant.* **2015**, *32*, 1302–1313. [[CrossRef](#)]
36. Gou, S.J.; Yuan, J.; Wang, C.; Zhao, M.H.; Chen, M. Alternative complement pathway activation products in urine and kidneys of patients with ANCA-associated GN. *Clin. J. Am. Soc. Nephrol.* **2013**, *8*, 1884–1891. [[CrossRef](#)]
37. Aendekerk, J.P.; Timmermans, S.A.M.E.G.; Busch, M.H.; Potjewijd, J.; Heeringa, P.; Damoiseaux, J.G.M.C.; Reutelingsperger, C.P.; van Paassen, P. Urinary Soluble CD163 and Disease Activity in Biopsy-Proven ANCA-Associated Glomerulonephritis. *Clin. J. Am. Soc. Nephrol.* **2020**, *15*, 1740–1748. [[CrossRef](#)]